

Signaling in symbiosis: The RNA signature of local and systemic interactions between partners

By
Silvia Moriano-Gutiérrez

A dissertation submitted in partial fulfillment of the requirements for the degree of

Doctor of Philosophy

(Molecular Biosciences and Bioengineering)

at the

University of Hawai‘i at Mānoa

August 2020

Margaret McFall-Ngai (Chair)

Edward Ruby

Alika Maunakea

Anthony Amend

Marla Berry

Daisuke Takagi

To my family, friends
and all scientific heroes
who inspired my pursuit of Science

ACKNOWLEDGEMENTS

I thank my thesis committee members: Marla Berry, Alike Maunakea, Anthony Amend, Daisuke Takagi, Edward Ruby and my doctoral adviser Margaret McFall-Ngai for their guidance during the research process. I thank my co-authors: Clotilde Bongrand, Eric Koch and Tara Essock-Burns for their work to foster successful collaborations, as well as lab members past and present, for training and great discussions. I especially thank Susannah Lawhorn for her valuable help proofreading this thesis.

My deepest gratitude goes to Margaret. The opportunity you granted me after that first email I sent you, set the course of my career as well as my personal life. Working with you has been a great adventure with fascinating challenges. I'm also very grateful to my co-supervisor. Ned, you have been instrumental and a great mentor, especially these last years. Discussions with you were always filled with laughter and always useful.

A key part of this whole process has been the great environment surrounding us. Clotilde, you have been the greatest support I had over all these seven years. Sharing a lab with you has been great. I really appreciate your craziness, laughs and our eternal discussions. Eric, thanks for your humor and your capacity to lighten the mood in any situation. Thanks for the invaluable beer meeting tradition that started in Madison.

Surviving my whole PhD also relied strongly on the support I've gotten from many others outside the lab. Specially to Angel, who has been incredibly supportive. You are one of the best things that has happened to me and I will be forever grateful for choosing this path that led me to my best friend. Thanks for all our useful discussions and limitless patience. Furthermore, I would not have chosen this path if it were not for the inspiration, support and motivation of my amazing friends from the University of Valencia. Dani, Andrea, Marta, Carmen, Ximo, Anselm, Ana Rosa, Jose, Borja and Dani M, I am very grateful for having all of you in my life.

Finally, to my parents, who taught me to be open-minded and supported me on every step of the way, thank you. Ana, Emma, Adriana, Ivan, Julia, María and Toñi, you all inspire me to work harder and keep hope that one day I will be able to return back home. A toda mi familia, muchísimas gracias, sin vosotros nada de esto hubiese sido posible.

Signaling in symbiosis: The RNA signature of local and systemic interactions between partners

Silvia Moriano Gutiérrez

Under the supervision of Professor Margaret McFall-Ngai.

Over the course of evolution, animals and bacteria have formed mutually beneficial partnerships, often characterized by an exchange of essential or fitness-enhancing goods and services, such as nutrients or safety. These symbioses, which have numerous effects on host fitness, can significantly impact host development and physiology. This dissertation uses the squid-vibrio symbiosis to examine the biochemical signaling that occurs between symbiotic partners, focusing on RNA-mediated host-microbe interactions. In the symbiosis between the marine bioluminescent bacterium *Vibrio fischeri* and the squid *Euprymna scolopes*, the host houses a monospecific association with *V. fischeri* in an organ specifically adapted to manipulate bacterial bioluminescence. This dissertation begins by describing the profound local and systemic influences of a single symbiont on the gene regulation of host tissues, highlighting the impact of the light-organ symbiosis on host expression networks across developmental time and daily rhythms. We found that the light produced by the bacteria is the main driver of changes of gene expression both within the light organ and throughout other organs. We next studied the role of bacterial small RNAs (sRNAs) in triggering responses in an animal host. We identified a symbiont sRNA called SsrA that is loaded into outer membrane vesicles (OMVs), and trafficked into the epithelium of the host. We determined that the delivery of SsrA is required to dampen the animal's immune response, which is necessary for a successful symbiosis. In addition, we found that the absence of this sRNA affects the host at the transcriptional, cellular, and physiological levels, negatively impacting fitness, and ultimately resulting in failure of the association to persist. As the light organ undergoes vast changes of gene expression in response to colonization by *V. fischeri*, we next studied the mechanisms of the regulation of host gene expression that orchestrates the main developmental and physiological changes in the light organ. We characterized the *E. scolopes* miRNA transcriptome as well as the extent of miRNA-mediated post-transcriptional regulation within the host light organ. The resultant miRNA transcriptome of the light organ drives gene expressional networks that both orchestrate developmental changes in symbiotic tissues and adapt the host immune response to integrate the symbiont into its biology.

KEYWORDS

Symbiosis, ncRNAs, miRNAs, sRNAs, Systemic, Transcriptomics, Squid-Vibrio

TABLE OF CONTENTS

Dedication	2
Acknowledgements	3
Abstract	4
Keywords	5
Table of contents	5
List of figures	6
List of tables	8
Chapter 1: General introduction	10
The immunogenic perception of symbionts	11
The squid-vibrio symbiosis	13
Non-coding RNAs in host-microbe interactions	14
References	18
Chapter 2: Critical symbiont signals drive both local and systemic changes in diel and developmental host gene expression	25
Abstract	26
Significance	26
Introduction	27
Results	29
Discussion	37
Materials and Methods	43
Acknowledgements	43
Figures	45
References	50
Supplementary Information	57
Chapter 3: The non-coding small RNA SsrA is secreted by <i>Vibrio fischeri</i> to modulate critical host responses	80

Summary	81
Keywords	81
Introduction	81
Results	83
Discussion	89
Acknowledgments	94
Tables	95
Figures	96
Star methods	102
Supplemental information	110
References	123
Chapter 4: miRNA-mediated regulation of host responses in a symbiotic organ	131
Abstract	132
Background	132
Material and Methods	134
Results	136
Discussion	140
Figures	145
Additional files	151
References	199
Appendix A: Additional Scientific contributions	206
Appendix B: Delivery of symbiont CsrB2 into host epithelium	209
Appendix C: Biogeography of symbiont gene expression in the light organ crypts	216

LIST OF FIGURES

Chapter 2

Fig. 1. Transcriptome profiling of <i>E. scolopes</i> organs	45
Fig. 2. Impact of light-organ symbiosis on gene expression in different adult organs	46
Fig. 3. Variation of symbiosis-responsive gene expression over the day/night cycle	47
Fig. 4. Impact of symbiont bioluminescence on juvenile gene expression	48

Fig. S1. Assessment of the assembly quality and read representation of the <i>E. scolopes</i> transcriptome and its annotation	63
Fig. S2. Data analysis of differentially expressed transcripts across each set of organs, identifying transcripts enriched in specific organs	64
Fig. S3. Symbiosis-responsive genes shared across squid organs and stages of development	65
Fig. S4. Validation of adult RNA-seq data by NanoString Technologies	66
Fig. S5. Patterns of differential gene expression in response to light-organ symbiosis in adult tissues	67
Fig. S6. Patterns of differential gene expression in juvenile tissues in response to light organ symbiosis by luminous and dark bacteria	68
Fig. S7. Transcriptional profiles of juvenile organs in response to light organ colonization by luminous or dark symbionts after 24 h	69
Fig. S8. Examples of symbiosis-responsive gene expression compared between juvenile and adult organs	70
Fig. S9. Differential gene expression early in symbiosis by NanoString Technologies	71
Fig. S10. Visualization of ANP-CE transcript in whole-mount light organs 24 h after colonization	72

Chapter 3

Figure 1. Symbiont non-coding RNA, SsrA, localizes within the crypt epithelium	96
Figure 2. The Δ <i>ssrA</i> mutant is able to initiate colonization normally, but persists poorly	97
Figure 3. Host responses to colonization by either WT or Δ <i>ssrA</i> differ	98
Figure 4. The absence of SsrA in the epithelium, but not SsrA activity in the symbiont, weakens the host	99
Figure 5. SsrA taken up by haemocytes is detected through host cytosolic RNA sensors	101
Figure S1. The symbiont sRNA SsrA, is found in the squid circulatory system, and within symbiont outer membrane vesicles (OMVs)	111
Figure S2. Effects of SsrA deletion on <i>V. fischeri</i> cells	112

Figure S3. Localization of the symbiont's 16S and SsrA transcripts within the host's light organ epithelial cells	113
Figure S4. Induction of apoptosis in the light-organ appendages of juvenile squid early in symbiosis	114
Figure S5. Effects of colonization by $\Delta ssrA$ on host physiology and health	115
Figure S6: Down-regulation of laccase-3 in the crypt epithelium requires the presence of symbiont SsrA	116

Chapter 4

Fig. 1. The molluscan argonaute and PIWI gene repertoire	145
Fig. 2. Expression of miRNA-synthesis associated proteins and light-organ miRNA database	146
Fig. 3. The effect of symbiosis on the light-organ miRNA profile	147
Fig. 4. Functional enrichment analysis of predicted miRNA target genes	148
Fig. 5. Profiling of the circulating miRNAs	149
Fig. 6. The impact of symbiosis on miRNA expression... ..	150
Fig. S1. Functional enrichment analysis of predicted miRNA target genes	151

LIST OF TABLES

Chapter 2

Table S1. Primer list for qRT-PCR	73
Table S2. HCR-FISH probe sequences	75

Chapter 3

Table 1: List of abundant small, non-coding RNAs	95
Key resources table	117
Table S1: Oligonucleotides information	120

Chapter 4

Table S1: miRNAs identified by sequence similarity in mirBase database but not found within the <i>E. scolopes</i> genome	152
Table S2. List of light-organ miRNAs found in the <i>E. scolopes</i> genome	154
Table S3. Differentially expressed miRNAs in response to symbiosis	161

Table S4. Predicted mRNA targets of miRNAs differentially up-regulated in aposymbiosis (APO) or symbiosis (WT)	162
Table S5. List of miRNAs found in squid hemolymph	176
Table S6. Differentially expressed miRNAs between hemolymph and light organ from colonized (WT) or uncolonized squid	197

CHAPTER 1

GENERAL INTRODUCTION

Symbiotic associations are ubiquitous across organisms. From plants, to fungi and animals, the occurrence of such associations is widespread and has provided different evolutionary strategies throughout the tree of life. The effects of microbial symbioses are apparent across biological levels, with molecular, organismal, and ecological consequences. Many organisms depend on beneficial associations with symbionts for nutrition, defense, normal development or other fitness features (McFall-Ngai et al. 2013). Rather than fostering total sterility in their bodies, hosts enable and often facilitate symbiotic colonization, and use signaling mechanisms that allow them to regulate the composition and behavior of their associated symbionts and to communicate with the microbes. Characterizing the ways in which hosts use this conserved dialog to distinguish beneficial associations from pathogenic ones is key for our understanding of host-microbe interactions.

The immunogenic perception of symbionts

Hosts and symbionts rely on a reciprocal biochemical language to establish and maintain specific associations, while resisting pathogenesis (Douglas, 2018; McFall-Ngai et al., 2010). This communication system is governed by the perception of microbe-associated molecular patterns (MAMPs) (Koropatnick, 2004; Round et al., 2011). These unique conserved molecular patterns are recognized by pattern-recognition receptors (PRRs) on host cells (Sellge and Kufer, 2015), thus mediating cross-talk between symbionts and their host. MAMPs are usually conserved structures that are essential for microbial life. Typical MAMPs include bacterial surface constituents such as lipopolysaccharides (LPS), the principal component of the outer membrane of Gram-negative bacteria, flagellin, the main structural component of the bacterial motility machinery, or peptidoglycan (PGN), found in both Gram-positive and Gram-negative bacteria a constituent of the cell wall (Altenbach and Robatzek, 2007; Erbs and Newman, 2012; Sommer and Bäckhed, 2013; Zhong et al., 2017). In fungi, cell-wall components such as chitin and ergosterol often serve as MAMPs or PAMPs (Nürnberg et al., 2004). Finally, host PRRs can also recognize certain nucleic acids derived from viral particles and bacteria (Gürtler and Bowie, 2013). By interacting with PRRs, bacterial ligands from the symbionts send signals to the host, promoting development of host tissue and of the immune system (Bäckhed et al., 2005; Koropatnick et al., 2004; Montgomery and McFall-Ngai, 1995).

The diversity of signaling pathways and host responses to various microbial molecules is reflected in the variety of PRRs. PRRs are divided into four families: toll-like receptors (TLR), Nucleotide-binding oligomerization domain-like receptors (NLR), C-type lectin receptors (CLR) and RIG-1 like receptors (RLR), providing a wide range of ligand recognition possibilities (Palm and Medzhitov, 2009; Sellge and Kufer, 2015). Having evolved in a microbial world, metazoans rely on exposure to microbial products for many aspects of their physiology. For example, LPS (Heath-Heckman et al., 2016; Koropatnick, 2004; Rakoff-Nahoum et al., 2004) and PGN (Bouskra et al., 2008; Buchon et al., 2009) are fundamental for normal development in many symbiotic organs. Another example of microbial products impacting symbiotic organs is that the proper maturation of the host's immune system also requires the presence of various microbial products (Kamada et al., 2013).

In addition to affecting host tissue development and biochemistry within symbiotic organs, symbionts can also impact host physiology in tissues far from the site of microbial symbiosis. Such systemic effects of symbiosis are an emerging area of research. For example, gut-microbiota produce short-chain fatty acids (SCFA) and other MAMPs, which are able to induce systemic immunomodulation, affecting both the immune system and host metabolism in distant organs (Spiljar et al., 2017). The gut-brain axis offers a striking example of this phenomenon; it is a bi-directional communication line between the intestinal environment and the central nervous system and functions as a regulatory pathway for immune responses in both the brain and gut tract. This well-studied host system, appears to be highly influenced by the activity of gut symbionts (Attar, 2016; Bauer et al., 2016). The ways in which microbes affect neural development and functioning have also been studied in invertebrates, such as *Drosophila* (Dus et al., 2015). In recent years, multiple gut-brain axis studies have emerged, situating gut symbionts at the intersection of several diseases (Schroeder and Bäckhed, 2016). Recent research focuses on the functional integration of the gut with distant organs such as the liver (Schneider et al., 2018; Yip et al., 2018), heart (Kamo et al., 2017; Serino et al., 2014), kidney (Coppo, 2018), lung (Budden et al., 2016; Samuelson et al., 2015), and retina (Rowan et al., 2017). However, further research is required in order to elucidate the ways in which changes in the gut microbial population indeed have far-reaching impacts on host metabolism, immune modulation, and/or disease progression when homeostasis is unbalanced. Yet another exciting discovery in research on system-wide effects of microbial symbiosis is the recent finding that gut microbes impact biological rhythms (Thaiss et al., 2016).

Many biological processes in the gut tract are influenced by a strong circadian rhythm control (Konturek et al., 2011), and signals derived from gut microbes influence the transcriptional and epigenetic activity of the gut tract, thus modulating the host's circadian physiology (Leone et al., 2015; Tahara et al., 2018; Thaiss et al., 2016, 2017). Deciphering the crosstalk between the host and its microbiota on a cellular and molecular level will elucidate the complex networks linking symbionts to host metabolism, homeostasis, and circadian rhythms. Innate immune responses triggered by PRR activation constitute another mechanism of host-microbe communication, with PRRs also enabling the host to distinguish microbes driving pathogenesis from those that are not. The mechanisms underlying host-responses to various microbial products require further investigation, as fine-scale variation in these signal-recognition pathways might be a key factor allowing the hosts not only to discern not only between friend and foe, but also to distinguish variability in symbiont quality. Thus, this form of host-microbe communication provides the biochemical tools for managing the onset, maintenance and persistence of a symbiosis.

Metazoans often host highly diverse and complex symbiont communities, which can make it challenging to decipher the complex interactions and molecular dialogs that occur between hosts and their microbiota. Among the metazoans, invertebrates generally have simpler symbiotic consortia. Furthermore, invertebrates lack an adaptive immune system, which provides an opportunity to study the innate immune system of the host with greater resolution. Therefore, invertebrates present model systems that present a variety of opportunities to study the mechanisms of communication between hosts and symbionts. The symbiosis of the marine bioluminescent bacterium *Vibrio fischeri* with its squid host *Euprymna scolopes* offers a simplified model system in which the squid forms a monospecific association with *V. fischeri* in a specific organ adapted to manipulate bacterial bioluminescence.

The squid-vibrio symbiosis.

The light-organ symbiosis between the Hawaiian bobtail squid *Euprymna scolopes* and the marine bioluminescent gammaproteobacterium *Vibrio fischeri* offers an experimentally accessible model for understanding the events and signals underlying animal-microbe symbioses. This partnership is very specific, wherein only *V. fischeri*, against a background of numerous other bacterial species in seawater, is capable of forming a stable relationship with the squid. In this horizontally-acquired symbiosis, the squid are aposymbiotic when they hatch, and within minutes,

the bacteria are acquired from the surrounding seawater. The *V. fischeri* cells are harbored within the epithelium-lined crypts of the squid light organ (Sycuro et al., 2006). The primary symbiont product of this mutualistic association is the bioluminescence provided by *V. fischeri* (Stabb and Millikan, 2009), which is most likely used as counterillumination for host nocturnal activities (McFall-Ngai and Montgomery 1990). Within hours of colonization, the symbiont induces the irreversible loss of the superficial ciliated epithelia of the juvenile light-organ, a process that facilitates symbiont acquisition (Doino and McFall-Ngai, 1995).

From the initial colonization of the light organ, the symbiont is maintained in a profound daily cycle determined by the host, in which the dawn light cue triggers loss of ~95% of the symbionts from the crypts (Lee and Ruby, 1994), leaving the remaining cells to repopulate the light organ. This rhythmic behavior is maintained throughout the host life-span (Boettcher et al., 1996; Lee and Ruby, 1994). The light organ crypts increase in morphological complexity in a developmental process that lasts several weeks (Essock-Burns et al., 2020; Montgomery and McFall-Ngai, 1998; Schwartzman et al., 2015; Sycuro et al., 2006). In the developmentally mature light organ, *V. fischeri* undergoes daily metabolic changes, transitioning from anaerobic respiration during the day to chitin fermentation at night (Schwartzman et al., 2015; Wier et al., 2010). This modulation of biological rhythms is not unidirectionally determined by the host, as symbionts affect host transcriptional rhythms as well (Heath-Heckman et al., 2013). Additionally, from the onset of symbiosis, through maturation of the light organ and maintenance of the daily rhythms, the light organ undergoes extensive transcriptomic responses (Chun et al., 2006, 2008; Kremer et al., 2013, 2018; Moriano-Gutierrez et al., 2019; Wier et al., 2010). The molecular basis of these dynamic changes in light-organ gene expression is yet not fully understood. Although other mechanisms such as epigenetic modification may play crucial roles in ensuring that proper gene expression patterns are established and maintained in any given moment and cell type, post-transcriptional regulation of gene expression by miRNAs is an evolutionarily conserved tool for inducing dynamic expressional changes, and could be key in regulating host responses.

Non-coding RNAs in host-microbe interactions

Non-coding RNA (ncRNA) constitutes the majority of the transcriptional products made in humans and other complex organisms. Further, ncRNAs represent key elements regulating eukaryotic gene expression (Michalak, 2006). One of the best-studied ncRNA is micro RNA

(miRNA), which usually down-regulate gene expression in a sequence-targeted manner. Briefly, miRNAs are transcribed from the genome, and the primary transcripts are processed in the nucleus and later in the cytosol by the RNase II enzymes Drosha and Dicer, respectively (Murphy et al., 2008). These short regulatory RNAs bind to Argonaute (AGO) proteins and affect gene expression through base pairing with target messenger RNAs (mRNAs). One strand of this mature miRNA duplex associates with the RNA-induced silencing complex (RISC), where it interacts with its mRNA target and cleaves it. miRNA control of gene expression is critical for the normal functioning of the mammalian immune system (Xiao and Rajwsky, 2009; Balakrishnan *et al.*, 2013), as well as many other critical biological processes including cell proliferation, differentiation, and normal development (Gomase and Parundekar, 2009). However, the role of miRNAs in host-microbe interactions is still not well understood. Recent studies show that the expression of host miRNAs is modulated in response to microbial colonization of the gut tract (Dalmaso et al., 2011), suggesting a possible role of miRNA in shaping host responses during the symbiont colonization process. In plants, ncRNAs from the fungal pathogen *Botrytis cinerea* hijack the plant interference RNA (RNAi) machinery by binding to Argonaute proteins (AGO), which direct host-gene silencing (Weiberg *et al.*, 2013). miRNAs have also been implicated in the interactions between plants and their associated arbuscular mycorrhizae (Devers *et al.*, 2011). Even more interesting, is the observation that secreted host miRNAs are able to modulate the composition of the gut microbiota composition. Surprisingly, host-secreted miRNAs are not only internalized by bacteria cells, but both regulate bacterial gene expression and affect bacterial growth (Liu et al., 2016; Moloney et al., 2018). Furthermore, miRNAs have been found circulating in different body fluids, protected by macrovesicles or exosomes (Cortez et al., 2011; Sohel, 2016). These circulating RNA molecules may influence cellular mRNA expression in the host if they are taken up into host cells, which could constitute a mechanism by which hosts respond systemically to microbial colonization. Several mechanisms for the uptake, internalization, and regulatory activity of microvesicles and circulating RNA complexes (Cortez et al., 2011; Valadi et al., 2007) have been described (Wang et al., 2012; Zhang et al., 2012). Thus, evidence to date suggests that miRNAs may play important roles in the control of symbiosis; nevertheless, but the extent to which they are critical and the precise underlying mechanisms for their influence, remain unexplored.

The regulatory ncRNAs produced by symbionts follow the same principles as those made by the host, and can be instrumental during all stages of gene expression (Storz et al., 2011). In

bacteria, ncRNA are commonly known as small regulatory RNAs (sRNAs) and they modulate gene expression in various ways. Some sRNAs promote or affect RNA stability, while others directly target translation (Wagner and Romby, 2015). sRNAs can also regulate genes by binding to a small protein that acts as a translational repressor (Repoila and Darfeuille, 2009; Vakulskas et al., 2016). In addition, sRNAs are key elements in bacterial cell physiology, stress responses, and control of pathogenesis (Citartan et al., 2016; Toledo-Arana et al., 2007; Wagner and Romby, 2015).

Pathogenic bacterial sRNAs have the potential not only to regulate bacterial gene expression and physiology, but also to alter the expression profile of infected host cells (Westermann et al., 2016), similar to the ways in which viral RNA can mediate host gene expression (Mehrabadi et al., 2013). For instance, *Mycobacterium marinum* has been found in association with the host RISC complex (Furuse et al., 2014) with concomitant effects on host translation; similarly, the sRNA PinT of *Salmonella enterica*, upon infecting host cells, temporally controls the expression of genes important for production of invasion-associated effector molecules and of virulence genes required for intracellular survival (Westermann et al., 2016). Nevertheless, whether these effects of microbial sRNAs on host gene expression are directed to specific host transcripts or to a global immunogenic response requires further investigation. Recognition by host cells of non-self nucleic acids, then, is not reserved only for viral responses, as bacterial RNA can also activate host innate immune responses (Chiu et al., 2009; Eberle et al., 2009; Lässig and Hopfner, 2017). For example, RNA from intracellular pathogens can activate the type I interferon (IFN) responses through RIG-I signaling (Abdullah et al., 2012; Chiu et al., 2009). Furthermore, while the chemical nature of MAMPs, such as LPS or DNA, remains relatively constant regardless of the bacterium's physiological state, the identity and proportions of sRNA can signal the metabolic condition of living microbes, and by responding to RNA signals hosts can shape their responses accordingly to the viability of the bacteria encountered (Barbet et al., 2018; Sander et al., 2011; Vabret and Blander, 2013). For example, ribosomal RNAs (rRNAs) are a major immunostimulatory component acting on specialized TLRs in immune cells (Eberle et al., 2009; Li and Chen, 2012). In addition, tRNA from the pathogen *Mycobacterium tuberculosis* has been shown to induce production of immune effector IL-12 (Keegan et al., 2019), indicating that evolutionary selection pressure to identify and respond to these RNAs has occurred in host cells.

Extracellular RNA has been extensively studied in the past several years (Akat et al., 2018;

Choi et al., 2017a; Sjöström et al., 2015; Sohel, 2016) and, interestingly, bacteria release RNA into their extracellular environment (Dorward et al., 1989). Furthermore, similar to the ways in which animal hosts package their regulatory RNAs in exosomes (Mittelbrunn et al., 2011; Sohel, 2016), bacteria constantly produce outer membrane vesicles (OMVs) that offer an RNA delivery system that protects their molecular cargo from degradation. sRNA delivered through OMVs from the pathogen *Pseudomonas aeruginosa* to mammalian epithelial cells attenuates the secretion of IL-8 (Koeppen et al., 2016). Similarly, sRNAs derived from periodontal pathogens regulate T-cell cytokine production (Choi et al., 2017b) in mice, and, when delivered via OMVs, down-regulate several cytokines in fibroblasts (Han et al., 2019). As shown in these recent studies on host-pathogen interactions, host sensing of bacterial RNA constitutes an additional mechanism by which a host can modulate its immune responses during infection. Thus, evidence to date suggests that non-coding RNAs may play important roles in host-microbe crosstalk. However, the precise underlying mechanisms for their influence require further investigation.

In summary, in this dissertation I explore the signaling that occurs in symbiosis, both locally within the light organ, and distally in tissues far from the symbionts using the squid-vibrio system as a model, focusing on RNA-mediated host-microbe interactions.

In **Chapter 2**, the transcriptional response of different host tissues to the symbiotic colonization of the light organ is studied. A comparative analysis is presented of the host expression networks under different symbiotic states of the light organ and in two anatomically remote organs: the eye and gill. The impact of symbiosis on the transcriptional responses across both developmental time and within daily rhythms is studied. Finally, I interrogated whether the symbiont luminescence drives changes in gene expression in host organs, both in local (light organ) and remote (eye and gill).

In **Chapter 3**, MAMP signaling via a bacterial sRNA called SsrA is characterized. The differential loading of SsrA into OMVs during growth on different carbon sources is studied, as well as the final localization of the secreted SsrA that has resulted from uptake of OMVs by host cells. Finally, I characterized a comparison of the host transcriptional, morphological, and physiological responses in the presence and absence of bacterial SsrA signaling.

In **Chapter 4**, the post-transcriptional regulation by miRNAs is characterized in the light organ tissue in response to symbiotic colonization. The potential mRNA targets of the miRNA are studied *in silico* and the functional effects of the differential miRNA response to symbiosis are characterized.

References

- Abdullah, Z., Schlee, M., Roth, S., Mraheil, M.A., Barchet, W., Böttcher, J., Hain, T., Geiger, S., Hayakawa, Y., Fritz, J.H., et al. (2012). RIG-I detects infection with live *Listeria* by sensing secreted bacterial nucleic acids. *EMBO J.* *31*, 4153–4164.
- Akat, K.M., Lee, Y.A., Hurley, A., Morozov, P., Max, K.E.A., and Brown, M. (2018). Detection of circulating extracellular mRNAs by modified small RNA-sequencing analysis. *JCI Insight* *4*, e127317.
- Altenbach, D., and Robatzek, S. (2007). Pattern recognition receptors: From the cell surface to intracellular dynamics. *Mol. Plant-Microbe Interact.* *20*, 1031–1039.
- Attar, N. (2016). Microbiome: Good for the gut, good for the brain. *Nat. Rev. Microbiol.* *14*, 269–269.
- Bäckhed, F., Ley, R.E., Sonnenburg, J.L., Peterson, D.A., and Gordon, J.I. (2005). Host-bacterial mutualism in the human intestine. *Science.* *307*, 1915–1920.
- Barbet, G., Sander, L.E., Geswell, M., Leonardi, I., Cerutti, A., and Iliev, I. (2018). Sensing microbial viability through bacterial RNA augments T follicular helper cell and antibody. *Immunity* *48*, 584–598.
- Bauer, K.C., Huus, K.E., and Finlay, B.B. (2016). Microbes and the mind: Emerging hallmarks of the gut microbiota-brain axis. *Cell. Microbiol.* *18*, 632–644.
- Boettcher, K.J., Ruby, E.G., and McFall-Ngai, M.J. (1996). Bioluminescence in the symbiotic squid *Euprymna scolopes* is controlled by a daily biological rhythm. *J. Comp. Physiol. A* *179*, 65–73.
- Bouskra, D., Brézillon, C., Bérard, M., Werts, C., Varona, R., Boneca, I.G., and Eberl, G. (2008). Lymphoid tissue genesis induced by commensals through NOD1 regulates intestinal homeostasis. *Nature* *456*, 507–510.
- Buchon, N., Broderick, N.A., Chakrabarti, S., and Lemaitre, B. (2009). Invasive and indigenous microbiota impact intestinal stem cell activity through multiple pathways in *Drosophila*. *Genes Dev.* *23*, 2333–2344.
- Budden, K.F., Gellatly, S.L., Wood, D.L.A., Cooper, M.A., Morrison, M., Hugenholtz, P., and Hansbro, P.M. (2016). Emerging pathogenic links between microbiota and the gut–lung axis. *Nat. Rev. Microbiol.* *15*, 55–63.

- Chiu, Y.H., MacMillan, J.B., and Chen, Z.J. (2009). RNA polymerase III detects cytosolic DNA and induces type I interferons through the RIG-I pathway. *Cell* 138, 576–591.
- Choi, J., Um, J., Cho, J., and Lee, H. (2017a). Minireview Tiny RNAs and their voyage via extracellular vesicles : Secretion of bacterial small RNA and eukaryotic microRNA. *1*, 1475–1481.
- Choi, J.W., Kim, S.C., Hong, S.H., and Lee, H.J. (2017b). Secretable small RNAs via outer membrane vesicles in periodontal pathogens. *J. Dent. Res.* 96, 458–466.
- Chun, C.K., Scheetz, T.E., Bonaldo, M. de F., Brown, B., Clemens, A., Crookes-Goodson, W.J., Crouch, K., DeMartini, T., Eyestone, M., Goodson, M.S., et al. (2006). An annotated cDNA library of juvenile *Euprymna scolopes* with and without colonization by the symbiont *Vibrio fischeri*. *BMC Genomics* 7, 154.
- Chun, C.K., Troll, J. V., Koroleva, I., Brown, B., Manzella, L., Snir, E., Almabrazi, H., Scheetz, T.E., de Fatima Bonaldo, M., Casavant, T.L., et al. (2008). Effects of colonization, luminescence, and autoinducer on host transcription during development of the squid-vibrio association. *Proc. Natl. Acad. Sci.* 105, 11323–11328.
- Citartan, M., Raabe, C.A., Hoe, C.H., Rozhdestvensky, T.S., and Tang, T.H. (2016). Bacterial sRNAs: Regulation in stress. *Stress Environ. Regul. Gene Expr. Adapt. Bact.* 1, 108–114.
- Coppo, R. (2018). The gut–kidney axis in IgA nephropathy: role of microbiota and diet on genetic predisposition. *Pediatr. Nephrol.* 33, 53–61.
- Cortez, M.A., Bueso-Ramos, C., Ferdin, J., Lopez-Berestein, G., Sood, A.K., and Calin, G.A. (2011). MicroRNAs in body fluids--the mix of hormones and biomarkers. *Nat. Rev. Clin. Oncol.* 8, 467–477.
- Dalmasso, G., Nguyen, H.T.T., Yan, Y., Laroui, H., Charania, M.A., Ayyadurai, S., Sitaraman, S. V., and Merlin, D. (2011). Microbiota modulate host gene expression via MicroRNAs. *PLoS One* 6, e19293.
- Doino, J.A., and McFall-Ngai, M.J. (1995). A transient exposure to symbiosis-competent bacteria induces light organ morphogenesis in the host squid. *Biol. Bull.* 189, 347–355.
- Dorward, D.W., Garon, C.F., and Judd, R.C. (1989). Export and intercellular transfer of DNA via membrane blebs of *Neisseria gonorrhoeae*. *J. Bacteriol.* 171, 2499–2505.
- Douglas, A.E. (2018). Fundamentals of microbiome science: How microbes shape animal biology.
- Dus, M., Lai, J.S.Y., Gunapala, K.M., Min, S., Tayler, T.D., Hergarden, A.C., Geraud, E., Joseph, C.M., and Suh, G.S.B. (2015). Nutrient sensor in the brain directs the action of the brain-gut axis in *Drosophila*. *Neuron* 87, 139–151.
- Eberle, F., Sirin, M., Binder, M., and Dalpke, A.H. (2009). Bacterial RNA is recognized by different sets of immunoreceptors. *7*, 2537–2547.
- Erbs, G., and Newman, M.A. (2012). The role of lipopolysaccharide and peptidoglycan, two glycosylated bacterial microbe-associated molecular patterns (MAMPs), in plant innate immunity. *Mol. Plant*

Pathol. *13*, 95–104.

- Essock-Burns, T., Bongrand, C., Goldman, W.E., Ruby, E.G., and McFall-Ngai, M.J. (2020). Interactions of symbiotic partners drive the development of a complex biogeography in the squid-vibrio symbiosis. *MBio* *11*, 1–18.
- Furuse, Y., Finethy, R., Saka, H.A., Xet-Mull, A.M., Sisk, D.M., Smith, K.L.J., Lee, S., Coers, J., Valdivia, R.H., Tobin, D.M., et al. (2014). Search for MicroRNAs Expressed by intracellular bacterial pathogens in infected mammalian cells. *PLoS One* *9*, e106434.
- Gomase, V.S., and Parundekar, A.N. (2009). microRNA: human disease and development. *Int. J. Bioinform. Res. Appl.* *5*, 479.
- Gürtler, C., and Bowie, A.G. (2013). Innate immune detection of microbial nucleic acids. *Trends Microbiol.* *21*, 413–420.
- Han, E.C., Choi, S.Y., Lee, Y., Park, J.W., Hong, S.H., and Lee, H.J. (2019). Extracellular RNAs in periodontopathogenic outer membrane vesicles promote TNF- α production in human macrophages and cross the blood-brain barrier in mice. *FASEB J.* *33*, 13412–13422.
- Heath-Heckman, E.A.C., Peyer, S.M., Whistler, C.A., Apicella, M.A., Goldman, W.E., and McFall-Ngai, M.J. (2013). Bacterial bioluminescence regulates expression of a host cryptochrome gene in the squid-Vibrio symbiosis. *MBio* *4*, e00167-13.
- Heath-Heckman, E.A.C., Foster, J., Apicella, M.A., Goldman, W.E., and McFall-Ngai, M. (2016). Environmental cues and symbiont microbe-associated molecular patterns function in concert to drive the daily remodelling of the crypt-cell brush border of the *Euprymna scolopes* light organ. *Cell. Microbiol.* *18*, 1642–1652.
- Kamada, N., Seo, S.-U., Chen, G.Y., and Núñez, G. (2013). Role of the gut microbiota in immunity and inflammatory disease. *Nat. Rev. Immunol.* *13*, 321–335.
- Kamo, T., Akazawa, H., Suzuki, J.I., and Komuro, I. (2017). Novel concept of a heart-gut axis in the pathophysiology of heart failure. *Korean Circ. J.* *47*, 663–669.
- Keegan, C., Krutzik, S., Schenk, M., Scumpia, O., Lu, J., Ling, Y., Pang, J., Brandon, S., Lim, K.S., Shell, S., et al. (2019). Mycobacterium tuberculosis transfer RNA induces IL-12p70 via synergistic activation of pattern recognition receptors within a cell network. *J. Immunol.* *200*, 3244–3258.
- Koepfen, K., Hampton, T.H., Jarek, M., Scharfe, M., Gerber, S.A., Mielcarz, D.W., Demers, E.G., Dolben, E.L., Hammond, J.H., Hogan, D.A., et al. (2016). A novel mechanism of host-pathogen interaction through sRNA in bacterial outer membrane vesicles. *PLoS Pathog.* *12*, 1–22.
- Konturek, P.C., Brzozowski, T., and Konturek, S.J. (2011). Gut clock: implication of circadian rhythms in the gastrointestinal tract. *J. Physiol. Pharmacol.* *62*, 139–150.
- Koropatnick, T.A. (2004). Microbial factor-mediated development in a host-bacterial mutualism. *Science.* *306*, 1186–1188.

- Koropatnick, T.A., Engle, J.T., Apicella, M.A., Stabb, E. V, Goldman, W.E., and McFall-Ngai, M.J. (2004). Microbial factor-mediated development in a host-bacterial mutualism. *Science*. *306*, 1186–1188.
- Kremer, N., Philipp, E.E.R., Carpentier, M.C., Brennan, C.A., Kraemer, L., Altura, M.A., Augustin, R., H??sler, R., Heath-Heckman, E.A.C., Peyer, S.M., et al. (2013). Initial symbiont contact orchestrates host-organ-wide transcriptional changes that prime tissue colonization. *Cell Host Microbe* *14*, 183–194.
- Kremer, N., Koch, E.J., Filali, A.E., Zhou, L., Heath-Heckman, E.A.C., Ruby, E.G., and Mcfall-ngai, M.J. (2018). Persistent interactions with bacterial symbionts direct mature-host cell morphology and gene expression in the squid. *MSystems* *3*, 1–17.
- Lässig, C., and Hopfner, K.P. (2017). Discrimination of cytosolic self and non-self RNA by RIG-I-like receptors. *J. Biol. Chem.* *292*, 9000–9009.
- Lee, K.H., and Ruby, E.G. (1994). Effect of the squid host on the abundance and distribution of symbiotic *Vibrio fischeri* in nature. *Appl. Environ. Microbiol.* *60*, 1565–1571.
- Leone, V., Gibbons, S.M., Martinez, K., Hutchison, A.L., Huang, E.Y., Cham, C.M., Pierre, J.F., Heneghan, A.F., Nadimpalli, A., Hubert, N., et al. (2015). Effects of diurnal variation of gut microbes and high-fat feeding on host circadian clock function and metabolism. *Cell Host Microbe* *17*, 681–689.
- Li, X.D., and Chen, Z.J. (2012). Sequence specific detection of bacterial 23S ribosomal RNA by TLR13. *Elife* *2012*, 1–14.
- Liu, S., Pires, A., Rezende, R.M., Comstock, L.E., Gandhi, R., Weiner, H.L., Liu, S., Pires, A., Rezende, R.M., Cialic, R., et al. (2016). The host shapes the gut microbiota via fecal article the host shapes the gut microbiota via fecal microRNA. *Cell Host Microbe* *19*, 32–43.
- McFall-Ngai, M., and Montgomery, M.K. (1990). The Anatomy and Morphology of the Adult Bacterial Light Organ of *Euprymna scolopes* Berry (Cephalopoda: *Sepiolidae*). *Biol. Bull.* *179*, 332–339.
- McFall-Ngai, M., Nyholm, S. V., and Castillo, M.G. (2010). The role of the immune system in the initiation and persistence of the *Euprymna scolopes-Vibrio fischeri* symbiosis. *Semin. Immunol.* *22*, 48–53.
- McFall-Ngai, M., Hadfield, M.G., Bosch, T.C.G., Carey, H. V., Domazet-Lošo, T., Douglas, A.E., Dubilier, N., Eberl, G., Fukami, T., Gilbert, S.F., et al. (2013). Animals in a bacterial world, a new imperative for the life sciences. *Proc. Natl. Acad. Sci.* *110*, 3229–3236.
- Mehrabadi, M., Hussain, M., and Asgari, S. (2013). MicroRNAome of *Spodoptera frugiperda* cells (Sf9) and its alteration following baculovirus infection. *J. Gen. Virol.* *94*, 1385–1397.
- Michalak, P. (2006). RNA world ? the dark matter of evolutionary genomics. *J. Evol. Biol.* *19*, 1768–1774.
- Mittelbrunn, M., Gutiérrez-Vázquez, C., Villarroya-Beltri, C., González, S., Sánchez-Cabo, F., González, M.Á., Bernad, A., and Sánchez-Madrid, F. (2011). Unidirectional transfer of microRNA-loaded exosomes from T cells to antigen-presenting cells. *Nat. Commun.* *2*.
- Moloney, G.M., Viola, M.F., Hoban, A.E., Dinan, T.G., and Cryan, J.F. (2018). Faecal microRNAs:

- indicators of imbalance at the host-microbe interface? *Benef. Microbes* 9, 175–183.
- Montgomery, M.K., and McFall-Ngai, M.J. (1995). The inductive role of bacterial symbionts in the morphogenesis of a squid light organ. *35*, 372–380.
- Montgomery, M.K., and McFall-Ngai, M.J. (1998). Late postembryonic development of the symbiotic light organ of *Euprymna scolopes* (Cephalopoda: Sepiolidae). *Biol. Bull.* 195, 326–336.
- Moriano-Gutierrez, S., Koch, E.J., Bussan, H., Romano, K., Belcaid, M., and Rey, F.E. (2019). Critical symbiont signals drive both local and systemic changes in diel and developmental host gene expression. *Proc. Natl. Acad. Sci.* 116, 7990–7999.
- Murphy, D., Dancis, B., and Brown, J.R. (2008). The evolution of core proteins involved in microRNA biogenesis. *BMC Evol. Biol.* 8, 1–18.
- Nürnberg, T., Brunner, F., Kemmerling, B., and Piater, L. (2004). Innate immunity in plants and animals: Striking similarities and obvious differences. *Immunol. Rev.* 198, 249–266.
- Palm, N.W., and Medzhitov, R. (2009). Pattern recognition receptors and control of adaptive immunity. *Immunol. Rev.* 227, 221–233.
- Rakoff-Nahoum, S., Paglino, J., Eslami-Varzaneh, F., Edberg, S., and Medzhitov, R. (2004). Recognition of commensal microflora by toll-like receptors is required for intestinal homeostasis. *Cell* 118, 229–241.
- Repoila, F., and Darfeuille, F. (2009). Small regulatory non-coding RNAs in bacteria: physiology and mechanistic aspects. *Biol. Cell* 101, 117–131.
- Round, J.L., Lee, S.M., Li, J., Tran, G., Jabri, B., Chatila, T.A., and Mazmanian, S.K. (2011). The toll-like receptor 2 pathway establishes colonization by a commensal of the human microbiota. *Science*. 332, 974–977.
- Rowan, S., Jiang, S., Korem, T., Szymanski, J., Chang, M.-L., Szelog, J., Cassalman, C., Dasuri, K., McGuire, C., Nagai, R., et al. (2017). Involvement of a gut–retina axis in protection against dietary glycemia-induced age-related macular degeneration. *Proc. Natl. Acad. Sci.* 114, E4472–E4481.
- Samuelson, D.R., Welsh, D.A., and Shellito, J.E. (2015). Regulation of lung immunity and host defense by the intestinal microbiota. *Front. Microbiol.* 6, 1–14.
- Sander, L.E., Davis, M.J., Boekschoten, M. V, Amsen, D., Dascher, C.C., Ryffel, B., Swanson, J.A., Muller, M., and Blander, J.M. (2011). Detection of prokaryotic mRNA signifies microbial viability and promotes immunity. *Nature* 474, 385–389.
- Schneider, K.M., Albers, S., and Trautwein, C. (2018). Role of bile acids in the gut-liver axis. *J. Hepatol.*
- Schroeder, B.O., and Bäckhed, F. (2016). Signals from the gut microbiota to distant organs in physiology and disease. *Nat. Med.* 22, 1079–1089.
- Schwartzman, J.A., Koch, E., Heath-Heckman, E.A.C., Zhou, L., Kremer, N., McFall-Ngai, M.J., and

- Ruby, E.G. (2015). The chemistry of negotiation: Rhythmic, glycan-driven acidification in a symbiotic conversation. *Proc. Natl. Acad. Sci.* *112*, 566–571.
- Sellge, G., and Kufer, T.A. (2015). PRR-signaling pathways: Learning from microbial tactics. *Semin. Immunol.* *27*, 75–84.
- Serino, M., Blasco-baque, V., and Nicolas, S. (2014). Far from the eyes , close to the heart : Dysbiosis of gut microbiota and cardiovascular consequences. *Current cardiology reports*, *16*, 540.
- Sjöström, A.E., Sandblad, L., Uhlin, B.E., and Wai, S.N. (2015). Membrane vesicle-mediated release of bacterial RNA. *Nat. Publ. Gr.* 1–10.
- Sohel, M.H. (2016). Extracellular/Circulating MicroRNAs: Release Mechanisms, Functions and Challenges. *Achiev. Life Sci.* *10*, 175–186.
- Sommer, F., and Bäckhed, F. (2013). The gut microbiota-masters of host development and physiology. *Nat. Rev. Microbiol.* *11*, 227–238.
- Spiljar, M., Merkle, D., and Trajkovski, M. (2017). The Immune System Bridges the Gut Microbiota with Systemic Energy Homeostasis: Focus on TLRs, Mucosal Barrier, and SCFAs. *Front. Immunol.* *8*, 1–10.
- Stabb, E. V., and Millikan, D.S. (2009). Is the *Vibrio fischeri-Euprymna scolopes* symbiosis a defensive mutualism? *Defensive mutualism in microbial symbiosis* (CRC Press).
- Storz, G., Vogel, J., and Wassarman, K.M. (2011). Regulation by Small RNAs in Bacteria: Expanding Frontiers. *Mol. Cell* *43*, 880–891.
- Sycuro, L.K., Ruby, E.G., and McFall-Ngai, M. (2006). Confocal microscopy of the light organ crypts in juvenile *Euprymna scolopes* reveals their morphological complexity and dynamic function in symbiosis. *J. Morphol.* *267*, 555–568.
- Tahara, Y., Yamazaki, M., Sukigara, H., Motohashi, H., Sasaki, H., Miyakawa, H., Haraguchi, A., Ikeda, Y., Fukuda, S., and Shibata, S. (2018). Gut microbiota-derived short chain fatty acids induce circadian clock entrainment in mouse peripheral tissue. *Sci. Rep.* *8*, 1–12.
- Thaiss, C.A., Levy, M., Korem, T., Dohnalová, L., Shapiro, H., Jaitin, D.A., David, E., Winter, D.R., Gury-BenAri, M., Tirovsky, E., et al. (2016). Microbiota diurnal rhythmicity programs host transcriptome oscillations. *Cell* *167*, 1495-1510.e12.
- Thaiss, C.A., Nobs, S.P., and Elinav, E. (2017). Previews NFIL-trating the host circadian rhythm-microbes fine-tune the epithelial clock. *Cell Metab.* *26*, 699–700.
- Toledo-Arana, A., Repoila, F., and Cossart, P. (2007). Small noncoding RNAs controlling pathogenesis. *Curr. Opin. Microbiol.* *10*, 182–188.
- Vabret, N., and Blander, J.M. (2013). Sensing microbial RNA in the cytosol. *Frontiers in immunology*, *4*, 468.

- Vakulskas, C.A., Leng, Y., Abe, H., Amaki, T., Okayama, A., Babitzke, P., Suzuki, K., and Romeo, T. (2016). Antagonistic control of the turnover pathway for the global regulatory sRNA CsrB by the CsrA and CsrD proteins. *Nucleic Acids Res.* *44*, 7896–7910.
- Valadi, H., Ekström, K., Bossios, A., Sjöstrand, M., Lee, J.J., and Lötvall, J.O. (2007). Exosome-mediated transfer of mRNAs and microRNAs is a novel mechanism of genetic exchange between cells. *Nat. Cell Biol.* *9*, 654–659.
- Wagner, E.G.H., and Romby, P. (2015). Chapter three. Small RNAs in Bacteria and Archaea: Who they are, what they do, and how they do it. *Advances in Genetics*, pp. 133–208.
- Wang, K., Li, H., Yuan, Y., Etheridge, A., Zhou, Y., Huang, D., Wilmes, P., and Galas, D. (2012). The complex exogenous RNA spectra in human plasma: an interface with human gut biota? *PLoS One* *7*, e51009.
- Westermann, A.J., Förstner, K.U., Amman, F., Barquist, L., Chao, Y., Schulte, L.N., Müller, L., Reinhardt, R., Stadler, P.F., and Vogel, J. (2016). Dual RNA-seq unveils noncoding RNA functions in host–pathogen interactions. *Nature* *529*, 496–501.
- Wier, A.M., Nyholm, S. V, Mandel, M.J., Massengo-Tiassé, R.P., Schaefer, A.L., Koroleva, I., Splinter-Bondurant, S., Brown, B., Manzella, L., Snir, E., et al. (2010). Transcriptional patterns in both host and bacterium underlie a daily rhythm of anatomical and metabolic change in a beneficial symbiosis. *Proc. Natl. Acad. Sci.* *107*, 2259–2264.
- Yip, L.Y., Aw, C.C., Lee, S.H., Hong, Y.S., Ku, H.C., Xu, W.H., Chan, J.M.X., Cheong, E.J.Y., Chng, K.R., Ng, A.H.Q., et al. (2018). The liver–gut microbiota axis modulates hepatotoxicity of tacrine in the rat. *Hepatology* *67*, 282–295.
- Zhang, L., Hou, D., Chen, X., Li, D., Zhu, L., Zhang, Y., Li, J., Bian, Z., Liang, X., Cai, X., et al. (2012). Exogenous plant MIR168a specifically targets mammalian LDLRAP1: evidence of cross-kingdom regulation by microRNA. *Cell Res.* *22*, 107–126.
- Zhong, M., Yan, H., and Li, Y. (2017). Flagellin: A unique microbe-associated molecular pattern and a multi-faceted immunomodulator. *Cell. Mol. Immunol.* *14*, 862–864.

CHAPTER 2

Critical symbiont signals drive both local and systemic changes in diel and developmental host gene expression

Published in PNAS, March 2019.

Silvia Moriano-Gutierrez^{a,b,c}, Eric J. Koch^{a,c}, Hailey Bussan^{c,1}, Kymberleigh Romano^{d,2}, Mahdi Belcaid^a, Federico E. Rey^d, Edward Ruby^{a,c}, and Margaret McFall-Ngai^{a,c,3}

^aPacific Biosciences Research Center, and ^bDepartment of Molecular Biosciences and Bioengineering, University of Hawai'i at Mānoa, Honolulu, HI 96822; ^cDepartment of Medical Microbiology and Immunology, and ^dDepartment of Bacteriology, University of Wisconsin-Madison, WI 53706

Short title: Symbiosis impact on host organ transcriptomes

Keywords: squid-vibrio, symbiosis, development, daily rhythm, bioluminescence

Author contributions: S.M.-G., F.E.R., E.G.R., and M.M.-N. designed research; S.M.-G., E.J.K., H.B., and K.R. performed research; S.M.-G. and M.B. analyzed data; S.M.-G., E.G.R., and M.M.-N. wrote the paper.

The authors declare no conflict of interests.

This article is a PNAS Contributed Submission

Data deposition: The sequences reported in this paper have been deposited in the GenBank database (BioProject accession nos. PRJNA473394, PRJNA498343, and PRJNA498345).

¹Present address: University of Wisconsin-Madison, School of Medicine and Public Health, Madison, WI 53706

²Present address: Department of Cellular and Molecular Medicine, Lerner Research Institute, Cleveland Clinic, Cleveland, OH 44106

³To whom correspondence should be addressed. Email: mcfallng@hawaii.edu

Abstract

The colonization of an animal's tissues by its microbial partners creates networks of communication across the host's body. We used the natural binary light-organ symbiosis between the squid *Euprymna scolopes* and its luminous bacterial partner, *Vibrio fischeri*, to define the impact of colonization on transcriptomic networks in the host. A night-active predator, *E. scolopes* coordinates the bioluminescence of its symbiont with visual cues from the environment to camouflage against moon and starlight. Like mammals, this symbiosis has a complex developmental program and a strong day-night rhythm. We determined how symbiont colonization impacted gene expression in the light organ itself, as well as in two anatomically remote organs: the eye and gill. While the overall transcriptional signature of light organ and gill were more alike, the impact of symbiosis was most pronounced and similar in light organ and eye, both in juvenile and adult animals. Further, the presence of a symbiosis drove daily rhythms of transcription within all three organs. Finally, a single mutation in *V. fischeri*, specifically, deletion of the *lux* operon, which abrogates symbiont luminescence, reduced the symbiosis-dependent transcriptome of the light organ by two-thirds. In addition, while the gills responded similarly to light-organ colonization by either the wild type or mutant, luminescence was required for all of the colonization-associated transcriptional responses in the juvenile eye. This study defines not only the impact of symbiont colonization on the coordination of animal transcriptomes, but also provides insight into how such changes might impact the behavior and ecology of the host.

Significance

Biologists now recognize that animal microbiomes have strong impacts not only on the organs with which they associate, but also anatomically remote tissues; however, the precise triggers underlying these impacts remain unknown. Here, using the squid-vibrio light-organ association, which affords unparalleled resolution of a natural binary partnership, we report both near-field (light organ) and far-field (eye and gill) symbiont-driven effects on host gene expression. Colonization by the symbiont results in unique transcriptional signatures for each organ. Further, distinct organ-specific patterns arise over the day-night cycle, and across the host's developmental trajectory. Most strikingly, the loss of a single genetic locus in the symbiont, that encoding bioluminescence, triggers a dominant and biologically relevant change of gene expression across the host's body.

Introduction

Recent studies of animal and plant microbiomes have demonstrated that they can have far reaching effects, influencing both the internal and external environments of the host (1, 2). For example, the human microbiota impacts both tissues with which it directly interacts and more remote tissues of the body (3), as well as the built and natural environment in which the human host resides (4, 5). These complex microbial networks profoundly influence host development, from embryogenesis through senescence, while maintaining physiological homeostasis along this trajectory (2).

The best-studied nexus of these complex interactions is the mammalian gut microbiota (6), which affects not only the gut tissues themselves, but also the immune system (7), brain (8), liver (9), heart (10, 11), kidney (12), lung (13, 14), and eye (15-17). The microbiota also helps coordinate the activities of these tissues and organs; e.g., the strong association of the gut microbiota with the control of host circadian rhythms (18, 19). Further, axes of influence between the gut and other organs have revealed that dysbiosis of the microbiota is a critical driver of seeming unrelated diseases (3).

Thus far, the mechanisms underlying these wide-ranging effects remain poorly studied. The integration of the gut microbiota into host biology is reflected in the transcriptomic regulation of genes in tissues both in direct contact with (20-22) and distant from (23, 24) the microbial assemblage. Available data suggest that the metabolomes of the blood, sweat and urine carry products of the gut microbiota, such as short-chain fatty acids (SCFA) and microbe-associated molecular patterns (MAMPs) (25, 26), to which these remote tissues respond. The complexity of the mammalian gut microbiota, however, renders it difficult to investigate the impact of a particular microbe on host biology under natural conditions, because the responses of adjacent and remote host tissues are the result of the cumulative effects of microbe-microbe and host-microbe interactions with 100s-1000s of microbial phylotypes. In contrast, here we use the binary light-organ symbiosis between the Hawaiian bobtail squid, *Euprymna scolopes*, and its luminous bacterial partner, *Vibrio fischeri* (27, 28), to define the impact of a single symbiotic partner on the transcriptomic responses of host tissues, both those housing the symbiont population and those remote from the symbionts.

The squid host acquires its symbiont each generation from the surrounding environment and, similar to the mammalian gut microbiota, the bacteria reside extracellularly along the apical

surfaces of epithelium-lined crypts (29). Also analogous to the mammalian gut microbiota, the squid-vibrio symbiosis undergoes significant development and maturation. Within hours following initial colonization of the juvenile animal, the symbionts trigger the regression of superficial ciliated fields of cells that promote light-organ inoculation (28). The symbionts also induce development of the crypt cells with which they directly associate throughout the animal's life, notably an increase in microvillar density and a swelling of the cells lining the crypts (Fig. 1A). A dark mutant derivative of *V. fischeri* ($\square lux$), defective in light production, the principal 'currency' of the symbiosis, is also defective in the induction of this latter hallmark event of early light-organ development (30-32).

Development of the light organ also involves the onset of diel cycles. Beginning during the first day of colonization, and thereafter, ~90% of the symbiont population is vented each day at dawn into the surrounding environment (33). Further, in response to luminous (but not $\square lux$) symbionts, the organ's cryptochrome-encoding clock gene, *escry1*, begins a day-night cycling, and the host concomitantly imposes a cycling of the symbiont's luminescence levels, which peak in the hours of the early evening (1900-2000 h), when the nocturnal squid host begins to forage. Then, after 3-4 weeks of colonization, the symbiosis undergoes a final maturation, with the onset of a strong daily rhythm of metabolic processes (34, 35), not unlike the circadian rhythms of metabolism described in the mammalian gut symbioses (18, 36). Specifically, the animal becomes fully nocturnal, and the symbiont metabolism begins a day-night fluctuation between respiration and fermentation in response to a change in nutrients provided by the host.

Here we compared the transcriptomes of three highly vascularized organs of the squid host: the light organ itself, and the eye and gill, manipulating both their symbiotic state and the genetics of the bacterial partner, in both juvenile and adult animals, and over the day-night cycle (Fig. 1A). The eye was chosen because, like the symbiotic organ, it is a light-sensing organ, and shows convergence in morphology, biochemistry (37), molecular biology (38, 39) and developmental pathways (40). As an immune organ, the gill, like the light organ, responds to bacterial colonization (41). Here, we present evidence that both light organ colonization and luminescence influence gene regulation of not only symbiotic tissue, but also host organs remote from the symbionts.

Results

De Novo Transcriptome Assembly, Annotation and Validation Provide the Resources for Analyses of Symbiosis Effects on Host Gene Expression.

To determine the extent to which symbiotic colonization impacts host gene expression, we sequenced transcripts isolated from the squid light organ, eye and gill (Fig. 1A&B). Samples were collected for RNA-Seq analysis from both juvenile (24 h post-hatch) and mature adult (5 month-old) animals, under two colonization states: symbiont-free (i.e., aposymbiotic, or APO) or colonized by the wild-type *V. fischeri* light-organ isolate ES114 (i.e., symbiotic, or SYM). An additional condition that was analyzed in juvenile animals was colonization by an isogenic, non-luminous ($\square lux$) mutant of ES114 (i.e., SYM-dark) (42) (see *SI Results* for details). The 2.2 billion paired-end reads obtained by Illumina sequencing, were de novo assembled to create a reference transcriptome (*SI Appendix*, Fig. S1 and Dataset S1). The large number of assembled transcripts is a common trait found in other *de novo* assembled transcriptomes of *E. scolopes* (43, 44). Cephalopods are known to expand certain gene families (45, 46). This feature, together with the high levels of heterozygosity and transcript editing (47) that are known to challenge assembly software (48), contributed to the high number of observed expressed transcripts. Transcriptomic profiles clustered by tissue type and, within each tissue type, by developmental stage, with a higher degree of variation among juvenile replicates (Fig. 1C and *SI Appendix*, Fig. S2). Irrespective of developmental stage, eye-derived samples showed the most divergent transcriptional profile. The light organ and gill displayed a more highly correlated expression pattern (Fig. 1C and *SI Appendix*, Fig. S2A), and shared more total expressed genes than either did with the eye (Fig. 1D), perhaps because they are both predominantly composed of epithelial tissue.

When considering the total number of genes that are expressed in each organ, depending on the host developmental stage and symbiotic state (*SI Appendix*, Fig. S3A), on average juvenile samples expressed 20% more detectable genes than their adult counterparts. Only 7,464 genes were expressed in all three organs, from both juveniles and adults, and in both the SYM and APO state (*SI Appendix*, Fig. S3B), suggesting that these genes encode core or ‘housekeeping’ functions (for more details of transcriptomic patterns, see Dataset S2). In contrast, when we determined tissue-specific genes, i.e., those that were expressed at least 8-fold higher in one organ relative to the other two, a total of 5,587 genes were identified (*SI Appendix*, Fig. S2E and Dataset S2). Not surprisingly, GO terms enriched for the eye were related to visual perception or synaptic signaling,

while for the gill were linked to gas exchange or pH regulation; similarly, the light organ was enriched in GO terms related to the expected activities of oxidative stress (49, 50) and chitin-associated processes (51) (*SI Appendix*, Fig. S2B-D and Dataset S3). Further, we validated the RNA-Seq data set by two methods, RT-qPCR, and the NanoString nCounter XT platform (*SI Appendix*, Fig. S4 and Dataset S4), which all had a high degree of congruity. These results provide strong evidence that the transcriptional patterns in response to colonization are robust, and clearly differentiate the three tissue types and their developmental states.

Adult Gene Expression in the Light Organ and Remote Tissues Responded Uniquely to Symbiont Colonization.

To identify whether and how the light organ, eye, and gill responded to colonization of the light organ, we compared the gene-expression patterns of these three organs when sampled from adult APO and SYM squid (Fig. 1A). According to the values for the differentially expressed transcripts, the samples clustered by condition (APO or SYM) within each organ (Fig. 2A). Transcripts having expression levels that differed significantly between APO and SYM were identified as up- or down-regulated by symbiosis (Fig. 2B). Unsurprisingly, the light organ, which harbors the symbionts, had the strongest transcriptional response to its colonization, with a total of 206 genes significantly differentially regulated, which clustered into 5 distinct expression profiles (Fig. 2 and *SI Appendix*, Fig. S5). Although they are in anatomically remote organs (Fig. 1B), the transcriptomes of both eye and gill also responded to colonization of the light organ. Because of the greater similarity between the number of total transcripts in light organ and gill (Fig. 1C&D and *SI Appendix*, Fig. S2A), and because both these organs respond to bacteria as part of their normal function, we anticipated that, compared to the eye, more symbiotically responsive genes would be detected in the gill, and they would overlap more significantly with the light organ. However, the eye had twice as many symbiotically regulated genes as the gill (84 vs. 42) (Fig. 2B and *SI Appendix*, Fig. S5 and Dataset S5). Furthermore, each organ had a distinctive transcriptional response to light-organ colonization: only one gene (annotated as ‘angiotensin-converting enzyme’ or ACE) was up-regulated in two of the organs (eye and gill).

To further analyze not only the possible functions of these symbiosis-responsive genes, but also whether there were shared functions (if not genes) among the three organs, we conducted a GO-enrichment analysis for all the differentially expressed genes. This analysis identified over-

represented terms in each organ, using the entire transcriptome as the background for the enrichment analysis. In APO animals, we found 40, 32 and 29 over-represented functions in eye, gill and light organ, respectively. In contrast, over-represented functions in response to symbiosis were highest in the light organ, followed by gill and eye (Dataset S6). In addition, each of the three organs expressed genes within a unique set of top 10 enriched biological processes, in a symbiosis-dependent manner (Fig. 2C), a further indication of the distinct ways in which they react to the presence of bacteria in the light organ. For example, in the light organ itself, the three major responses to symbiosis, encompassing 9 of the 20 enriched biological functions (Fig. 2C), could be associated with: (i) vascularization and an increased oxygen demand driven by the symbiont's bioluminescence; (ii) tissue stress from the presence of the symbionts; and, (iii) an easing of innate immune responses once the organ is colonized. All of these functions are consistent with previous studies (40, 52, 53). In contrast, in the eye, light-organ colonization resulted in an up-regulation of genes encoding structural proteins, and down-regulation of genes encoding elements of sensory perception and oxidative stress, while the gill exhibited an increased expression of genes encoding stress responses and transcriptional regulation.

Because a robust systemic response to colonization was observed that included functions associated with light-perception in the squid eye (Fig. 2C), an organ convergent in form and function with the mammalian eye (39), we asked whether and how eyes of another well-studied symbiosis model, the mouse, respond to host colonization; to our knowledge, the impact of the gut microbiota on the transcriptomic profile of the mouse eye has not been reported. We compared, by RNA-Seq, the expression profile of the eye of conventionalized mice, i.e., mice in which the gut microbiota was present, to that of germ-free mice. Adult mice and squid were compared to diminish any effect of their different developmental trajectories. Applying the same level of stringency as used for the squid eye (i.e., an adjusted p-value < 0.05) only 5 genes were detected as differentially expressed in the mouse eye in response to conventionalization (Dataset S7). One 'predicted gene' was down-regulated, and 4 genes were up-regulated, including lactotransferrin, which was previously reported as present in the transcriptome of mouse eye (54), interferon-activated gene 205, a mitochondrial tRNA, and a non-coding RNA of the RIKEN family. Although the evolutionarily convergent eyes of cephalopods and vertebrates share a large number of conserved genes with similar expression levels (55, 56), we detected no shared symbiosis-regulated genes in the eyes of these two organisms.

In summary, in the mature squid symbiosis: (i) functionally distinct and anatomically distant tissues are influenced by the presence of symbiotic bacteria; (ii) unlike the total expression profile for each of the three organs, the transcriptional responses to symbiosis, and their functional annotations, were specific and non-overlapping (Fig. 1D and Fig. 2B); and, (iii) although the evolutionarily convergent eyes of cephalopods and vertebrates share a large number of conserved genes with similar expression levels (55, 56), no shared gene regulation was detected within eyes of squid and mouse in response to microbial colonization of distant tissues.

Colonization of Juvenile Hosts had a Rapid Impact on Gene Expression, Even in Remote Tissues.

In the adult host, transcriptional responses to symbiosis are evident both locally and systemically (Figs. 2 and 3), but how quickly during symbiotic development does this outcome appear? The transcriptional response of the light organ has been reported to occur as early as 3 h following exposure to environmental *V. fischeri* (52). To determine the manner and timing of symbiosis-specific responses in other organs, more distant from the light-organ symbionts, we compared the RNA-Seq gene expression data of light organ, eye, and gill, 24 h after the initiation of symbiosis, when the bacteria have fully colonized and are brightly luminous (28). At this point, we found that the light organ already exhibits a distinct transcriptional response; specifically, when comparing APO and SYM conditions, a total of 1919 differentially regulated genes was detected, including 17% of the 206 genes characteristic of the adult SYM light-organ response (Fig. 2B). Analysis of this overlapping set of 36 genes revealed that ~40% are associated with osmoregulatory and immune functions (Dataset S8 and S9). Subclusters 3 and 4 of light-organ differential gene expression comprise highly up-regulated genes in only two out of the three analyzed SYM light organs (*SI Appendix*, Fig. S6), indicating a response whose onset is either variable or transitory. Interestingly, these two subclusters contained genes related to light perception, with significantly enriched functions such as “structural components of the lens”, “visual perception” or “phototransduction” (*SI Appendix*, Dataset S9), perhaps reflecting the development of the light organ’s capacity to perceive light (39).

As expected, a smaller number of symbiosis-responsive genes (44 in the eye and 184 in the gill) were detected (*SI Appendix*, Figs. S6 and S7), and there was essentially no overlap with the adult response in either of these organs. Nevertheless, a trend in which eye (but not gill) genes

clustered with colonization state was detected (*SI Appendix*, Fig. S7). Unlike the light organ, the responses of eye and gill at 24 h were highly variable between samples; thus, we hypothesized that many genes that were differentially regulated in these organs in adults may have not yet become apparent in 24-h juveniles (*SI Appendix*, Fig. S8A). Thus, we used the NanoString platform to determine whether the patterns of a selected set of 23 genes that were not significantly regulated at 24 h (Dataset S4), but were either trending toward induction at 24 h or would become induced in adult eye and gill, had, by 72 h, become significantly differentially regulated by symbiosis. While such a temporal comparison can be made with juvenile eye or gill tissues, changes in the light organ transcriptome are confounded by this organ's substantial morphogenic transformation between 24 and 72 h (28).

Of the 13 selected adult eye-specific, symbiosis-responsive genes, 4 became clearly differentially regulated in juvenile eye tissue between 24 and 72 h post-colonization (e.g., *SI Appendix*, Figs. S8A' and S9), indicating that during this period much of the transcriptional signature of the adult eye was still developing. For the gill, we chose two groups of genes: 6 that were significantly up-regulated in adults, and 4 that were not, but were trending toward significance in 24-h juveniles. Of the first group, only one (ACE) had become differentially regulated by 72 h, while all 4 of the 24-h trending genes had. Thus, the data suggest that the gill has a more juvenile-specific response that is not retained in adults. In summary, the analysis of juvenile organs indicates that: (i) a robust transcriptional response to symbiosis appeared in the light organ within 24 h post-colonization, (ii) a smaller systemic response by eye and gill also became apparent, and (iii) by 24 h, the juvenile eye began to show an adult-like response, which became more significant at 72 h.

Expression of Some Symbiosis-Responsive Genes was Regulated over the Day/Night Cycle.

Because the light organ has a well-described daily rhythm of transcriptional regulation (35) that is reflected in crypt-cell ultrastructural remodeling, symbiont luminescence, and metabolic activity in both partners (34, 35), we asked whether the symbiosis-regulated gene expression detected in remote organs also changed over the day (Fig. 1A). Based on the NanoString data for 72 h juveniles at 2000 h (*SI Appendix*, Fig. S9), we characterized symbiosis-responsive gene expression from juvenile organs by RT-qPCR at three times: two hours before dusk (1600 h, at ~70 h post-colonization) and two hours before dawn (0400 h), both times when the host is

quiescent and symbiont luminescence is reduced, as compared to two hours after dusk (2000 h, at ~74 h post-colonization) (Fig. 1A), when the host is active and the symbionts are brightly luminous (34).

Expression levels of three genes (atrial natriuretic peptide-converting enzyme [ANP-CE], ACE, and galaxin 1 [Gal1]) were determined across all of the organs. In the light organ, while ACE was not significantly regulated by symbiosis, ANP-CE and Gal1 remained up-regulated in SYM relative to APO at all times tested (Fig. 3A). In contrast, Gal1 and ACE were up-regulated by symbiosis in the eye only at 2000 h although, in gill, ACE was up at both 2000 and 0400 h (Fig. 3BC). Thus, ANP-CE is specifically regulated in the light organ, as is ACE regulated only in the eye and gill.

Expression of an additional 4 eye-specific and 2 gill-specific genes that were symbiosis-regulated at 2000 h were likewise dependent on time of day. While there are trends of down-regulation of these genes in the eye at 1600 h, no significant differences appeared beyond 2000 h (Fig. 3B). Similarly, in gill, opsin is up-regulated at 2000 relative to 1600 h, while reflectin 2d becomes down-regulated (relative to APO) at 0400 h (Fig. 3C). Cephalopods are noted for extraocular photoreceptors (57), but these structures are associated with the surface of the animal, and not with internal organs, such as the gills (58).

In summary, symbiosis-responsive genes that were regulated in one organ at one time of day, can be differentially expressed in other organs at a different time, emphasizing the time- and context-dependency of the response. In addition, among the genes examined here, the symbiosis-dependent up-regulation of expression in gill, and especially in eye, was generally most prominent early in the evening (2000 h), when the host is ecologically active. In contrast, in the light organ, no pattern was observed for these genes (Fig. 3A), although other genes show strong patterns of temporal regulation (35).

Symbiont Luminescence was the Principal Driver of Transcriptomic Patterns in both the Light Organ and the Eye.

Because symbiosis-induced up-regulation of gene expression occurred at night, coincident with high levels of symbiont luminescence, we asked whether light-emission itself is a factor driving gene expression. To this end, the gene-expression profiles of the juvenile light organ, eye and gill were compared when the light organ was colonized by either a wild-type, light-producing

strain (SYM), or a non-luminous Δlux mutant derivative (SYM-dark). Because such dark mutants can only maintain normal levels of colonization for the first day post-inoculation (32), we focused our analyses on 24 h after symbiosis had initiated.

At this time, under normal conditions of SYM colonization, 1919 genes are regulated in the light organ compared to APO (Fig. 4A). Comparison of the SYM expression profile with that of the SYM-dark animals revealed that at 24 h the light organ has a strong transcriptional response, independent of light production. Specifically, a total of 636 genes were regulated by both strains, over two-thirds of which were down-regulated. The functional annotation of >25% of these down-regulated genes was dominated by GO categories associated with maintenance of ciliary structure and function (Fig. 4A), which is not surprising, as both SYM and SYM-dark bacteria induce the cell death and loss of the ciliated surface that mediates initial colonization (28). Also enriched in this shared set were genes up-regulated in immune response and stress (Fig. 4A), which is also not unexpected, as the morphogenesis of the ciliated surface is driven largely by symbiont MAMPs.

However, it is most striking that over 2/3 of the 1919 genes regulated by colonization required that the symbionts be luminescent, underscoring how critical a role *V. fischeri* bioluminescence plays in shaping the symbiosis. In direct contrast to the luminescence-independent response, nearly 70% of the genes of the luminescence-specific response were up-regulated. Notably, the 39 GO categories of up-regulated genes included ‘visual perception’, ‘phototransduction’, ‘photoreceptor activity’, and ‘structural constituent of eye lens’, all involved with light perception or modulation, as well as homophilic cell adhesion and oxidative-reduction processes (Fig. 4A and Dataset S9). The light organs that were colonized by the dark mutant not only failed to regulate these luminescence-specific genes, but also had an expression signature of their own. The dark mutant regulated 875 genes, only 46% the number regulated by the wild-type strain (1919), with just over one-quarter of their regulated genes specific to the SYM-dark colonization, compared to the two-thirds of genes specific to the luminous SYM colonization. Further, unlike the SYM animals, the SYM-dark condition resulted principally in down-regulated genes, with no significant functional enrichment in any GO category (Fig. 4A). Finally, when gene regulation was compared directly between SYM and SYM-dark animals, 143 annotated genes were up-regulated in SYM, and only 15 down-regulated (Fig. 4B). Thirty-nine percent of these up-regulated genes were associated with sensory perception of light stimulus or modulation of light (e.g., lens proteins) (Dataset S9).

A particularly interesting difference between colonization conditions was the ~7-fold up-regulation in SYM compared to SYM-dark of atrial natriuretic peptide-converting enzyme (ANP-CE), which regulates cell volume and inflammation in a variety of systems (59). One of the key developmental features of the light organ is the SYM-induced swelling of the crypt cells with which the bacteria directly associate (Fig. 1A); however, the dark mutant is defective in inducing this phenotype (32). If ANP-CE were involved in such a cell-swelling and inflammation phenotype, we would predict that the transcript for this protein would specifically localize to the crypt epithelium in the SYM host, and be at a higher abundance than in SYM-dark-colonized animals. Using HCR-FISH, we compared the localization of the ANP-CE transcript in light organs at 24 h post-inoculation. Abundant transcript localized specifically to the cytoplasm of the crypt cells in SYM-colonized animals (*SI Appendix*, Movies S1-S3). In contrast, only low levels were detected in either APO or SYM-dark animals, with no significant difference between these conditions (Fig. 4C and C').

Unlike the light organ, no difference in colonization-dependent gene expression was detected between gill tissue of SYM and SYM-dark juveniles at 24 h, perhaps due to this organ's high variability in development at this time point. However, the eye showed a uniform, down-regulation in the expression of all 44 of the genes that responded in any way to colonization by the luminous symbiont (Fig. 4D); in contrast, no significant change in expression of any of those genes was detected when the symbiont was the dark mutant. These data suggest that, like the light organ, the eye's principal reaction to symbiotic colonization is mediated by the presence of light production. Interestingly, eye genes down-regulated by symbiont colonization were enriched in biological processes related to oxidation state or tissue reorganization (Fig. 4D, Dataset S9). Only 4 of the 44 genes down-regulated in the eye were shared with the light-organ's response: specifically, ANP-CE, MAM/LDL-receptor class A domain-containing 2-like, dynein heavy chain axonemal, as well as the hypothetical protein KGM_03810, which is also regulated in the adult light organ. However, unlike with the juvenile light-organ, the first three of these eye genes are up- (not down-) regulated in response to symbiosis. In summary, symbiosis-dependent gene expression in both the light organ and eye was more dependent on the existence of bacterium's luminescence than on the presence of the bacteria themselves.

Discussion

The data presented here demonstrate that, beginning within hours of the onset of the *E. scolopes* light-organ symbiosis, localized colonization of tissues by the specific symbiont *V. fischeri* creates a network of communication across the host's body that reprograms transcription system-wide. The coordination of this network persists throughout the developmental trajectory of the association, beginning with early symbiosis-induced changes in light-organ form and function, and continuing well into the maturation of the partnership. Further, the network reprograms remote organs to respond to the daily rhythms set by the *V. fischeri* population within the light organ. Finally, genetic manipulation of the symbiosis revealed that bioluminescence, the principal 'currency' of the symbiont, while having no effect on the gill response, is not only the major symbiosis-dependent driver of transcriptional regulation in the light organ, but also the *only* driver in the eye.

Transcriptomes of the Host's Organs Reflect their Biological Functions through Development.

The transcriptomes examined in this study, which segregated both by organ and by life stage, reflect known functions of the light organ, eye and gill, i.e., control of symbiont luminescence, vision and respiration, respectively (*SI Appendix*, Fig. S3 and Dataset S3). The light organ, eye and gill transcriptomes clustered separately between juveniles and adults (Fig. 1C and *SI Appendix*, Fig. S2A), a finding that may reflect the dramatic change in the animal's ecology upon its maturation. Briefly, from hatching to ~4 weeks post-colonization, the juvenile's behavior is not controlled by a daily rhythm, being either active or quiescent at all times of day and night; however, by about a month, the animal has assumed a profound diel rhythm of burying in the substrate during the day and coming out to forage at night, a behavior that will persist throughout its ~1-year life (60). This change in lifestyle coincides with a dramatic shift in the daily cycling of host and symbiont metabolism (34), a shift that promotes a brighter luminescence of the bacteria in the evening, when the squid is active and using the light emission of the symbionts to camouflage itself by 'counterilluminating' (28, 61). We hypothesize that the eye may be responding transcriptionally not only to its commitment to a diel rhythm of environmental light, but also to the requirement that the eye coordinate its function with the light organ's emission. Specifically, during counterillumination, the light organ modulates its luminescence in response to the intensity

of down-welling moonlight and starlight, which is monitored by the eye, through as yet undefined mechanisms. With such developmental changes in day-night behavior, it is not surprising that the transcriptomes of both the light organ and eye adopt new patterns as these organs mature. Similarly, the respiratory and immune functions of gill tissue, like its transcriptome (Fig. 1C), change between juvenile and adults as the animal begins to bury in the substrate each day by 4 weeks of age.

Symbiosis-induced changes in squid-host gene expression show similarities with those reported for the mammalian microbiota.

As with the global patterns of squid gene expression (Fig. 1C), both the light organ and remote tissues reacted robustly to colonization by *V. fischeri*, and several features of this life-stage and organ-specific transcriptomic response appear to be evolutionarily conserved between the squid light-organ and mammalian-gut symbioses. For example, a comparison of intestinal epithelial cell (IEC) transcriptomes from germ-free and conventionalized mice found that the response of IECs to the presence of the microbiota was only a fraction of the genes expressed in these cells and, as in squid, little overlap in this response occurs between juvenile and adult mice (62). In the squid, such largely stage-specific patterns of symbiosis reprogramming apply not only to the colonized tissue, i.e., the light organ, but also to the anatomically remote eye and gill. As yet, we know little about how remote tissues receive information about the colonization state or activity of symbiotic organs, but two modes are possible. The first is a chemical signal, such as a bacterial metabolite, delivered through the circulation (63, 64); one such metabolite, acetate, is generated in the light organ as byproduct of symbiont metabolism (34). For example, the presence of *V. fischeri* in the light organ has a systemic effect on hemocyte signaling (65). The second mode is neural: cephalopods, in particular, produce both targeted and systemic responses via their nervous system, similar to mammals, where the vagus nerve conveys information about the gut microbiota to the brain (66). However they are delivered, the transcriptional changes appearing during postnatal development in the mouse and squid organs reveal only part of the impact of symbiosis. In fact, many of these effects are deployed during embryogenesis, when symbionts are not yet present; i.e., both in the squid-vibrio system and in mammals, the developing host creates specific target-tissue conditions that are poised to respond to the eventual arrival of their symbiotic partners (28). Conversely, in a synoptic study comparing digestive-system transcriptomes of four

regions of the mouse intestine and liver (67), as with the squid, very little overlap in the transcriptional response to symbiosis occurred across the body.

To our knowledge, an integrated comparison both across tissues and through development has not yet been addressed in the mouse; thus whether the trajectory of the robust mammalian transcriptional response to symbiont colonization over early development varies among organs, as it did in the squid (i.e., first the light organ, then eye, then gill; *SI Appendix*, Datasets S4 & S8) remains to be determined. However, taken together, these similarities in life-stage and organ/tissue-specific responses to symbiosis in the two distantly related animal taxa suggest that, rather than having a generalized response to bacteria or their products, as they develop each tissue or organ, near to or distant from sites of colonization, integrates the partnership into its specific function. For example, in the squid association, we observed an up-regulation of genes involved in vascular development of tissues (Fig. 2C; *SI Appendix*, Dataset S6), which has also been reported for the nutrition-based gut symbioses of mammals (68). The finding that the squid system, wherein bioluminescence and not nutrition is the principal benefit to the host suggests, not surprisingly, that increased vascularization is important for other aspects of this symbiosis, such as facilitating the support of the bacterial population and their dialog with host tissues (34, 53).

Symbiotic Regulation of Genes Encoding Specific Functions Occurs on a Diel Cycle.

In addition to sharing life-stage and tissue-specific responses to symbiosis, in both mammalian (69) and squid hosts, there exist diel transcriptomic rhythms in colonized and remote tissues that are influenced by their bacterial partners. For example, although the overall transcriptomes of the three squid organs examined here differed greatly (Fig. 1C), the juvenile light organ shared with eye and gill a symbiosis-dependent diel regulation of two genes: angiotensin converting enzyme (ACE) and the antimicrobial peptide Galaxin 1 (Gal1). ACE occurs widely among animals, controlling blood pressure and electrolyte balance, although the conserved function of this protein family is immune modulation in both vertebrates (70, 71) and invertebrates (59, 72). Immunity is also likely to be its ancestral role because ACE occurs even in taxa without a closed circulatory system; however, in the squid, whose circulation is closed, this protein may serve both an immune and a vascular function. In contrast, galaxins are invertebrate-specific proteins, first identified in corals; in *E. scolopes*, Gal1 is an antimicrobial peptide present in the light organ (73). Although the genes encoding ACE and Gal1 were both regulated (either up

or down) by symbiosis, each had a different daily rhythm of expression depending on the host organ (Fig. 3).

What biological purposes might underlie the diel regulation of these genes? At all times analyzed, i.e., 0400, 1600 h, and 2000 h, the light organs were fully colonized (74); however, at 1600 and 0400, the per-cell luminescence of the symbionts is relatively low, compared to its maximum at 2000 h (75). The light organ expressed ACE and Gal1 constitutively throughout the day, whereas ACE and Gal1 expression was up-regulated in the eye only when luminescence was highest (2000 h). In addition, the light organ had symbiosis-induced expression of atrial natriuretic peptide-converting enzyme (ANP-CE), which transforms a pro-peptide to the edema-related peptide ANP (76). Because ANP-CE and ACE often offset one another's functions in immunity and vascular homeostasis (77), these findings suggests that an ACE-driven modulation of ANP-CE activity in the light organ releases ANP into the host blood stream, modulating the biochemistry of the eye and gill during the day-night cycle. Taken together, the transcriptional data are consistent with an organ-specific expression of an increased immune potential at particular times of day.

Light Organ and Eye are More Similar in their Responses to Symbiosis.

The repertoire of gene expression characteristic of light organ and gill tissues overlapped more in gene identity and number (Fig. 1D), consistent with both their similar relationship to the environment (i.e., both are bathed with bacteria-rich seawater during ventilation) and their shared immune function. In contrast, the interior portions of the eye examined here are protected from any direct exposure to environmental microbes. Yet, compared to the gill, the differential gene expression in symbiosis responses of the squid's eye and light organ were more similar in magnitude (Fig. 2B), reinforcing the hypothesis proposed above, that a coordination between these organs facilitates the host's counterillumination behavior within the ambient light field (61).

The squid eye also had a stronger relative response to light-organ colonization (84 genes; Fig. 2B) than the mouse eye did to colonization of the gut by the microbiota (5 genes; *SI Appendix, Dataset S7*). This difference in the scale of transcriptional response was unexpected because, while the mice were an inbred strain, the squid were genetically diverse, reared from wild-caught parents, and such genetic variation should lead to an underestimation of significant transcriptomic differences. However, the relatively weak reprogramming of the mouse by the presence of its gut

microbiota may reflect the vertebrate eye's status as a site of immune privilege (17). Nevertheless, colonization has been reported to influence the mouse eye's lipid content (16), and metabolomics studies have revealed a gut-retina axis that correlates with a proclivity toward development of macular degeneration (15, 78). In short, the difference between squid and mouse responses may be either due to differences in how the immune system interacts with the eye, or because of a greater need for light-organ/eye coordination in bioluminescent symbiotic associations. The latter hypothesis could be tested by a study of fishes with light-organ symbioses, which have both the vertebrate immune privilege of the eye, and the need to modulate luminescence by the symbiotic organ (79, 80).

Symbiont Luminescence has a Disproportionately Large Transcriptomic Effect.

A striking feature of symbiont-induced gene expression was discovered during a comparison of the organ transcriptomes of squid colonized with either the wild-type or the $\square lux$ mutant symbiont. The results highlight the remarkable dominance of luminescence in reprogramming gene regulation in not only the symbiont-containing light organ (Fig. 4AB), but also the anatomically remote eye (Fig. 4D). In many other associations, studies of such systemic consequences of losing the symbiont's principal activity have been clouded by the resultant physiological effects on the host. For example, in the rhizobium-legume symbiosis, bacterial mutants defective in nitrogen fixation similarly have a differential affect on transcription in both nodule tissue (81) and other plant organs (82); however, it was difficult to separate functions within the nodule from their general nutritional role. Similarly, animal-microbe interactions within gut tracts and bacteriomes also revolve around the symbiont's provision of an important nutrition function (83). That is, unlike bioluminescence, these functions directly impact the host's general physiology and health. Because the light-organ symbiosis plays an ecological role for the squid (i.e., anti-predation), under lab conditions, the physiology of the host is not negatively affected by carriage of a dark mutant (32). As such, this system serves as a paradigm for studies of the reprogramming of remote-tissue by other microbiota assemblages with non-nutritional functions (e.g., an antibiotic or defensive toxin (84, 85)), like those of the skin and urogenital tract of humans (86).

ANP-CE is one of the most abundant and highly regulated genes in the squid transcriptomes; specifically, it is overexpressed in SYM relative to APO tissues (Fig. 4C), it's level fluctuates on

a day-night cycle in eye and gill (Fig. 3BC), and in light organ and eye, its expression is induced by the symbiont's luminescence (*SI Appendix*, Dataset S8). Because ANP-CE plays a role in inducing cell edema (76), and the epithelia lining the symbiont-containing crypts swell when colonized by wild-type, but not dark-mutant, *V. fischeri* (32, 87), we predicted that ANP-CE expression would be reduced in the epithelium when the symbionts are dark mutants (Fig. 4C). This reduction suggested a direct link between symbiont function and host-tissue response, and may indicate a mechanism by which dark mutants are sanctioned (32, 88), possibly by withholding the nutrients typically delivered by the crypt's edematous epithelium.

The data presented here demonstrate that different tissues can have different transcriptional drivers in response to symbiosis, and future work will address the array of symbiont features that trigger the systemic response to light-organ colonization. Here we demonstrate that, among several effects on remote tissues, the most remarkable was the role of the symbiont's product (luminescence), rather than the presence of the symbiont itself, as the sole driver reprogramming the eye's transcriptome (Fig. 4D). As yet, it is unclear how the eye recognizes the presence of a luminous symbiont: perhaps a signal is delivered indirectly through a humoral or neural signal from the light organ (39). In any case, determining the mechanisms underlying this response presents a rich horizon for discovering shared principles of microbe-organ communication. The transcriptomic responses described here not only document symbiosis-induced molecular networks across the host, but also reveal how these networks may influence the behavior and ecology of the host, e.g., mediating the counterillumination antipredatory strategy.

In conclusion, we determined three types of organ-specific transcriptional responses to symbiont colonization, over the trajectory of development and over the day-night cycle: (i) a strong reaction to both the microbe and its primary product, luminescence (light organ), (ii) a response to the presence of the symbionts, independent of their luminescence (gill), and (iii) a response triggered solely by the luminescence product (eye). Determining the presence and mechanistic basis of the inter-organ network that connects symbiotic and remote tissues, enabling a coordinated response, is a critical area of exploration, and will eventually reveal the degree to which symbioses can influence host health and homeostasis throughout life.

Materials and Methods

Sample Collection.

Animals were collected 24 and 72 h after hatching (juveniles), or ~5 mos (adults) (Fig. 1A), and anesthetized in seawater containing 2% ethanol, juveniles were stored whole in RNAlater (Sigma-Aldrich) as previously described (52), while adult tissues were dissected prior to storage. With the exception of day/night cycle studies, all samples were collected at 2000 h, 2 h after dusk.

RNA-Seq Assembly and Analysis.

A total of 2.2 billion paired-end reads were *de novo* assembled using the Trinity-v2.4.0 RNA-Seq assembler (89) (Dataset S1), and annotated by BLASTx against the NCBI non-redundant protein database. For functional annotation of the reference transcriptome, gene ontology (GO) mapping of the transcripts was performed with Blast2GO software (90). To estimate the relative expression value for transcripts, RSEM software (91) was used in combination with the R package edgeR (92) to identify the significantly differentially expressed transcripts. Statistical enrichment of GO terms for differentially expressed genes was performed in Blast2Go using the Fisher exact test with an FDR<0.01. In addition, Gene-Set Weighted Enrichment Analysis (GSEA) with 500 permutations and FDR < 0.1 was performed on the differentially expressed transcripts (*SI Appendix*).

Transcript Quantification by qPCR or NanoString nCounter Analysis.

Changes in host gene expression were measured by qPCR using LightCycler[®] 480 SYBR Green I Master Mix (Roche). Ribosomal protein 19L, serine hydroxymethyl transferase, and heat-shock protein 90 were used to normalize the transcript level (*SI Appendix*, Table S1). The nCounter Custom CodeSet Kit (NanoString Technologies) was used to detect changes in gene expression (Dataset S4). Assay and spike-in controls were used for normalization based on identical amounts of input RNA. Analysis was performed with nSolverAnalysis Software v3.0.

See *SI Materials and Methods* for additional experimental details.

ACKNOWLEDGMENTS.

We thank members of the McFall-Ngai and Ruby labs for helpful discussions. We specially thank Dr. Tara Essock-Burns for her assistance with confocal imaging. This work was funded by NIH grants to M.M.-N. (R37 AI50661), and to E.G.R. (R01 OD11024). F.R. was supported by

the Office of the Vice-Chancellor for Research and Graduate Education at the University of Wisconsin–Madison, with funding from the Wisconsin Alumni Research Foundation.

Figures

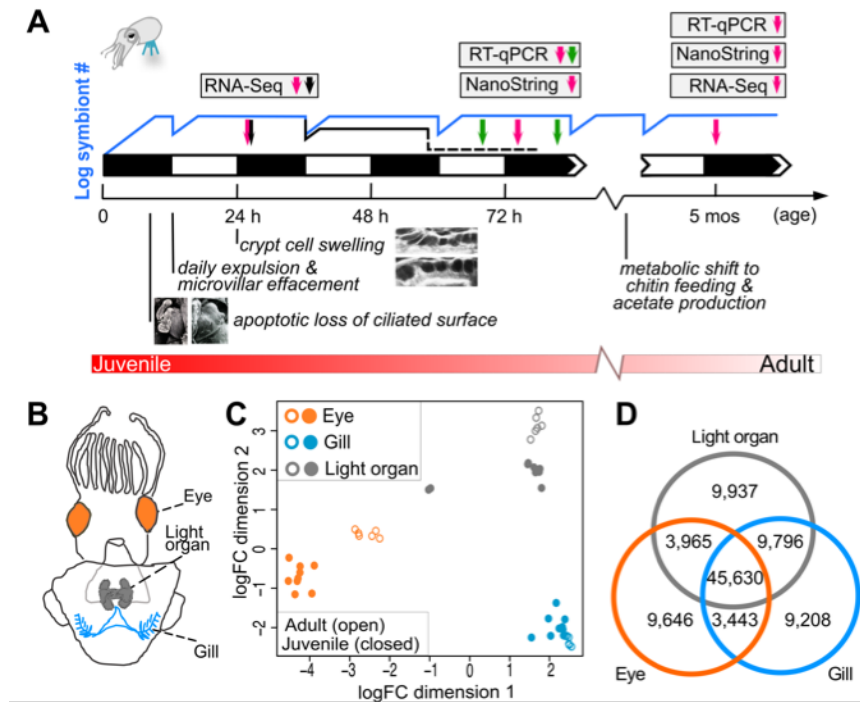


Fig. 1. Transcriptome profiling of *E. scolopes* organs. (A) Transcriptome sampling scheme during symbiotic development. On the night (black squares) that they hatch, juvenile squid become inoculated by *V. fischeri* cells, which proliferate, (blue line), filling the light-organ crypts and producing bioluminescence. Colonization triggers developmental events in the light organ's tissues, including apoptosis of the surface epithelium (left panel inset = APO; right panel inset = SYM), and edematous swelling of the crypt epithelial cells (upper panel inset = APO; lower panel inset = SYM). Each dawn, the nocturnally active host effaces the crypt-cell microvilli and expels most of its symbiont population, which grows back up by noon. A dark mutant ($\square lux$) colonizes normally, but is unable to persist in the organ (dotted black line), and doesn't induce normal crypt cell swelling. After one month, the host begins providing chitin to the symbionts, which ferment it to acetate. Transcriptomes of light organ, eye and gill were constructed by RNA-Seq or NanoString from organs sampled at 2000 h (magenta arrows) in APO and SYM hosts of juvenile and adult animals. SYM-dark hosts, colonized by a dark-mutant strain, were also sampled (black arrow). For day/night comparisons, APO and SYM organs were sampled at 1600 and 0400 h (green arrows) as well. Levels of transcripts of interest were confirmed by NanoString and RT-qPCR. (B) Schematic drawing of *E. scolopes* indicating tissue types collected from both juvenile and adult squid. (C) Multi-dimensional scaling plot of gene expression for the *E. scolopes* reference transcriptome. (D) Venn diagram of the number of shared and specific genes, expressed by tissue type. A gene is considered expressed when FPKM (fragments per kilobase million) >0.5 in at least 2 samples per tissue.

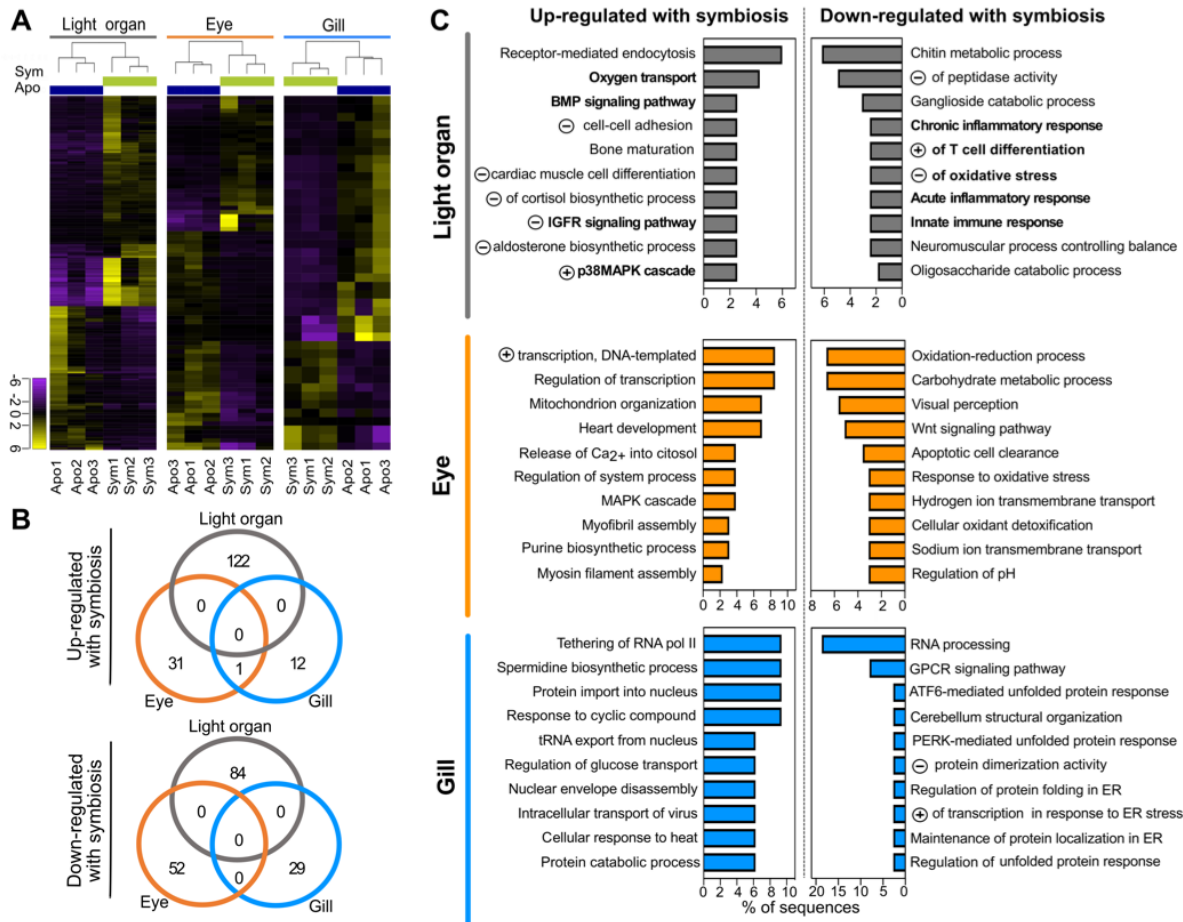


Fig. 2. Impact of light-organ symbiosis on gene expression in different adult organs. (A) Heat map of expression values, log₂-transformed and median centered, for genes significantly differentially expressed (>2 fold, P_{adj} < 0.05) in adult light organ, eye and gill. Apo: aposymbiotic, in dark blue; Sym: symbiotic (colonized by wild type *V. fischeri*) in green. (B) Venn diagrams indicating the numbers of significantly differentially expressed genes (>2 fold, P_{adj} < 0.05) in response to symbiosis. (C) Functional annotation of symbiosis-responsive genes in remote tissues. The differentially expressed genes were enriched in functional categories based on gene ontology (GO) annotation. The top 10 enriched Biological Processes are shown ordered by percentages of sequences with that function, and by its significance level (Fisher exact test, FDR < 0.05). “Negative (or positive) regulation of..” is abbreviated by a circled minus (or plus) symbol. Complete GO-term names and codes are in *SI Appendix*, Dataset S6. Bold lettering indicates GO terms described in Results section.

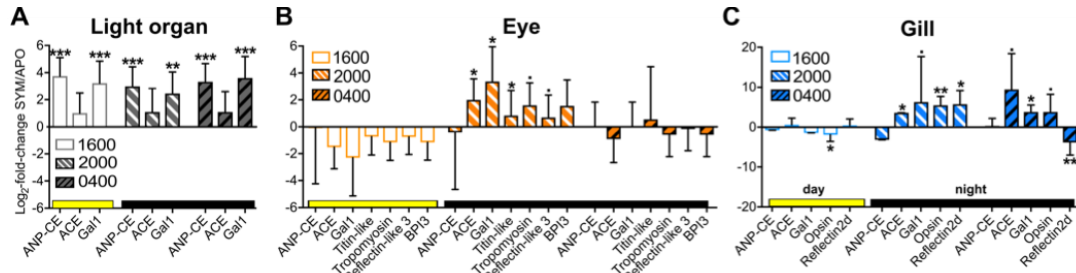


Fig. 3. Variation of symbiosis-responsive gene expression over the day/night cycle. Gene expression changes in SYM (compared to APO) light organ (A), eye (B) and gill (C) tissue at different times of day: 0400 h = 2 h before dawn; 1600 h = 2 h before dusk; 2000 h = 2 h after dusk. Juvenile squid were maintained for 3 days under a 12-12 light-dark schedule. Candidate genes were chosen for RT-qPCR based on expression changes observed at 72 h (SI Appendix, Fig. S9, Table S1; Dataset S4). ANP-CE= atrial natriuretic peptide-converting enzyme; ACE= angiotensin-converting enzyme; Gal1= galaxin1; BPI3= bactericidal/permeability-increasing protein 3. P-value code (SYM vs. APO): ***, <0.001; **, <0.01; *, <0.05; ; <0.1.

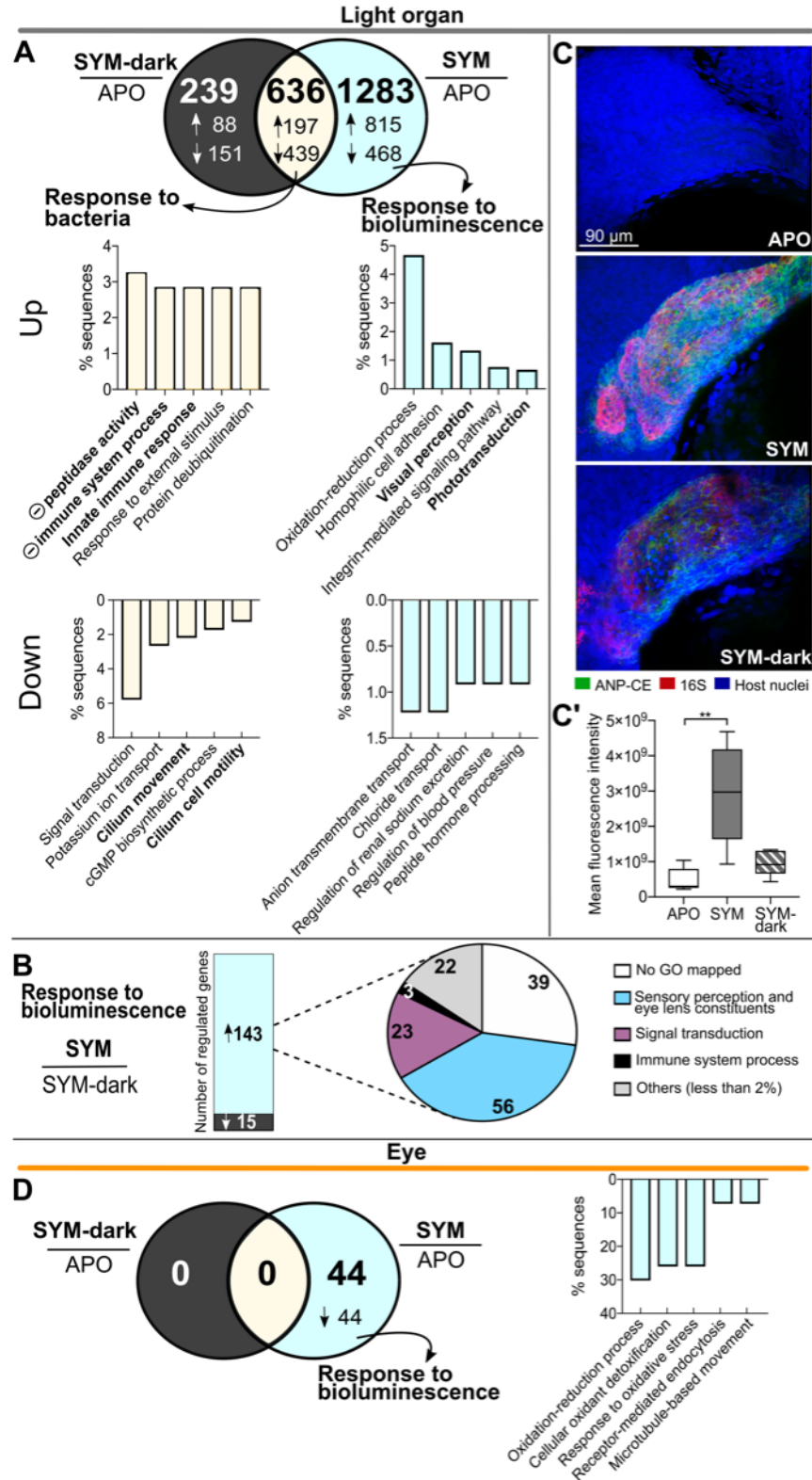


Fig. 4. Impact of symbiont bioluminescence on juvenile gene expression. (A) Venn diagram of numbers of differentially expressed genes in the light organ, 24 h after colonization by either SYM (wild-type) or SYM-dark (Δlux) strains, compared to APO (>2 fold, $P_{adj} < 0.05$). Arrows indicate either up (\uparrow) or down (\downarrow) regulation. Bar graphs: functional enrichment of genes significantly up-regulated and down-regulated

with symbiosis. For each set, the top 5 biological process terms are represented (Fisher exact test, FDR <0.01). Notations as in Fig. 2. (B) (left) number of genes significantly up- or down-regulated in SYM compared to SYM-dark colonized light organs; (right) proportion of annotated Biological Processes accounting for >2% of up-regulated genes. (C) Visualization of ANP-CE transcript in whole-mount light organs 24 h after colonization. Representative confocal images showing ANP-CE expression in crypt epithelium of APO, SYM or SYM-dark colonized juvenile squid; merged mid-section of Z-stack of crypt #1; ANP-CE (green), 16S RNA (symbionts, red) and host nuclei (TOPRO, blue) (*SI Appendix*, Fig. S10, Movies S1-S3). (C') Quantification of ANP-CE signal by fluorescence intensity from Z stacks of crypt #1 in five light organs. *P* values were calculated using Kruskal–Wallis test and Dunn's multiple comparison test. Error bar: SD (**, *P*<0.01). (D) Venn diagram of differentially expressed genes in the eye, 24 h after colonization by either SYM (wild-type) or SYM-dark (Δlux) strains, compared to APO (>2 fold, P_{adj} <0.05). Arrow indicates down (\downarrow) regulation. Bar graph: notations as in (A) (*SI Appendix*, Datasets S8 & S9).

References

1. Blaser MJ, *et al.* (2016) Toward a predictive understanding of Earth's microbiomes to address 21st-century challenges. *mBio* 7(3):e00714-00716.
2. Bosch TC & McFall-Ngai MJ (2011) Metaorganisms as the new frontier. *Zoology (Jena)* 114(4):185-190.
3. Schroeder BO & Backhed F (2016) Signals from the gut microbiota to distant organs in physiology and disease. *Nat Med* 22(10):1079-1089.
4. Hsu T, *et al.* (2016) Urban transit system microbial communities differ by surface type and interaction with humans and the environment. *mSystems* 1(3):e00018-00016.
5. Kembel SW, *et al.* (2014) Architectural design drives the biogeography of indoor bacterial communities. *PLoS One* 9(1):e87093.
6. Goyal MS, Venkatesh S, Milbrandt J, Gordon JI, & Raichle ME (2015) Feeding the brain and nurturing the mind: Linking nutrition and the gut microbiota to brain development. *Proc Natl Acad Sci U S A* 112(46):14105-14112.
7. Chu H & Mazmanian SK (2013) Innate immune recognition of the microbiota promotes host-microbial symbiosis. *Nat Immunol* 14(7):668-675.
8. Sharon G, Sampson TR, Geschwind DH, & Mazmanian SK (2016) The central nervous system and the gut microbiome. *Cell* 167(4):915-932.
9. Schneider KM, *et al.* (2018) Successful fecal microbiota transplantation in a patient with severe complicated *Clostridium difficile* infection after liver transplantation. *Case Rep Gastroenterol* 12(1):76-84.
10. Kamo T, Akazawa H, Suzuki JI, & Komuro I (2017) Novel concept of a heart-gut axis in the pathophysiology of heart failure. *Korean Circ J* 47(5):663-669.
11. Serino M, Blasco-Baque V, Nicolas S, & Burcelin R (2014) Far from the eyes, close to the heart: dysbiosis of gut microbiota and cardiovascular consequences. *Curr Cardiol Rep* 16(11):540.
12. Coppo R (2018) The gut-kidney axis in IgA nephropathy: role of microbiota and diet on genetic predisposition. *Pediatr Nephrol* 33(1):53-61.
13. Budden KF, *et al.* (2017) Emerging pathogenic links between microbiota and the gut-lung axis. *Nat Rev Microbiol* 15(1):55-63.
14. Samuelson DR, Welsh DA, & Shellito JE (2015) Regulation of lung immunity and host defense by the intestinal microbiota. *Front Microbiol* 6:1085.

15. Lin P (2018) The role of the intestinal microbiome in ocular inflammatory disease. *Curr Opin Ophthalmol* 29(3):261-266.
16. Oresic M, Seppanen-Laakso T, Yetukuri L, Backhed F, & Hanninen V (2009) Gut microbiota affects lens and retinal lipid composition. *Exp Eye Res* 89(5):604-607.
17. Zarate-Blades CR, *et al.* (2017) Gut microbiota as a source of a surrogate antigen that triggers autoimmunity in an immune privileged site. *Gut Microbes* 8(1):59-66.
18. Liang X & FitzGerald GA (2017) Timing the microbes: The circadian rhythm of the gut microbiome. *J Biol Rhythms* 32(6):505-515.
19. Zhao L & Zhang C (2017) Microbiome: keeping rhythm with your gut. *Nat Microbiol* 2:16273.
20. Barr T, *et al.* (2018) Concurrent gut transcriptome and microbiota profiling following chronic ethanol consumption in nonhuman primates. *Gut Microbes* 9(4):338-356.
21. Chowdhury SR, *et al.* (2007) Transcriptome profiling of the small intestinal epithelium in germfree versus conventional piglets. *BMC Genomics* 8:215.
22. Sommer F, Nookaew I, Sommer N, Fogelstrand P, & Backhed F (2015) Site-specific programming of the host epithelial transcriptome by the gut microbiota. *Genome Biol* 16:62.
23. Thaiss CA, *et al.* (2016) Microbiota diurnal rhythmicity programs host transcriptome oscillations. *Cell* 167(6):1495-1510.
24. Thion MS, *et al.* (2018) Microbiome influences prenatal and adult microglia in a sex-specific manner. *Cell* 172(3):500-516.
25. Holmes E, Li JV, Athanasiou T, Ashrafi H, & Nicholson JK (2011) Understanding the role of gut microbiome-host metabolic signal disruption in health and disease. *Trends Microbiol* 19(7):349-359.
26. Postler TS & Ghosh S (2017) Understanding the holobiont: how microbial metabolites affect human health and shape the immune system. *Cell Metab* 26(1):110-130.
27. McFall-Ngai M (2014) Divining the essence of symbiosis: insights from the squid-vibrio model. *PLoS Biol* 12(2):e1001783.
28. McFall-Ngai MJ (2014) The importance of microbes in animal development: lessons from the squid-vibrio symbiosis. *Annu Rev Microbiol* 68:177-194.
29. Dethlefsen L, McFall-Ngai M, & Relman DA (2007) An ecological and evolutionary perspective on human-microbe mutualism and disease. *Nature* 449(7164):811-818.

30. Heath-Heckman EA, Foster J, Apicella MA, Goldman WE, & McFall-Ngai M (2016) Environmental cues and symbiont microbe-associated molecular patterns function in concert to drive the daily remodelling of the crypt-cell brush border of the *Euprymna scolopes* light organ. *Cellul Microbiol* 18(11):1642-1652.
31. Lamarcq LH & McFall-Ngai MJ (1998) Induction of a gradual, reversible morphogenesis of its host's epithelial brush border by *Vibrio fischeri*. *Infect Immun* 66(2):777-785.
32. Visick KL, Foster J, Doino J, McFall-Ngai M, & Ruby EG (2000) *Vibrio fischeri lux* genes play an important role in colonization and development of the host light organ. *J Bacteriol* 182(16):4578-4586.
33. Graf J & Ruby EG (1998) Host-derived amino acids support the proliferation of symbiotic bacteria. *Proc Natl Acad Sci U S A* 95(4):1818-1822.
34. Schwartzman JA, *et al.* (2015) The chemistry of negotiation: rhythmic, glycan-driven acidification in a symbiotic conversation. *Proc Natl Acad Sci U S A* 112(2):566-571.
35. Wier AM, *et al.* (2010) Transcriptional patterns in both host and bacterium underlie a daily rhythm of anatomical and metabolic change in a beneficial symbiosis. *Proc Natl Acad Sci U S A* 107(5):2259-2264.
36. Carey HV & Duddleston KN (2014) Animal-microbial symbioses in changing environments. *J Therm Biol* 44:78-84.
37. Montgomery MK & McFall-Ngai MJ (1992) The muscle-derived lens of a squid bioluminescent organ is biochemically convergent with the ocular lens: evidence for recruitment of aldehyde dehydrogenase as a predominant structural protein. *J Biol Chem* 267(29):20999-21003.
38. Peyer SM, Heath-Heckman EAC, & McFall-Ngai MJ (2017) Characterization of the cell polarity gene crumbs during the early development and maintenance of the squid-vibrio light organ symbiosis. *Dev Genes Evol* 227(6):375-387.
39. Tong D, *et al.* (2009) Evidence for light perception in a bioluminescent organ. *Proc Natl Acad Sci U S A* 106(24):9836-9841.
40. McFall-Ngai M, Heath-Heckman EA, Gillette AA, Peyer SM, & Harvie EA (2012) The secret languages of coevolved symbioses: insights from the *Euprymna scolopes-Vibrio fischeri* symbiosis. *Semin Immunol* 24(1):3-8.
41. Gestal C & Castellanos-Martinez S (2015) Understanding the cephalopod immune system based on functional and molecular evidence. *Fish Shellfish Immunol* 46(1):120-130.

42. Bose JL, Rosenberg CS, & Stabb EV (2008) Effects of *luxCDABEG* induction in *Vibrio fischeri*: enhancement of symbiotic colonization and conditional attenuation of growth in culture. *Arch Microbiol* 190(2):169-183.
43. Casaburi G, Goncharenko-Foster I, Duscher AA, & Foster JS (2017) Transcriptomic changes in an animal-bacterial symbiosis under modeled microgravity conditions. *Sci Rep* 7:46318.
44. Kremer N, *et al.* (2018) Persistent interactions with bacterial symbionts direct mature-host cell morphology and gene expression in the squid-vibrio symbiosis. *mSystems* 3(5).
45. Albertin CB, *et al.* (2015) The octopus genome and the evolution of cephalopod neural and morphological novelties. *Nature* 524(7564):220-224.
46. Belcaid M, *et al.* (2019) Symbiotic organs shaped by distinct modes of genome evolution in cephalopods. *Proc Natl Acad Sci U S A*.
47. Alon S, *et al.* (2015) The majority of transcripts in the squid nervous system are extensively recoded by A-to-I RNA editing. *Elife* 4.
48. da Fonseca RR, *et al.* (2016) Next-generation biology: Sequencing and data analysis approaches for non-model organisms. *Mar Genomics* 30:3-13.
49. Bose JL, *et al.* (2007) Bioluminescence in *Vibrio fischeri* is controlled by the redox-responsive regulator ArcA. *Mol Microbiol* 65(2):538-553.
50. Ruby EG & McFall-Ngai MJ (1999) Oxygen-utilizing reactions and symbiotic colonization of the squid light organ by *Vibrio fischeri*. *Trends Microbiol* 7(10):414-420.
51. Schwartzman JA & Ruby EG (2016) A conserved chemical dialog of mutualism: lessons from squid and vibrio. *Microbes Infect* 18(1):1-10.
52. Kremer N, *et al.* (2013) Initial symbiont contact orchestrates host-organ-wide transcriptional changes that prime tissue colonization. *Cell Host Microbe* 14(2):183-194.
53. Nyholm SV, Stewart JJ, Ruby EG, & McFall-Ngai MJ (2009) Recognition between symbiotic *Vibrio fischeri* and the haemocytes of *Euprymna scolopes*. *Environ Microbiol* 11(2):483-493.
54. Rageh AA, *et al.* (2016) Lactoferrin expression in human and murine ocular tissue. *Curr Eye Res* 41(7):883-889.
55. Ogura A, Ikeo K, & Gojobori T (2004) Comparative analysis of gene expression for convergent evolution of camera eye between octopus and human. *Genome Res* 14(8):1555-1561.

56. Yoshida MA, *et al.* (2015) Molecular evidence for convergence and parallelism in evolution of complex brains of cephalopod molluscs: insights from visual systems. *Integr Comp Biol* 55(6):1070-1083.
57. Kingston AC, Kuzirian AM, Hanlon RT, & Cronin TW (2015) Visual phototransduction components in cephalopod chromatophores suggest dermal photoreception. *J Exp Biol* 218():1596-1602.
58. Mathger LM, Roberts SB, & Hanlon RT (2010) Evidence for distributed light sensing in the skin of cuttlefish, *Sepia officinalis*. *Biol Lett* 6(5):600-603.
59. Takei Y (2001) Does the natriuretic peptide system exist throughout the animal and plant kingdom? *Comp Biochem Physiol B Biochem Mol Biol* 129:559-573.
60. McFall-Ngai MJ & Ruby EG (1998) Sepiolid and vibrios: when first they meet. *Bioscience* 48:257-265.
61. Jones BW & Nishiguchi MK (2004) Counterillumination in the Hawaiian bobtail squid, *Euprymna scolopes* Berry (Mollusca: Cephalopoda). *Mar Biol* 144:1151-1155.
62. Pan WH, *et al.* (2018) Exposure to the gut microbiota drives distinct methylome and transcriptome changes in intestinal epithelial cells during postnatal development. *Genome Med* 10(1):27.
63. Pluznick JL, *et al.* (2013) Olfactory receptor responding to gut microbiota-derived signals plays a role in renin secretion and blood pressure regulation. *Proc Natl Acad Sci U S A* 110(11):4410-4415.
64. Fujisaka S, *et al.* (2018) Diet, genetics, and the gut microbiome drive dynamic changes in plasma metabolites. *Cell Rep* 22(11):3072-3086.
65. McAnulty SJ & Nyholm SV (2016) The role of hemocytes in the Hawaiian bobtail squid, *Euprymna scolopes*: a model organism for studying beneficial host-microbe interactions. *Front Microbiol* 7:2013.
66. Bonaz B, Bazin T, & Pellissier S (2018) The vagus nerve at the interface of the microbiota-gut-brain Axis. *Front Neurosci* 12:49.
67. Mardinoglu A, *et al.* (2015) The gut microbiota modulates host amino acid and glutathione metabolism in mice. *Mol Syst Biol* 11(10):834.
68. Stappenbeck TS, Hooper LV, & Gordon JI (2002) Developmental regulation of intestinal angiogenesis by indigenous microbes via Paneth cells. *Proc Natl Acad Sci U S A* 99(24):15451-15455.

69. Tahara Y, *et al.* (2018) Gut microbiota-derived short chain fatty acids induce circadian clock entrainment in mouse peripheral tissue. *Sci Rep* 8(1):1395.
70. De Vito P (2014) Atrial natriuretic peptide: an old hormone or a new cytokine? *Peptides* 58:108-116.
71. Moskowitz DW & Johnson FE (2004) The central role of angiotensin I-converting enzyme in vertebrate pathophysiology. *Curr Top Med Chem* 4(13):1433-1454.
72. Salzet M & Verger-Bocquet M (2001) Elements of angiotensin system are involved in leeches and mollusks immune response modulation. *Brain Res Mol Brain Res* 94:137-147.
73. Heath-Heckman EA, *et al.* (2014) Shaping the microenvironment: evidence for the influence of a host galaxin on symbiont acquisition and maintenance in the squid-*Vibrio* symbiosis. *Environ Microbiol* 16(12):3669-3682.
74. Nyholm SV & McFall-Ngai MJ (1998) Sampling the light-organ microenvironment of *Euprymna scolopes*: description of a population of host cells in association with the bacterial symbiont *Vibrio fischeri*. *Biol Bull* 195:89-97.
75. Boettcher KJ, Ruby EG, & McFall-Ngai MJ (1996) Bioluminescence in the symbiotic squid *Euprymna scolopes* is controlled by a daily biological rhythm. *J Comp Physiol* 179:65-73.
76. Theilig F & Wu Q (2015) ANP-induced signaling cascade and its implications in renal pathophysiology. *Am J Physiol Renal Physiol* 308(10):1047-1055.
77. Boudoulas KD, Triposkiadis F, Parissis J, Butler J, & Boudoulas H (2017) The cardio-renal interrelationship. *Prog Cardiovasc Dis* 59(6):636-648.
78. Rinninella E, *et al.* (2018) The role of diet, micronutrients and the gut microbiota in age-related macular degeneration: new perspectives from the gut-retina axis. *Nutrients* 10(11):E1677.
79. Gould AL, Dougan KE, Koenigbauer ST, & Dunlap PV (2016) Life history of the symbiotically luminous cardinalfish *Siphamia tubifer* (Perciformes: Apogonidae). *J Fish Biol* 89(2):1359-1377.
80. Haygood MG (1993) Light organ symbioses in fishes. *Crit Rev Microbiol* 19(4):191-216.
81. Barnett MJ, Toman CJ, Fisher RF, & Long SR (2004) A dual-genome Symbiosis Chip for coordinate study of signal exchange and development in a prokaryote-host interaction. *Proc Natl Acad Sci U S A* 101(47):16636-16641.
82. O'Rourke JA, *et al.* (2014) An RNA-Seq based gene expression atlas of the common bean. *BMC Genomics* 15:866.

83. Douglas AE (2010) *The Symbiotic Habit* (Princeton University Press) p 214.
84. McCutcheon JP (2013) Genome evolution: a bacterium with a Napoleon complex. *Curr Biol* 23(15):R657-659.
85. Sharp KH, Davidson SK, & Haygood MG (2007) Localization of 'Candidatus Endobugula sertula' and the bryostatins throughout the life cycle of the bryozoan *Bugula neritina*. *ISME J* 1(8):693-702.
86. Meisel JS, *et al.* (2018) Commensal microbiota modulate gene expression in the skin. *Microbiome* 6(1):20.
87. Sycuro LK, Ruby EG, & McFall-Ngai M (2006) Confocal microscopy of the light organ crypts in juvenile *Euprymna scolopes* reveals their morphological complexity and dynamic function in symbiosis. *J Morphol* 267(5):555-568.
88. Koch EJ, Miyashiro T, McFall-Ngai MJ, & Ruby EG (2014) Features governing symbiont persistence in the squid-vibrio association. *Mol Ecol* 23(6):1624-1634.
89. Grabherr MG, *et al.* (2011) Full-length transcriptome assembly from RNA-Seq data without a reference genome. *Nat Biotechnol* 29(7):644-652.
90. Gotz S, *et al.* (2008) High-throughput functional annotation and data mining with the Blast2GO suite. *Nucleic Acids Res* 36(10):3420-3435.
91. Li B & Dewey CN (2011) RSEM: accurate transcript quantification from RNA-Seq data with or without a reference genome. *BMC Bioinformatics* 12:323.
92. Robinson MD, McCarthy DJ, & Smyth GK (2010) edgeR: a Bioconductor package for differential expression analysis of digital gene expression data. *Bioinformatics* 26(1):139-140.

Supplementary Information for:

Critical symbiont signals drive both local and systemic changes in diel and developmental host gene expression

Silvia Moriano-Gutierrez, Eric J. Koch, Hailey Bussan, Kymberleigh Romano, Mahdi Belcaid, Federico E. Rey, Edward Ruby, and Margaret McFall-Ngai

Margaret McFall-Ngai
Email: mcfallng@hawaii.edu

This PDF file includes:

Supplementary text
Figs. S1 to S10
Tables S1 to S3
Captions for movies S1 to S3
Captions for databases S1 to S10
References for SI reference citations

Other supplementary materials for this manuscript can be found online at <https://www.pnas.org/content/116/16/7990/tab-figures-data>; and include the following:

Movies S1 to S3
Datasets S1 to S10

Supplementary Information Text

SI Results

Sequencing, Assembly and Annotation. We sequenced total RNA isolated from 45 samples across 3 distinct tissue types and two developmental stages. The 2.2 billion paired-end reads were de novo assembled, yielding 788,971 contigs (Fig. S1 and Dataset S1). Ninety percent of the expression was represented by only 16,295 transcripts, and 70% of all transcripts with an open reading frame had BLASTx annotations, which had highest representation within closely related taxa (Fig. S1C and D). For all three squid organs considered together, the ‘biological process’ category constituted the highest percentage (47%) of Gene Ontology (GO) mapping of the transcripts, followed by ‘cellular component’ (35%) and ‘molecular function’ (18%) (Fig. S1E).

SI Materials and Methods

General Procedures. Adult *Euprymna scolopes* squid were collected from Paikō Lagoon, Oahu, Hawai'i, and either transferred to outdoor tanks to maintain natural light cues or transported to the University of Wisconsin (Madison, WI) and maintained in the laboratory as previously described (1). Juveniles from the breeding colony were collected within minutes of hatching, and placed in either filter-sterilized Instant Ocean (FSIO) artificial seawater (Aquarium Systems, Mentor, OH) or filter-sterilized coastal ocean water. Within 2 h of hatching, juveniles were either made symbiotic (SYM) by overnight exposure to cells of *Vibrio fischeri* in filter-sterilized ocean water (FSIO), or kept aposymbiotic (APO) (2). For all experiments, animals were maintained on a 12-h light-dark cycle and, when needed, squid males were raised for 5-6 months to adulthood, following standard procedures (3). All of the adult squid used, including both, reared or wild-caught, were males, and had mantle lengths between 2.51 and 2.82 cm, indicating that they were fully mature.

Two strains of *V. fischeri* were used in this study: the wild-type ES114 (2) and its dark-mutant derivative EVS102 (Δlux), in which the genes required for luminescence were deleted (4). To prepare the strains as an inoculum, they were first cultured overnight in Luria-Bertani salt medium (LBS) (5). They were then subcultured (1:100) into seawater tryptone medium (SWT) (2), and grown to mid-log phase at 28 °C with shaking. This subculture was diluted into seawater to a final concentration of 3,000-5,000 cells/ml, and juvenile squid added. Colonization of the host was monitored by checking for animal luminescence with a TD 20/20 luminometer (Turner Designs,

Sunnyvale, CA) or, in animals colonized by EVS102, by plating the surrounding water after the dawn expulsion. Juvenile animals were collected at the indicated times after inoculation, anesthetized in seawater containing 2% ethanol, and stored frozen at -80 °C in RNAlater (Ambion), as previously described (6), until further processing.

Host Organ RNA Extraction and Sequencing. Total RNA was purified using QIAGEN RNeasy columns, immediately followed by treatment with TURBO™ DNase (Ambion). The RNA concentration for each sample was then determined with a Qubit RNA BR assay kit (Invitrogen). The Illumina TruSeq protocol v2.0, with polyA selection, was used throughout to generate bar-coded sequencing libraries for all 24 h samples. Paired-end 100-bp sequencing was performed at the University of Wisconsin-Madison Biotechnology and Gene Expression Center. The Illumina TruSeq Stranded mRNA Sample Prep with polyA selection v4.0 protocol was used for all adult samples of light organ and gill tissues (at the University of Utah High-Throughput Genomics Core Facility) and for eye tissues (at SeqMatic, Fremont, CA. All sequencing data was used to build the reference transcriptome (see below).

De Novo RNA-Seq Assembly and Annotation. Trimmomatic (7), was used to trim and discard reads containing the Illumina adaptor sequences with a minimum length threshold of 36 bp. A total of 2.2 billion paired-end reads were *de novo* assembled into the Trinity-v2.4.0 RNA-Seq assembler (8) incorporating an *in silico* normalization step (Dataset S1). A BLASTx search against the NCBI non-redundant protein database was used to annotate the reference transcriptome. For the functional annotations of the reference transcriptome, Gene Ontology (GO) mapping of the transcripts and gene set enrichment analysis (GSEA) (9) as performed with Blast2go software (10).

Transcript Abundance Estimation and Differential Expression Analysis. Reads were mapped against the reference transcriptome with bowtie2 (11), and their relative expression values for each tissue were estimated with RSEM software (12). The statistical analysis of the RNA-Seq data was performed with the R package edgeR (13), identifying the significantly differentially expressed transcripts in each of the pairwise comparisons, and employing a false discovery rate (FDR) threshold of 0.05 with at least a 2-fold change in expression difference. However, when we determined the sets of tissue-specific genes, the cut off for fold-change difference was set to 8-

fold. Only genes with expression values of >0.5 FPKM (fragments per kilobase of transcript per million fragments mapped) in at least 2 samples of the pairwise comparisons were included in the analysis. The count data of the remaining genes were normalized and log-transformed in edgeR. All normalized mean expression values are shown in Dataset S2. All normalized expression values were used to determine the threshold of expression for all tissues, where a gene is considered expressed if it has an expression value equal to or larger than 0.5 FPKM in all samples of that tissue. Due to the large differences in expression profiles of the different tissues at both developmental stages, the determination of expressed genes per tissue was performed separately for juvenile and adult samples. Venn diagrams were drawn using the venn function of ggplot R package. Heatmaps of expression values and hierarchical clustering were created with heatmap3 and hclust functions, respectively, in the R environment (14). Statistical enrichment of Gene Ontology (GO) terms for differentially expressed genes was performed in Blast2Go software (10) using the Fisher exact test with an $FDR < 0.01$. In addition, gene-set weighted enrichment analysis (GSEA) with 500 permutations and $FDR < 0.1$ was performed on the differentially expressed transcripts (Dataset S10). No significant difference was seen for the top enriched terms between the two methods.

Quantitative NanoString nCounter Analysis and Gene Transcript Quantification by qPCR.

The nCounter Custom CodeSet (Dataset S3) Kit (NanoString Technologies) was used to detect changes in gene expression following the manufacturer's protocol. Total RNA, was extracted as described above. Assay and spike-in controls were used for normalization based on identical amounts of input RNA. Welch's t-test analysis was performed with nSolverAnalysis Software v3.0. Ribosomal protein 19L, serine hydroxymethyl transferase and peptidyl-prolyl cis-trans isomerase were used as internal reference genes to normalize expression levels of each candidate gene, using their geometric means (15). Pearson correlation of expression data obtained by RNA-Seq and NanoString was calculated with GraphPad Prism v7.00 software. Host gene expression changes were in addition measured by qPCR using LightCycler[®] 480 SYBR Green I Master Mix (Roche). Total RNA, was extracted as described previously. Synthesis of the single-stranded complementary DNA was performed with SMART MMLV Reverse Transcriptase (Clontech) using Oligo(dT)12–18 primers (Invitrogen). All reactions were performed with no-RT and no-template controls to confirm that the reaction mixtures were not contaminated. Specific primers

(Table S1) were designed with Primer3plus (16). Primer efficiencies ranged between 98% and 105% with an annealing temperature of 60 °C for all primer pairs. The amplification efficiency was determined by in-run standard curves with a 10-fold dilution template. Each reaction was done in duplicate with a starting level of 12.5 ng cDNA. The generation of specific PCR products was confirmed by melting-curve analysis. Expression analyses of candidate genes were normalized to the geometric mean of the expression levels of three reference genes: ribosomal protein 19L, serine hydroxymethyl transferase and heat-shock protein 90. Analyses were performed with the MCMC.qpcr R package (17) using an *informed* MCMC qpcr model. Results are reported as log₂ fold-changes with *p*-values calculated using the posterior distribution and corrected for multiple testing. Bar graphs of expression values were produced with GraphPad Prism v7.00 software.

Experimental Procedures with Mice. All experiments involving mice were performed using protocols approved by the University of Wisconsin - Madison Animal Care and Use Committee. C57BL/6 mice were maintained in a controlled environment in plastic flexible-film gnotobiotic isolators [germ-free (GF) mice] or filter-top cages [conventionally raised (CONVR) mice] under a strict 12:12 light:dark cycle, and received sterilized water and food *ad libitum*. The sterility of germ-free animals was assessed by incubating freshly collected fecal samples under aerobic and anaerobic conditions using standard microbiology methods. In total, six 8-week-old female mice, three GF and three CONVR, had both left and right eyes collected 5 h after facility lights were turned on. Animals were euthanized by cervical dislocation and were non-fasted at the time of sacrifice. Collected tissue was preserved in RNAlater, left overnight at 4 °C, and shipped frozen to the University of Hawaii at Manoa, where samples were kept at -80 °C until further processing.

RNA Extraction from Mouse Eyes. Total RNA from eye tissue was purified with RNeasy Fibrous Tissue Mini Kit (QIAGEN), immediately followed by treatment with TURBO™ DNase (Ambion) and quantified with Qubit RNA BR assay kit (Invitrogen). The Illumina TruSeq protocol v4.0, TruSeq Stranded RNA kit with Ribo-Zero Gold with polyA selection was done. Sequencing was performed with HiSeq 125 Cycle Paired-End sequencing V4 (New York University, Genome Technology center). Sequencing reads were trimmed and cleaned of adapters with Trimmomatic (7) and then mapped to the mouse genome. Then gene annotations (mm_ref_GRCm38.p4) were derived using TopHat v2.013 (18) with default settings for paired-end samples. Samtools (19) was

used to index and sort the alignments and FeatureCounts (20) in paired-end (-p) exon mode to assign their gene annotations. To identify differentially expressed transcripts the R package edgeR (13) was implemented with a threshold of FDR<0.05 and 2-fold change difference in expression.

Whole-mount Hybridization Chain Reaction, Fluorescence in Situ Hybridization (HCR-FISH) to Detect the Transcript of Atrial Natriuretic-Converting Enzyme. HCR-FISH probes (version3) specific for the host atrial natriuretic-converting enzyme and *V. fischeri* 16S RNA (Table S2) were designed and provided by Molecular Instruments (www.molecularinstruments.org). Juvenile squid were collected 24 h post-colonization under standard procedures explained previously, with the following modifications. After anesthetization with 2% ethanol in seawater, squid were fixed overnight in 4% paraformaldehyde in marine phosphate-buffered saline (mPBS) (3) at 4 °C. The light organs were then dissected out and the hybridization procedure was followed as described in (21), with the following modifications. Probe hybridization was conducted at 37 °C in 30% DNA hybridization buffer (version3; Molecular Instruments). Probe wash buffer (version 3) was used to remove nonspecifically bound probe as specified earlier (21). Samples were counterstained with TO-PRO-3 (Thermo Fisher Scientific) to label host nuclei, and imaged using a Zeiss LSM 710 confocal microscope. Z-stack images of 1024 x 1024 pixels were acquired at acquisition speed 7, with an averaging of 4 images. Fluorescence intensity for all sections of each Z-stack was measured using FIJI (22). The brightness of the final images was adjusted for visual clarity using IMARIS bitplane software.

ACCESSION NUMBERS

The data have been deposited with links to BioProject accession numbers PRJNA473394, PRJNA498343, and PRJNA498345 in the NCBI BioProject database (<https://www.ncbi.nlm.nih.gov/bioproject/>).

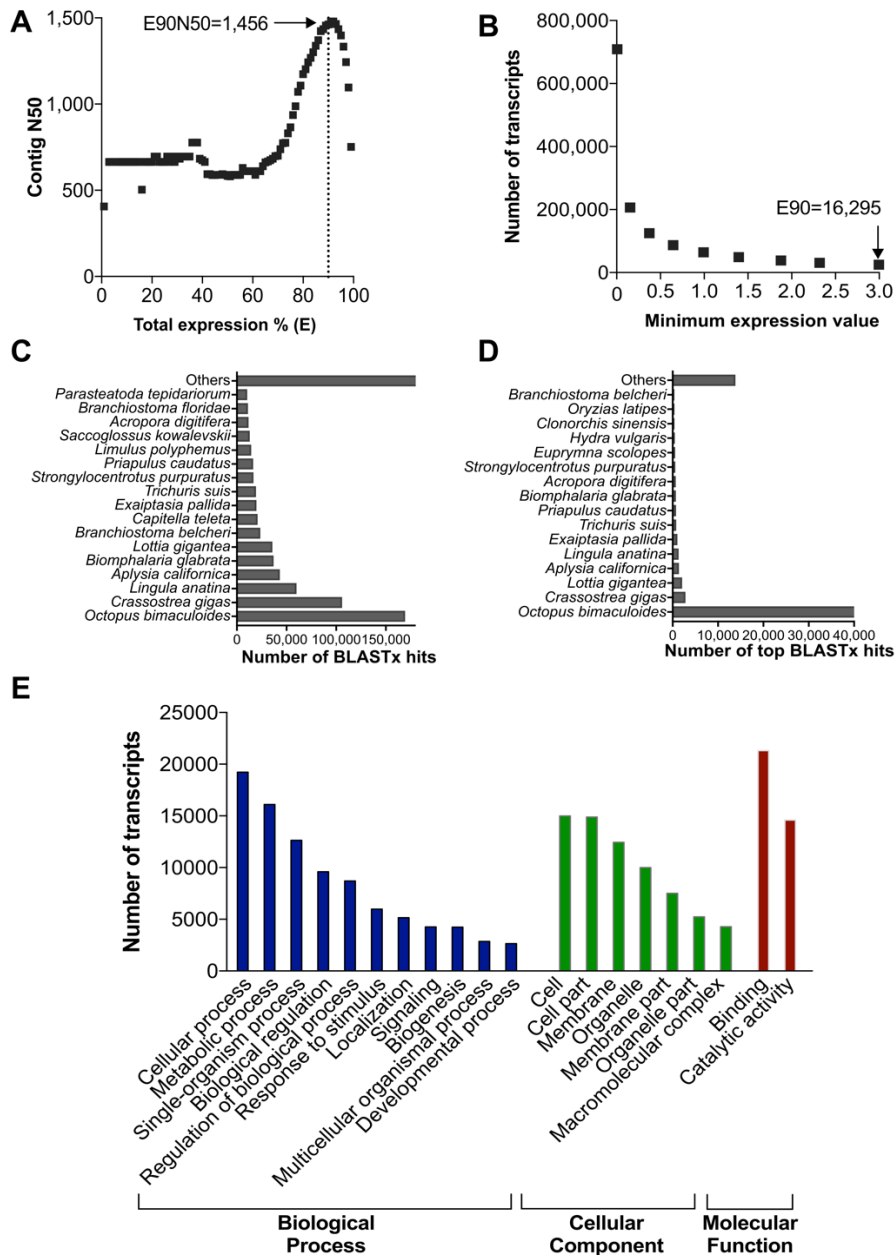


Fig. S1. Assessment of the assembly quality and read representation of the *E. scolopes* transcriptome and its annotation. **A.** The N50 contig value is calculated from the cumulative sets of the top most highly expressed transcripts that represent the total TMM (Trimmed Mean of M-values)-normalized expression data. $E_{90}N_{50} = 1,456$. **B.** The number of most highly expressed transcripts is plotted against the minimum expression value. Ninety percent of the total transcriptional activity is represented by a set of 16,295 transcripts. The expression value is measured as fragments per kilobase million reads (FPKM). **C.** BLASTx species distribution for all blast hits for the squid transcriptome. **D.** Species distribution of blast hits for all top-hit species for the squid transcriptome. To identify homologous genes, the squid transcripts were compared (using BLASTx) against the non-redundant protein database (nr). The E-value cut-off was set at 1.0×10^{-3} . **E.** Functional annotation of *E. scolopes* transcriptome at the 2nd-level GO terms (Dataset S1).

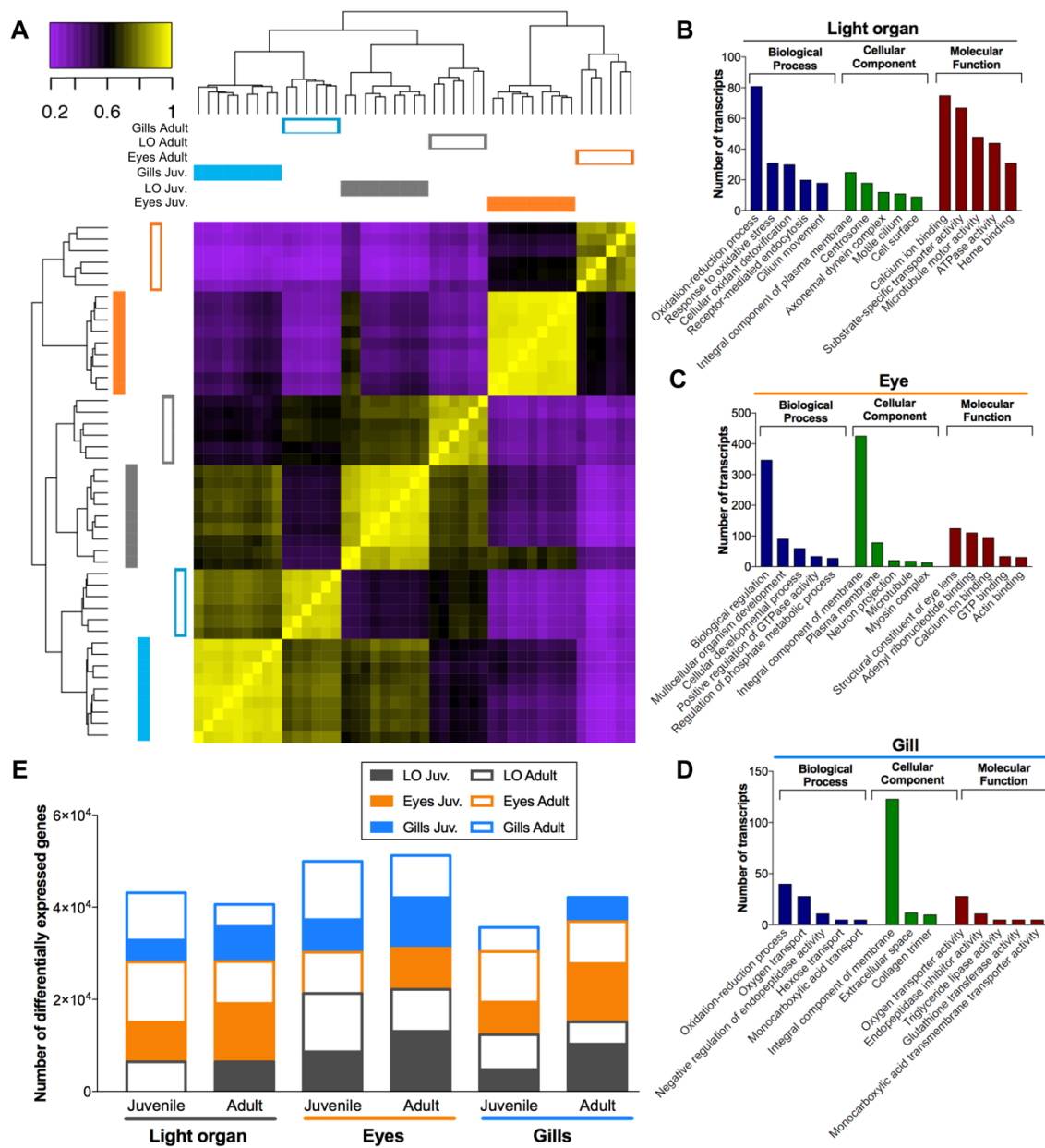


Fig. S2. Data analysis of differentially expressed transcripts across each set of organs, identifying transcripts enriched in specific organs ($P_{adj} < 0.05$, fold-change > 8). **A.** Hierarchically clustered heatmap based on 21,013 differentially expressed genes, visualizing a correlation matrix of the reference transcriptome. **B-D.** Top 5 GO term enrichment for each category. GO enrichment ($p < 0.01$ FDR corrected) for differentially expressed genes in **B.** Light organ, **C.** Eyes and **D.** Gills. **E.** The number of differentially expressed genes in each of the five pairwise comparisons between the three analyzed organs, for each of two developmental stages ($P_{adj} < 0.05$, fold-change > 8). LO= light organ, Juv= 24-h. (Datasets S2 and S3).

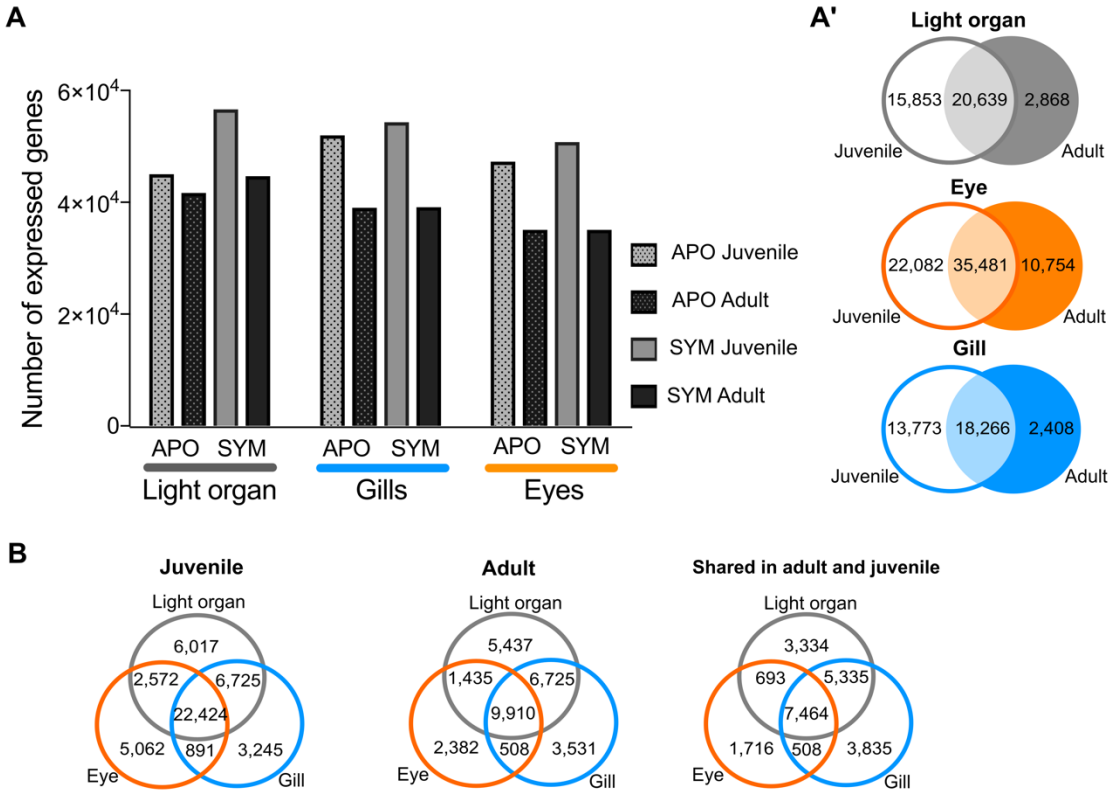


Fig. S3. Symbiosis-responsive genes shared across squid organs and stages of development. A. Summary of distribution of gene abundance across two developmental stages (juvenile and adult) in aposymbiotic (APO) and symbiotic (SYM) individuals. **A'** Venn diagrams of expressed genes shared between juveniles and adults in each organ. A gene is considered expressed when FPKM > 0.5 in at least two samples. **B.** Venn diagrams of shared expressed genes when FPKM > 0.5 in all samples within the comparison. (Dataset S1).

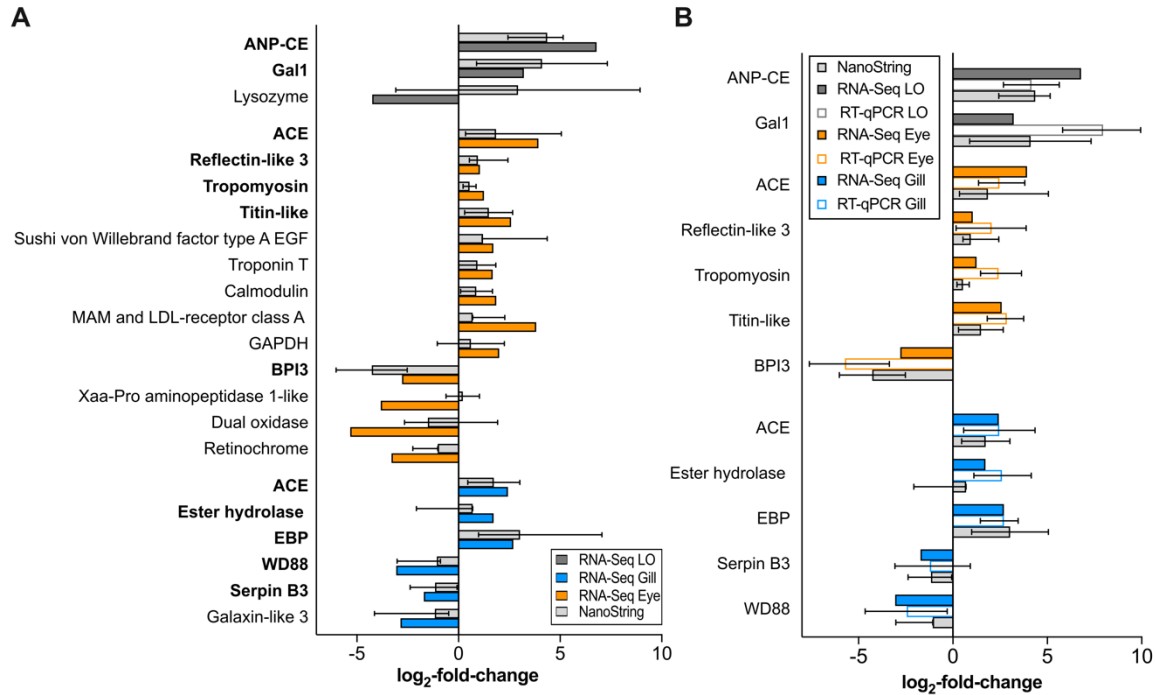


Fig. S4. Validation of adult RNA-seq data by NanoString Technologies. **A.** The \log_2 -fold change values determined by NanoString Technologies validated 21 of the set of 22 differentially expressed genes selected from the mature eye, gill and symbiotic light organ (LO) tissues. Significant correlations between data based on NanoString and RNA-Seq expression profiles were observed (Pearson coefficient correlation of 0.7119, $p < 0.0002$), indicating the reliability of RNA-Seq for gene-expression analyses. In bold, genes co-validated with RT-qPCR. **B.** Comparison of \log_2 -fold change values of transcripts of the same three organs determined by RT-qPCR and NanoString Technologies. (Pearson coefficient of correlation = 0.992, $p < 0.01$). Genes were either up-regulated (+); or, down-regulated (-) with symbiosis. ANP-CE; atrial natriuretic peptide-converting enzyme; ACE: angiotensin-converting enzyme, BPI3: bactericidal/permeability-increasing protein 3; GAPDH: glyceraldehyde-3-phosphate dehydrogenase; Ester hydrolase: ester hydrolase C11orf54 homolog; EBP: emopamil-binding protein; WD88: WD repeat-containing protein 88. Error bars in the NanoString and RT-qPCR expression data represent 95% CI (Dataset S4).

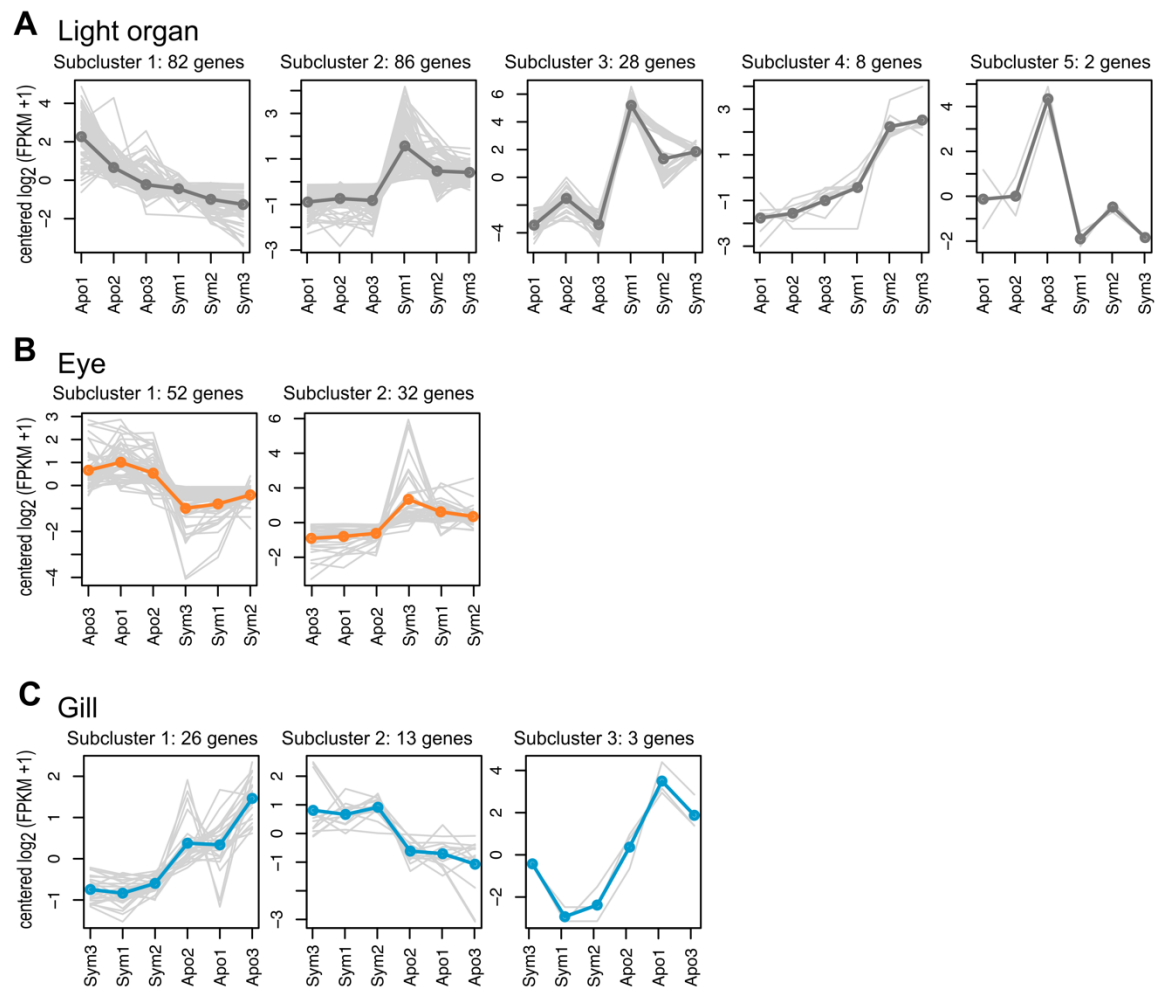


Fig. S5. Patterns of differential gene expression in response to light-organ symbiosis in adult tissues. Differentially expressed genes were grouped into subclusters at 60% of height of the hierarchically clustered gene tree of gene expression. The y-axis gives the median-centered \log_2 FPKM, whereas horizontal axes list the different samples. The gray lines represent all mean expression level for all genes in each sub-cluster in **A.** light organ (dark gray); **B.** eye (orange), and **C.** gill (blue). Sym: symbiotic; Apo: aposymbiotic.

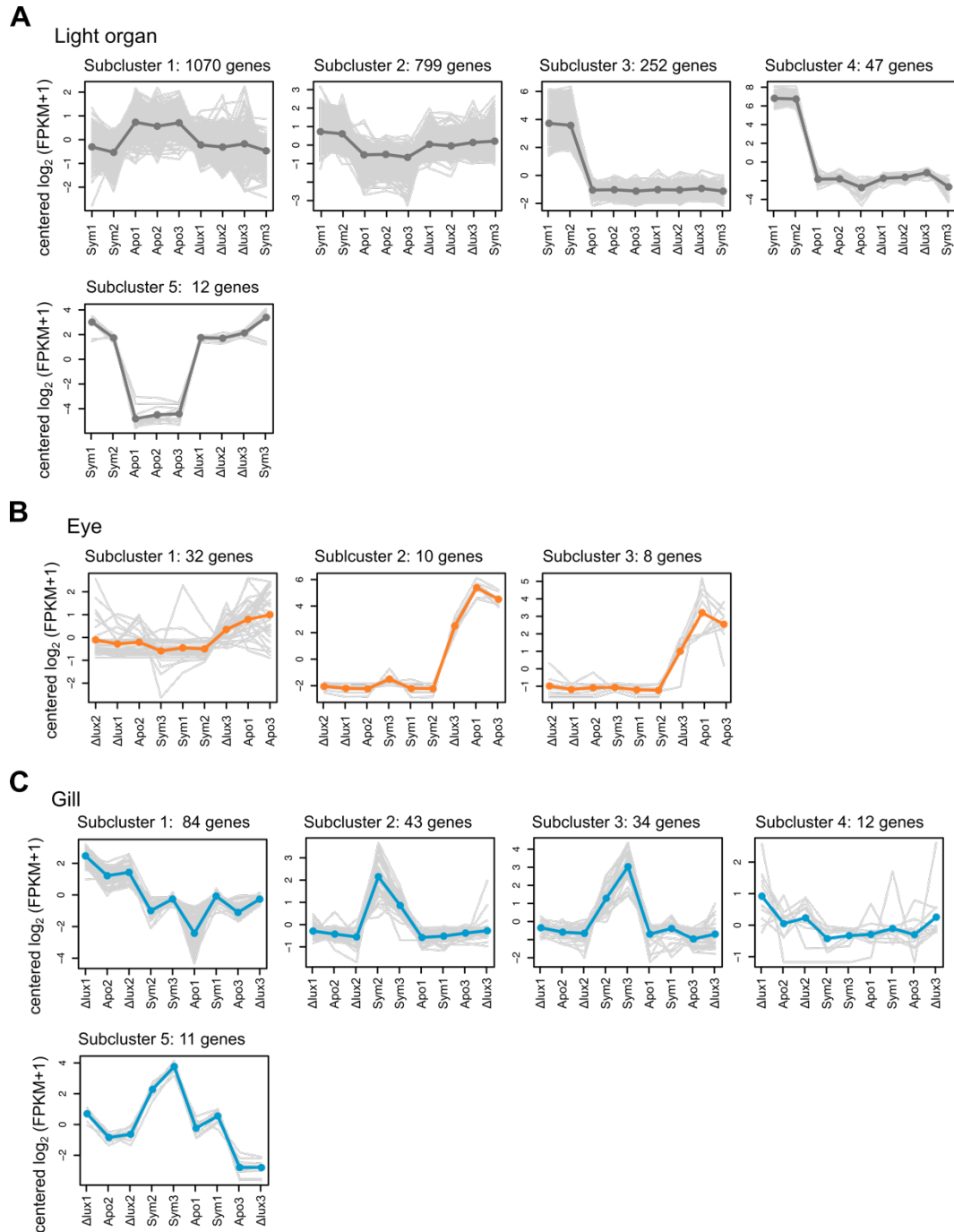


Fig. S6. Patterns of differential gene expression in juvenile tissues in response to light organ symbiosis by luminous and dark bacteria. Differentially expressed genes were grouped into subclusters at 60% of height of the hierarchically clustered gene tree of gene expression. The y-axis gives the median-centered \log_2 FPKM, whereas horizontal axes represent the different samples. The light gray lines represent all mean expression level for all genes in each sub-cluster. **A.** light organ (dark gray), **B.** eye (orange), and **C.** gill (blue). Apo (= APO): aposymbiotic; Sym (= SYM): symbiotic, colonized by the wild-type strain ES114; Δlux (= SYM-dark): symbiotic, colonized by the dark mutant Δlux strain EVS102 (4).

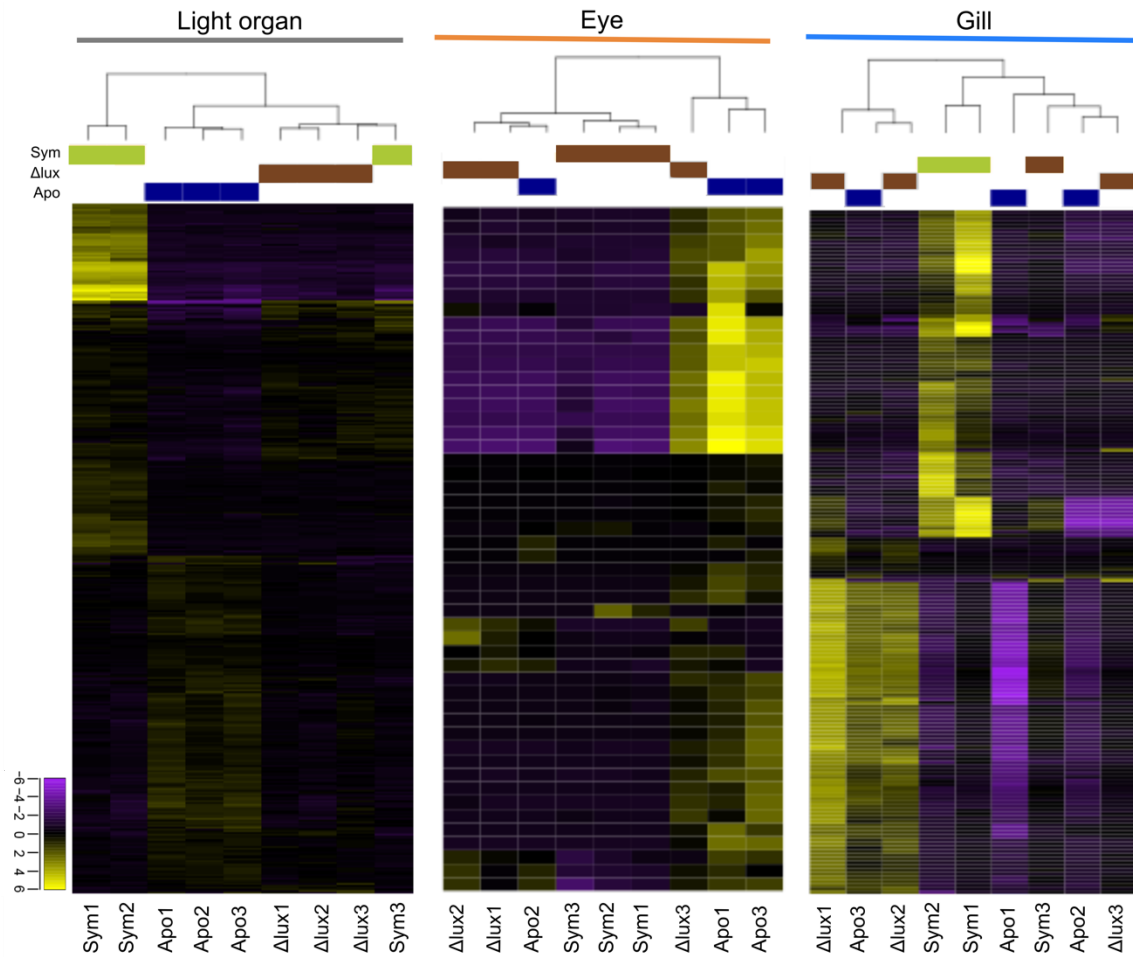


Fig. S7. Transcriptional profiles of juvenile organs in response to light organ colonization by luminous or dark symbionts after 24 h. A heat map of expression values, \log_2 -transformed and median centered, for genes significantly differentially expressed (>2 fold, $P_{\text{adj}} < 0.05$) in juvenile light organ, eye and gill. Apo (= APO): aposymbiotic, (dark blue); Sym (= SYM): symbiotic, colonized with the luminous wild-type strain (in green); Δlux (= SYM-dark): symbiotic, colonized by a dark mutant Δlux strain (in maroon).

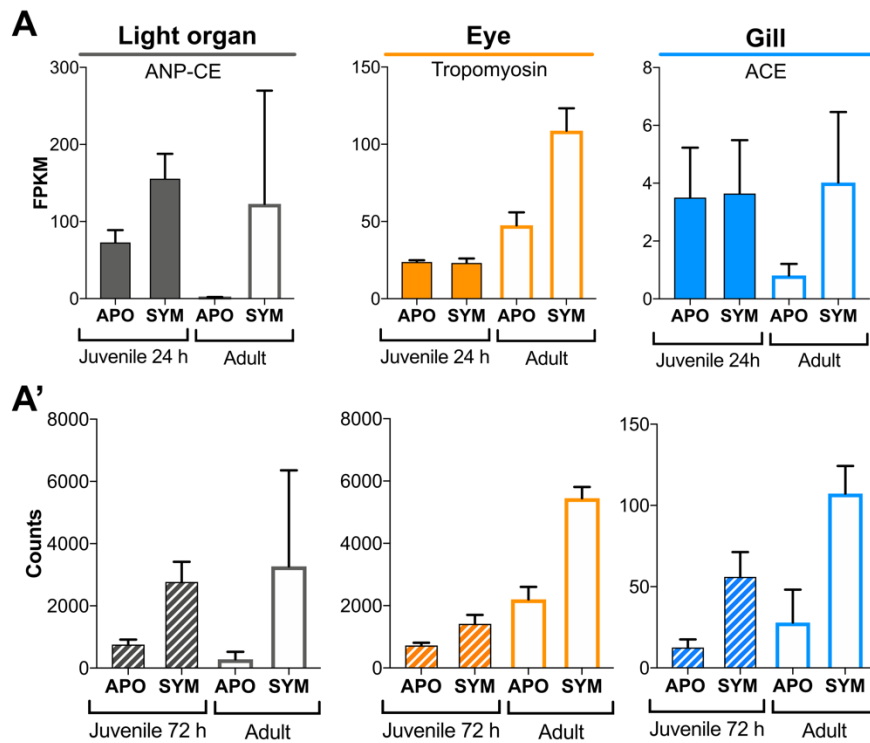


Fig. S8. Examples of symbiosis-responsive gene expression compared between juvenile and adult organs. **A.** Expression of three genes determined by RNA-Seq in 24-h juvenile and in adult animals that had been shown to be differentially regulated in APO and SYM adults, but not in all tissues of 24-h juveniles. **A'.** Expression of the same set of genes determined by NanoString Technologies in 72-h juvenile and in adult animals. APO: aposymbiotic; SYM: symbiotic; ANP-CE: atrial natriuretic-converting enzyme, ACE: angiotensin-converting enzyme.

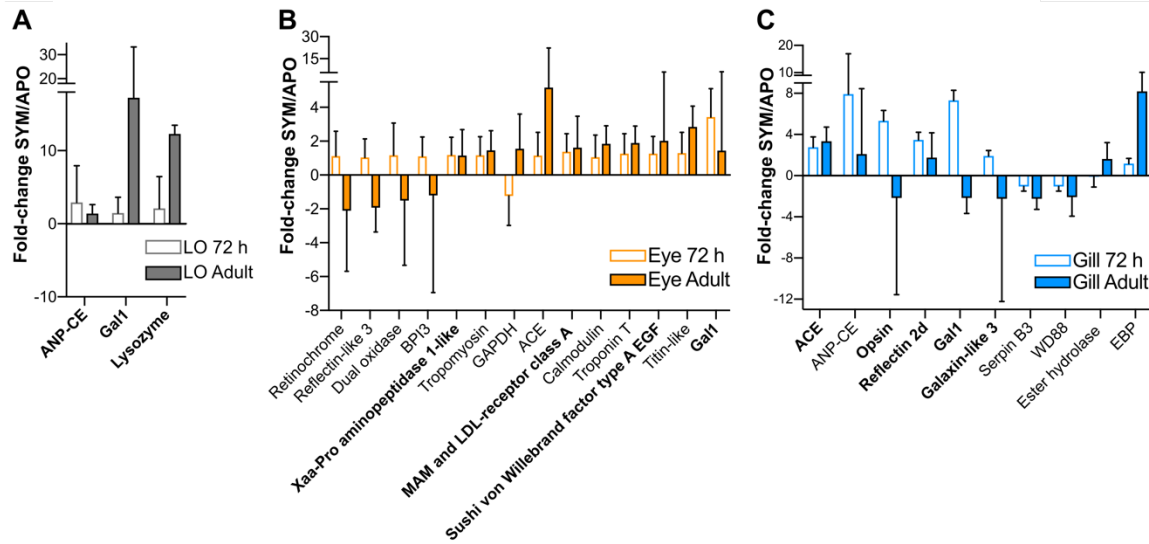


Fig. S9. Differential gene expression early in symbiosis by NanoString Technologies. The \log_2 -fold change (SYM/APO) values determined by NanoString Technologies, comparing expression values of genes in symbiotic and aposymbiotic squid: light organ (LO) (A), eye (B) and gill (C). ANP-CE; atrial natriuretic peptide-converting enzyme; ACE: angiotensin-converting enzyme. BPI3: bactericidal/permeability-increasing protein 3; GAPDH: glyceraldehyde-3-phosphate dehydrogenase; Ester hydrolase: ester hydrolase C11orf54 homolog; EBP: emopamil-binding protein; WD88: WD repeat-containing protein 88. Error bars indicate one standard deviation. In bold shown 72 h significant fold-changes, p -value <0.05 (significance in Dataset S4).

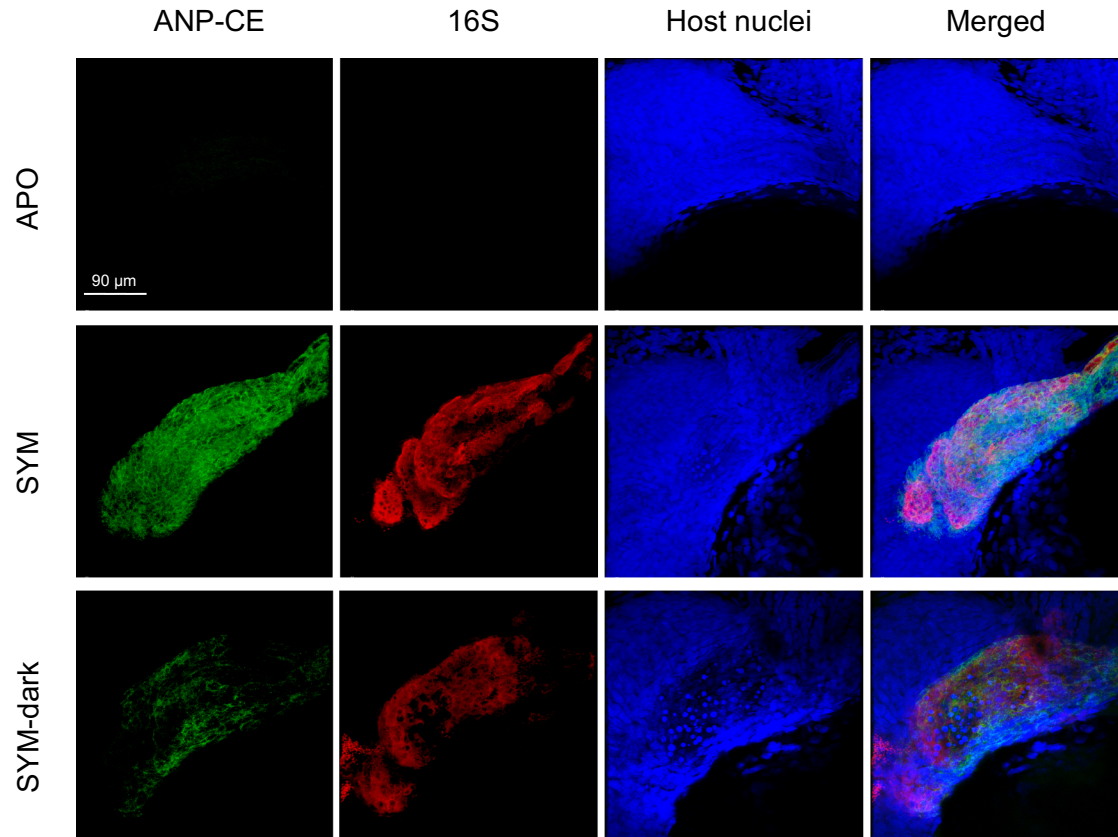


Fig. S10. Visualization of ANP-CE transcript in whole-mount light organs 24 h after colonization. Representative confocal images showing ANP-CE expression in crypt epithelium of APO, or SYM or SYM-dark colonized, juvenile squid; merged mid-section of Z-stack of crypt #1. Separate and merged channels: ANP-CE (green), 16S RNA (symbionts, red) and host nuclei (TOPRO, blue) (Movies S1-S3).

Table S1. Primer list for RT-qPCR

<i>Gene</i>	<i>Primer name</i>	<i>Primer sequence (5' > 3')</i>	<i>Primer reference</i>
<i>S19 ribosomal protein</i>	40S-qF3	AAGGCTTTGTCCA CCTTCCT	This study
	40S-qR3	TAAATGCTCCAAC ACCAGCA	
<i>Serine hydroxymethyl transferase</i>	HMT-qF	GTCCTGGTGACAA GAGTGCAATGA	(23)
	HMT-qR	TTCCAGCAGAAAG GCACGATAGGT	
<i>Heat shock protein 90</i>	HSP90_ F	AGACTGCAAGGCT TCCATAAA	This study
	HSP90_ R	TTCCGAACAAGGA GGACAATA	
<i>Galaxin 1</i>	esgal1_ q2	GAACTCGAATCTG TTGTTCTGGCG	(24)
	esgal1_ R q2	GTTGGTTTCATGG TAACACGGCCA	
<i>Titin-like</i>	titin_ Fq	GCAAAAGTTCTTG GTGCTCA	This study
	titin_ Rq	TTGCAACATCTTT GGGCATA	
<i>Tropomyosin</i>	tropomy_ Fq	ATGCTGACCGGAA GTTTGAC	This study
	tropomy_ Rq	GTTGCCCAACAAC TTCAACT	
<i>Bactericidal/permeability-increasing protein 3</i>	BPI3_ Fq	GCCAAGTTCGAAA TCGTAGC	This study
	BPI3_ Rq	AATCACCAACAAC CGCAGTC	
<i>Reflectin-like 3</i>	Ref13like_ Fq	GACATATCGAAGT ATCTTTCTGGGTA	This study
	Ref13like_ Rq	GACAGGTGGGGAC GTTACTG	
<i>Angiotensin-converting enzyme-like isoform X1</i>	ACE_ Fq	AGGTAATATGTGG GCGCAAG	This study
	ACE_ Rq	CGAAGACGGAGTT TTCCAG	
<i>Galaxin-like isoform X3</i>	galx3_ Fq	ACCCAAACGACAA TTCTTGC	This study

<i>Opsin</i>	galx3_R	CAGAGTTTTTCGC	This study
	q	TGGTTGA	
	opsin2_F	GTAAACGGTTTCC	
	q	CCCTCAT	
<i>Reflectin 2d</i>	opsin2_R	TCTGTGGCTCATA	This study
	q	TGCTTCG	
	Ref2d_F	CAACCCATGTCCC	
	Ref2d_R	GTCCATCATCCAG	
<i>Atrial natriuretic peptide-converting enzyme</i>		CCGTAGT	This study
	ANPq_F	CATTTCCACCAGC	
		CTTCCTC	
	ANPq_R	ATTCGCTTTCGTCC	
<i>WD repeat-containing 88-like</i>		ACAACC	This study
	WD88_F	TGAATGGACACAT	
	q	GGATTGG	
	WD88_R	CGAGGGTTGGTCA	
<i>Emopamil-binding family-containing</i>	q	CTTGAAT	This study
	EBP_Fq	ATGGCAACATGAA	
		CGATTCC	
	EBP_Rq	ATGCAAGAGGGAC	
<i>Ester hydrolase C11orf54 homolog isoform X1</i>		TGTGTGTC	This study
	EsterHy_F	GGATGCACCTTTG	
	q	ATCTGCT	
	EsterHy_R	GGCTCGGTATGAC	
<i>Serpin B3-like isoform X1</i>		ACTTCGT	This study
	serpinB3_F	AGCCAGACAACCTG	
	q	GAAGAGGT	
	serpinB3_R	ATGCGGCTGACTG	
		ATTTGA	

Table S2. HCR-FISH probe sequences

Probe	Amplifier/Fluorophore	Probe sequence
<i>E. scolopes</i> -ANP-CE #1	B1 / Alexa 488	GCTTGCCTTTATCAAACCTGGACAAAA AATATTTCCCTGCATAGAGTCCGAC
<i>E. scolopes</i> -ANP-CE #2	B1 / Alexa 488	AACAGCTGTGCCCCGACAGTCTTTCCC TTGGCGACAACAGTACGTGCTGGTT
<i>E. scolopes</i> -ANP-CE #3	B1 / Alexa 488	TACCACGGTTGTGGACGAAAGCGAAT TGGTGCTCTCCCTTTTGCAGTGGAT
<i>E. scolopes</i> -ANP-CE #4	B1 / Alexa 488	ATCCTAACTCTCTGCAGACAACGTCAG CGTTACTCTGAGACCAATATCCACA
<i>E. scolopes</i> -ANP-CE #5	B1 / Alexa 488	CTGCGGGCTGCATATTGCACGTACACC AAGAGGTGCACTTAGATATGGAGCA
<i>E. scolopes</i> -ANP-CE #6	B1 / Alexa 488	GTCCTGCGGAATGCATTCATAGTTAA GGCATTGGAATTGGTTCCGATCGCA
<i>E. scolopes</i> -ANP-CE #7	B1 / Alexa 488	AACAATGGAATTCATCGGATCCGCTTT TGCAATTTCTGACGCCATCACATTG
<i>E. scolopes</i> -ANP-CE #8	B1 / Alexa 488	AGATGCCTTTACCGCGATAGACGGAT GGACCAACTGAGGCATCTCCTTTTCC
<i>E. scolopes</i> -ANP-CE #9	B1 / Alexa 488	TTTTGTAACCGGGCAATACGGGATTTT TTGCTGCTGCTCCTCTATAGGTA
<i>E. scolopes</i> -ANP-CE #10	B1 / Alexa 488	CATCCTGACCGTATAGGATCATGGGAT CATAAATTTGGAACCTCCGTGTTCC
<i>E. scolopes</i> -ANP-CE #11	B1 / Alexa 488	TACAGTGTGCAGCTGTGAGAACGTGC CATCTGTCAACAATTGCTGCACCACA
<i>E. scolopes</i> -ANP-CE #12	B1 / Alexa 488	CTATCGGCGAAGTCACACGCAATACA GCAATATCGTTGTGCAGTTTCACCTC
<i>E. scolopes</i> -ANP-CE #13	B1 / Alexa 488	GTGGAACCCACGGTTTAGAAGGAAGA CATATGGGTCGGATGTAATCAGTCAT
<i>E. scolopes</i> -ANP-CE #14	B1 / Alexa 488	TCGATGTTTCGATTATTTTGCATGCGTC CCCAACCCGATAGAAAGCATTGCGT
<i>E. scolopes</i> -ANP-CE #15	B1 / Alexa 488	GACCTCTGCAGCCTTTGTGTCCGAAGC TGACGAGTCCAACACTTCCCAATA
<i>E. scolopes</i> -ANP-CE #16	B1 / Alexa 488	GGACCCAACCTTTTCATTGCATAAACAT CGGTAAAGAACAGCGAGTAGTATAC
<i>E. scolopes</i> -ANP-CE #17	B1 / Alexa 488	AGGACCTACCAGCCATTCGTTTTCGGA CTGTTGCTTCCCTCCACTTTATTGT
<i>E. scolopes</i> -ANP-CE #18	B1 / Alexa 488	GCAGGAATCTCCTATTTTCGGCGGTGGA GTTGTCCGCCTCTTGCATCTACTTC
<i>E. scolopes</i> -ANP-CE #19	B1 / Alexa 488	ATGCGTGTAGTCTGATGTAACCTGAGA ACGAGTGTGTTTACTCGGGCGTTTT
<i>E. scolopes</i> -ANP-CE #20	B1 / Alexa 488	GTGCAGGTTTTCGAATAATGCGTCCTG AACGTGTAGTCAGCTGTTGGCTGTC

<i>V. fischeri</i> -16S #1	B3 / Alexa 546	GTTCATTAAGTCAGATGTGAAAGCCC GGGGCTCAACCTCGGAACCGCATTG
<i>V. fischeri</i> -16S #2	B3 / Alexa 546	ACTGGTGAACCTAGAGTGCTGTAGAGG GGGGTAGAATTCAGGTGTAGCGGTG

Caption for Movie S1. Z-stack of confocal microscopy sections from a representative uncolonized (APO) light-organ crypt #1 (see Fig. 4B, top panel, for single image). The tissue was probed by HCR-FISH to localize symbiont 16S (green) and host ANP-CE (red) RNA, and counterstained to show the epithelial cell nuclei (blue).

Caption for Movie S2. Z-stack of confocal microscopy sections from a representative wild-type *V. fischeri* colonized (SYM) light-organ crypt #1, produced from a Z-stack of confocal microscopy images (see Fig. 4B, middle panel, for single image). The tissue was probed by HCR-FISH to localize symbiont 16S (green) and host ANP-CE (red) RNA, and counterstained to show the epithelial cell nuclei (blue).

Caption for Movie S3. Z-stack of confocal microscopy sections from a representative dark-mutant *V. fischeri* colonized (SYM-dark) light-organ crypt #1, produced from a Z-stack of confocal microscopy images (see Fig. 4B, lower panel, for single image). The tissue was probed by HCR-FISH to localize symbiont 16S (green) and host ANP-CE (red) RNA, and counterstained to show the epithelial cell nuclei (blue).

Dataset S1. *E. scolopes* transcriptome gene expression description. [Sheet 1](#): A description of the raw read counts of the samples sequenced in this study for the *E. scolopes* transcriptome. [Sheet 2](#): Trinity Assembly Statistics. [Sheet 3](#): Top-BLAST hits annotation for the *E. scolopes* transcriptome. [Sheet 4](#): Functional annotation for the *E. scolopes* transcriptome.

Dataset S2. Normalized transcript abundance expressed as FPKM.

Dataset S3. Functional enrichment by tissue type. [Sheet 1](#): GO terms enriched in light organ. [Sheet 2](#): GO terms enriched in eye. [Sheet 3](#): GO terms enriched in gill. [Sheet 4](#): summary of the number of enriched genes by tissue type and number of enriched GO terms. [Sheet 5](#): Enriched GO terms in all juvenile tissues. [Sheet 6](#): Enriched GO terms in all adult tissues.

Dataset S4. Host organ gene-expression data obtained by NanoString Technologies codeset. [Sheet 1](#): NanoString Technologies probe sequences. [Sheet 2](#): 72-h juvenile light-organ expression data. [Sheet 3](#): Adult light-organ expression data. [Sheet 4](#): 72-h juvenile eye expression data. [Sheet 5](#): Adult eye expression data. [Sheet 6](#): 72-h juvenile gill expression data. [Sheet 7](#): Adult gill expression data.

Dataset S5. Transcripts identified as differentially expressed in adult squids by edgeR. Sheet 1, 2: light organ, differently expressed transcripts, raw counts, and annotations. Sheet 3, 4: eye, differently expressed transcripts, raw counts, and annotations. Sheet 5, 6: gill, differently expressed transcripts, raw counts, and annotations.

Dataset S6. Functional enrichment in response to symbiosis. Sheet 1: GO terms enriched in light organ symbiosis-responsive genes. Sheet 2: GO terms enriched in eye symbiosis-responsive genes. Sheet 3: GO terms enriched in gill symbiosis-responsive genes. Sheet 4: Top 5 biological processes enriched within each tissue, as indicated in Fig. 2C.

Dataset S7. Transcripts Identified as Differentially Expressed in adult mice eye. Sheet 1: A description of the raw read counts of the samples sequenced in this study for the *M. musculus* eye transcriptome. Sheet 2: Differentially expressed transcripts, raw counts per sample and annotation. Sheet 3: Functional annotation of differentially expressed transcripts.

Dataset S8. Transcripts identified as differentially expressed in juvenile squid by edgeR. Sheet 1, 2: light organ differently expressed transcripts, raw counts, and its annotations in SYM vs APO pairwise comparisons. Sheet 3, 4: light organ differently expressed transcripts, raw counts, and its annotations in SYM-dark (LUX) vs APO pairwise comparisons. Sheet 5, 6: light organ, differently expressed transcripts, raw counts, and its annotations in SYM vs SYM-dark (LUX) pairwise comparisons. Sheet 7, 8: eye, differently expressed transcripts, raw counts, and its annotations in SYM vs APO pairwise comparisons.

Dataset S9. Functional enrichment in response to symbiosis in juvenile squid. Sheet 1: GO terms enriched in juvenile light organ symbiosis-responsive genes. Sheet 2: GO terms enriched in juvenile light organ bioluminescence-specific response. Sheet 3: GO terms enriched in juvenile light organ bacteria-specific response (shared SYM and SYM-dark response). Sheet 4: GO terms enriched in symbiosis-shared response with adult light organ. Sheet 5: GO terms enriched in juvenile eye symbiosis-responsive genes

Dataset S10. Functional gene-set enrichment analysis (GSEA). Sheet 1: Adult light organ GSEA analysis. Sheet 2: Adult eye GSEA analysis. Sheet 3: Adult gill GSEA analysis. Sheet 4: Juvenile light organ GSEA analysis. Sheet 5: Juvenile eye GSEA analysis.

References

1. Naughton LM & Mandel MJ (2012) Colonization of *Euprymna scolopes* squid by *Vibrio fischeri*. *J Vis Exp* (61):e3758.
2. Boettcher KJ & Ruby EG (1990) Depressed light emission by symbiotic *Vibrio fischeri* of the sepiolid squid *Euprymna scolopes*. *J Bacteriol* 172(7):3701-3706.
3. Koch EJ, Miyashiro T, McFall-Ngai MJ, & Ruby EG (2014) Features governing symbiont persistence in the squid-vibrio association. *Mol Ecol* 23(6):1624-1634.
4. Bose JL, Rosenberg CS, & Stabb EV (2008) Effects of *luxCDABEG* induction in *Vibrio fischeri*: enhancement of symbiotic colonization and conditional attenuation of growth in culture. *Arch Microbiol* 190(2):169-183.
5. Graf J, Dunlap PV, & Ruby EG (1994) Effect of transposon-induced motility mutations on colonization of the host light organ by *Vibrio fischeri*. *J Bacteriol* 176(22):6986-6991.
6. Kremer N, *et al.* (2013) Initial symbiont contact orchestrates host-organ-wide transcriptional changes that prime tissue colonization. *Cell Host Microbe* 14(2):183-194.
7. Bolger AM, Lohse M, & Usadel B (2014) Trimmomatic: a flexible trimmer for Illumina sequence data. *Bioinformatics* 30(15):2114-2120.
8. Grabherr MG, *et al.* (2011) Full-length transcriptome assembly from RNA-Seq data without a reference genome. *Nat Biotechnol* 29(7):644-652.
9. Subramanian A, *et al.* (2005) Gene set enrichment analysis: a knowledge-based approach for interpreting genome-wide expression profiles. *Proc Natl Acad Sci U S A* 102(43):15545-15550.
10. Gotz S, *et al.* (2008) High-throughput functional annotation and data mining with the Blast2GO suite. *Nucleic Acids Res* 36(10):3420-3435.
11. Langmead B & Salzberg SL (2012) Fast gapped-read alignment with Bowtie 2. *Nat Methods* 9(4):357-359.
12. Li B & Dewey CN (2011) RSEM: accurate transcript quantification from RNA-Seq data with or without a reference genome. *BMC Bioinformatics* 12:323.
13. Robinson MD, McCarthy DJ, & Smyth GK (2010) edgeR: a Bioconductor package for differential expression analysis of digital gene expression data. *Bioinformatics* 26(1):139-140.
14. de Hoon MJ, Imoto S, Nolan J, & Miyano S (2004) Open source clustering software. *Bioinformatics* 20(9):1453-1454.
15. Vandesompele J, *et al.* (2002) Accurate normalization of real-time quantitative RT-PCR data by geometric averaging of multiple internal control genes. *Genome Biol* 3(7):RESEARCH0034.
16. Untergasser A, *et al.* (2012) Primer3--new capabilities and interfaces. *Nucleic Acids Res* 40(15):e115.
17. Matz MV, Wright RM, & Scott JG (2013) No control genes required: Bayesian analysis of qRT-PCR data. *PLoS One* 8(8):e71448.
18. Kim D & Salzberg SL (2011) TopHat-Fusion: an algorithm for discovery of novel fusion transcripts. *Genome Biol* 12(8):R72.
19. Li H (2011) A statistical framework for SNP calling, mutation discovery, association mapping and population genetical parameter estimation from sequencing data. *Bioinformatics* 27(21):2987-2993.

20. Liao Y, Smyth GK, & Shi W (2014) featureCounts: an efficient general purpose program for assigning sequence reads to genomic features. *Bioinformatics* 30(7):923-930.
21. Nikolakakis K, Lehnert E, McFall-Ngai MJ, & Ruby EG (2015) Use of hybridization chain reaction-fluorescent *in situ* hybridization to track gene expression by both partners during initiation of symbiosis. *Appl Environ Microbiol* 81(14):4728-4735.
22. Schindelin J, *et al.* (2012) Fiji: an open-source platform for biological-image analysis. *Nat Methods* 9(7):676-682.
23. Wier AM, *et al.* (2010) Transcriptional patterns in both host and bacterium underlie a daily rhythm of anatomical and metabolic change in a beneficial symbiosis. *Proc Natl Acad Sci U S A* 107(5):2259-2264.
24. Heath-Heckman EA, *et al.* (2014) Shaping the microenvironment: evidence for the influence of a host galaxin on symbiont acquisition and maintenance in the squid-*Vibrio* symbiosis. *Environ Microbiol* 16(12):3669-3682.

CHAPTER 3

The non-coding small RNA SsrA is secreted by *Vibrio fischeri* to modulate critical host responses

To be submitted to Cell Host & Microbe

Silvia Moriano-Gutierrez^{1,2}, Clotilde Bongrand¹, Tara Essock-Burns¹,
Leo Wu¹, Margaret J McFall-Ngai¹ and Edward G Ruby^{1,3,*}

¹ **Pacific Biosciences Research Center.** University of Hawai‘i at Mānoa; Honolulu; 96813. USA

² Molecular Biosciences and Bioengineering. University of Hawai‘i at Mānoa

³ Lead Contact

*Correspondence: eruby@hawaii.edu

Summary

The regulatory non-coding small RNAs (sRNAs) of bacteria are key elements influencing gene expression; however, there has been little evidence that beneficial bacteria use these molecules to communicate with their animal hosts. We report here that the bacterial sRNA SsrA plays an essential role in the light-organ symbiosis between *Vibrio fischeri* and the squid *Euprymna scolopes*. The symbionts load SsrA into outer membrane vesicles, which are transported specifically into the epithelial cells surrounding the symbiont population in the light organ. While an SsrA deletion mutant (Δ *ssrA*) colonized the host to a normal level after 24 h, it produced only 1/10 the luminescence per bacterium, and its persistence began to decline by 48 h. The host's response to colonization by the Δ *ssrA* strain was also abnormal: the epithelial cells underwent premature swelling, and host robustness was reduced. Most notably, when colonized by the Δ *ssrA* strain, the light organ differentially up-regulated 10 genes, including several encoding heightened immune-function or antimicrobial activities. This study reveals the potential for a symbiont's sRNAs not only to control its own activities, but also to trigger critical responses promoting homeostasis in its host. In the absence of this communication, there are dramatic fitness consequences for both partners.

Keywords

symbiosis, tmRNA, SsrA, cytoplasmic RNA sensing, non-coding RNA, extracellular RNA, outer membrane vesicles.

INTRODUCTION

In host-microbe associations with horizontally transmitted symbionts, the partners must rely upon a predictable and reciprocal biochemical language through which they establish and maintain an often highly specific association, while resisting pathogenic encounters (Douglas, 2018; McFall-Ngai et al., 2010). This communication system typically includes the host's pattern-recognition receptors (PRRs) (Sellge and Kufer, 2015), which sense a series of microbe-associated molecular patterns (MAMPs) (Koropatnick, 2004; Round et al., 2011). As with other, well studied MAMPs, such as lipopolysaccharides (LPS) or peptidoglycan (PGN), nucleic acids can be recognized by PRRs. For example, retinoic-acid inducible gene I (RIG-I)-like receptors (RLR) play a key role in recognizing foreign RNA in the cytoplasm (Goubau et al., 2013; Rehwinkel et al., 2010). In

vertebrates, such RNA activates RIG-I, leading to the induction of innate immune effectors, including type I interferons (IFN) and inflammatory cytokines (Kell and Gale, 2015). Certain invertebrates display characteristic trademarks of vertebrate IFN responses by inducing a non-specific immune reaction (Wang et al., 2015). For example, mollusks, such as oysters, octopus or squid, encode in their genomes homologs of several evolutionary conserved PRRs that sense nucleic acids, as well as other elements involved in signaling-cascade pathways such as RLRs, toll-like receptors (TLRs), and members of the *interferon*-regulatory factor (IRF) family (Albertin et al., 2015; Belcaid et al., 2019; Wang et al., 2012; Zhang et al., 2015). Not surprisingly, expression of these genes is up-regulated in response to infection, indicating that the mollusk antimicrobial signaling pathway is complex and reactive (Green et al., 2015; He et al., 2015).

Intracellular bacterial pathogens like *Legionella pneumophila* and *Listeria monocytogenes* activate the host's innate immune responses (Chiu et al., 2009; Eberle et al., 2009; Lässig and Hopfner, 2017) by releasing RNAs that trigger the type-I IFN pathway through RIG-I signaling (Abdullah et al., 2012; Chiu et al., 2009). Extracellular pathogens also release RNA into their environment (Dorward et al., 1989), often protected within outer membrane vesicles (OMVs) (Bitar et al., 2019; Blenkiron et al., 2016; Choi et al., 2017b; Ghosal et al., 2015; Han et al., 2019; Koeppen et al., 2016; Malabirade et al., 2018; Zhang et al., 2020). This RNA is mainly non-coding (ncRNA), such as regulatory small RNAs (sRNAs) (Dauros-Singorenko et al., 2018) that can gain access to host cytoplasm when they are released from their OMVs (Keegan et al., 2019; Song et al., 2008). Interestingly, while the nature of MAMPs like PGN or DNA is likely to remain the same regardless of the bacterium's physiological state, the suite of different sRNAs produced provides an indicator of the cell's metabolism and growth rate (Chen et al., 2019; Ugolini and Sander, 2018). Thus, by recognizing which RNAs are present, the host might shape its responses according not only to the identity, but also to the physiological state, of the bacteria encountered (Barbet et al., 2018; Sander et al., 2011; Vabret and Blander, 2013).

Compared to these pathogenic interactions, there are very few reports describing ncRNA signaling between beneficial microbes and their hosts (Ren et al., 2018; Silvestri et al., 2019). While it is well established that an animal's microbiome is critical to its health and development, little has been reported about these beneficial bacteria using ncRNA communication to initiate and maintain these associations, possibly because they are so phylogenetically complex and difficult to visualize. In contrast, the monospecific light-organ symbiosis between the Hawaiian bobtail

squid, *Euprymna scolopes*, and the marine bioluminescent γ -proteobacterium *Vibrio fischeri* offers an experimentally accessible model system for discovering how ncRNAs produced by a beneficial symbiont can be sensed by the host and modulate its responses. This association begins when a newly hatched juvenile squid is colonized by planktonic *V. fischeri* cells that enter pores on the surface of the nascent light organ, proceeding down a migration path that ends at epithelium-lined crypt spaces (Figure 1A). Once there, the bacteria proliferate on host-provided nutrients (Schwartzman et al., 2015; Wier et al., 2010), and induce bioluminescence used by the squid in its behavior (Jones and Nishiguchi, 2004). The initiation of this highly specific association occurs within hours, and involves a carefully choreographed exchange of signals (McFall-Ngai, 2014) that change gene expression in both partners (Morianio-Gutierrez et al., 2019; Thompson et al., 2017).

Like other Gram-negative bacteria, *V. fischeri* continuously produces OMVs, and these vesicles trigger host responses during symbiosis (Aschtgen et al., 2016). In this study, we report the profile of RNAs carried in these OMVs, including a ncRNA called SsrA, and identify and visualize SsrA within the crypt epithelial lining. SsrA is a small stable RNA molecule that, together with its required chaperon, SmpB (Karzai et al., 2000), participates in the ribosome rescue system of many bacteria by tagging partially synthesized proteins for degradation (Bhaskarla et al., 2018; Muto et al., 1996). By comparing the host's responses to colonization by either the wild-type strain or its Δ *ssrA* derivative, we determined that the absence of signaling by SsrA within host cells has dramatic consequences for the partnership. *V. fischeri* cells that produce OMVs lacking SsrA do not persist in the light organ, and, in the absence of SsrA, the colonization leads to a heightened immune response and a loss of host robustness. Taken together, these data demonstrate the first example of a symbiont using its sRNA to modulate responses in its animal host, and reveal the potential for functional RNA molecules to be key elements in the language of beneficial host-microbe associations.

RESULTS

The Bacterial sRNA SsrA Is Found within OMVs.

In a recent study (Morianio-Gutierrez et al., 2019), we reported that symbiotic colonization resulted in transcriptional changes not only in the light organ, but also in the expression of host genes in anatomically remote organs. To begin to understand the mechanisms underlying those

distal responses, we analyzed the haemolymph of adult squid to detect signal molecules being sent through the body via the circulation. One such RNA-seq study (PRJNA629011), revealed sequences that unexpectedly mapped against the *V. fischeri* genome. This finding indicated that the haemolymph of symbiotic squid carried RNAs produced by the bacterial population of the light organ. Specifically, 166 *V. fischeri* open reading frames (ORFs) were identified, the majority being tRNAs (74%) and ribosomal RNA (22%), with a lesser complement of small ncRNAs (4%) (Table 1, Figure 1B, Supplementary File 1). These latter small ncRNAs (sRNAs) were of particular interest to us because this class contains important regulators of gene expression and other cellular activities (Gottesman, 2004). Among these, the bacterial translation quality-control molecule, SsrA, was the most abundant in the haemolymph (Table 1).

When OMVs were isolated from a culture of the light-organ symbiont *V. fischeri* strain ES114 (Boettcher and Ruby, 1990), RNAs encoding 73 genomic regions were identified in their contents by Illumina sequencing. The majority of these reads also mapped to ribosomal RNA and tRNA genes (Figure 1B). The remaining RNAs in OMVs were sRNAs (Figure 1B) and, as with the haemolymph samples, SsrA was one of the major species in both *V. fischeri* cells and their OMVs (Table 1) regardless of the growth medium (Figure S1A,A').

In summary, *V. fischeri* symbionts continuously release OMVs containing SsrA into the crypt environment (Aschtgen et al., 2016; Kuehn and Kesty, 2005), from which they may find their way into the circulation. To determine whether this release plays a regulatory role in the light organ, we constructed a *V. fischeri* clean-deletion mutant of *ssrA* ($\Delta ssrA$), whose OMVs differed only in the absence of SsrA (Figures 1C and S1B); similarly, the major species of proteins (Lynch et al., 2019) in OMVs from the two strains were indistinguishable (Figure S1C). When compared to its wild-type (WT) parent, the *V. fischeri* $\Delta ssrA$ mutant had no growth deficiency in either rich or minimum media (Figure S2A), had similar rates of motility (Figure S2B) and respiration (Figure S2C), and initiated colonization, but failed to persist, as well as WT (Figure 2A). Thus, the absence of SsrA has little effect on *V. fischeri* physiology, but may compromise symbiotic homeostasis.

Symbiont SsrA Localizes within the Crypt Epithelium of the Light Organ.

To better understand the occurrence of SsrA within host tissues, we contrasted its absence in the $\Delta ssrA$ mutant (Figure S2D) to its localization in light organs colonized by either the WT parent or the genetic complement ($\Delta ssrA + ssrA$). Using HCR-FISH (see STAR METHODS),

SsrA transcripts were found in WT-colonized crypts (Figure 1B; upper panels) while no signal was detected in Δ *ssrA*-colonized ones (Figure 1B, lower panels). Surprisingly, SsrA was observed not only inside the symbiont cells, but also within the epithelial cell-layer that directly contacted the symbionts. After the majority of the symbionts were vented from the crypts, the signal disappeared within minutes (data not shown), suggesting that the transcript must be continuously delivered to maintain its level within host cells. A higher magnification (Figure 1C) revealed abundant SsrA within the cytoplasm (but little detected in the nucleus) of crypt epithelial cells. In addition, other non-coding RNAs found within OMVs, such as 16S rRNA, were also observed within host epithelium (Figure S3), indicating that the epithelial cells contacting the symbionts may be particularly susceptible (Cohen et al., 2020) to taking up bacterial OMVs and their RNA cargo.

The Δ *ssrA* Mutant Initiates Symbiosis Normally, and Can Trigger Typical Host Responses.

We next asked whether host cells exhibited any SsrA-dependent responses during the initiation of symbiosis. For instance, colonization by *V. fischeri* cells causes symbiont-induced morphogenesis in the light organ (McFall-Ngai, 2014), including (i) trafficking of macrophage-like haemocytes into the blood sinus of the ciliated epithelial appendages (Figure 1A, middle), induced principally by the PGN monomer (Koropatnick et al., 2007), and (ii) apoptosis in these appendages, triggered primarily by the lipid-A portion of LPS (Foster et al., 2000). The presence of both these MAMPs works synergistically on the two events, which in nature result from colonization, or by exposure to *V. fischeri* OMVs (Aschtgen et al., 2016). When we compared a colonization by the Δ *ssrA* mutant and its WT parent, or a 3-h exposure to OMVs isolated from those two strains, we observed no difference in either haemocyte trafficking (Figure 2B-C) or apoptosis (Figures 2D and S4). Thus, the Δ *ssrA* mutation has no qualitative effect on the bacterium's production of these two MAMPs.

The Δ *ssrA* Mutant Initiates Several Abnormal Symbiotic Responses.

WT- and Δ *ssrA*-colonized light organs contained the same number of symbionts by 24 h (Figure 2A); however, Δ *ssrA*-colonized animals emitted only 1/10 the luminescence (Figure 2E). Nevertheless, when each symbiont population was released from its light organ, the light emission produced per bacterium was comparable. This result indicated that, while the Δ *ssrA* symbionts

have the same luminescence potential as WT, when they are within the light organ their light emission is constrained, possibly due to oxygen limitation (Ruby and McFall-Ngai, 1999).

Another symbiosis-triggered host response is an increase in the volume of the crypt epithelial cells that requires that the symbionts not be ‘dark’ mutants (Visick et al., 2000). To determine whether symbionts lacking SsrA still induced this cell swelling, we compared the cytoplasmic cross-sectional area of epithelial cells in light organs colonized by the WT, Δ *ssrA* or, as a negative control, a non-luminescent Δ *lux* strain. Unlike the Δ *lux*, at 48 h post colonization both WT- and Δ *ssrA*-colonized squid exhibited normal crypt-cell swelling relative to aposymbiotic animals (Figure 3A,A’). In contrast, after 24 h, only light organs colonized by Δ *ssrA* cells had an increased cytoplasmic area, showing that colonization by a symbiont that produces no SsrA induced a significantly earlier swelling of the crypt epithelium.

Symbiont-induced changes in light-organ gene expression occur within a few hours of colonization (Chun et al., 2008; Moriano-Gutierrez et al., 2019). To investigate whether this transcriptional response is influenced by the presence of SsrA, we performed a comparative RNA-seq analysis on WT- and Δ *ssrA*-colonized light organs 24 h after colonization. Compared to WT-colonized animals, 10 host genes were significantly up-regulated in the Δ *ssrA*-colonized organs, including typical microbe-responsive genes with known immune-function or antimicrobial activities. These genes encoded laccase-3, a galaxin-like protein and chitinases, among others (Figure 3B, Supplementary File 2), and their induction suggested that the host treats the Δ *ssrA* colonization as an undesirable infection.

Because laccase-3 encodes an extracellular enzyme involved in the synthesis of melanin, a key component of the invertebrate immune response to pathogens (Luna-Acosta et al., 2017), we asked where this transcript occurred within the light organ. At 24 h post-colonization, the laccase-3 transcript is localized to the crypt epithelium (Figure 3C) in direct contact with the symbionts (Figure 1A). While the HCR signal for laccase-3 is downregulated after colonization by an SsrA-producing strain (Figure 3C,C’), the epithelium’s laccase-3 expression remains high if the symbiont fails to produce SsrA. These findings were validated by qRT-PCR (Figure 3D). Thus, delivery of SsrA into the crypt epithelium appears to be required to down-regulate the expression of this, and possibly other, immune defenses.

The Absence of SsrA Signaling, but not SsrA Activity in the Symbiont, Weakens the Host.

In the bacterial cell, SsrA requires its chaperone, SmpB, to function as part of the stalled-ribosome rescue system (Karzai et al., 2000). We used this dependency to ask whether the function of SsrA within the symbiont is necessary to induce the SsrA-dependent host responses, by constructing a clean-deletion mutant of *smpB*. Like Δ *ssrA* cells, the Δ *smpB* mutant had no growth defect in culture (Figure S2A), but it expressed normal levels of SsrA (Figure S2D) that accessed the cytoplasm of crypt epithelia (Figures 4A and S5A) similarly to WT (Figures 1D-E and S3). Thus, colonization with the mutant results in SsrA delivery to the host without SsrA function in the symbiont, and any host response to Δ *ssrA* that is not also evoked by Δ *smpB* is likely due to a direct, signal-like, activity of SsrA within the host.

Due to the early cell swelling and immune-like transcriptional responses of crypt epithelial cells colonized by Δ *ssrA* symbionts, we sought to determine whether the absence of cytoplasmic SsrA in the epithelium compromised the host's health and, if so, whether SsrA was acting directly. To address these questions, we performed a survival assay on juvenile hatchlings that were colonized either by WT, Δ *ssrA*, Δ *ssrA* + *ssrA*, or Δ *smpB* strains. Those squid colonized by Δ *ssrA*, but not Δ *smpB*, had a survival defect relative to WT-colonized squid (Figures 4B and S5B), indicating that the absence of SsrA within the crypt epithelium, and not the lack of SsrA activity within symbiont cells, compromised the survival of the host. In a similar experiment, the expression of laccase-3 transcript within the Δ *smpB*-colonized light organ was down-regulated like WT, rather than unregulated, as with Δ *ssrA* (Figure S6A, A'). Interestingly, the absence of this down-regulation in the Δ *ssrA*-colonized epithelium was not rescued by the SsrA within externally provided wild-type OMVs (Figure S6B), indicating that curbing the expression of this immune-defense enzyme likely requires that SsrA be delivered from the symbiont population within the crypts.

Because an increased immune response can be expected to impose an energetic cost on the host, as a proxy for such increased metabolic activity, we measured the weight loss of juvenile squid between hatching and 4 days post-colonization by either WT, Δ *ssrA*, or Δ *lux*. The latter strain is included as a control because, like Δ *ssrA*, Δ *lux* is unable to maintain a normal colonization level after the first 24 h (Koch et al., 2014). We found that animals colonized by the Δ *ssrA* mutant lost weight more rapidly than either aposymbiotic animals or symbiotic animals colonized by WT or Δ *lux* (Figure 4C). To assure that the differential in weight loss was not due simply to a difference in the activity level of juveniles colonized by the different strains, the respiration rates of the squid

were measured. We found that the rate of oxygen consumption was indistinguishable between newly hatched animals or animals colonized for 48 h by WT, Δlux or $\Delta ssrA$ (Figure S5C). Thus, neither establishing the symbiosis (i.e., APO vs. WT) nor losing the symbiont (i.e., WT vs. Δlux) significantly impacted the weight of the juveniles; however, the absence of SsrA (WT vs. $\Delta ssrA$) did.

In cephalopods, an internal yolk sac provides a reservoir of nutrients that is used by juveniles after hatching (Boletzky, 2003; Vidal et al., 2002). The animal's observed weight loss over the first four days post-hatch (Figure 4C), led us to ask whether there was a more rapid depletion of these stored nutrients by $\Delta ssrA$ -colonized squid. Because of its high lipid content, the size of the yolk sac could be estimated by confocal microscopy using a lipophilic stain (Figure 4D, see STAR METHODS). We found that after 2 days of colonization, in $\Delta ssrA$ -colonized animals the yolk sac significantly decreased not only in area, but also to a significantly greater extent (Figure 4D') as confirmed by scanning electron microscopy (Figure 4E). Further, when comparing the yolk sac's size in 2 day-old juveniles, only those colonized by $\Delta ssrA$ had a significantly smaller yolk sac (Figure S5D), indicating that it is neither the lack of SsrA activity within the symbionts nor the decrease in their number, but instead the failure to deliver SsrA to the host, that leads to its faster depletion of yolk-sac resources.

SsrA Is Detected Through Host Cytosolic RNA Sensors

The range of distinct host phenotypes observed with $\Delta ssrA$ symbionts suggested that, to trigger normal symbiosis development and persistence, the presence of cytoplasmic SsrA (Figure 1E) must be sensed by the crypt epithelial cells. Therefore, we asked whether the expression of host cytosolic RNA sensors might normally respond to this SsrA but, in its absence, the lack of this response might contribute to the host's aberrant phenotypes. We further hypothesized that SsrA is delivered into host cells by the uptake of sRNA-containing symbiont OMVs. Haemocytes, the immune effector cells of mollusks, are professional phagocytes and take up symbiont OMVs not only in culture (Aschtgen et al., 2016) but also in haemocytes observed within the crypts (Figure 5A). Using isolated host haemocytes as a simplified model, we determined the changes in gene expression triggered by OMV-delivered SsrA (see STAR METHODS) Because a change in the levels of complement protein 3 (C3) (Castillo et al., 2009) is a highly conserved innate-immunity reaction, we used an increased expression of its transcript as a positive control for OMV

detection. However, to determine the specific nature of the response, we monitored the expression of the cytosolic-RNA sensor RIG-I, and the IL-17 associated adapter protein CIKS (Rosani et al., 2015). As expected, haemocyte expression of C3 was up-regulated after exposure to either WT or Δ *ssrA* OMVs, indicating that both types of OMVs were sensed (Figure 5B); however, only haemocytes that were exposed to WT OMVs responded with a significant increase in RIG-I expression. In contrast, those that were presented with Δ *ssrA* OMVs increased their expression of CIKS, instead. The differential transcriptional response of host haemocytes to SsrA-containing OMVs suggests that they induce an immune response through the RIG-I pathway that is missing in Δ *ssrA* OMV-exposed haemocytes (Figure 5C).

DISCUSSION

A fundamental characteristic of host-microbe interactions is the reciprocal signaling that allows an animal or plant host to distinguish between beneficial symbionts and potential pathogens, and respond appropriately. Here, we identify the small RNA SsrA as a novel molecular signal that modulates an animal host's response to its beneficial microbial partner. SsrA produced by symbiotic *V. fischeri* enters host epithelial tissue that surrounds the symbionts (Figure 1D-E), and induces changes in light-organ gene expression (Figure 3B), dampening the host's immune response. In the absence of this signal, the host's normal recognition of its symbiont is impaired and, as a consequence, the host apparently perceives the presence of the symbiont as a danger signal, resulting in a heightened immunological response. Thus, the ability of symbionts to modulate host defenses properly by transmitting an sRNA signal is a key element underlying homeostasis and persistence.

Bacteria Deliver sRNA through OMVs

The regulatory activities of extracellular RNA have been studied extensively in recent years (Akat et al., 2018; Caruana and Walper, 2020; Choi et al., 2017a), and a common theme is that OMVs provide a mechanism for safely delivering such cargo molecules to nearby cells. As in other species (Biller et al., 2014; Blenkiron et al., 2016; Ghosal et al., 2015), rRNA and tRNA are the major RNA classes present in *V. fischeri* OMVs (Figure 1B). The third abundant class, the small-RNA (sRNA) component, often includes SsrA, SsrS and/or CsrB (Koeppen et al., 2016; Malabirade et al., 2018). The packaging of these particular sRNAs into OMVs is a shared

characteristic among different bacteria, perhaps because: (i) they are among the most highly expressed sRNAs, and/or (ii) their localization within the bacterial cell may facilitate packaging (Nevo-Dinur et al., 2012). In any case, *V. fischeri* OMVs and their sRNA cargo readily transit from the symbionts into the epithelial cells of the light organ (Aschtgen et al., 2016; Cohen et al., 2020) and, from there, may cross into the host's vascular system as reported for other animals (Park et al., 2017). Significantly, while the symbionts traverse a long epithelium-lined migration path on their way to the crypts (Figure 1A), these cells show a high degree of localized functional differentiation (Esseck-Burns et al., 2020), with only the epithelium lining the crypt becoming labeled with SsrA (Figure S3). We conclude that the crypt epithelium may be particularly susceptible to signals presented by symbiont-derived OMVs and secreted molecules (Cohen et al., 2020).

Bacterial RNA Regulates Host Immune Responses

As with their response to other MAMPs, host cells identify and react immunologically to the presence of bacterial ncRNAs. When the microbe encountered is a pathogen, the host's goal is to heighten its defenses; e.g., bacterial rRNAs induce a major immunostimulatory reaction through specialized TLRs of dendritic cells and macrophages (Eberle et al., 2009; Li and Chen, 2012), and tRNA from *Mycobacterium tuberculosis* induces the production of the immune effector IL-12 in blood mononuclear cells (Keegan et al., 2019). However, a pathogen can also use ncRNAs to evade host responses; e.g., sRNAs delivered through OMVs by *Pseudomonas aeruginosa* attenuate the secretion of IL-8 by mammalian epithelia (Koeppen et al., 2016). Likewise, pathogen-derived sRNAs can both curb T-cell cytokine production (Choi et al., 2017b), and down-regulate cytokines when delivered via OMVs (Han et al., 2019).

To successfully initiate a symbiotic association, beneficial bacteria must similarly restrain the immune system of their host; for example, certain plant symbionts use sRNAs to control host responses and foster a cooperative colonization (Ren et al., 2018; Silvestri et al., 2019). However, while some symbionts can inhibit an animal's immune system, no example of such bacteria using RNA to achieve this outcome has been reported, except after genetic engineering (Leonard et al., 2020). Instead, other mechanisms have been described, e.g., zebrafish immunomodulate their response to symbiotic aeromonads that produces a lipocalin-like molecule (Rolig et al., 2018) and, in the mammalian gut, *Faecalibacterium prausnitzii* promotes health by inducing IL-10 (Rossi et

al., 2016). During colonization of the squid light organ, *V. fischeri* down-regulates several antimicrobial immune responses in the host, including phagocytosis (Nyholm et al., 2009), and the production of nitric oxide (Davidson et al., 2004) and halide peroxidase (Small and McFall-Ngai, 1999). Nevertheless, the mechanisms for achieving these and other responses resulting in symbiotic homeostasis have remained unexplained.

Symbionts Defective in SsrA Signaling Produce a Dysfunctional Association

As in the reaction to some pathogenic infections (Mogensen, 2009), symbiont colonization of the light organ results in a several-fold increase in the cytoplasmic volume of the crypt epithelium (Visick et al., 2000). Colonization by Δ *ssrA* bacteria induces swelling significantly earlier than WT (Figure 3A), suggesting that the absence of SsrA signaling generates a dysregulated host response. In addition, we found that, while laccase-3 expression (Figure 3B-D), which is a key component of the invertebrate immune response to pathogens (Luna-Acosta et al., 2017), is down-regulated by WT colonization, after Δ *ssrA* colonization, expression of this antimicrobial remains at high levels. These results indicate that Δ *ssrA* symbionts do not suppress the program of host immune response that WT symbionts do. Further, the Δ *ssrA* population produced only 1/10 the luminescence per cell when within the light organ (Figure 2E), suggesting a limited availability of oxygen to drive the luminescence reaction. We hypothesize that the increased oxidase activity (Mate and Alcalde, 2017) resulting from the higher laccase concentration within Δ *ssrA*-colonized crypts (Figure 5C) depletes tissue oxygen that otherwise would be available for symbiont light production.

These data suggest that, if SsrA is absent from its epithelium, the host responds to *V. fischeri* as a pathogen. Immunological rejection of a pathogen requires a substantial commitment of cellular resources. For instance, when activated, macrophages use ATP more rapidly (Newsholme and Newsholme, 1989), and defending against a septic infection increases energy demand by 30% (Carlson et al., 1997; Kreyman et al., 1993). Because of the heightened immune response to a Δ *ssrA* symbiont, we used a survival assay to assess the health of mutant-colonized squid compared to those colonized by WT. We hypothesized that the effort to reject the Δ *ssrA* symbiont entails a cost for the host. Supporting this assumption, there was a significantly greater rate of depletion of the juvenile's internal yolk sac (Figure 5D-E), leading to an overall faster loss of weight by the host (Figure 5C), when colonized by the mutant.

While not yet fully understood, the mechanism by which the SsrA molecule impacts the host appears to be direct, rather than indirect through its activity within the symbionts. *V. fischeri* encodes a second ribosome-rescue system, ArfAB (Garza-Sánchez et al., 2011), allowing the normal growth of both the Δ *ssrA* mutant and a mutant in SsrA's specific chaperon, SmpB, (Figure S2A). This result, together with the normal responses to the Δ *smpB* mutant (Figures 4B, S5D and S6A), provide strong evidence that a critical part of initiating a stable symbiosis is that the host sense, and respond specifically to, the SsrA signal entering the crypt epithelium.

OMV-delivered SsrA May Regulate Immune Responses through RIG-I

Mechanisms underlying the impact of bacterial sRNA on host cells have been successfully investigated through the use of tissue culture models (Choi et al., 2019). In the same way, we used isolated squid haemocytes as a proxy for the less easily manipulated crypt epithelial cells. These studies demonstrated a different transcriptional response to the delivery of RNA by OMVs produced by either WT or the Δ *ssrA* mutant, whose only detectable difference in RNA content (Figure 1C and S1B) is in the presence of SsrA. The SsrA-dependent induction of the gene encoding RIG-I (Figure 5B) leads us to speculate that (i) a functional RIG-I signaling pathway exists in the Hawaiian bobtail squid, and (ii), as in other mollusks challenged with viral RNA (Huang et al., 2017), the up-regulation of RIG-I indicates that this RNA-sensor protein is involved in the recognition of symbiont SsrA. In vertebrates, RIG-I activates NF- κ B and IRF transcription factors, which coordinately regulate the expression of type-I IFNs (Seth et al., 2005). Although no IFN homologs have been identified in *E. scolopes*, genes encoding several key elements of the IFN pathway are present in the squid genome, including those involved in JAK/STAT signaling, NF-kappaB (Goodson et al., 2005) and IRFs (Belcaid et al., 2019). The latter study hypothesized that the functional role of IFN in the squid may be filled by products of unannotated genes lacking a recognizable homology to vertebrate IFN. Together, these results indicate that RIG-I may function as a molecular PRR that recognizes symbiont SsrA, and acts as a crucial trigger for downstream signaling cascades in the squid (Figure 5C). Because two RIG-I homologs exist in the *E. scolopes* genome (Belcaid et al., 2019), the extent and specificity of RNA-sensing mechanisms in this host require further investigation, e.g., functional diversification may have occurred during RIG-I evolution, allowing its paralogs to participate both in communicating with symbionts and

in antiviral sensing. Additional studies will be required to determine the actual *in vivo* mechanisms of RIG-I-associated signaling.

Regarding the response of haemocytes to the delivery of OMVs that lack SsrA, we found a specific up-regulation of the expression of a homolog of CIKS (Act1), an adapter acting downstream in the pro-inflammatory IL-17 signaling pathway of mammals (Rosani et al., 2015; Seon et al., 2006). We predict that induction of CIKS leads to an increased inflammatory state in host cells in contact with Δ *ssrA* symbionts. Such inflammation is apparently not a response to an increased delivery of other MAMPs (i.e., PGN monomer and lipid A) because colonization by either WT or Δ *ssrA* symbionts induces an equivalent level of both haemocyte trafficking and apoptosis (Figure 2C-D), (Krasity et al., 2011; McFall-Ngai et al., 2010). Similarly, when the host is presented with WT or Δ *ssrA* OMVs, there is apparently no functionally significant difference either in the identity of the major proteins (Figure S1C), or in the level of PGN cargo, delivered by the two vesicle types (Figure 2B). Nevertheless, we recognize there may still be differences in low abundance proteins (Lynch et al., 2019) or in sRNAs that our library preparation could not efficiently capture.

The particular mechanism(s) by which SsrA is sensed within the epithelium remains to be determined, but the possibilities include secondary structure or sequence specificity playing a role in the recognition of SsrA by the host. The sequences of SsrAs are relatively conserved across bacteria but, like 16S, can be used to identify different species (Dong et al., 2007; Schönhuber et al., 2001); thus, an investigation of the degree of specificity with which host cells discern and respond to SsrA molecules from bacteria other than their symbionts will be the subject of future studies.

Conclusions

Because all animal hosts must protect themselves against colonization by unsuitable or dangerous bacteria, distinct signaling molecules that detect microbial presence and viability have evolved to ensure that the appropriate response to a pathogenic threat or a beneficial encounter is executed. Thus, it is not surprising that hosts will have evolved mechanisms by which to sense not only MAMPs, but also common sRNA species such as SsrA. Here we hypothesize that, in a host colonized by Δ *ssrA* cells, RIG-I is not activated, leading to a dysregulation of normal host responses (Figure 5C), and resulting in a heightened immune reaction that ultimately affects the

health and stability of the association. Whether and how other symbiont RNAs are sensed by the host, and lead to specific tissue responses, will require further exploration. We anticipate that host recognition of such RNAs will emerge as a major new category of communication between symbionts and the tissues they inhabit.

Acknowledgments

We thank members of the McFall-Ngai and Ruby labs for helpful discussions. We especially thank Fredrik Bäckhed for excellent advice and helpful discussions. We also thank Susan Gottesmann for suggesting the *smpB* mutant studies, and Gabriela Aguirre and Susannah Lawhorn for their valuable technical help. Tina Carvalho (University of Hawaii-Manoa) provided scanning-electron microscopy (SEM) training, and the Histology & Imaging Core Facility at JABSOM, performed the tissue sectioning. The research was supported by NIH grants R37 AI50661 (Margaret McFall-Ngai and E.G.R.), R01 OD11024 and GM135254 (E.G.R. and M.M.-N.), and NSF INSPIRE Grant MCB1608744 (Eva Kanso, USC). Acquisition of the Leica TCS SP8 X confocal microscope was supported by NSF DBI 1828262 (Marilyn Dunlap, E.G.R., and M.M.-N.), and SEM and confocal microscopy was performed in the MICRO Core facility, supported by COBRE P20 GM125508 (M.M.-N. and E.G.R.).

Author Contributions

SMG, MMN and EGR designed and conceptualized the study; SMG conducted most experiments; CB made *V. fischeri* mutants; TEB assisted with Leica imaging and image analysis; LW conducted plating experiments; SMG, MMN and EGR discussed the results and wrote the manuscript.

Declaration of Interests

The authors declare no competing interests.

Tables

Table 1: List of abundant small, non-coding RNAs.

Gene product	Locus tag	No. of reads per fraction	
		OMV RNA	Haemolymph RNA
CsrB1	VF 2593	5455	ns
CsrB2	VF 2577	10804	11
RnpB	VF 2654	3411	18
SsrA	VF 2639	8390	306
SsrS	VF 2651	1234	70
Ffs	VF 2599	ns	31

Figures

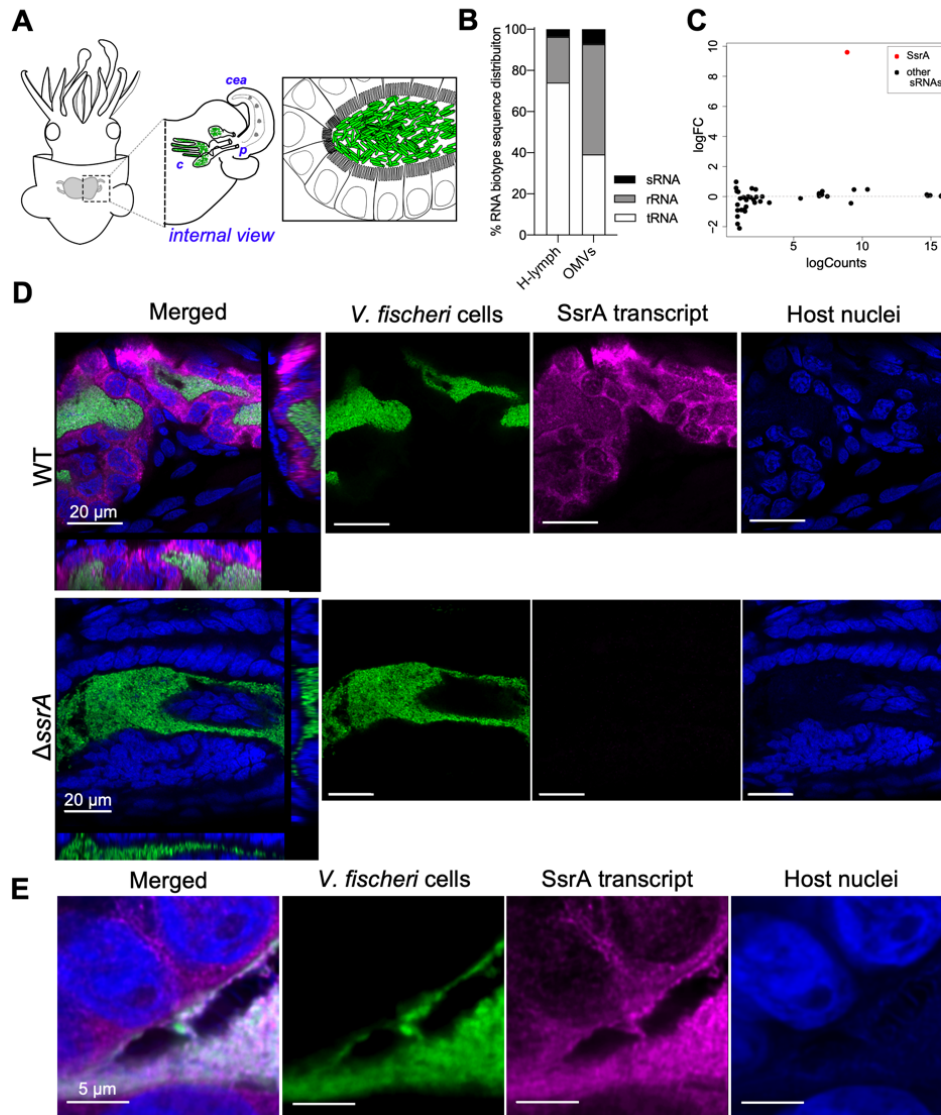


Figure 1. Symbiont Non-coding RNA, SsrA, Localizes within the Crypt Epithelium (A) Diagram of a juvenile squid showing the anatomical location (Left), and internal aspects (Middle) of the light organ, with one of its two pair of ciliated epithelial appendages (cea), and three entry pores (p) through which the symbionts reach the migration path to internal crypts (c). Grey dots inside the sinus of the cea represent symbiosis-induced trafficking of haemocytes. (Right) Illustration of the close contact between the *V. fischeri* population (green) and the light-organ epithelial cells in a crypt. (B) Relative proportions of types of *V. fischeri* RNAs present in squid haemolymph (H-lymph), or in the RNA cargo of OMVs. (C) Volcano plot representation of a differential-expression analysis (logFC) of the RNA cargo in OMVs produced by WT or $\Delta ssrA$ strains; the only significant difference in RNA content is the presence (in WT) or absence (in $\Delta ssrA$) of SsrA. (D) Localization of symbiont SsrA transcript by confocal microscopy, 24 h after colonization by wild-type (WT) or the *ssrA*-deletion mutant ($\Delta ssrA$) bacteria. Left: merged images with orthogonal views; other panels: images of individual labels. (E) Higher magnification of WT *V. fischeri* cells (green) colonizing the light organ, showing the location of SsrA transcript (magenta) within the cytoplasm of host epithelial cells.

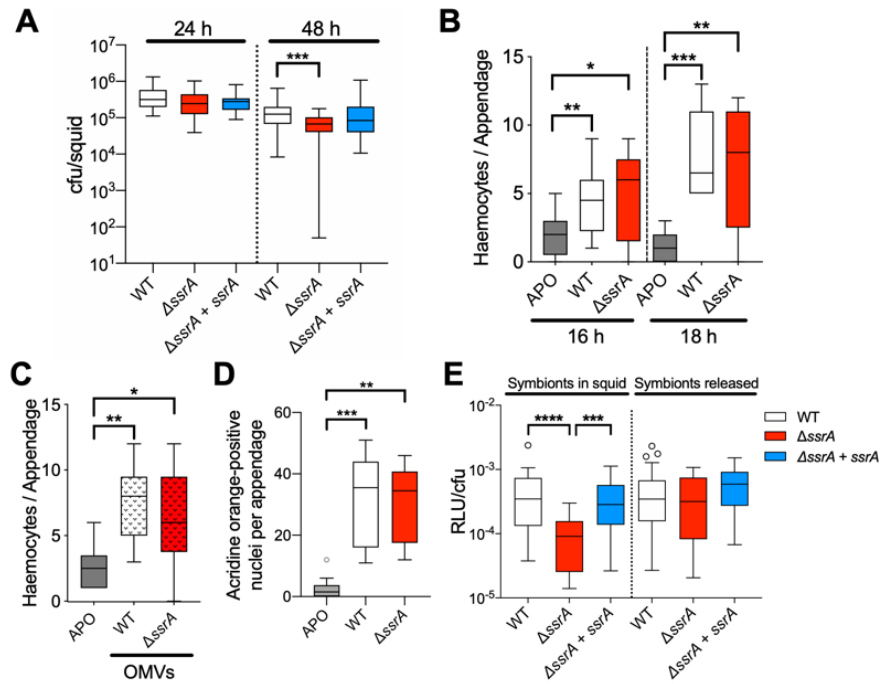


Figure 2. The $\Delta ssrA$ Mutant Is Able to Initiate Colonization Normally, but Persists Poorly

(A) Number of *V. fischeri* colony-forming units (cfu) per light organ 24 or 48 h post-colonization in animals colonized by WT, $\Delta ssrA$, or the genetically complemented $\Delta ssrA + ssrA$ strains. A 1-way Kruskal–Wallis Analysis of Variance, followed by Dunn’s Multiple Comparison test (DMC). Ten squid/condition from 6 different clutches were used in this experiment (n=60).

(B) Levels of haemocyte trafficking into the light-organ’s anterior appendages at 16 and 18 h post-colonization. Significant differences, as indicated by a 1-way ANOVA with Tukey’s multiple comparison test (TMC) (n=10).

(C) Levels of haemocyte trafficking 3 h after exposure to 100 μg of OMVs per ml. Significant differences, as indicated by a 1-way ANOVA with TMC test (n=10).

(D) Degree of apoptosis in the light-organ’s ciliated epithelium, as indicated by the number of acridine orange-staining nuclei, in animals that were uncolonized (APO), or colonized by either WT or the $\Delta ssrA$ strain (Figure S4). Statistical significance determined by a 1-way ANOVA, followed by DMC (n=10).

(E) Specific luminescence [relative light units (RLU) per cfu] of symbionts either within the light organ, or within a homogenate of the light organ of a 24-h juvenile. Animals were uncolonized (APO), or colonized by either WT or the $\Delta ssrA$ strain. Significant differences, as indicated by a 1-way ANOVA, followed by DMC. The experiment was repeated twice with the same outcome. P-value code: ****, < 0.0001; ***, < 0.0002; **, < 0.001; * < 0.021 for all graphs.

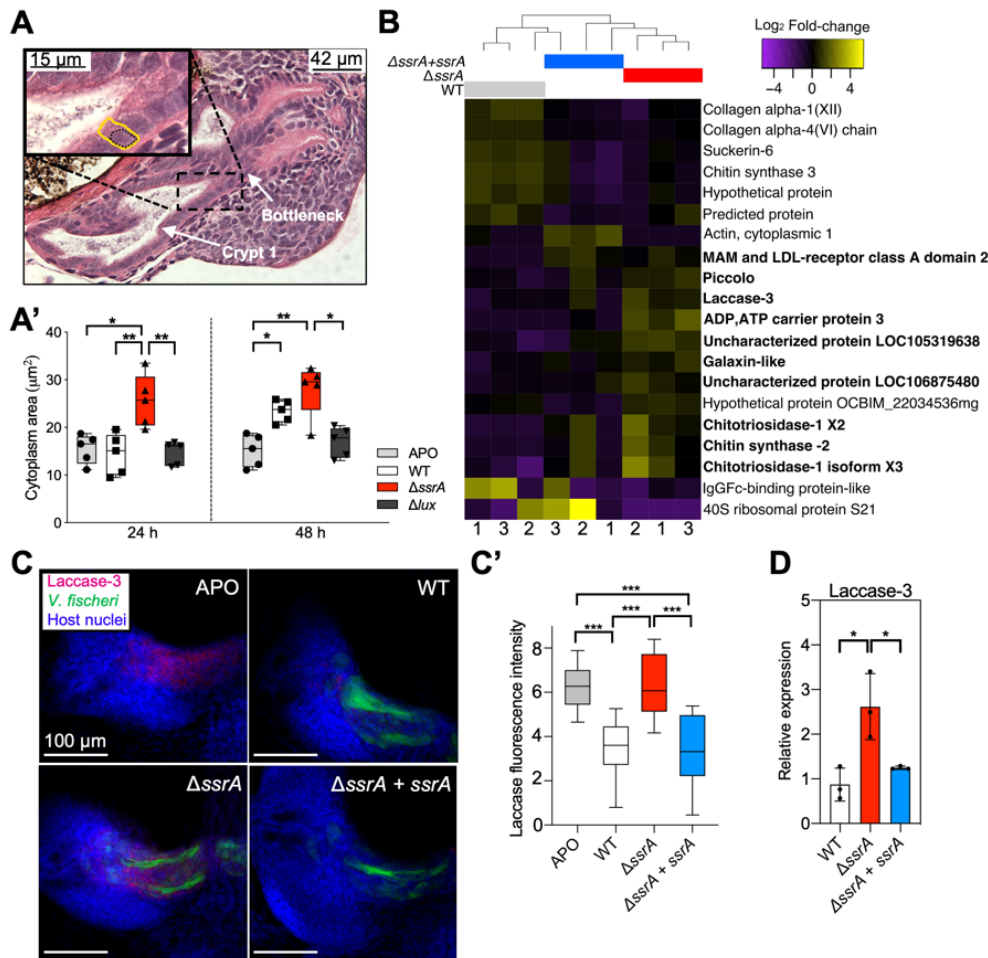


Figure 3. Host Responses to Colonization by either WT or $\Delta ssrA$ Differ

(A) Paraffin-section image of a WT-colonized light organ after 48 h, illustrating how crypt-cell cytoplasmic volume was measured. The nuclear area (black dotted line) was subtracted from the total cell area (yellow line). The areas of 10 epithelial cells in crypt 1, just inside of the bottleneck, were measured per light organ. Details in STAR METHODS.

(A') Cytoplasmic volume of the crypt epithelium at 24 and 48 h post-inoculation with WT, $\Delta ssrA$ or Δlux strains, or left uncolonized (APO). (n=5). (B) Heat map depicting fold-change differences in significantly differently expressed genes in light organs colonized by WT, the $\Delta ssrA$ mutant, or its genetically complemented ($\Delta ssrA + ssrA$) strain. Genes that are up-regulated in $\Delta ssrA$ -colonized animals compared to WT-colonized are indicated in bold. The replicate number for each condition (Supplementary File 2) is indicated beneath the heatmap.

(C) Localization of the Laccase-3 transcript (magenta) on one side of the light organ using hybridization chain-reaction fluorescence *in situ* hybridization (HCR) labeling. Light organs were colonized by the indicated strains of GFP-labeled symbionts (green).

(C') Quantification of Laccase-3 signal using relative fluorescence intensity of a Z series of the light organ (n=9). P values were calculated using a 1-way ANOVA with TMC.

(D) Relative expression of Laccase-3 after 24 h post-colonization in light organs colonized by WT, $\Delta ssrA$ or $\Delta ssrA + ssrA$, determined by qRT-PCR. Expression was normalized to ribosomal protein S19 and expressed as $2^{\Delta\Delta CT}$ normalized to WT expression. Significant differences, as indicated by a 1-way ANOVA with Tukey's multiple comparison test (n=3). Data presented as the mean \pm SD. P-value code: ****, < 0.0001; ***, < 0.0002; **, < 0.001; *, < 0.021.

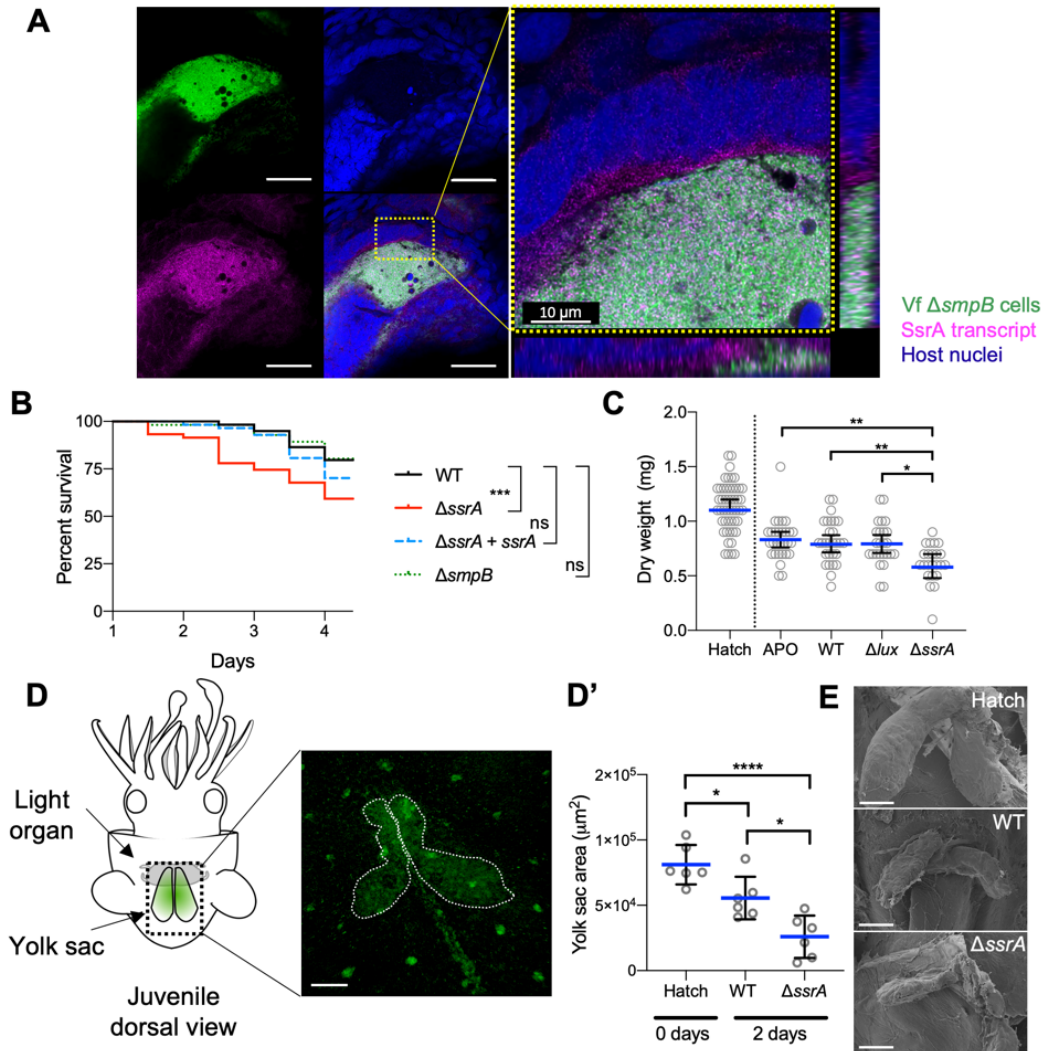


Figure 4. The Absence of SsrA in the Epithelium, but Not SsrA Activity in the Symbiont, Weakens the Host

(A) Visualization by HCR of SsrA transcript (magenta) in a whole-mount light organ, 24 h after colonization with a GFP-labeled $\Delta smpB$ strain of *V. fischeri* (green). A representative confocal image indicates that symbiont SsrA transcript is within the crypt epithelial cells. Scale bar, left panel = 30 μm . See Figure S5A.

(B) Kaplan-Meier survival plot of juvenile squid colonized by WT, $\Delta ssrA$, the complement ($\Delta ssrA + ssrA$) or $\Delta smpB$ strains. A calculation based on three separate experiments (Figure S5B) is shown, consisting of WT ($n = 59$), $\Delta ssrA$ ($n = 59$), $\Delta ssrA + ssrA$ ($n = 57$), or $\Delta smpB$ ($n = 56$) colonized animals. Survival curve analysis by a Log Rank Mantel-Cox test, with Bonferroni multiple testing adjustment for pairwise comparisons. P-value = 0.016.

(C) Dry weight of juvenile squid immediately after hatching (Hatch), or at 4 days post-hatching when kept aposymbiotic (APO) or colonized with WT, $\Delta ssrA$, or a dark mutant (Δlux) strain. Analysis by a 1-way ANOVA with TMC indicated that hatchlings had a significantly higher dry weight compared to all other conditions ($P < 0.0001$). Data are represented as the median, with 95% confidence intervals.

(D) Left: dorsal view of a juvenile squid, illustrating the location of the internal yolk sac (dotted box). Right: representative confocal Z-stack image of a hatchling yolk sac stained with the lipophilic lipidspot-488

(green) and depicting how the area (dotted region) was measured; scale bar = 100 μm . Details in STAR METHODS.

(D') Quantification of internal yolk-sac area, determined from confocal Z-stack images. Data are represented as mean \pm SD, analyzed by a 1-way ANOVA with TMC.

(E) Representative scanning electron microscopy (SEM) images of the yolk sac of a hatchling squid, and animals colonized for 2 days by the WT or the ΔssrA -mutant strain. Scale bar = 100 μm . P-value code: ****, < 0.0001; ***, < 0.0002; **, <0.001; *, < 0.021 for all figures.

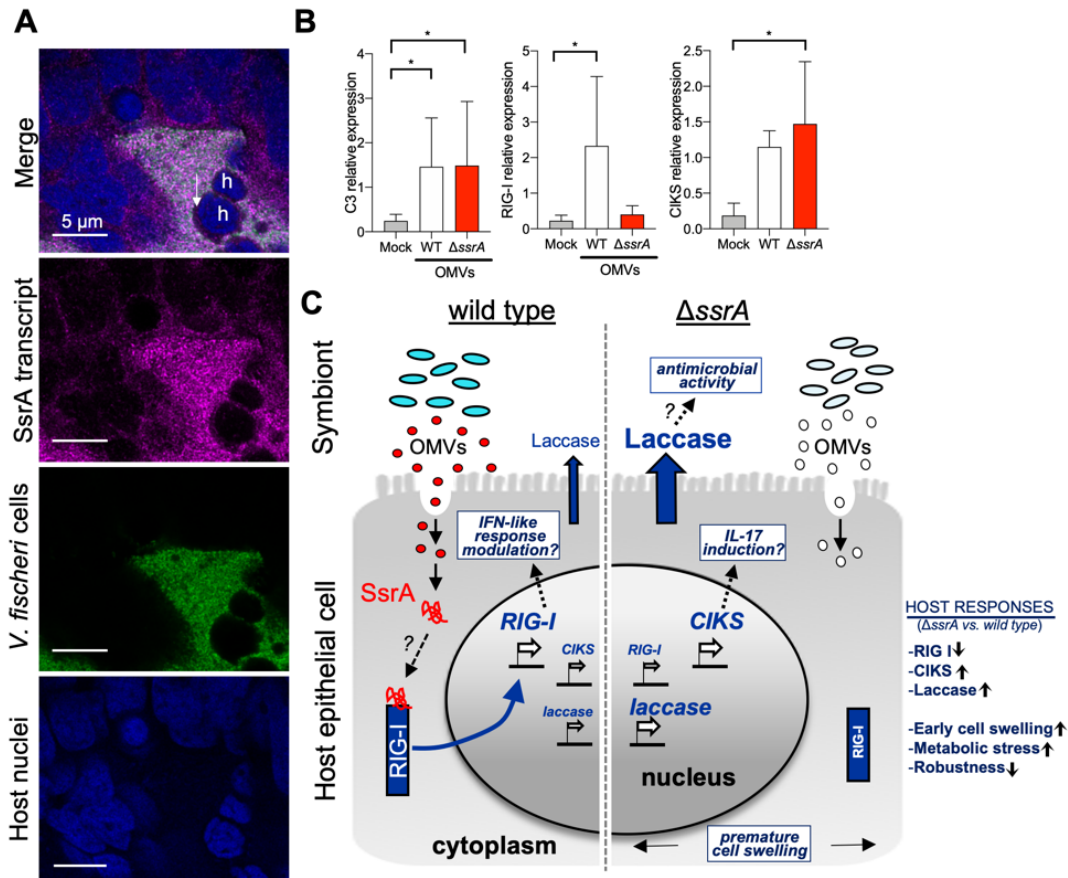


Figure 5. SsrA Taken Up by Haemocytes Is Detected through Host Cytosolic RNA Sensors

(A) HCR visualization of SsrA transcript (magenta) in a whole-mount light organ, 24 h after colonization with a GFP-labeled WT strain (green). A representative confocal image indicates that symbiont SsrA transcript is within the crypt epithelial cells (nuclei, TOPRO-3; blue). White arrow indicates symbiont SsrA transcript in a host haemocyte (h) within the crypt space.

(B) Changes in gene expression 30 min after challenging isolated juvenile haemocytes with OMVs purified from exponential cultures of either WT or Δ ssrA cells, or after addition of dPBS (Mock). Relative expression levels were determined by qPCR for complement 3 (C3); retinoic-acid inducible gene I (RIGI), and adapter protein CIKS (CIKS). Error bars = SD. P-value code: * < 0.021.

(C) Proposed model for SsrA modulation of host immune response. During WT colonization, OMVs containing SsrA enter the host cell. The OMV cargo is released in the cytoplasm where it associates with RIG-I, triggering a signaling cascade that induces its own upregulation as well as the activation of a IFN-like response for symbiont modulation. During Δ ssrA colonization, there is no SsrA to associate with RIG-I. As a consequence, there is no modulation of IFN response, leading to inflammation through IL-17 signaling. This results lead to an increase of laccase and cell swelling, and overall less robustness of the host due to the rapid depletion of its yolk sac by the increased immune response.

STAR METHODS

LEAD CONTACT AND MATERIALS AVAILABILITY

Please contact the Lead Contact, Edward Ruby (eruby@hawaii.edu) for further information and any request for strains and reagents.

EXPERIMENTAL MODEL AND SUBJECT DETAILS

Squid

The breeding colony of Hawaiian bobtail squid (*Euprymna scolopes*) was supplied by collecting adult animals from Maunalua Bay, Oahu, Hawai'i, and transferring them to the Kewalo Marine Laboratory in sun-lite, outdoor, flow-through seawater tanks. Adult females laid egg clutches that were kept in seawater and maintained on a natural 12:12-h light:dark cycle. While the IACUC committee of the University of Hawaii at Manoa only reviews vertebrate protocols, all squid experiments reported here conform to the relevant standards established by the University's senior veterinarian.

Bacterial Strains

Detailed information of the *V. fischeri* strains used in this study are provided in the Key Resources Table.

Generation of Bacterial Mutants

The *V. fischeri* wild-type symbiont strain ES114 (Boettcher and Ruby, 1990) was used as the parental strain for all mutant constructions. The enzymes used for cloning were the platinum Taq polymerase (Invitrogen), Fast digest restriction enzyme (Thermo Fischer Scientific), and a T4 DNA ligase (New England Biolabs). SsrA mutant was constructed by allelic exchange with pSMG3, a derivative of the counter-selectable suicide vector pKV363 (Le Roux et al., 2007; Stabb and Ruby, 2002). To build pSMG3, we amplified two fragments PCRa, ~600 bp up-stream region of SsrA, and PCRb product, ~500 bp down-stream region of SsrA (Table S1). Both products were digested with BamHI at 37°C for 1 h and ligated overnight at 4 °C. The ligated product was amplified (PCRab) and inserted it between EcoRI and XhoI of pKV363. To construct the plasmid pSMG5 that complement the *ssrA* deletion, we amplified a fragment of ES114 gDNA, including *ssrA* and *smpB* genes region. PCR product was digested it with KpnI and XbaI and inserted it in those sites into pVSV105 (Dunn et al., 2006). SmpB mutants was constructed using a sucrose-based selection with pCBNR36, a derivative of pSMV3 vector (Lynch et al., 2019). To build this vector, we amplified two fragments: PCRa, ~900 bp up-stream region of *smpB*, and PCRb product,

~800 bp down-stream region of *smpB* (Table S1). Both products were digested with BamHI at 37°C for 1 h and ligated overnight at 4 °C. The ligate product was amplified and inserted it between ApaI and SpeI of pSMV3.

For labeling strains, pVSV102 carrying GFP and a kanamycin-resistance expression cassette was transferred from *E. coli* DH5 α to each *V. fischeri* receiver strain by triparental mating (Stabb and Ruby, 2002) using the conjugative helper strain CC118 λ *pir* as described previously (Dunn et al., 2006).

When necessary, antibiotics were added to the media at the following concentrations: 50 μ g ml⁻¹ and 100 μ g ml⁻¹ for kanamycin, and 25 and 2,5 μ g ml⁻¹ for chloramphenicol in respectively Luria-Bertani (LB: 950 ml DI H₂ O, 10 g Bacto-Tryptone, 5 g yeast extract, 10 g NaCl, 50 ml of 1 M Tris; pH 7.5-7.6) and Luria-Bertani salt medium (LBS) (Graf et al., 1994).

METHOD DETAILS

Light-Organ Colonization Assays

Juvenile squid from the breeding colony were collected within minutes of hatching, and placed in FSOW. Within 2 h of hatching, juveniles were either made symbiotic (SYM) by overnight exposure to ES114 *V. fischeri* WT or derived mutant strains suspended in filter-sterilized ocean water (FSOW), or kept aposymbiotic (APO) in FSOW without additions. Animals were maintained on a 12:12-h light:dark cycle. To prepare bacterial inocula for colonization, strains were cultured overnight in Luria-Bertani salt medium (LBS) (Graf et al., 1994) with any appropriate antibiotic selection, if necessary. These cells were sub-cultured into seawater tryptone medium (SWT) (Boettcher and Ruby, 1990), and grown to mid-log phase at 28°C with 220 rpm shaking. The final inoculum was a dilution of this subculture into FSOW to achieve a concentration of 4,000-8,000 cfu/ml. Colonization of the host was monitored by checking for animal luminescence with a TD 20/20 luminometer (Turner Designs, Sunnyvale, CA). Unless otherwise indicated, SYM or APO juvenile animals were analyzed at 24 h post-colonization (i.e., 2 h after dusk). The squid were anesthetized in seawater containing 2% ethanol, and either flash frozen and stored at -80°C in RNAlater (Sigma-Aldrich) as previously described (Kremer et al., 2013) until further processing, or fixed overnight in 4% paraformaldehyde (PFA) in marine phosphate-buffered saline (mPBS: 450 mM NaCl, 50 mM sodium phosphate buffer, pH 7.4).

Bacterial Growth Assays

Cells were grown in LBS medium to an OD of 0.6 ± 0.1 , and then diluted to an optical density at 600 nm (OD_{600}) of 0.02 with either fresh LBS or a minimal medium (MSM: composed of 1 g of Bacto-tryptone, 20 g of NaCl, and 50 ml of 1 M Tris-HCl buffer [pH 7.5] per liter of deionized water). Depending on the experimental condition, LBS was supplemented with glycerol (32.6 mM) or *N*-acetyl-glucosamine (GlcNAc; 10 mM). Growth of 1-ml cultures in 24-well plates was monitored at OD_{600} using a GENiosPro plate reader (Tecan, Research Triangle Park, NC) with continuous shaking at 28°C. Absorbance readings were corrected for a nonstandard path length by linear transformation.

Host RNA Extraction and Sequencing

For light organ-RNA extraction, 20 juvenile light organs were pooled, and total extracted RNA was purified using QIAGEN RNeasy columns, immediately followed by treatment with TURBO™ DNase (Thermo Fisher Scientific). The RNA concentration for each sample was then determined with a Qubit RNA BR assay kit (Invitrogen). The Illumina TruSeq Stranded mRNA Sample Prep with polyA selection v4.0 protocol was used for library preparation. Illumina HiSeq 4000 using a paired end, 100 nucleotides in length, run mode was used for sequencing either at the NYU Genome Center, for light-organ tissue samples.

Transcript Abundance Estimation and Differential Expression Analysis

Reads from the RNA-Seq analyses were mapped against the reference transcriptome (Belcaid et al., 2019) with bowtie2 (Langmead and Salzberg, 2012), and their relative expression values were estimated with RSEM software (Li and Dewey, 2011). To identify the differentially expressed transcripts, the R package edgeR (Robinson et al., 2009) was used for the statistical analysis of the RNA-Seq data, employing a false discovery rate (FDR) threshold of 0.05. Heatmaps of expression values and hierarchical clustering were created with heatmap3 (Zhao et al., 2014) in the R environment.

Fluorescence *In Situ* Hybridization Chain Reaction (HCR-FISH)

Fixed juvenile squid were washed three times for 30 min in mPBS prior to dissection of the host tissues. HCR-FISH probes (version3 chemistries, (Choi et al., 2018)) specific for the host's laccase and *V. fischeri* 16S RNA transcripts (Key Resources Table) were designed and provided by Molecular Instruments (www.molecularinstruments.com). Juvenile squid were collected 24 h post-colonization under the standard procedures explained previously. The light organs were then dissected out and the hybridization procedure was followed as described previously (Moriano-

Gutierrez et al., 2019). Samples were counterstained overnight with TO-PRO-3 (Thermo Fisher Scientific) to label host nuclei, and imaged using a Zeiss LSM 710 upright laser-scanning confocal microscope (Carl Zeiss AG, Jena, Germany) located at the University of Hawaii-Manoa (UHM) Kewalo Marine Laboratory. Fluorescence intensity for all sections of each Z-stack was measured using FIJI (Schindelin et al., 2012).

For symbiont SsrA transcript detection, HCR-FISH probes (version2 chemistry, (Choi et al., 2014)) were designed and provided by Molecular Instruments. The hybridization procedure was followed as described in (Nikolakakis et al., 2015) and, after counterstaining with TO-PRO-3, the samples were imaged using an upright Leica SP8 confocal microscope (Leica Camera AG, Wetzlar, Germany). Images were adjusted to optimize visual resolution using the Lightning Adaptive deconvolution, and the Leica LasX software, located at UHM.

Quantitative Real-Time PCR (qPCR)

Gene expression changes were confirmed by qRT-PCR using LightCycler[®] 480 SYBR Green I Master Mix (Roche) and the same total RNA extracts as described previously. Synthesis of the single-stranded complementary DNA was performed with SMART MMLV Reverse Transcriptase (Clontech) using either Oligo(dT)12–18 primers (Invitrogen) for host gene expression, or random hexamers (Invitrogen) for symbiont gene expression. Following the MIQE guidelines (Bustin et al., 2009), all reactions were performed with no-RT and no-template controls to confirm that the reaction mixtures were not contaminated. Specific primers (Key Resources Table) were designed with Primer3plus (Untergasser et al., 2012). The amplification efficiency was determined by in-run standard curves, with a 10-fold dilution template. Each reaction was performed in duplicate with a starting level of 12.5 ng cDNA. The generation of specific PCR products was confirmed by melting-curve analysis. Expression analyses of candidate genes were normalized to either the ribosomal protein S19 for host-gene expression analysis, or to polymerase A for symbiont-gene expression analyses. Bar graphs of expression values were produced with GraphPad Prism v8.00 software.

Paraffin Sectioning and Histology

Squid were collected after 24 h or 48 h post-colonization, fixed in 4% PFA in mPBS, and the light organs were dissected out and dehydrated by serial washes in ethanol. Afterwards the light organs were embedded in paraffin wax, histologically sectioned (5 μ m), stained with haematoxylin and eosin, and mounted on slides at the Microscopy and Imaging Core (MICRO) facility of UHM. FIJI

(Schindelin et al., 2012) was used to measure the cytoplasmic area of light-organ epithelial cells by subtraction of the nucleus area from the total cell area. Five light organs were analyzed, and 10 cells on each border of the crypt side of the crypt #1 bottleneck were measured per light organ.

Dry Weight Measurement

Squid were collected at hatching, and at 4 days post-colonization, anesthetized in seawater containing 2% ethanol and flash frozen until further processing. Each squid was placed in pre-weighted aluminum foil tray, dried at 90°C, and weighed on an Ohaus AX124 balance until a constant dry-weight value had been reached.

Scanning Electron Microscopy

Squid were collected 48 h post-colonization, fixed and washed in mPBS, before dehydrating through an ethanol series, and critical-point dried as previously described (Doino and McFall-Ngai, 1995). The samples were mounted on stubs, gold sputter-coated, and viewed with a Hitachi S-4800 FESEM scanning electron microscope at the UHM MICRO facility.

Yolk Sac Staining and Measurement

Squid were collected after 48 h of colonization, and incubated at room temperature for 2 h in 1:1000 of the lipid stain, lipidspot488 (Biotium). Afterwards, the squid were washed in seawater, anesthetized in seawater containing 2% ethanol and imaged using a Zeiss LSM 710 confocal microscope. Z-stack images were acquired and the area of the internal yolk sac measured using FIJI (Schindelin et al., 2012) from the sum slices of each Z-stack.

Purification of Outer Membrane Vesicles (OMVs)

V. fischeri cultures were grown at 28°C in LBS until late exponential phase ($OD \approx 3$). The cells were removed by low-speed centrifugation ($8000 \times g$) at 4°C, and the culture supernatant was filtered through a 0.22 μm pore-size PVDF membrane filter (Millipore, Inc.). OMVs were then collected from the filtered supernatant by centrifugation for 2 h in a TLA-45 rotor using a Max-XP ultracentrifuge (Beckman Coulter) at $180,000 \times g$ and 4°C. The pelleted OMVs were washed by resuspension in Dulbecco's phosphate-buffered saline (DPBS) with added salt (0.4 M NaCl) (Aschtgen et al., 2016), and re-centrifugation at $200,000 \times g$ for 1 h, at 4°C using either a MLA-50 or TLA-110 rotor in an Optima-XP centrifuge (Beckman Coulter). The resulting pellets were resuspended in saline DPBS, and filter-sterilized through 0.45 μm -pore-size PVDF membrane filter (Millipore, Inc.) before storing at -80°C. Before OMVs were added to live squid, they were further purified with a sucrose density-gradient as previously described (Aschtgen et al., 2016).

To estimate the OMV concentration, total protein of the sample was determined with the Qubit™ Protein Assay Kit (Invitrogen).

Protein Gel Electrophoresis

Samples containing 10 ug of total protein from *E. scolopes* OMVs were loaded onto a pre-cast 12% bis-tris polyacrylamide gel (Invitrogen), together with a Precision Plus Protein™ standard (Bio-Rad™). The proteins were separated for 1 h at 150 V at 4°C in a Mini-Vertical Electrophoresis System (Bio-Rad™), stained overnight in 90% Protoblue Safe (National Diagnostics,) in ethanol, rinsed in deionized water, and imaged with GelDoc-It® (UVP) system.

Sequencing of RNA Extracted From OMVs

To determine the nature of their RNA cargo, 500 µL (2500 µg of protein per ml) of purified OMVs were first treated with 4 mg of RNaseA (Promega) per ml for 10 min at 37°C to remove any surface contamination. The added RNase was then inhibited by the addition of 1 ul of Murine RNase inhibitor (NEB). The RNA within these treated OMVs was purified using a mirVana PARIS kit (Invitrogen), followed by DNase I treatment (Thermo Fisher Scientific). The RNA concentration for each sample was then determined with a Qubit RNA BR assay kit (Invitrogen). Library preparation and sequencing was performed by SeqMatic (Fremont, CA), with paired-end stranded RNA (2x75 bp). Size selection of the library with inserts smaller than 300 nucleotides was performed before sequencing on an Illumina MySeq platform. Reads were mapped to the *V. fischeri* genome (GenBank: CP000020, CP000021 and CP000022), and their relative abundance was estimated with Feature Counts (Liao et al., 2014). Differential-expression analysis was performed using the R package edgeR (Robinson et al., 2009) with an FDR threshold of 0.05. Heatmaps of expression values were originated with the R package heatmap3 (Zhao et al., 2014).

Isolation of Host Haemocytes and Purification of their RNA

Haemocytes from aposymbiotic juveniles were isolated as described previously (Heath-Heckman and McFall-Ngai, 2011). For expression analysis, haemocytes from 20 juveniles were pooled and spread into 12-well plates (Millipore-Sigma), allowed to adhere for 20 min at room temperature, and washed 3 times in Squid-Ringer's solution (SRS: 530 mM NaCl, 10 mM CaCl₂, 10 mM KCl, 25 mM MgCl₂, and 10 mM HEPES buffer, pH 7.5). After these washes, purified OMVs from either the WT or Δ *ssrA* strain were delivered at a concentration of 50 µg/ml of SRS, and incubated for 30 min at room temperature. For the mock condition, the same volume of saline DPBS was delivered to the haemocytes. Following the incubation, haemocytes were washed in SRS once, and

TRIzol™ Reagent (Invitrogen) was immediately added and incubated for 5 min, and the sample was kept at -80°C until further processing. For RNA extraction, 200 µl of chloroform was added to the sample, which was vortexed, incubated for 5 min, and centrifuged at 120,000 × g. The upper aqueous phase was removed and, after adding 1 vol of 100% ethanol, placed on a silica spin column from the Monarch RNA clean-up kit (NEB) following standard procedures. RNA was then eluted in 20 µl of nuclease-free water, and the RNA concentration of each sample was determined with a Qubit RNA BR assay kit. Subsequent synthesis of cDNA and qPCR reactions were performed as described above. The *E. scolopes* genome encodes two RIG-I genes; the RIG-I homolog with greater sequence identity to human RIG-I sequence (O95786-1) was chosen for primer design.

Haemocyte Trafficking Assay

Juvenile squid were collected at 16 and 18 h post-colonization, and fixed as described above. Light organs were dissected out and permeabilized overnight at 4°C in 1% Triton X-100 (Sigma-Aldrich) in mPBS. Haemocytes were stained as previously described (Koropatnick et al., 2007), with a solution of 1 mg of deoxyribonuclease I conjugated to Alexa Fluor 488 (Thermo Fisher Scientific, Inc.) per ml of 1% Triton X mPBS for 24 h at 4°C. Samples were counterstained with rhodamine phalloidin (Invitrogen) to visualize the actin cytoskeleton. The migration of haemocytes into the blood sinus of the light-organ appendages were visualized and counted by a Zeiss LSM 710 confocal microscope.

Apoptosis Assay

Juvenile squid were collected at 14 h post-colonization, anesthetized in 2% ethanol, and placed in 0.0001% acridine orange (Invitrogen, A1301) in seawater for 1 min, as previously described (Foster et al., 2000). Light-organ appendages were visualized to determine the number of acridine orange-positive nuclei using a Zeiss LSM 710 fluorescence confocal microscope.

Squid Survival Assay

Juvenile squid were colonized following standard procedures. To control for inter-clutch variation, 3 independent experiments were performed using juveniles from 3 different clutches. After overnight inoculation with the appropriate strains, squid were transferred into clean glass scintillation vials containing 4 ml of FSOW. Each morning for the duration of the experiment, the squid were placed in new vials with 4 ml of fresh FSOW but were not fed. Under these conditions, the squid survive until the nutrients in their internal yolk sac are depleted. Approximately every

12 h, colonization of the light organ was monitored by checking for animal luminescence with a TD 20/20 luminometer, and the squid's viability was assessed by recording their responsiveness.

Measurement of Bacterial and Host Respiration Rates

Respiration-rate assays were performed using a digital respirometer system (Model 10, Rank Brothers Ltd, Cambridge, UK), whose data were collected via the analogical-digital interface ADC-20 Picolog 1216 data logger (Picolog PicoTechnology Ltd.,UK). Prior to data collection, the oxygen sensor was calibrated at 100% with air-saturated deionized water. The seawater in the respirometer chamber was fully aerated prior to adding the squid, and continuously stirred to maintain a uniform oxygen concentration during the measurement. The linear rate of decline in the oxygen concentration within the sealed chamber was used to calculate oxygen-consumption rates.

For the determination of bacterial respiration rates, overnight LBS cultures were diluted 1:100 in SWT and grown at 28°C until an OD₆₀₀ of 0.3 for replicate #1, 0.4 for replicate #2, or 0.5 for replicate #3. One ml of culture was placed in the chamber, and the rate of decline in the oxygen concentration was measured. The final respiration rate was normalized to the OD as follows: $\Delta O_2(t_0 - t_n)/\Delta OD(t_n - t_0)$, where t_0 is the time the measurements started, and t_n is the time the measurements ended. For the squid respiration-rate measurement, animals were placed in the chamber with 1 ml of seawater, and the measurement made without stirring to avoid disturbing the animal.

QUANTIFICATION AND STATISTICAL ANALYSIS

All data are expressed either as mean and standard deviation, or as median with 95% confident intervals. A normality test was applied, where appropriate, to ensure a normal distribution of the data. A 1-way ANOVA or Kruskal–Wallis analysis of variance was used for statistical analysis. The data were considered significant at a P-value < 0.05. When appropriate, P-values were adjusted for multiple comparison. The sample number (n) indicates the number of independent biological samples tested. Independent experimental replicates are indicated when performed. Information on relevant statistical analysis is provided for each experiment in the figure legends.

DATA AVAILABILITY

The datasets generated during this study have been deposited in the NCBI SRA repository with accession numbers: PRJNA629992 and PRJNA629425.

Supplemental Information

Supplemental information includes 6 figures, one table and two supplementary files.

Figure S1. The Symbiont sRNA SsrA, Is Found in the Squid Circulatory System, and within Symbiont Outer Membrane Vesicles (OMVs). Related to Figure 1.

Figure S2. Effects of SsrA Deletion on *V. fischeri* Cells. Related to Figure 2.

Figure S3. Localization of the Symbiont's 16S and SsrA Transcripts within the Host's Light Organ Epithelial Cells. Related to Figure 1.

Figure S4. Induction of Apoptosis in the Light-Organ Appendages of Juvenile Squid Early in Symbiosis. Related to Figure 2.

Figure S5. Effects of Colonization by Δ *ssrA* on Host Physiology and Health. Related to Figure 4.

Figure S6: Down-Regulation of Laccase-3 in the Crypt Epithelium Requires the Presence of Symbiont SsrA. Related to Figure 3 and Figure 4.

Table S1: Oligonucleotides information. Related to STAR METHODS.

Supplementary File 1. OMV RNA-Seq. Sheet 1: Relative expression. Sheet 2: Differential expression analysis. Related to STAR METHODS and Figure S1.

Supplementary File 2. Light Organ RNA-Seq. Sheet 1: Differential expression analysis. Related to STAR METHODS and Figure 3.

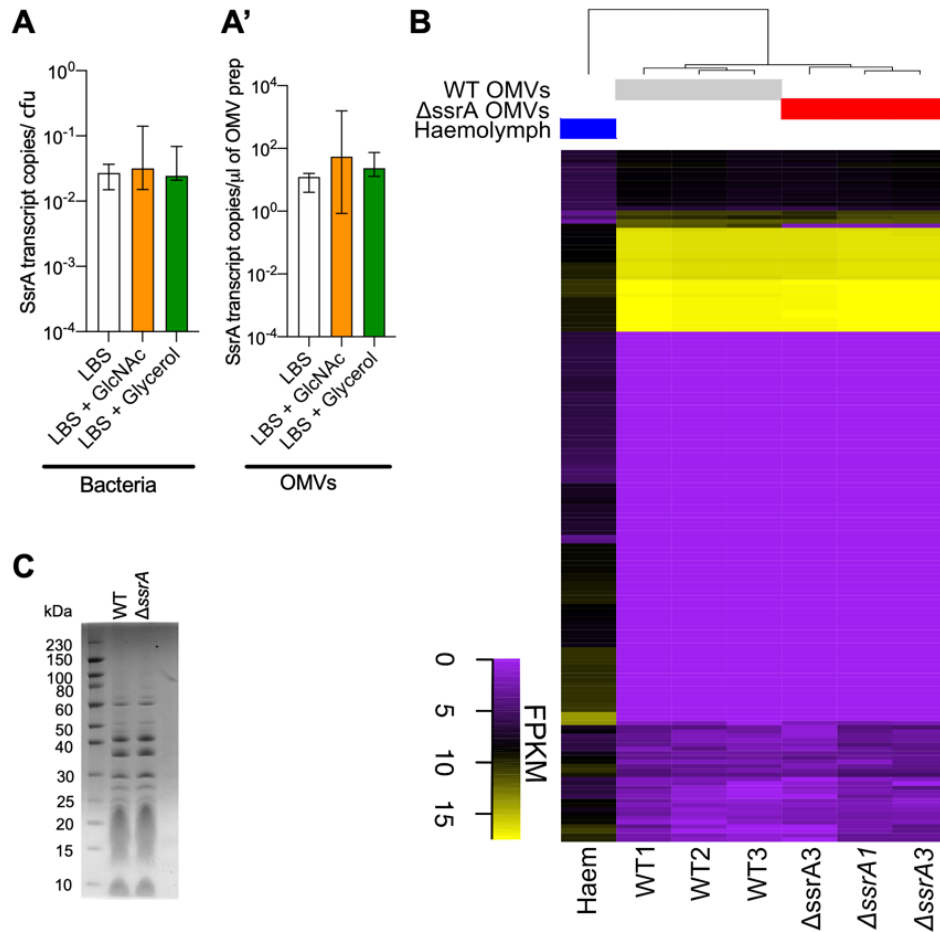


Figure S1. The Symbiont sRNA SsrA, Is Found in the Squid Circulatory System, and Within Symbiont Outer Membrane Vesicles (OMVs). Related to Figure 1.

(A) qPCR measurements of SsrA expression by WT *V. fischeri* grown in 3 different media: a tryptone-based medium (LBS), or LBS with the addition of either glycerol (32.6 mM) or *N*-acetyl-glucosamine (GlcNAc; 10 mM). Data are presented as the number of transcript copies per colony forming units (cfu) in late log phase (n=3).

(A') qPCR measurements of SsrA expression within purified OMVs, presented as the number of transcript copies per volume of purified OMV preparation (n=3).

(B) Heat map of expression levels of *V. fischeri* RNA detected in squid haemolymph and in the RNA contents of OMVs. Haemolymph was collected from adult field-caught animals. OMVs were purified from cultures of WT *V. fischeri*, or its Δ ssrA derivative.

(C) Soluble proteins present in purified OMVs isolated from cultures of WT or Δ ssrA cells.

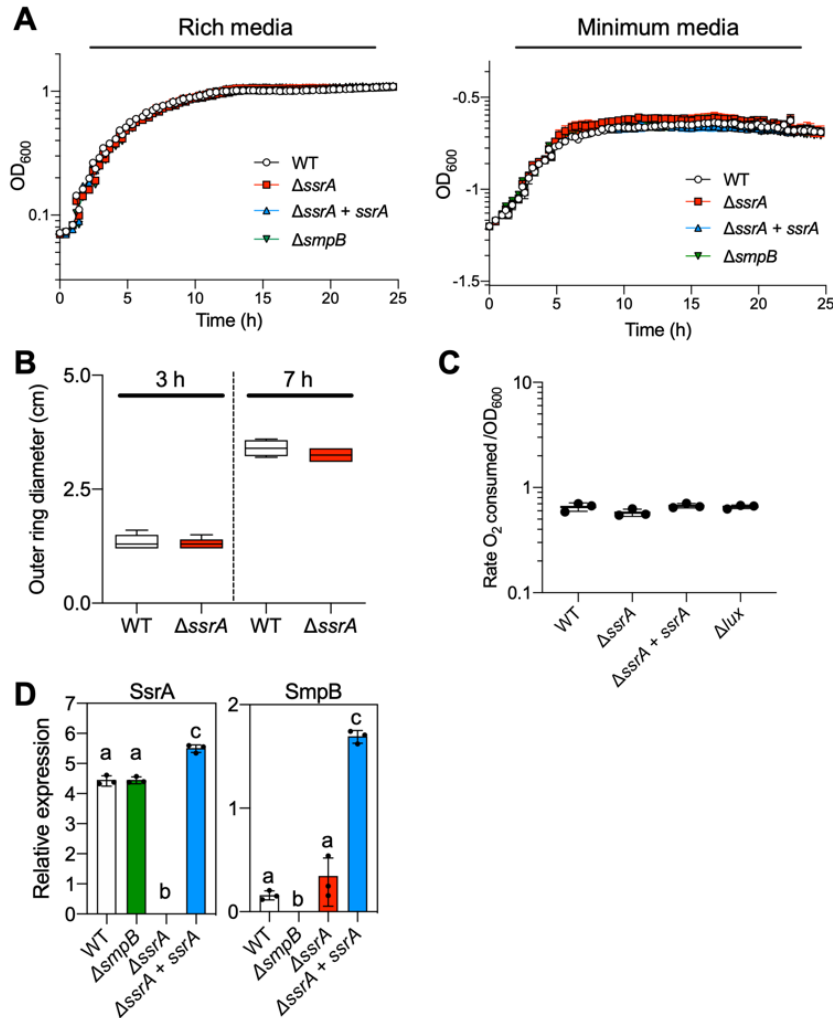


Figure S2. Effects of SsrA Deletion on *V. fischeri* Cells. Related to Figure 2.

(A) Growth characteristics in (left) the tryptone-based medium LBS, or (right) a minimal-salts medium, by the wild-type *V. fischeri* strain ES114 (WT), the $\Delta ssrA$ mutant derivative, its genetic complement ($\Delta ssrA + ssrA$), and a deletion mutant ($\Delta smpB$) of the SsrA chaperone, SmpB.

(B) Rate of motility in soft agar of WT and $\Delta ssrA$ cells. The diameter of the outer ring was measured at 3 and 7 h post-inoculation. Data presented as the mean \pm SD.

(C) Normalized respiration rates of WT, $\Delta ssrA$, $\Delta ssrA + ssrA$, and a non-luminescent, *lux*-deletion mutant (Δlux) in SWT medium. Data presented as the mean \pm SD.

(D) Relative expression of *ssrA* and *smpB* transcripts by cells of WT and its mutant derivatives during exponential phase of growth (OD₆₀₀ between 0.65 and 0.74) in LBS medium. Expression was normalized to polymerase A, and expressed as $2\Delta\Delta CT$. Significant differences are indicated by letters, based on a Bonferroni multiple-testing adjustment for pairwise comparisons. P-value = 0.0083.

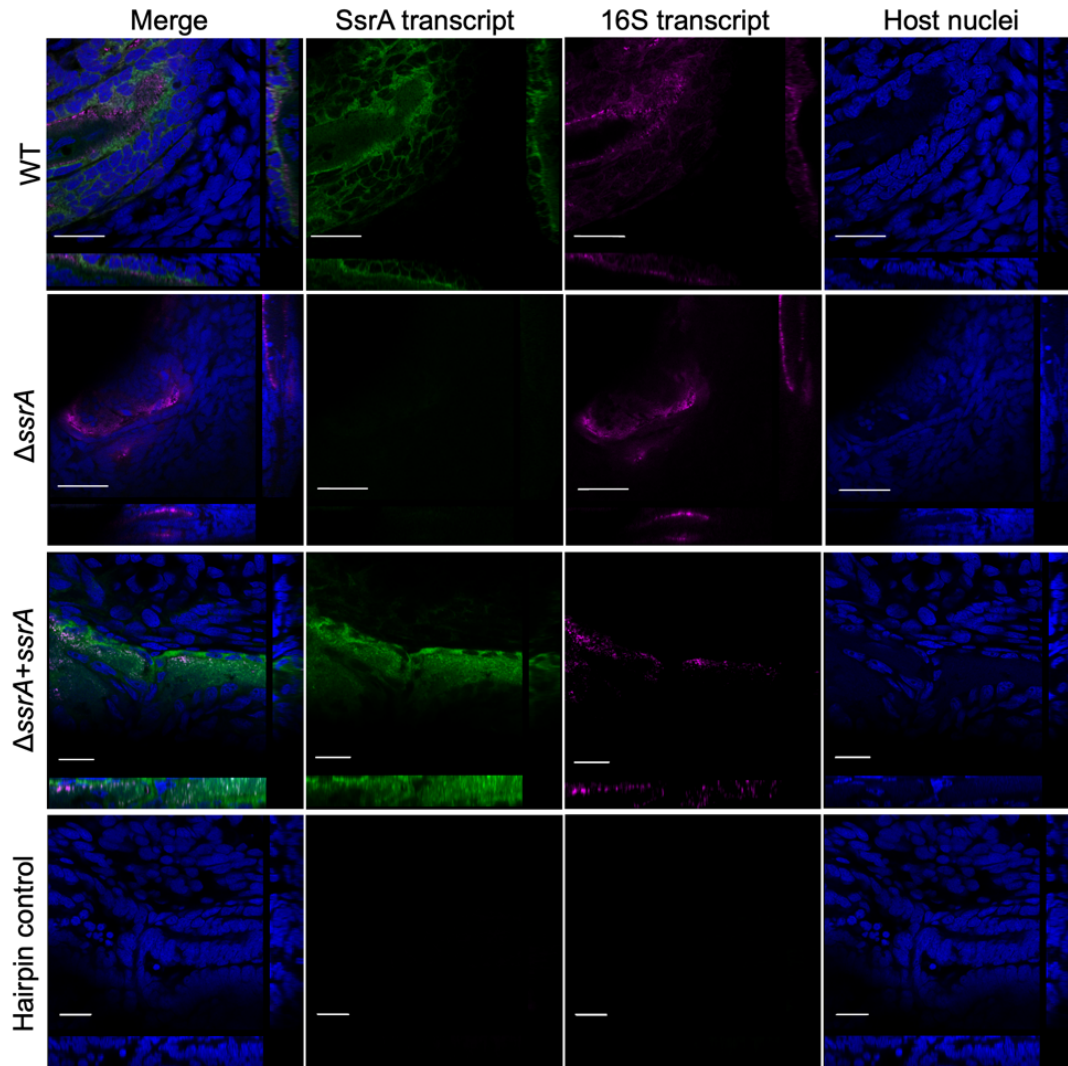


Figure S3. Localization of the Symbiont's 16S and SsrA Transcripts within the Host's Light Organ Epithelial Cells. Related to Figure 1.

Representative confocal microscopy images with orthogonal projections localizing symbiont SsrA (green) and 16S (magenta) transcripts within the crypt epithelium of light organs colonized by WT, $\Delta ssrA$, or $\Delta ssrA + ssrA$, compared to the HCR hairpin negative control; host nuclei (blue). Scale bars = 20 μm .

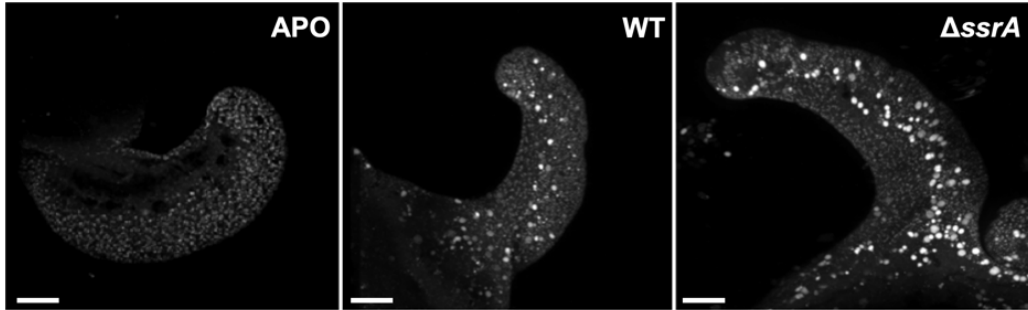


Figure S4. Induction of Apoptosis in the Light-Organ Appendages of Juvenile Squid Early in Symbiosis. Related to Figure 2.

Representative confocal microscopy images of acridine orange (AO)-stained juvenile light organs, after exposure to no (APO), wild-type (WT) or *ssrA*-deletion mutant ($\Delta ssrA$) *V. fischeri*, as described in STAR METHODS. Scale bar = 60 μm for all images.

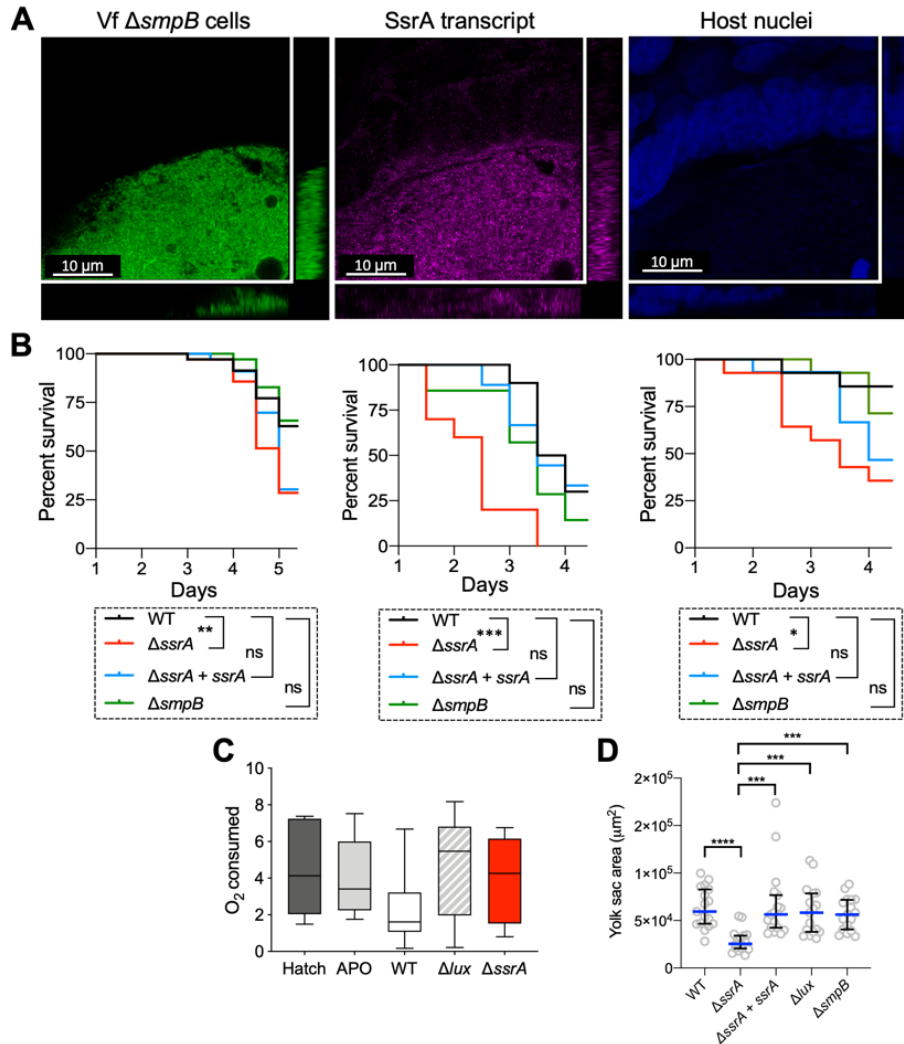


Figure S5. Effects of Colonization by $\Delta ssrA$ on Host Physiology and Health. Related to Figure 4.

Visualization of SsrA transcript (magenta) in a whole-mount light organ, 24 h after colonization with a GFP-labeled $\Delta smpB$ strain of *V. fischeri* (green). A representative confocal image indicates that symbiont SsrA transcript is within the crypt epithelial cells. Scale bar = 10 μm .

(A) Visualization by HCR of SsrA transcript (magenta) in crypt 1 of a whole-mount light organ, 24 h after colonization with a GFP-labeled $\Delta smpB$ strain of *V. fischeri* (green), including orthogonal views of a confocal microscopy Z-stack; host nuclei (TOPRO-3, blue).

(B) Kaplan-Meier survival plots of juvenile squid colonized by WT, $\Delta ssrA$, its complement ($\Delta ssrA + ssrA$) or $\Delta smpB$ strain. Data are from replicate #1 (left), #2 (middle) or #3 (right). Survival-curve analysis used the Log Rank Mantel-Cox test, with Bonferroni multiple testing adjustment for pairwise comparisons. P-value = 0.016.

(C) Respiration rates of newly hatched squid (Hatch, n=5), or of animals after 24 h, that were either maintained aposymbiotic (APO, n=12), or colonized by WT (n=12), $\Delta ssrA$ (n=11) or Δlux (n=11) strains. No significant difference between treatments was noted.

(D) Internal yolk sac areas, two days post-colonization with wild-type (WT), $\Delta ssrA$, its complement ($\Delta ssrA + ssrA$), the dark-mutant (Δlux), or $smpB$ strains. Analysis used Kruskal–Wallis ANOVA, followed by Dunn’s Multiple Comparison test (n=17). Data are represented as the median, with 95% confidence interval. P-value code: ****, < 0.0001; ***, < 0.0002; **, < 0.001; *, < 0.021. ns: non-significant for all figures.

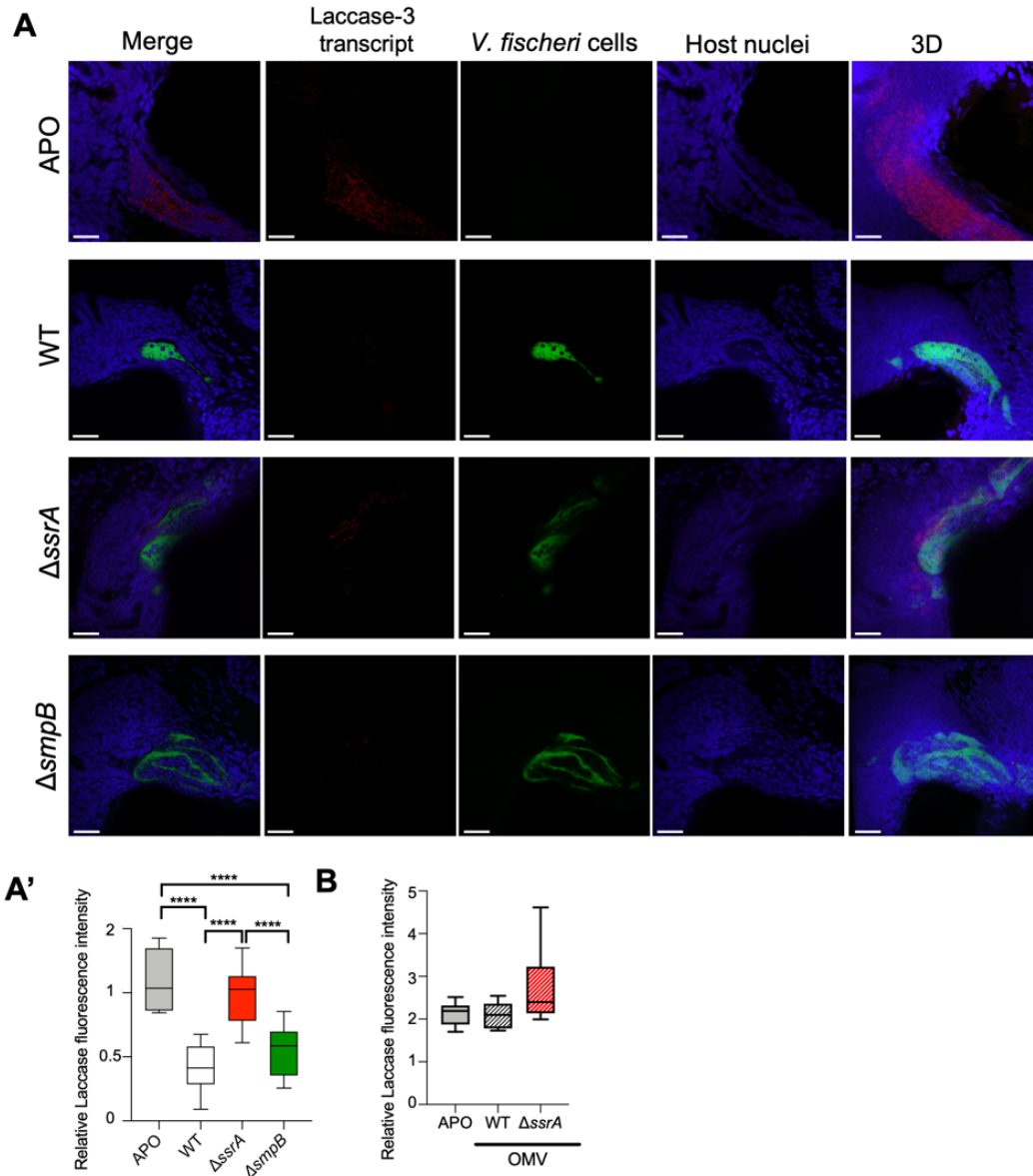


Figure S6: Down-Regulation of laccase-3 in the Crypt Epithelium Requires the Presence of Symbiont SsrA. Related to Figure 3 and Figure 4.

(A) Localization of the Laccase-3 transcript (magenta) in whole-mount light organs, 24 h post-colonization. Representative confocal images showing Laccase-3 expression in the crypt epithelia of APO (uncolonized) and WT, $\Delta ssrA$ or $\Delta smpB$ -colonized light organs; merged mid-section of Z-stack, and 3D reconstruction of the stack.

(B) Quantification of Laccase-3 presence by HCR fluorescence signal intensity from a Z-series of light organs (n=5), 3 h after incubation with OMVs isolated from either WT or $\Delta ssrA$ cultures. The symbiont OMVs by themselves do not significantly change the expression of Laccase-3 in the crypt epithelium.

KEY RESOURCES TABLE

REAGENT or RESOURCE	SOURCE	IDENTIFIER
Antibodies		
Deoxyribonuclease I, Alexa Fluor™ 488 Conjugate	Thermo Fisher Scientific	Cat# D12371
Bacterial Strains		
<i>V. fischeri</i> ES114 (WT strain)	(Boettcher and Ruby, 1990)	N/A
<i>E. coli</i> strain DH5 α carrying GFP-expression plasmid pVSV102	(Dunn et al., 2006)	N/A
<i>E. coli</i> strain DH5 α <i>pir</i> carrying conjugative helper plasmid CC118 <i>pir</i> (pEVS104)	(Dunn et al., 2006)	N/A
<i>E. coli</i> strain DH5 carrying expression vector (pEVS105)	(Dunn et al., 2006)	N/A
<i>E. coli</i> strain β 3914 carrying counter-selectable suicide vector pKV363	(Shibata and Visick, 2012)	N/A
<i>E. coli</i> strain WM3064 carrying deletion vector pSMV3	(Lynch et al., 2019)	N/A
<i>V. fischeri</i> SMG7 (Δ <i>ssrA</i>)	This study	N/A
<i>V. fischeri</i> SMG11 (Δ <i>ssrA</i> + <i>ssrA</i>)	This study	N/A
<i>V. fischeri</i> SMG12, Δ <i>ssrA</i> carrying GFP-expression plasmid pVSV102	This study	N/A
<i>V. fischeri</i> CBNR166 (Δ <i>smpB</i>)	This study	N/A
Chemicals, Peptides, and Recombinant Proteins		
Platinum® Taq DNA Polymerase High Fidelity	Invitrogen	Cat# 11304011
T4 DNA ligase	New England Biolabs	Cat# M0202T
FastDigest BamHI	Thermo Fisher Scientific	Cat# FD0054
FastDigest EcoRI	Thermo Fisher Scientific	Cat# FD0275
FastDigest XhoI	Thermo Fisher Scientific	Cat# FD0694
FastDigest KpnI	Thermo Fisher Scientific	Cat# FD0524
FastDigest XbaI	Thermo Fisher Scientific	Cat# FD0684
FastDigest ApaI	Thermo Fisher Scientific	Cat# FD1414
FastDigest SpeI	Thermo Fisher Scientific	Cat# FD1254

Kanamycin	DOT Scientific Inc	Cat# DS102120
Chloramphenicol	RPI	Cat# C61000
RNAlater®	Sigma-Aldrich	Cat# R0901-500ML
16% Paraformaldehyde Aqueous Solution	Grade Electron Microscopy Sciences	Cat# 15710
TURBO DNA- <i>free</i> ™ Kit	Thermo Fisher Scientific	Cat# AM1907
QIAGEN Proteinase K	Qiagen	Cat# 19131
TO-PRO™-3 Iodide (642/661) - 1 mM Solution in DMSO	Thermo Fisher Scientific	Cat# T3605
Random hexamers	Invitrogen	Cat# N8080127
Oligo(dT)12–18	Invitrogen	Cat# 18418012
Precision Plus Protein™ standard	Bio-Rad™	Cat# 374
ProtoBlue Safe	National Diagnostics	Cat# EC-722
RNaseA	Promega	Cat# A797C
Murine RNase inhibitor	New England Biolabs	Cat# M0314S
TRIzol™ Reagent	Invitrogen	Cat# 15596026
Chloroform ≥99%	MP Biomedicals	Cat# 0219400225
Triton™ X-100	Sigma-Aldrich	Cat# X100
Rhodamine phalloidin	Invitrogen	Cat# R415
Acridine orange	Invitrogen	Cat# A1301
Critical Commercial Assays		
QIAGEN RNeasy RNA extraction kit	Qiagen	Cat# 74104
Qubit RNA BR assay kit	Invitrogen	Cat# Q10210
LightCycler® 480 SYBR Green I Master	Roche	Cat# 04707516001
SMART™ MMLV Reverse Transcriptase	Clontech	Cat# 639523
Qubit™ Protein Assay Kit	Invitrogen	Cat# Q33211
mirVana PARIS kit	Invitrogen	Cat# AM1556
LipidSpot™ Lipid Droplet Stains	Biotium	Cat# 70065-T
Monarch RNA clean-up kit	New England Biolabs	Cat# T2030
Other lab reagents		
33 mm Millex Filter Units, .22um filter, PVDF membrane	EMD Millipore	Cat# SLGV033RS
TLA-45 rotor	Beckman Coulter	Cat# 10380
MLA-50 rotor	Beckman Coulter	Cat# A91774
TLA-110 rotor	Beckman Coulter	Cat# 366735
Millipore Durapore Membrane, PVDF, 0.45	EMD Millipore	Cat# HVLP04700

Invitrogen Novex NuPAGE 12% Bis Tris Protein Gels, 1.0mm, 10 well	Thermo Fisher Scientific	Cat# NP0341BOX
12-well plates	Millipore-Sigma	Cat# CLS3513
Scintillation vials 20ml	Thermo Fisher Scientific	Cat# 033374
Media		
Luria-Bertani broth (<i>LB</i>)	(Sambrook J. et al., 1989)	N/A
Luria-Bertani salt medium (LBS)	(Graf et al., 1994)	N/A
Minimal salts medium (MSM)	(Adin et al., 2008)	N/A
Seawater tryptone medium (SWT)	(Boettcher and Ruby, 1990)	N/A
Squid-Ringer's solution (SRS)	(Collins et al., 2012)	N/A
Oligonucleotides		
Primers used for cloning (Table S1)	This study	N/A
HCR probes (Table S1)	This study	N/A
Primers used for qRT-PCR (Table S1)	This study	N/A
Plasmids		
pSMG3, derivative of pKV363	This study	N/A
pSMG5, derivative of pVSV105	This study	N/A
pCBNR36, derivative of pSMV3	This study	N/A
Software and Algorithms		
Bowtie2	(Langmead and Salzberg, 2012)	N/A
RSEM software	(Li and Dewey, 2011)	N/A
R package edgeR	(Robinson et al., 2009)	N/A
heatmap3	(Zhao et al., 2014)	N/A
FIJI	(Schindelin et al., 2012)	N/A
Primer3plus	(Untergasser et al., 2012)	N/A
GraphPad Prism v8.00 software	GraphPad Software	N/A
Leica LasX software	Leica Microsystems	N/A
Feature Counts	(Liao et al., 2014)	N/A
Deposited Data		
RNA Seq OMV	This study	PRJNA629425
RNA Seq light organ tissue	This study	PRJNA629992

Table S1: Oligonucleotides information.

Oligonucleotide ID	Description	Sequence 5' to 3'	Source
Cloning primers			
EcoRI-ssrAups-F2	Up-stream SsrA amplification (PCRa)/PCRa to insert into pKV363	GCATGGAATTCGGTTATCTAG TCAAACCACTTCCCT	This study
ssrAdel-BamHI-R6	Up-stream SsrA amplification (PCRa)	GTACGGATCCAGCCCCAAAGT TTTGTTACCAG	This study
BamHI-ssrAdel-F7	Down-stream SsrA amplification (PCRa)	CGATCGGATCCGGGTTTTTCG TTTTAATGGCG	This study
SsrAdown-XhoI-R3	Down-stream SsrA amplification (PCRa)/PCRa to insert into pKV363	CGTACCTCGAGTCTCTTCGTG GCGCTCATT	This study
KpnI-ssrAcomp-F1	SsrA and smpB amplification to insert into pVSV105	GCATGGGTACCGACTAAATCG TACATCTGCTTTG	This study
XbaI-ssrAcomp-R2	SsrA and smpB amplification to insert into pVSV105	CGTACTCTAGACCCCTGTAAC CTATTGATTAC	This study
ApaI-smpB_A-F1	Up-stream smpB amplification (PCRa)/PCRa to insert into pSMV3	CGATCGGGCCCCGTTACGGCT AAACACACCG	This study
BamHI-smpB_A-R1	Up-stream smpB amplification (PCRa)	CGATCGGATCCTGCCATAATG CCCACATTATAC	This study
BamHI-smpB_B-F1	Down-stream smpB amplification (PCRa)	CGATCGGATCCAGTAGTTTGC GTTAATTTCAACCAG	This study
SpeI-smpB_B-R1	Down-stream smpB amplification (PCRa)/PCRa to insert into pSMV3	CGTACACTAGTGTTAGAGATG GATAGCGTGG	This study
<i>V. fischeri</i> qRT-PCR primers			
ssrA_qF2	Target gene <i>ssrA</i> amplification	AGCTCTCCTGCCCTAGCTTC	This study
ssrA_qR2	Target gene <i>ssrA</i> amplification	ATCCGTTCTAGCTCGTTTGG	This study
smpB_qF	Target gene <i>smpB</i> amplification	CACACCGCTACAAGCAGCAT	This study
smpB_qR	Target gene <i>smpB</i> amplification	CTTCACGGTTTACACGGCCA	This study
polA_qF2	Reference gene <i>polA</i> amplification	AGAGCCAAACGTAGATGAGT TGA	This study
polA_qR2	Reference gene <i>polA</i> amplification	CGATCTTACCGTCGCTTCCA	This study
<i>E. scolopes</i> qRT-PCR primers			

40S-qF3	Reference gene <i>S19</i> ribosomal protein amplification	AAGGCTTTGTCCACCTTCCT	(Moriano- Gutierrez et al., 2019)
40S-qR3	Reference gene <i>S19</i> ribosomal protein amplification	TAAATGCTCCAACACCAGCA	(Moriano- Gutierrez et al., 2019)
RIGI-3_F1q	Target gene <i>RIG-I</i> amplification	ACAGCAGCGTCCATCATCAA	This study
RIGI-3_R1q	Target gene <i>RIG-I</i> amplification	GGACCAGGTAAAGGACACGG	This study
laccase-3_F1q	Target gene <i>laccase</i> amplification	CTCCGTCCAATGAATGTGTG	This study
laccase-3_R1q	Target gene <i>laccase</i> amplification	TAGGGACAGAAAGCCGATGT	This study
C3_F1q	Target gene <i>complement 3</i> amplification	TGCTGTTCCGTTCTGTGAGCA CTA	Collins et al 2012
C3_R1q	Target gene <i>complement 3</i> amplification	GCAACACACTCTCTTTGAG CGCAT	Collins et al 2012
CIKS_F1q	Target gene <i>CIKS</i> amplification	GGTGAAGTGCCGATAACAT	This study
CIKS_R1q	Target gene <i>CIKS</i> amplification	TGCTGAAACCCATTTTAGGG	This study
HCR probes version 2			
<i>V. fischeri</i> 16S Probe #1	Target 16S rRNA	TGTGCGGGCCCCGTC AATTC ATTTGAGTTTTAATCTTGC GA CCGTA CT C	(Nikolakakis et al 2015)
<i>V. fischeri</i> 16S Probe #2	Target 16S rRNA	GTAGGTAAGGTTCTTCGCGTT GCATCGAATTAACCACATGC TCCACCGC	(Nikolakakis et al 2015)
<i>V. fischeri</i> SsrA Probe #1	Target SsrA RNA	ACGACATGCTCCTCGGGTTTC AAAATTCCCGTCGAATCCTGA ATCAGCCC	This study
<i>V. fischeri</i> SsrA Probe #3	Target SsrA RNA	CCGTCTTACAAGCAGAAGCTA GGGCAGGAGAGCTCTCAGCA GGTTATTAA	This study
<i>V. fischeri</i> SsrA Probe #4	Target SsrA RNA	AATTCGAAGTTCATCTCTCAG GCGGGAGAATCCGTTCTAGCT CGTTTGGG	This study
<i>V. fischeri</i> SsrA Probe #5	Target SsrA RNA	CGATCTTTGATTTACCGTAA AACTGCGAACCACGACGCTAT CTTATGGC	This study
HCR probes version 3			
<i>E. scolopes</i> Laccase-3 Probe #1	Target Laccase-3 RNA	TGATGACGTCATCTATTGGAA CCGGGTTTCGCTGCACTCGTGT TAACGACTTC	This study
<i>E. scolopes</i> Laccase-3 Probe #2	Target Laccase-3 RNA	GGATTGTTCCATTAACCGCCA CAACAAGTCGTGACTCAGTGT AACCATCTAA	This study

<i>E. scolopes</i> Laccase-3 Probe #3	Target Laccase-3 RNA	TCTCAACGTTGATAATTACAG TTTGGCCAACGTAGACTTCAA TCGCCGGACC	This study
<i>E. scolopes</i> Laccase-3 Probe #4	Target Laccase-3 RNA	CTTTCTGCTCCAATCCGTGCC AATGAATGGTAACGCCACTA GAGTAGAGATG	This study
<i>E. scolopes</i> Laccase-3 Probe #5	Target Laccase-3 RNA	CAGGTCCTATAGGACACTGGG TTACATAGGGGACACCGTCCA TAAACGGCGT	This study
<i>E. scolopes</i> Laccase-3 Probe #6	Target Laccase-3 RNA	TGTAATCGCTGATGACCATAA GATGTTTCGGGCATAGACATCG GCTTTCTGTC	This study
<i>E. scolopes</i> Laccase-3 Probe #7	Target Laccase-3 RNA	CGTACATAACCATGCACCATCT TAAGATAAGCTACATCAGATT CCCAATGATG	This study
<i>E. scolopes</i> Laccase-3 Probe #8	Target Laccase-3 RNA	GAGTTCCTGGTTAACTGTGA ATTTAGCAATTGGCGCTTCGT TGTGAACGCC	This study
<i>E. scolopes</i> Laccase-3 Probe #9	Target Laccase-3 RNA	CAGATATTTCAAACGGATAAA GAGCTCCAGCTGCGATTACTC TAAAACGATA	This study
<i>E. scolopes</i> Laccase-3 Probe #10	Target Laccase-3 RNA	GTGGCTCCAATTCACAGCCGT CAGACGAGACAATCTGAAGC TTATGACCGTC	This study
<i>E. scolopes</i> Laccase-3 Probe #11	Target Laccase-3 RNA	CGAATTCTGTCGTTATCCAC GAATCCAGTAGTTCGCTGGTG GTTGGTTGGC	This study
<i>E. scolopes</i> Laccase-3 Probe #12	Target Laccase-3 RNA	CTTCATCAGGGGAACCTTCGT AGTGCAGAATAGCTTCAAAG GTGTGGTTTTT	This study
<i>E. scolopes</i> Laccase-3 Probe #13	Target Laccase-3 RNA	TTAAGACCCACACGGGTCAT TTCCGAGCAGTTCTTACTTG CAGAATTCGG	This study
<i>E. scolopes</i> Laccase-3 Probe #14	Target Laccase-3 RNA	GCTGGTATAATGGGTTTACAG ACGGCTCCTGGTATTTGCGCC CGTTTACTGA	This study
<i>E. scolopes</i> Laccase-3 Probe #15	Target Laccase-3 RNA	ATATCCGATCAACTCCGCAGT CTTGCTTATCGCATAATGTGT CTACTTCGTT	This study
<i>E. scolopes</i> Laccase-3 Probe #16	Target Laccase-3 RNA	CTCCTGTAGTCGTATTAATA TAGGGTATCCCATTTTTACAA GCGAAAACGA	This study
<i>E. scolopes</i> Laccase-3 Probe #17	Target Laccase-3 RNA	CGGGAATGTTATCTCCACCCC AGTTGCTGTTTCGACCAGGTGG CATCGTTACA	This study
<i>E. scolopes</i> Laccase-3 Probe #18	Target Laccase-3 RNA	AATGCATGAACCACAGACCT GGGTTATCAGCCTTGATCCGA ATAACAGCATA	This study
<i>E. scolopes</i> Laccase-3 Probe #19	Target Laccase-3 RNA	GTGTGAAACTCCGACACACA GGAAAATGGGCAGGTGCCTC GGGCACATCAGC	This study

<i>E. scolopes</i>		GGGTCGTCGTGCCGTCCTCG	
Laccase-3 Probe	Target Laccase-3 RNA	TTTCCATCATTGGTATGCGAC	This study
#20		TGATTGCTTC	

References

- Abdullah, Z., Schlee, M., Roth, S., Mraheil, M.A., Barchet, W., Böttcher, J., Hain, T., Geiger, S., Hayakawa, Y., Fritz, J.H., et al. (2012). RIG-I detects infection with live *Listeria* by sensing secreted bacterial nucleic acids. *EMBO J.* *31*, 4153–4164.
- Akat, K.M., Lee, Y.A., Hurley, A., Morozov, P., Max, K.E.A., and Brown, M. (2018). Detection of circulating extracellular mRNAs by modified small RNA- sequencing analysis. *JCI Insight* *4*, e127317.
- Albertin, C.B., Simakov, O., Mitros, T., Wang, Z.Y., Pungor, J.R., Edsinger-Gonzales, E., Brenner, S., Ragsdale, C.W., and Rokhsar, D.S. (2015). The octopus genome and the evolution of cephalopod neural and morphological novelties. *Nature* *524*, 220–224.
- Aschtgen, M.-S., Wetzel, K., Goldman, W., McFall-Ngai, M., and Ruby, E. (2016). *Vibrio fischeri*-derived outer membrane vesicles trigger host development. *Cell. Microbiol.* *18*, 488–499.
- Barbet, G., Sander, L.E., Geswell, M., Leonardi, I., Cerutti, A., and Iliev, I. (2018). Sensing microbial viability through bacterial RNA augments T follicular helper cell and antibody. *Immunity* *48*, 584–598.
- Belcaid, M., Casaburi, G., McAnulty, S.J., Schmidbaur, H., Suria, A.M., Moriano-Gutierrez, S., Sabrina Pankey, M., Oakley, T.H., Kremer, N., Koch, E.J., et al. (2019). Symbiotic organs shaped by distinct modes of genome evolution in cephalopods. *Proc. Natl. Acad. Sci. U. S. A.* *116*, 3030–3035.
- Bhaskarla, C., Bhosale, M., Banerjee, P., Chandra, N., and Nandi, D. (2018). Protein tagging , destruction and infection. *Curr. Protein Pept. Sci.* *19*, 155–171.
- Biller, S.J., Schubotz, F., Roggensack, S.E., Thompson, A.W., Summons, R.E., and Chisholm, S.W. (2014). Bacterial vesicles in marine ecosystems. *Science.* *343*, 183–186.
- Bitar, A., Aung, K.M., Wai, S.N., and Hammarström, M.L. (2019). *Vibrio cholerae* derived outer membrane vesicles modulate the inflammatory response of human intestinal epithelial cells by inducing microRNA-146a. *Sci. Rep.* *9*, 1–11.
- Blenkiron, C., Simonov, D., Muthukaruppan, A., Tsai, P., Dauros, P., Green, S., Hong, J., Print, C.G., Swift, S., and Phillips, A.R. (2016). Uropathogenic *Escherichia coli* releases extracellular vesicles that are associated with RNA. *PLoS One* *11*, 1–16.
- Boettcher, K.J., and Ruby, E.G. (1990). Depressed light emission by symbiotic *Vibrio fischeri* of the sepiolid squid *Euprymna scolopes*. *J. Bacteriol.* *172*, 3701–3706.
- Boletzky, S. V. (2003). Biology of early life stages in cephalopod molluscs. *Adv. Mar. Biol.* *44*, 143–203.

- Bustin, S.A., Benes, V., Garson, J.A., Hellems, J., Huggett, J., Kubista, M., Mueller, R., Nolan, T., Pfaffl, M.W., Shipley, G.L., et al. (2009). The MIQE guidelines: Minimum information for publication of quantitative real-time PCR experiments. *Clin. Chem.* *55*, 611–622.
- Carlson, G.L., Gray, P., Arnold, J., Little, R.A., and Irving, M.H. (1997). Thermogenic, hormonal and metabolic effects of intravenous glucose infusion in human sepsis. *Br. J. Surg.* *84*, 1454–1459.
- Caruana, J.C., and Walper, S.A. (2020). Bacterial membrane vesicles as mediators of microbe-microbe and microbe-host community interactions. *Front. Microbiol.* *11*, 432.
- Castillo, M.G., Goodson, M.S., and McFall-Ngai, M. (2009). Identification and molecular characterization of a complement C3 molecule in a lophotrochozoan, the Hawaiian bobtail squid *Euprymna scolopes*. *Dev. Comp. Immunol.* *33*, 69–76.
- Chen, J., Morita, T., and Gottesman, S. (2019). Regulation of transcription termination of small RNAs and by small RNAs: Molecular mechanisms and biological functions. *Front. Cell. Infect. Microbiol.* *9*, 201.
- Chiu, Y.H., MacMillan, J.B., and Chen, Z.J. (2009). RNA polymerase III detects cytosolic DNA and induces type I interferons through the RIG-I pathway. *Cell* *138*, 576–591.
- Choi, H.M.T., Beck, V.A., and Pierce, N.A. (2014). Next-generation in situ hybridization chain reaction: Higher gain, lower cost, greater durability. *ACS Nano* *8*, 4284–4294.
- Choi, H.M.T., Schwarzkopf, M., Fornace, M.E., Acharya, A., Artavanis, G., Stegmaier, J., Cunha, A., and Pierce, N.A. (2018). Third-generation in situ hybridization chain reaction: Multiplexed, quantitative, sensitive, versatile, robust. *Dev.* *145*, dev165753.
- Choi, J., Um, J., Cho, J., and Lee, H. (2017a). Minireview Tiny RNAs and their voyage via extracellular vesicles: Secretion of bacterial small RNA and eukaryotic microRNA. *1*, 1475–1481.
- Choi, J., Kim, Y.K., and Han, P.L. (2019). Extracellular vesicles derived from *Lactobacillus plantarum* increase BDNF expression in cultured hippocampal neurons and produce antidepressant-like effects in mice. *Exp. Neurobiol.* *28*, 158–171.
- Choi, J.W., Kim, S.C., Hong, S.H., and Lee, H.J. (2017b). Secretable small RNAs via outer membrane vesicles in periodontal pathogens. *J. Dent. Res.* *96*, 458–466.
- Chun, C.K., Troll, J. V., Koroleva, I., Brown, B., Manzella, L., Snir, E., Almabrazi, H., Scheetz, T.E., de Fatima Bonaldo, M., Casavant, T.L., et al. (2008). Effects of colonization, luminescence, and autoinducer on host transcription during development of the squid-vibrio association. *Proc. Natl. Acad. Sci.* *105*, 11323–11328.
- Cohen, S.K., Aschtgen, M.S., Lynch, J.B., Koehler, S., Chen, F., Escrig, S., Daraspe, J., Ruby, E.G., Meibom, A., and McFall-Ngai, M. (2020). Tracking the cargo of extracellular symbionts into host tissues with correlated electron microscopy and nanoscale secondary ion mass spectrometry imaging. *Cell. Microbiol.* *22*, e13177.
- Dauros-Singorenko, P., Blenkiron, C., Phillips, A., and Swift, S. (2018). The functional RNA cargo of bacterial membrane vesicles. *FEMS Microbiol. Lett.* *365*, 1–9.
- Davidson, S.K., Koropatnick, T.A., Kossmehl, R., Sycuro, L., and McFall-Ngai, M.J. (2004). NO

- means “yes” in the squid-vibrio symbiosis: Nitric oxide (NO) during the initial stages of a beneficial association. *Cell. Microbiol.* 6, 1139–1151.
- Doino, J.A., and McFall-Ngai, M.J. (1995). A transient exposure to symbiosis-competent bacteria induces light organ morphogenesis in the host squid. *Biol. Bull.* 189, 347–355.
- Dong, Q., Zhang, L., Goh, K.L., Forman, D., O’Rourke, J., Harris, A., and Mitchell, H. (2007). Identification and characterisation of *ssrA* in members of the *Helicobacter* genus. *Antonie van Leeuwenhoek, Int. J. Gen. Mol. Microbiol.* 92, 301–307.
- Dorward, D.W., Garon, C.F., and Judd, R.C. (1989). Export and intercellular transfer of DNA via membrane blebs of *Neisseria gonorrhoeae*. *J. Bacteriol.* 171, 2499–2505.
- Douglas, A.E. (2018). *Fundamentals of microbiome science: How microbes shape animal biology.*
- Dunn, A.K., Millikan, D.S., Adin, D.M., Bose, J.L., and Stabb, E. V. (2006). New *rfp*- and *pES213*-derived tools for analyzing symbiotic *Vibrio fischeri* reveal patterns of infection and *lux* expression in situ. *Appl. Environ. Microbiol.* 72, 802–810.
- Eberle, F., Sirin, M., Binder, M., and Dalpke, A.H. (2009). Bacterial RNA is recognized by different sets of immunoreceptors. 7, 2537–2547.
- Esseck-Burns, T., Bongrand, C., Goldman, W.E., Ruby, E.G., and McFall-Ngai, M.J. (2020) Interactions of symbiotic partners drive the development of a complex biogeography in the squid-vibrio symbiosis. *mBio* (in press)
- Foster, J.S., Apicella, M.A., and McFall-Ngai, M.J. (2000). *Vibrio fischeri* lipopolysaccharide induces developmental apoptosis, but not complete morphogenesis, of the *Euprymna scolopes* symbiotic light organ. *Dev. Biol.* 226, 242–254.
- Garza-Sánchez, F., Schaub, R.E., Janssen, B.D., and Hayes, C.S. (2011). tmRNA regulates synthesis of the ArfA ribosome rescue factor. *Mol. Microbiol.* 80, 1204–1219.
- Ghosal, A., Upadhyaya, B.B., Fritz, J. V., Heintz-Buschart, A., Desai, M.S., Yusuf, D., Huang, D., Baumuratov, A., Wang, K., Galas, D., et al. (2015). The extracellular RNA complement of *Escherichia coli*. *Microbiologyopen* 4, 252–266.
- Goodson, M.S., Kojadinovic, M., Troll, J. V., Scheetz, T.E., Casavant, T.L., Bento Soares, M., and McFall-Ngai, M.J. (2005). Identifying components of the NF- κ B pathway in the beneficial *Euprymna scolopes*-*Vibrio fischeri* light organ symbiosis. *Appl. Environ. Microbiol.* 71, 6934–6946.
- Gottesman, S. (2004). The small RNA regulators of *Escherichia coli*: Roles and mechanisms. *Annu. Rev. Microbiol.* 58, 303–328.
- Goubau, D., Deddouche, S., and Reis e Sousa, C. (2013). Cytosolic sensing of viruses. *Immunity* 38, 855–869.
- Graf, J., Dunlap, P. V., and Ruby, E.G. (1994). Effect of transposon-induced motility mutations on colonization of the host light organ by *Vibrio fischeri*. *J. Bacteriol.* 176, 6986–6991.
- Green, T.J., Raftos, D., Speck, P., and Montagnani, C. (2015). Antiviral immunity in marine molluscs. *J. Gen. Virol.* 96, 2471–2482.
- Han, E.C., Choi, S.Y., Lee, Y., Park, J.W., Hong, S.H., and Lee, H.J. (2019). Extracellular RNAs in periodontopathogenic outer membrane vesicles promote TNF- α production in human

- macrophages and cross the blood-brain barrier in mice. *FASEB J.* *33*, 13412–13422.
- He, Y., Jouaux, A., Ford, S.E., Lelong, C., Sourdain, P., Mathieu, M., and Guo, X. (2015). Transcriptome analysis reveals strong and complex antiviral response in a mollusc. *Fish Shellfish Immunol.* *46*, 131–144.
- Heath-Heckman, E.A.C., and McFall-Ngai, M.J. (2011). The occurrence of chitin in the hemocytes of invertebrates. *Zoology* *4*, 191–198.
- Huang, B., Zhang, L., Du, Y., Xu, F., Li, L., and Zhang, G. (2017). Characterization of the mollusc RIG-I / MAVS pathway reveals an archaic antiviral signalling framework in invertebrates. *Sci. Rep.* *7*, 1–13.
- Jones, B.W., and Nishiguchi, M.K. (2004). Counterillumination in the Hawaiian bobtail squid, *Euprymna scolopes* Berry (Mollusca: Cephalopoda). *Mar. Biol.* *144*, 1151–1155.
- Karzai, A.W., Roche, E.D., and Sauer, R.T. (2000). The SsrA – SmpB system for protein tagging, directed degradation and ribosome rescue. *Nat. Struct. Biol.* *7*, 449–455.
- Keegan, C., Krutzik, S., Schenk, M., Scumpia, O., Lu, J., Ling, Y., Pang, J., Brandon, S., Lim, K.S., Shell, S., et al. (2019). Mycobacterium tuberculosis transfer RNA induces IL-12p70 via synergistic activation of pattern recognition receptors within a cell network. *J. Immunol.* *200*, 3244–3258.
- Kell, A.M., and Gale, M. (2015). RIG-I in RNA virus recognition. *Virology* *479*, 110–121.
- Koch, E.J., Miyashiro, T., McFall-Ngai, M.J., and Ruby, E.G. (2014). Features governing symbiont persistence in the squid-vibrio association. *Mol. Ecol.* *23*, 1624–1634.
- Koeppen, K., Hampton, T.H., Jarek, M., Scharfe, M., Gerber, S.A., Mielcarz, D.W., Demers, E.G., Dolben, E.L., Hammond, J.H., Hogan, D.A., et al. (2016). A novel mechanism of host-pathogen interaction through sRNA in bacterial outer membrane vesicles. *PLoS Pathog.* *12*, 1–22.
- Koropatnick, T.A. (2004). Microbial factor-mediated development in a host-bacterial mutualism. *Science* (80-.). *306*, 1186–1188.
- Koropatnick, T.A., Kimbell, J.R., and McFall-Ngai, M.J. (2007). Responses of host hemocytes during the initiation of the squid-vibrio symbiosis. *Biol. Bull.* *212*, 29–39.
- Krasity, B.C., Troll, J. V., Weiss, J.P., and McFall-Ngai, M.J. (2011). LBP/BPI proteins and their relatives: Conservation over evolution and roles in mutualism. *Biochem. Soc. Trans.* *39*, 1039–1044.
- Kremer, N., Philipp, E.E.R., Carpentier, M.C., Brennan, C.A., Kraemer, L., Altura, M.A., Augustin, R., Hasler, R., Heath-Heckman, E.A.C., Peyer, S.M., et al. (2013). Initial symbiont contact orchestrates host-organ-wide transcriptional changes that prime tissue colonization. *Cell Host Microbe* *14*, 183–194.
- Kreymann, G., Grosser, S., Buggisch, P., Gottschall, C., Matthaei, S., and Greten, H. (1993). Oxygen consumption and resting metabolic rate in sepsis, sepsis syndrome, and septic shock. *Crit. Care Med.* *21*, 1012–1019.
- Kuehn, M.J., and Kesty, N.C. (2005). Bacterial outer membrane vesicles and the host-pathogen interaction. *Genes Dev.* *19*, 2645–2655.

- Langmead, B., and Salzberg, S.L. (2012). Fast gapped-read alignment with Bowtie 2. *Nat. Methods* 9, 357–359.
- Lässig, C., and Hopfner, K.P. (2017). Discrimination of cytosolic self and non-self RNA by RIG-I-like receptors. *J. Biol. Chem.* 292, 9000–9009.
- Leonard, S.P., Powell, J.E., Perutka, J., Geng, P., Heckmann, L.C., Horak, R.D., Davies, B.W., Ellington, A.D., Barrick, J.E., and Moran, N.A. (2020). Engineered symbionts activate honey bee immunity and limit pathogens. *Science* 367, 573–576.
- Li, B., and Dewey, C. (2011). RSEM: accurate transcript quantification from RNA-Seq data with or without a reference genome. *BMC Bioinformatics* 12, 323.
- Li, X.D., and Chen, Z.J. (2012). Sequence specific detection of bacterial 23S ribosomal RNA by TLR13. *eLife* 2012, 1–14.
- Liao, Y., Smyth, G.K., and Shi, W. (2014). featureCounts: an efficient general purpose program for assigning sequence reads to genomic features. *Bioinformatics* 30, 923–930.
- Luna-Acosta, A., Breitwieser, M., Renault, T., and Thomas-Guyon, H. (2017). Recent findings on phenoloxidases in bivalves. *Mar. Pollut. Bull.* 122, 5–16.
- Lynch, J.B., Schwartzman, J.A., Bennett, B.D., McAnulty, S.J., Knop, M., Nyholm, S.V., and Ruby, E.G. (2019). Ambient pH alters the protein content of outer membrane vesicles, driving host development in a beneficial symbiosis. *J. Bacteriol.* 201, e00319-19.
- Malabirade, A., Habier, J., Heintz-buschart, A., and May, P. (2018). The RNA complement of outer membrane vesicles from *Salmonella enterica* serovar Typhimurium under distinct culture conditions. *Front. Microbiol.* 9, 1–21.
- Mate, D.M., and Alcalde, M. (2017). Laccase: a multi-purpose biocatalyst at the forefront of biotechnology. *Microb. Biotechnol.* 10, 1457–1467.
- McFall-Ngai, M. (2014). The importance of microbes in animal development: Lessons from the squid-vibrio symbiosis. *Annu. Rev. Microbiol.* 68, 177–194.
- McFall-Ngai, M., Nyholm, S. V., and Castillo, M.G. (2010). The role of the immune system in the initiation and persistence of the *Euprymna scolopes*-*Vibrio fischeri* symbiosis. *Semin. Immunol.* 22, 48–53.
- Mogensen, T.H. (2009). Pathogen recognition and inflammatory signaling in innate immune defenses. *Clin. Microbiol. Rev.* 22, 240–273.
- Moriano-Gutierrez, S., Koch, E.J., Bussan, H., Romano, K., Belcaid, M., and Rey, F.E. (2019). Critical symbiont signals drive both local and systemic changes in diel and developmental host gene expression. *Proc. Natl. Acad. Sci.* 116, 7990–7999.
- Muto, A., Sato, M., Tadaki, T., Fukushima, M., Ushida, C., and Himeno, H. (1996). Structure and function of 10Sa RNA: Trans-translation system. *Biochimie* 78, 985–991.
- Nevo-Dinur, K., Govindarajan, S., and Amster-Choder, O. (2012). Subcellular localization of RNA and proteins in prokaryotes. *Trends Genet.* 28, 314–322.
- Newsholme, P., and Newsholme, E.A. (1989). Rates of utilization of glucose, glutamine and oleate and formation of end-products by mouse peritoneal macrophages in culture. *Biochem. J.* 261, 211–218.

- Nikolakakis, K., Lehnert, E., McFall-Ngai, M.J., and Ruby, E.G. (2015). Use of hybridization chain reaction-fluorescent in situ hybridization to track gene expression by both partners during initiation of symbiosis. *Appl. Environ. Microbiol.* *81*, 4728–4735.
- Nyholm, S. V., Stewart, J.J., Ruby, E.G., and McFall-Ngai, M.J. (2009). Recognition between symbiotic *Vibrio fischeri* and the haemocytes of *Euprymna scolopes*. *Environ. Microbiol.* *11*, 483–493.
- Park, J.Y., Choi, J., Lee, Y., Lee, J.E., Lee, E.H., Kwon, H.J., Yang, J., Jeong, B.R., Kim, Y.K., and Han, P.L. (2017). Metagenome analysis of bodily microbiota in a mouse model of Alzheimer disease using bacteria-derived membrane vesicles in blood. *Exp. Neurobiol.* *26*, 369–379.
- Rehwinkel, J., Tan, C.P., Goubau, D., Schulz, O., Pichlmair, A., Bier, K., Robb, N., Vreede, F., Barclay, W., Fodor, E., et al. (2010). RIG-I detects viral genomic RNA during negative-strand RNA virus infection. *Cell* *140*, 397–408.
- Ren, B., Wang, X., Duan, J., and Ma, J. (2018). Rhizobial tRNA-derived small RNAs are signal molecules regulating plant nodulation. *Science* (80-.). *294*, 16930–16941.
- Robinson, M.D., McCarthy, D.J., and Smyth, G.K. (2009). edgeR: A Bioconductor package for differential expression analysis of digital gene expression data. *Bioinformatics* *26*, 139–140.
- Rolig, A.S., Sweeney, E.G., Kaye, L.E., Desantis, M.D., Perkins, A., Banse, A. V., Hamilton, M.K., and Guillemin, K. (2018). A bacterial immunomodulatory protein with lipocalin-like domains facilitates host–bacteria mutualism in larval zebrafish. *Elife* *7*, e37172.
- Rosani, U., Varotto, L., Gerdol, M., Pallavicini, A., and Venier, P. (2015). IL-17 signaling components in bivalves : Comparative sequence analysis and involvement in the immune responses. *Dev. Comp. Immunol.* *52*, 255–268.
- Rossi, O., Van Berkel, L.A., Chain, F., Tanweer Khan, M., Taverne, N., Sokol, H., Duncan, S.H., Flint, H.J., Harmsen, H.J.M., Langella, P., et al. (2016). *Faecalibacterium prausnitzii* A2-165 has a high capacity to induce IL-10 in human and murine dendritic cells and modulates T cell responses. *Sci. Rep.* *6*, 18507.
- Round, J.L., Lee, S.M., Li, J., Tran, G., Jabri, B., Chatila, T.A., and Mazmanian, S.K. (2011). The toll-like receptor 2 pathway establishes colonization by a commensal of the human microbiota. *Science*. *332*, 974–977.
- Le Roux, F., Binesse, J., Saulnier, D., and Mazel, D. (2007). Construction of a *Vibrio splendidus* mutant lacking the metalloprotease gene *vsm* by use of a novel counterselectable suicide vector. *Appl. Environ. Microbiol.* *73*, 777–784.
- Ruby, E.G., and McFall-Ngai, M.J. (1999). Oxygen-utilizing reactions and symbiotic colonization of the squid light organ by *Vibrio fischeri*. *Trends Microbiol.* *7*, 414–420.
- Sander, L.E., Davis, M.J., Boekschoten, M. V, Amsen, D., Dascher, C.C., Ryffel, B., Swanson, J.A., Muller, M., and Blander, J.M. (2011). Detection of prokaryotic mRNA signifies microbial viability and promotes immunity. *Nature* *474*, 385–389.
- Schindelin, J., Arganda-Carreras, I., Frise, E., Kaynig, V., Longair, M., Pietzsch, T., Preibisch, S., Rueden, C., Saalfeld, S., Schmid, B., et al. (2012). FIJI: an open-source platform for biological-image analysis. *Nat. Methods* *9*, 676–682.

- Schönhuber, W., Le Bourhis, G., Tremblay, J., Amann, R., and Kulakauskas, S. (2001). Utilization of tmRNA sequences for bacterial identification. *BMC Microbiol.* *1*, 1–20.
- Schwartzman, J.A., Koch, E., Heath-Heckman, E.A.C., Zhou, L., Kremer, N., McFall-Ngai, M.J., and Ruby, E.G. (2015). The chemistry of negotiation: Rhythmic, glycan-driven acidification in a symbiotic conversation. *Proc. Natl. Acad. Sci.* *112*, 566–571.
- Sellge, G., and Kufer, T.A. (2015). PRR-signaling pathways: Learning from microbial tactics. *Semin. Immunol.* *27*, 75–84.
- Seon, H.C., Park, H., and Dong, C. (2006). Act1 adaptor protein is an immediate and essential signaling component of interleukin-17 receptor. *J. Biol. Chem.* *281*, 35603–35607.
- Seth, R.B., Sun, L., Ea, C.K., and Chen, Z.J. (2005). Identification and characterization of MAVS, a mitochondrial antiviral signaling protein that activates NF- κ B and IRF3. *Cell* *122*, 669–682.
- Silvestri, A., Fiorilli, V., Miozzi, L., Accotto, G.P., Turina, M., and Lanfranco, L. (2019). In silico analysis of fungal small RNA accumulation reveals putative plant mRNA targets in the symbiosis between an arbuscular mycorrhizal fungus and its host plant. *BMC Genomics* *20*, 169.
- Small, A.L., and McFall-Ngai, M.J. (1999). Halide peroxidase in tissues that interact with bacteria in the host squid *Euprymna scolopes*. *J. Cell. Biochem.* *72*, 445–457.
- Song, T., Mika, F., Lindmark, B., Liu, Z., Schild, S., Bishop, A., Zhu, J., Camilli, A., Johansson, J., Vogel, J., et al. (2008). A new *Vibrio cholerae* sRNA modulates colonization and affects release of outer membrane vesicles. *Mol. Microbiol.* *70*, 100–111.
- Stabb, E. V., and Ruby, E.G. (2002). RP4-based plasmids for conjugation between *Escherichia coli* and members of the Vibrionaceae. *Methods Enzymol.*
- Thompson, L.R., Nikolakakis, K., Pan, S., Reed, J., Knight, R., and Ruby, E.G. (2017). Transcriptional characterization of *Vibrio fischeri* during colonization of juvenile *Euprymna scolopes*. *Environ. Microbiol.* *19*, 1845–1856.
- Ugolini, M., and Sander, L.E. (2018). Dead or alive : how the immune system detects microbial viability. *Curr. Opin. Immunol.* *56*, 60–66.
- Untergasser, A., Cutcutache, I., Koressaar, T., Ye, J., Faircloth, B.C., Remm, M., and Rozen, S.G. (2012). Primer3--new capabilities and interfaces. *Nucleic Acids Res.* *40*, e115.
- Vabret, N., and Blander, J.M. (2013). Sensing microbial RNA in the cytosol. *4*, 1–9.
- Vidal, E.A.G., DiMarco, F.P., Wormuth, J.H., and Lee, P.G. (2002). Influence of temperature and food availability on survival, growth and yolk utilization in hatchling squid. *Bull. Mar. Sci.* *71*, 915–931.
- Visick, K.L., Foster, J., Doino, J., McFall-Ngai, M., and Ruby, E.G. (2000). *Vibrio fischeri* lux genes play an important role in colonization and development of the host light organ. *J. Bacteriol.* *182*, 4578–4586.
- Wang, J., Zhang, G., Fang, X., Guo, X., Li, L., Luo, R., Xu, F., Yang, P., Zhang, L., Wang, X., et al. (2012). The oyster genome reveals stress adaptation and complexity of shell formation. *Nature* *490*, 49–54.

- Wang, P.H., Weng, S.P., and He, J.G. (2015). Nucleic acid-induced antiviral immunity in invertebrates: An evolutionary perspective. *Dev. Comp. Immunol.* *48*, 291–296.
- Wier, A.M., Nyholm, S. V, Mandel, M.J., Massengo-Tiassé, R.P., Schaefer, A.L., Koroleva, I., Splinter-Bondurant, S., Brown, B., Manzella, L., Snir, E., et al. (2010). Transcriptional patterns in both host and bacterium underlie a daily rhythm of anatomical and metabolic change in a beneficial symbiosis. *Proc. Natl. Acad. Sci.* *107*, 2259–2264.
- Zhang, H., Zhang, Y., Song, Z., Li, R., Ruan, H., Liu, Q., and Huang, X. (2020). sncRNAs packaged by *Helicobacter pylori* outer membrane vesicles attenuate IL-8 secretion in human cells. *Int. J. Med. Microbiol.* *310*, 151356.
- Zhang, L., Li, L., Guo, X., Litman, G.W., Dishaw, L.J., and Zhang, G. (2015). Massive expansion and functional divergence of innate immune genes in a protostome. *Sci. Rep.* *5*, 8693.
- Zhao, S., Guo, Y., Sheng, Q., and Shyr, Y. (2014). Advanced heat map and clustering analysis using Heatmap3. *Biomed Res. Int.* *2014*, 986048.

CHAPTER 4

microRNA-mediated regulation of host responses in a symbiotic organ

To be submitted to BMC Genomics

Silvia Moriano-Gutierrez^{1,2}, Edward G Ruby¹ and Margaret J McFall-Ngai^{1*}

¹ Pacific Biosciences Research Center. University of Hawai‘i at Mānoa; Honolulu; 96813. USA

² Molecular Biosciences and Bioengineering. University of Hawai‘i at Mānoa

*Correspondence: mcfallng@hawaii.edu

Abstract

Background:

In horizontally acquired symbioses, hosts require specific tissues and/or organs to maintain their symbionts. Symbiotic colonization is accompanied by vast changes in the gene expression within these tissues. MicroRNAs (miRNAs) are short, non-coding RNAs that bind to target mRNAs, shaping the cellular expression landscape by post-transcriptional control of mRNA translation and decay.

Results: Using the experimentally tractable, binary squid-vibrio model for understanding the events and signals underlying host-microbe symbioses, we show that colonization of the light organ induces changes in the miRNA transcriptome. A total of 215 host miRNAs were identified as being expressed in the light organ, 26 of which were differentially expressed with symbiosis. A functional enrichment analysis revealed that target genes of miRNAs down-regulated in symbiosis are enriched in the categories of neurodevelopment and tissue remodeling, while targets of miRNAs up-regulated in symbiosis are enriched in the depression of immune responses.

Conclusion: Our data provide evidence that, upon colonization, the miRNA transcriptome in the light organ drives gene expression changes that orchestrate developmental changes in symbiotic tissues as well as adapting the host immune response to integrate the symbiont into its biology

Keywords: miRNA, non-coding RNA, symbiosis

Background

Symbiotic interactions are ubiquitous, diverse and have emerged multiple times across evolutionary time, highlighting such alliances as powerful source for innovative evolutionary strategies [1]. Many organisms rely on beneficial associations with specific symbionts for nutrition, defense, normal development, physiology or other fitness aspects [2]. In horizontally transmitted symbioses, in which an animal or plant acquires new symbionts each generation, the host requires specific tissues and/or organs to harbor its symbionts and must adapt its morphology, physiology and immune responses to accommodate symbiotic colonization [3]. Ultimately, these accommodations are driven by changes in gene expression during the onset of the symbiosis [4–7]. Post-transcriptional regulation by microRNAs (miRNAs) is crucial to ensuring that proper gene expression patterns are established and maintained in each cell type [8]. miRNAs are small regulatory RNAs, constituents of the RNA-induced silencing complex (RISC), that regulate target

genes via complementary binding to the 3' untranslated region (3'UTR) of mRNA. Although target transcripts are commonly downregulated by either inhibition of translation or mRNA degradation [8, 9], some studies have revealed that specific miRNAs are capable of activating gene expression directly or indirectly in different cell types [10, 11]. Regardless of their mechanism of action, miRNAs are known key regulators of biological processes such as early development, stress responses, apoptosis, cell proliferation and differentiation, as well as host-microbe interactions [12–15].

The miRNA biogenesis machinery is highly conserved among organisms [16]. After the miRNAs are transcribed from the genome, the primary transcripts are processed first in the nucleus and then in the cytosol by RNase II enzymes Drosha and Dicer, respectively, ultimately generating a mature miRNA associated with the RISC complex [17]. miRNAs have been discovered in a wide range of organisms. The miRNA database (mirBase v22), for instance, encompasses 38,589 hairpin precursors (pre-miRNA) in at least 271 different organisms [18]. However, the collection of known miRNAs among Lophotrochozoa is still relatively limited, with only 461 precursors belonging to this group. Among Mollusca, just 65 miRNA precursors are represented in the latest version of mirBase and, to date, no miRNA high-throughput sequencing studies have been published in any cephalopod.

To study miRNA-mediated regulation in response to symbiosis, we used as a model the highly specific symbiosis between the Hawaiian bobtail squid, *Euprymna scolopes*, and the luminescent bacterium *Vibrio fischeri*. In this horizontally transmitted association, the nascent light organ is poised to interact with planktonic *V. fischeri* from the surrounding seawater [19]. Moving cilia on the external appendages of the light organ (Fig. 1A) aid symbiont recruitment [20] to a set of surface pores, through which the symbionts migrate into the deep crypts of the light organ where they proliferate [21]. Within days following colonization, the ciliated field on the light organ surface appendages is completely lost by an early induction of apoptosis [22]. Furthermore, the crypt epithelial cells that are in direct contact with the symbionts change shape and size [23]. These symbiont-driven changes in the light organ involve vast changes of gene expression [4, 5, 24, 25]. In this study, we compared miRNA expression profiles in uncolonized and colonized juvenile squid light organs. Additionally, we compared the miRNAs present in the circulatory system of a symbiotic host to those found within the symbiotic light organ. Our data provide evidence that, upon colonization, the miRNA transcriptome in the light organ drives gene

expression changes that orchestrate the development of symbiotic tissues, and affect the host immune response to promote symbiont tolerance.

Material and Methods

Squid light-organ colonization assays

The breeding colony of Hawaiian bobtail squid (*Euprymna scolopes*) was collected from Maunalua Bay, Oahu, Hawai'i, and maintained in flow-through seawater tanks on a natural 12:12-h light:dark cycle in the Kewalo Marine Laboratory. Within 2 h of hatching, juvenile squid were either exposed overnight to *V. fischeri* cells (*i.e.*, wild-type (WT) strain ES114 [26]) at a concentration of 3,000-6,000 CFU*ml⁻¹ overnight, or kept aposymbiotic (APO) in filter-sterilized ocean water (FSOW). Bacterial cells were cultured overnight in Luria-Bertani salt medium (LBS) [26], sub-cultured into seawater tryptone medium (SWT) [27], and grown to mid-log phase at 28°C with shaking at 220 rpm. Colonization of the host was monitored by monitoring animal luminescence with a TD 20/20 luminometer (Turner Designs, Sunnyvale, CA). After 24 h post-colonization, squid were anesthetized in seawater containing 2% ethanol and stored at -80°C in RNAlater (Sigma-Aldrich) until further processing.

Hemolymph RNA isolation and sequencing

Adult wild-caught squid were anesthetized with 2% ethanol in seawater prior to hemolymph extraction from the cephalic artery. Each squid was sampled only once at either 4 PM or 2 AM, with 200-300 µl of hemolymph recovered. Circulating hemocytes were removed by centrifuging the samples at 5,000 rpm for 10 min at 4°C to pellet the cells. Pooled cell-free hemolymph from two adults was used for RNA purification at each time point. Total extracted RNA was purified using the mirVana PARIS kit (Invitrogen), which was followed by treatment with DNase I (Thermo Fisher Scientific). The RNA concentration was determined with a Qubit RNA BR assay kit (Invitrogen). The small RNA libraries were constructed using the TruSeq Small RNA Sample Preparation kit according to the manufacturer's instructions. The quality of the RNA libraries was assessed with the Agilent 2100 Bioanalyzer System. The single-end 50-cycle sequencing was performed using an Illumina HiSeq2500 platform at the University of Wisconsin-Madison Biotechnology and Gene Expression Center.

Phylogenetic tree reconstruction of the Argonaute and PIWI proteins

The sequences of annotated molluscan argonaute-like and PIWI like proteins were obtained from NCBI. *E. scolopes* sequences were obtained from the reference transcriptome [28] by blastx [29], and translated to amino acid sequence by ExPASy [30]. Protein sequences were aligned with mafft [31], trimmed for sites with over 50% gaps with trimAl [32] before tree reconstruction. A phylogenetic tree was constructed with RAxML with the PROTGAMMAWAG model [33]. Support values were generated by 1000 bootstrap pseudoreplications.

To obtain light-organ expression levels of miRNA machinery proteins, the 24-h light-organ transcriptome was downloaded from SRA (PRJNA473394) and mapped against the *E. scolopes* reference transcriptome [28] with bowtie2 [34]. Relative expression values for each tissue were estimated with RSEM software [35]. A bar graph of expression values was produced with GraphPad Prism v8.00 software.

Light organ RNA isolation and sequencing

For RNA isolation, 20 juvenile light organs were pooled, and total extracted RNA was purified using the mirVana PARIS kit (Invitrogen), which was followed by treatment with DNase I (Thermo Fisher Scientific). RNA concentration was determined with a Qubit RNA BR assay kit (Invitrogen). The small RNA libraries were constructed using the TruSeq Small RNA Sample Preparation kit according to the manufacturer's instructions. The quality of the RNA libraries was assessed with Agilent 2100 Bioanalyzer System. The single-end 50-cycle sequencing was performed using an Illumina HiSeq2500 platform at the University of Wisconsin-Madison Biotechnology and gene expression center.

Analysis of known and predicted miRNAs.

FastQC [36] was used to evaluate raw sequencing reads. The low quality nucleotide bases and adapter-contamination sequences were identified and removed with trimmomatic [37] and cutadapt [38]. Reads ranging from 14-36 bp were collected for alignment with the *E. scolopes* genome [28] using miRDeep2 software [39]. In addition, reads were mapped to the latest miRbase database (v22.1), allowing one mismatch to the precursor sequence. Any miRNA already present in miRbase was designated as "known", while miRNAs identified in the squid genome uniquely

were considered to be “predicted” miRNAs. Only potential predicted miRNAs with mirDeep2 scores greater than 0 were considered.

To identify *E. scolopes* predicted miRNAs in other mollusks, the identified precursors were mapped against the genomes of four species: *Octopus bimaculoides* (GCA_001194135.1), *Crassostrea gigas* (GCA_000297895.1), *Lymnaea stagnalis* (GCA_900036025.1), and *Lottia gigantea* (GCF_000327385.1) and, as an outgroup, *Drosophila melanogaster* (GCF_000001215.4).

Differential expression analysis of miRNAs

Identified precursors in the *E. scolopes* genome or in the mirBase database were quantified with the miRDeep2 module quantifier.pl [39]. Principal component analysis of expression values was performed with DESeq2. The R package edgeR [40] was used to detect differentially expressed miRNAs among conditions. miRNAs with an adjusted p-value < 0.05 were considered significantly differentially expressed. Heatmaps of expression values of such miRNAs, as well as a hierarchical clustering, were created with heatmap3 [41] in the R environment.

Target-gene prediction and functional annotation

The potential targets of the differentially expressed miRNA were obtained using miRanda [42] and the three prime UTR regions of the reference transcriptome [28]. Only targets with both a score ≥ 160 , and a free energy ≤ -25 kcal/mol, were considered. Functional annotation of the miRNA targets was performed by Gene Ontology (GO) mapping with Blast2go software [43]. Statistical enrichment of GO terms was determined by a Fisher exact test with FDR < 0.01 in Blast2go, and visualized with REVIGO [44].

Results

Evolution and expression of *E. scolopes* miRNA machinery

Using a phylogenetic framework, we studied the distribution of the guide-RNA protein repertoire of *E. scolopes* in the context of other mollusks and reference organisms, including the fruit fly and humans. The Argonaute and PIWI protein sequence data were obtained from available annotations in NCBI of 6 different molluscan species (*Aplysia californica*, *Crassostreas gigas*,

Lottia gigantea, *Lymnaea stagnalis*, *Mizuhopecten yessoensis* and *Octopus bimaculoides*). In addition, we identified two unique candidate Argonaute-like sequences and two PIWI-like sequences within existing *E. scolopes* transcriptional databases [5, 28]. We found that unlike the octopus, which encodes only one argonaute-like protein in its genome, the squid has two putative orthologs of argonaute-like proteins that cluster within the Argonaute (AGO) clade and are supported by high bootstrap values (Fig. 1B). PIWI family members, by contrast, are relatively conserved in cephalopods where both octopus and squid have PIWI1-like and PIWI2-like members (Fig. 1B). Furthermore, in agreement with previously reported gene trees, *D. melanogaster* AGO3 shares a common ancestral gene with the PIWI-like clade members [45, 46]. In summary, the data provide evidence that the squid light organ contains evolutionarily conserved RNA-guide proteins within the PIWI and argonaute subclades.

We furthermore confirmed that additional proteins involved in the miRNA machinery are expressed in the light organ. Members of the microprocessor complex, PAHSA and DROSHA, as well as the RISC loading protein Dicer, together with the miRNA-guide AGO1 and AGO2, exhibited relatively low expression (Fig. 2A). In comparison, PIWI members and Exportin 5, involved in the transport of the pre-miRNA to the cytoplasm for the final maturation steps, were more highly expressed (Fig. 2A). Regardless of expression level, all major proteins of the miRNA machinery were found in the *E. scolopes* light organ, indicating that the squid has all the necessary components to use miRNA machinery for post-transcriptional regulation of gene expression.

Identification of known and predicted *E. scolopes* miRNAs in the squid light organ

To study miRNA expression in response to symbiont colonization of the juvenile squid light organ, colonized (WT) or uncolonized (APO) juvenile light organs were collected 24 h post-colonization for small RNA sequencing. After removing contaminating *V. fischeri* sequences and well-characterized non-coding RNAs (rRNAs, tRNAs, snoRNAs), reads ranging from 14-36 bp were collected for alignment with both the *E. scolopes* genome [28] and the latest miRbase database (v22.1) using miRDeep2 software [39]. By comparison with both the genome and the miRbase database, we identified a total of 215 miRNAs in the combined WT-colonized and aposymbiotic juvenile light organs. Sixty-six of these identified miRNAs were found only in miRbase database and, although they were isolated from the squid host, could not be identified within the *E. scolopes* genome (Table S1). Among the miRNAs localized in the genome, 34 were

found within the mirBase database, and were designated as “known” miRNAs, while the remaining 115 miRNAs were not found within miRbase and were therefore considered to be “predicted” (Fig. 2B, Table S2). To further characterize the miRNA light-organ database, we compared the miRNAs found in the squid genome to four other mollusk genomes (*C. gigas*, *L. gigantea*, *L. stagnalis* and *O. bimaculoides*), as well as to *D. melanogaster* as an outgroup. Remarkably, but not unexpectedly, the number of matching predicted miRNA sequences increases with taxonomic proximity (Fig. 2C), and only 35% of the predicted miRNAs are specific to the *E. scolopes* lineage. Known miRNAs remain relatively constant across the molluscan species studied, with only 50% of these known miRNAs also identified in *D. melanogaster*.

Differential expression profile of miRNAs in response to light-organ symbiosis

To determine the effect of symbiosis on the miRNA population, the expression of miRNAs in WT-colonized light organs was compared to that of APO light organs. Principal Component Analysis (PCA) revealed that colonization state was the primary factor affecting global miRNA expression in squid light organs; *i.e.*, PC1 (55% of the overall variance) separated APO animals from WT-colonized animals (Fig. 3A). A total of 26 miRNAs were found differentially expressed, with 16 miRNAs up-regulated and 10 miRNAs down-regulated with symbiosis (Fig. 3B, Table S3). Interestingly, only two known (*i.e.*, present in miRbase) miRNAs change their expression levels with symbiosis, and are down-regulated, while many predicted (*i.e.*, not present in miRbase) miRNAs were up-regulated with symbiosis, perhaps suggesting that the symbiotic state requires an miRNA response unique to *E. scolopes*.

Target prediction of light-organ regulated miRNAs

To understand more precisely why miRNAs are regulated in response to light-organ symbiosis, candidate mRNA targets were predicted with miRanda software. The miRNAs up-regulated in APO animals had 108 predicted mRNA targets, while the miRNAs up-regulated in WT animals had 188 predicted mRNA targets. For each group of targeted mRNAs, a functional enrichment analysis using annotated Gene Ontology (GO) terms was performed (Fig. 4, Table S4). Interestingly, targets of miRNAs up-regulated in symbiotic animals were enriched in the depression of immune responses, with associated frequent keywords such as “immunological”, “immunogenic” or “stimulus” (Fig. 4, Fig. S1, Table S4). As miRNAs typically down-regulate

gene expression, these data indicate that light-organ symbiosis turns down host-tissue immune responses. In contrast, targets of miRNAs down-regulated in symbiotic animals are enriched in neurodevelopmental functions, with associated frequent keywords such as “chemotaxis”, “migration”, “pathfinding” or “cytoskeleton directed” which, in turn, indicates that with the establishment of symbiosis there is an up-regulation of tissue remodeling activities (Fig. 4, Fig. S1, Table S4).

A comparison between circulating miRNAs and light organ miRNAs

E. scolopes develops a closed circulatory system to transport in the hemolymph nutrients, excreta, minerals and ions to and from various tissues and cells. Not surprisingly, circulating miRNAs have the potential to influence cellular gene expression and activity within these tissues [47–49]. Symbiotic colonization alters gene expression in tissues situated far from the light organ [5], perhaps through the agency of mature miRNAs secreted into the circulation in a protected condition and incorporated within exosomes [47].

To characterize the population of circulating miRNAs in *E. scolopes*, we performed RNA-seq analyses on the circulating small RNA fraction of two hemolymph samples of adult wild-caught squid. A total of 268 predicted miRNAs and 18 known miRNAs were identified in the circulating miRNAs population (Table S5). To determine whether the miRNA population specific to the light organ could be detected among the hemolymph miRNAs, we compared the miRNAs isolated from these two locations. All 18 known miRNAs identified in circulation were also expressed in light organ tissue. However, only 46 of the predicted miRNAs were found in both the light organ and in circulation, and with 222 and 93 predicted miRNAs specific to the hemolymph and light organ, respectively (Fig. 5A). PCA of the miRNA profile revealed that the sample origin was the primary factor affecting global miRNA expression, where PC1 (68.2% of the overall variance) separated light organ from hemolymph samples, while PC2 (11.0% of the overall variance) separated symbiotic from aposymbiotic samples (Fig. 5B). When comparing expression values of individual miRNAs, samples clustered by condition (Fig. 5C); significantly, the number of differentially expressed miRNAs between hemolymph and aposymbiotic light organ samples was nearly double that between hemolymph and colonized light organs (Fig. 6, Table S6), again

indicating that symbiosis is the main variable driving both the tissue-specific and circulating miRNA populations.

Discussion

In host-microbe associations with horizontally transmitted symbionts, hosts require symbiotic tissues and organs to harbor their symbionts that colonize anew each generation. These tissues harbor a dynamic population of symbionts and, as such, must respond actively to maintain homeostasis. Upon contact with bacteria and bacterial products, many tissues undergo post-embryonic development [3] with morphological changes that are orchestrated by vast changes in tissue gene expression. MicroRNAs (miRNAs) are small regulatory RNAs that shape the cellular expression landscape by post-transcriptional control of mRNA decay and translation, thereby regulating biological processes in different tissues. In this study, we characterized the shifts in miRNA expression that occur in the light organ tissues of *E. scolopes* upon colonization by symbiotic *V. fischeri*, and linked miRNA expressional changes to the transcriptional response previously observed in symbiotic light organs [4, 5, 24, 50].

A total of 361 miRNAs were identified in the *E. scolopes* genome, 139 of which were expressed in the light organ, with 268 appearing in the hemolymph (Fig. 5A, Table S1, Table S2). The total number of miRNAs described in other systems ranges widely from ~2000 miRNAs in most vertebrates [51] to only a few hundred in some invertebrates [13, 52]. Orthologs of miRNAs present in other organisms indicate conservation of miRNAs across organisms, and are described as “known” miRNAs. Of the miRNAs identified in the *E. scolopes* light organ, 24% were known and, of those identified in the hemolymph, 13% were known. These percentages are in agreement with those found in other mollusk genomes [53, 54]. However, the relative abundance of conserved miRNAs varies greatly among other high-throughput sequencing studies of mollusks, with percentages ranging from ~7% to ~50% conserved miRNAs [53–57]. Such variation might be attributed to the differing levels of completeness of each mollusk genome, which can influence the efficiency of discovering new miRNA families. While the miRNA repertoire has increased during the evolution of metazoans, the rate of appearance of these molecules is highly diverse over evolutionary time [16]. Nearly 88% of the known miRNAs found within the *E. scolopes* genome show sequence conservation within the Mollusca, and 50% appear across even larger evolutionary distances. The number of shared predicted miRNA sequences increases with taxonomic proximity

(Fig. 2C). For example, 65% of the predicted *E. scolopes* miRNAs are also found in *O. bimaculoides*, making them cephalopod-specific miRNAs, while 35% of the squid's predicted miRNAs are lineage-specific, highlighting the uniqueness of the light organ. Furthermore, in both subclades of RNA-guide proteins, AGO and PIWI, cephalopod proteins cluster together with high confidence (Fig. 1B). All other proteins involved in the miRNA machinery and biogenesis are present in the squid genome and expressed in the light organ, indicating that cephalopods have an active and complex post-transcriptional regulation of gene expression by miRNAs.

Symbiotic organs are tightly regulated in order to maintain yet control their symbiont population in homeostasis. In the light organ of *E. scolopes*, colonization by *V. fischeri* drives several post-embryonic developmental changes. For instance, within hours after the symbiont enters the crypts, apoptosis [22, 58] is induced, resulting in loss of the ciliated field on the exterior appendages of the light organ (Fig. 1A). Additionally, the light-organ crypts mature and differentiate as the symbiosis matures, with changes in cell size and shape in the layer of epithelial cells that interacts directly with the bacterial symbionts [3, 59]. Other, non-developmental changes occur as well in the light organ after symbiotic colonization. For example, the host secretes several enzymes into the lumen of the crypts in order to detoxify symbiont products [60, 61], and effectively shuts down mucus shedding on the light-organ surface within 48 h of symbiont colonization [62]. All of these changes are accompanied by a vast shift in gene expression within the light organ in response to symbiosis [4, 5, 24, 50]. The way in which these expressional changes are regulated is not yet known. Although DNA and chromatin modifiers may play crucial roles in ensuring that proper gene expression patterns are established and maintained in any given moment and cell type, post-transcriptional regulation of gene expression by miRNAs is an evolutionarily conserved mechanism for dynamic changes, and could be key in regulating symbiosis-mediated expressional changes. In this study we have shown that the miRNA population expressed in the light organ changes in response to symbiosis (Fig. 3A). Interestingly, we found that only miRNAs down-regulated in colonized animals are conserved among other organisms (Fig. 3B). Because targets of these miRNAs would be predicted to be up-regulated in symbiotic light organs, this finding suggests that the response to symbiotic colonization is an evolutionarily conserved phenomenon. Additionally, orthologs of this set of miRNA, including members of the family miR-92 as well as miR-184 [14, 63], have previously been implicated in studies of host-microbe associations. Specifically, miR-92 family members are generally found to be up-regulated in

pathogenesis [63–66] while, similar to their orthologs in the light organ, they are down-regulated in response to either symbiont metabolites [67], *Wolbachia* infection in mosquitos [15], or TLR activation in innate inflammatory responses [68]. Thus, members of the miR-92 family of miRNAs might be key regulators of host responses between both beneficial and pathogenic interactions.

By contrast, all miRNAs that are found with increased expression in colonized organs are “predicted”, and the majority of these are specific to *E. scolopes*; *i.e.*, only 23% of them also present in *O. bimaculoides*. These findings suggest that the majority of predicted miRNAs that are regulated with symbiosis are unique to light-organ tissue. Furthermore, all miRNAs differentially expressed in aposymbiosis (APO) compared to symbiosis (WT) are also differentially expressed in hemolymph samples, which likewise indicates that they belong to a light-organ specific response (Figs. 5 & 6).

To identify the possible functions of the differentially expressed miRNAs more fully, putative target genes were predicted using the 3' UTR regions of the *E. scolopes* transcriptome [28]. These presumed targets were then subjected to a GO enrichment analysis to classify their expected functions. The results indicated that targets of miRNAs up-regulated in symbiosis are enriched in genes that function to attenuate immune responses, with associated frequent keywords such as “immunological”, “immunogenic” or “stimulus” (Fig. 4). As miRNAs typically down-regulate the expression of their target genes, this result suggested that upon colonization, host cells within the light organ down-regulate their immune responses. Consistent with this finding, *V. fischeri* colonization triggers, within the light organ, a dramatic decrease in nitric oxide (NO) as well as NO synthase [69], laccase (as described earlier, in Chapter 3) and halide peroxidase [70], all antimicrobial immune responses. The underlying mechanism of such responses had previously remained unexplored, yet, based on our findings, it seems that post-transcriptional regulation by miRNA might be key to achieving symbiotic homeostasis. By contrast, targets of miRNAs down-regulated by symbiosis are enriched in genes affiliated with neurodevelopment and tissue remodeling, with associated frequent keywords such as “chemotaxis”, “migration”, or “cytoskeleton directed”. As colonization of the light organ induces morphological changes in the organ tissues [3, 22, 58, 59], it is not unexpected that symbiosis would trigger up-regulation of genes involved in tissue remodeling.

In conclusion, this study provides evidence of host miRNA-mediated regulation of gene expression in response to symbiotic colonization. Specifically, our results demonstrate that upon

the initiation of symbiosis a down-regulation of immune responses and an up-regulation of neurodevelopment are driven by changes in miRNA expression within the light organ. Thus, the evidence to date is inconsistent with the hypothesis that miRNAs play important roles in the adaptation to and control of symbiosis.

Additional files

Table S1: List of “known” *E. scolopes* light-organ miRNAs found only in mirBase.

Table S2. List of light-organ miRNAs found in the *E. scolopes* genome

Table S3: List of light-organ differentially expressed miRNAs.

Table S4: List of miRNA target genes.

Table S5: List of miRNAs found in squid hemolymph.

Table S6. Differentially expressed miRNAs between hemolymph and light organ from colonized (WT) or uncolonized squid

Figure S1: Tag cloud displaying of overrepresented words in the functional enrichment analysis of predicted miRNA target genes.

Abbreviations

FDR: False discovery rate; PCA: Principal component analysis; miRNA: Micro RNA; rRNA: Ribosomal RNA; tRNA: Transfer RNA; UTR: Untranslated region.

Acknowledgements

We would like to thank members of McFall-Ngai and Ruby lab for helpful discussions. We specially thank Susannah Lawhorn for proofreading the manuscript.

Funding

The research was supported by NIH grants R37 AI50661 (M.M.-N. and E.G.R.), R01 OD11024 and R01 GM135254 (E.G.R. and M.M.-N.), and NSF INSPIRE Grant MCB1608744 (Eva Kanso, USC). Acquisition of the Leica TCS SP8 X confocal microscope was supported by NSF DBI 1828262 (Marilyn Dunlap, E.G.R., and M.M.-N.), and SEM and confocal microscopy was

performed in the MICRO Core facility, supported by COBRE P20 GM125508 (M.M.-N. and E.G.R.).

Availability of data and materials

The datasets generated during this study have been deposited in the NCBI SRA repository with accession numbers: PRJNA629011 and PRJNA629996.

Authors' contributions

SMG and MMN conceived and designed the experiments; SMG performed all the experiments and analyzed the data; SMG, MMN and EGR wrote the manuscript.

Competing interests

The authors declare that they have no competing interests.

Ethics approval

All animal experiments were performed according to the local regulations of the University of Hawaii.

Author details

¹ Pacific Biosciences Research Center. University of Hawai'i at Mānoa; Honolulu; 96813. USA

² Molecular Biosciences and Bioengineering. University of Hawai'i at Mānoa

*Correspondence: mcfallng@hawaii.edu

References

1. Moya A, Peretó J, Gil R, Latorre A. Learning how to live together: genomic insights into prokaryote–animal symbioses. *Nat Rev Genet.* 2008;9:218–29. doi:10.1038/nrg2319.
2. McFall-Ngai M, Hadfield MG, Bosch TCG, Carey H V., Domazet-Lošo T, Douglas AE, et al. Animals in a bacterial world, a new imperative for the life sciences. *Proc Natl Acad Sci.* 2013;110:3229–36. doi:10.1073/pnas.1218525110.
3. Montgomery MK, McFall-Ngai M. Bacterial symbionts induce host organ morphogenesis during early postembryonic development of the squid *Euprymna scolopes*. *Development.* 1994;120:1719–29. papers3://publication/uuid/BF5BB089-FA96-4EF6-8ED3-CAB940D15B66.
4. Kremer N, Philipp EER, Carpentier MC, Brennan CA, Kraemer L, Altura MA, et al. Initial symbiont contact orchestrates host-organ-wide transcriptional changes that prime tissue colonization. *Cell Host Microbe.* 2013;14:183–94.
5. Moriano-Gutierrez S, Koch EJ, Bussan H, Romano K, Belcaid M, Rey FE. Critical symbiont signals drive both local and systemic changes in diel and developmental host gene expression. *Proc Natl Acad Sci.* 2019;116:7990–9.
6. El Aidy S, Van Baarlen P, Derrien M, Lindenbergh-Kortleve DJ, Hooiveld G, Levenez F, et al. Temporal and spatial interplay of microbiota and intestinal mucosa drive establishment of immune homeostasis in conventionalized mice. *Mucosal Immunol.* 2012;5:567–79.
7. Rawls JF, Samuel BS, Gordon JI. Gnotobiotic zebrafish reveal evolutionarily conserved responses to the gut microbiota. *Proc Natl Acad Sci U S A.* 2004;101:4596–601.
8. Bartel DP, Chen CZ. Micromanagers of gene expression: The potentially widespread influence of metazoan microRNAs. *Nat Rev Genet.* 2004;5:396–400.
9. Agarwal V, Bell GW, Nam JW, Bartel DP. Predicting effective microRNA target sites in mammalian mRNAs. *Elife.* 2015;4:1–38.
10. Orang AV, Safaralizadeh R, Kazemzadeh-Bavili M. Mechanisms of miRNA-mediated gene regulation from common downregulation to mRNA-specific upregulation. *Int J Genomics.* 2014;2014 June 2013.

11. Vasudevan S, Steitz JA. AU-Rich-Element-Mediated Upregulation of Translation by FXR1 and Argonaute 2. *Cell*. 2007;128:1105–18.
12. Berezikov E. Evolution of microRNA diversity and regulation in animals. *Nat Rev Genet*. 2011;12:846–60. doi:10.1038/nrg3079.
13. Wheeler BM, Heimberg AM, Moy VN, Sperling EA, Holstein TW, Heber S, et al. The deep evolution of metazoan microRNAs. *Evol Dev*. 2009;11:50–68.
14. Mehrabadi M, Hussain M, Asgari S. MicroRNAome of *Spodoptera frugiperda* cells (Sf9) and its alteration following baculovirus infection. *J Gen Virol*. 2013;94 Pt_6:1385–97. doi:10.1099/vir.0.051060-0.
15. Mayoral JG, Hussain M, Joubert DA, Iturbe-Ormaetxe I, O’Neill SL, Asgari S. Wolbachia small noncoding RNAs and their role in cross-kingdom communications. *P Natl Acad Sci USA*. 2014;111:18721–6. doi:10.1073/pnas.1420131112.
16. Bartel DP. Metazoan MicroRNAs. *Cell*. 2018;173:20–51. doi:10.1016/j.cell.2018.03.006.
17. Murphy D, Dancis B, Brown JR. The evolution of core proteins involved in microRNA biogenesis. *BMC Evol Biol*. 2008;8:1–18.
18. Kozomara A, Birgaoanu M, Griffiths-Jones S. MiRBase: From microRNA sequences to function. *Nucleic Acids Res*. 2019;47:D155–62.
19. Lee KH, Ruby EG. Effect of the squid host on the abundance and distribution of symbiotic *Vibrio fischeri* in nature. *Appl Environ Microbiol*. 1994;60:1565–71. <http://www.ncbi.nlm.nih.gov/pubmed/16349257>.
20. Nawroth JC, Guo H, Koch E, Heath-Heckman EAC, Hermanson JC, Ruby EG, et al. Motile cilia create fluid-mechanical microhabitats for the active recruitment of the host microbiome. *Proc Natl Acad Sci U S A*. 2017;114:9510–6.
21. Nyholm S V., Stabb E V., Ruby EG, McFall-Ngai MJ. Establishment of an animal-bacterial association: Recruiting symbiotic vibrios from the environment. *Proc Natl Acad Sci U S A*. 2000;97:10231–5.
22. Montgomery MK, McFall-Ngai MJ. The inductive role of bacterial symbionts in the morphogenesis of a squid light organ. 1995;35:372–80.

23. Lamarca LH, Mcfall-Ngai MJ. Induction of a Gradual , Reversible Morphogenesis of Its Host ' s Epithelial Brush Border by *Vibrio fischeri*. *Infect Immun*. 1998;66:777–85.
24. Chun CK, Scheetz TE, Bonaldo M de F, Brown B, Clemens A, Crookes-Goodson WJ, et al. An annotated cDNA library of juvenile *Euprymna scolopes* with and without colonization by the symbiont *Vibrio fischeri*. *BMC Genomics*. 2006;7:154.
25. Chun CK, Troll J V., Koroleva I, Brown B, Manzella L, Snir E, et al. Effects of colonization, luminescence, and autoinducer on host transcription during development of the squid-vibrio association. *Proc Natl Acad Sci U S A*. 2008;105:11323–8.
26. Graf J, Dunlap P V, Ruby EG. Effect of transposon-induced motility mutations on colonization of the host light organ by *Vibrio fischeri*. *J Bacteriol*. 1994;176:6986–91. doi:10.1128/jb.176.22.6986-6991.1994.
27. Boettcher KJ, Ruby EG. Depressed light emission by symbiotic *Vibrio fischeri* of the sepiolid squid *Euprymna scolopes*. *J Bacteriol*. 1990;172:3701–6. doi:10.1128/JB.172.7.3701-3706.1990.
28. Belcaid M, Casaburi G, McAnulty SJ, Schmidbaur H, Suria AM, Moriano-Gutierrez S, et al. Symbiotic organs shaped by distinct modes of genome evolution in cephalopods. *Proc Natl Acad Sci U S A*. 2019;116:3030–5.
29. Camacho C, Coulouris G, Avagyan V, Ma N, Papadopoulos J, Bealer K, et al. BLAST+: Architecture and applications. *BMC Bioinformatics*. 2009;10:1–9.
30. Gasteiger E, Gattiker A, Hoogland C, Ivanyi I, Appel RD, Bairoch A. ExPASy: The proteomics server for in-depth protein knowledge and analysis. *Nucleic Acids Res*. 2003;31:3784–8.
31. Katoh K, Standley DM. MAFFT multiple sequence alignment software version 7: Improvements in performance and usability. *Mol Biol Evol*. 2013;30:772–780.
32. Capella-Gutiérrez S, Silla-Martínez JM, Gabaldón T. trimAl: A tool for automated alignment trimming in large-scale phylogenetic analyses. *Bioinformatics*. 2009;25:1972–3.
33. Stamatakis A. RAxML version 8: A tool for phylogenetic analysis and post-analysis of large phylogenies. *Bioinformatics*. 2014;30:1312–3.

34. Langmead B, Salzberg SL. Fast gapped-read alignment with Bowtie 2. *Nat Methods*. 2012;9:357–9. doi:10.1038/nmeth.1923.
35. Li B, Dewey C. RSEM: accurate transcript quantification from RNA-Seq data with or without a reference genome. *BMC Bioinformatics*. 2011;12:323.
36. Andrews S, Krueger F, Seaman P, Pichon A, Biggins F, Wingett S. FastQC. A quality control tool for high throughput sequence data. Babraham Bioinformatics. Babraham Institute. 2015;; Available online at: <http://www.bioinformatics.babraham.ac.uk/projects/fastqc/>.
37. Bolger AM, Lohse M, Usadel B. Trimmomatic: a flexible trimmer for Illumina sequence data. *Bioinformatics*. 2014;30:2114–20. doi:10.1093/bioinformatics/btu170.
38. Martin M. Cutadapt removes adapter sequences from high-throughput sequencing reads. *EMBnet J*. 2011;17:10–2.
39. Friedländer MR, MacKowiak SD, Li N, Chen W, Rajewsky N. MiRDeep2 accurately identifies known and hundreds of novel microRNA genes in seven animal clades. *Nucleic Acids Res*. 2012;40:37–52.
40. Robinson MD, McCarthy DJ, Smyth GK. edgeR: A Bioconductor package for differential expression analysis of digital gene expression data. *Bioinformatics*. 2009;26:139–40.
41. Zhao S, Guo Y, Sheng Q, Shyr Y. Advanced Heat Map and Clustering Analysis Using Heatmap3. *Biomed Res Int*. 2014;2014:986048.
42. Enright AJ, John B, Gaul U, Tuschl T, Sander C, Marks DS. MicroRNA targets in *Drosophila*. *Genome Biol*. 2003;5:R1.
43. Götz S, García-Gómez JM, Terol J, Williams TD, Nagaraj SH, Nueda MJ, et al. High-throughput functional annotation and data mining with the Blast2GO suite. *Nucleic Acids Res*. 2008;36:3420–35.
44. Supek F, Bošnjak M, Škunca N, Šmuc T. Revigo summarizes and visualizes long lists of gene ontology terms. *PLoS One*. 2011;6:e21800.
45. Jehn J, Gebert D, Pipilescu F, Stern S, Kiefer JST, Hewel C, et al. PIWI genes and piRNAs are ubiquitously expressed in mollusks and show patterns of lineage-specific adaptation.

- Commun Biol. 2018;1:137. doi:10.1038/s42003-018-0141-4.
46. Zhou X, Liao Z, Jia Q, Cheng L, Li F. Identification and characterization of Piwi subfamily in insects. *Biochem Biophys Res Commun.* 2007;362:126–31.
47. Sohel MH. Extracellular/Circulating MicroRNAs: Release Mechanisms, Functions and Challenges. *Achiev Life Sci.* 2016;10:175–86. doi:10.1016/J.ALS.2016.11.007.
48. Valadi H, Ekström K, Bossios A, Sjöstrand M, Lee JJ, Lötvall JO. Exosome-mediated transfer of mRNAs and microRNAs is a novel mechanism of genetic exchange between cells. *Nat Cell Biol.* 2007;9:654–9. doi:10.1038/ncb1596.
49. Cortez MA, Bueso-Ramos C, Ferdin J, Lopez-Berestein G, Sood AK, Calin GA. MicroRNAs in body fluids--the mix of hormones and biomarkers. *Nat Rev Clin Oncol.* 2011;8:467–77. doi:10.1038/nrclinonc.2011.76.
50. Kremer N, Koch EJ, Filali AE, Zhou L, Heath-Heckman EAC, Ruby EG, et al. Persistent interactions with bacterial symbionts direct mature-host cell morphology and gene expression in the squid. *MSystems.* 2018;3:1–17.
51. Alles J, Fehlmann T, Fischer U, Backes C, Galata V, Minet M, et al. An estimate of the total number of true human miRNAs. *Nucleic Acids Res.* 2019;47:3353–64.
52. Wei P, He P, Zhang X, Li W, Zhang L, Guan J, et al. Identification and characterization of microRNAs in the gonads of *Crassostrea hongkongensis* using high-throughput sequencing. *Comp Biochem Physiol - Part D Genomics Proteomics.* 2019;31:100606. doi:10.1016/j.cbd.2019.100606.
53. Jiao Y, Zheng Z, Du X, Wang Q, Huang R, Deng Y, et al. Identification and characterization of microRNAs in pearl oyster *Pinctada martensii* by solexa deep sequencing. *Mar Biotechnol.* 2014;16:54–62.
54. Zhou Z, Wang L, Song L, Liu R, Zhang H, Huang M, et al. The identification and characteristics of immune-related MicroRNAs in haemocytes of oyster *Crassostrea gigas*. *PLoS One.* 2014;9:1–9.
55. Zhao X, Yu H, Kong L, Liu S, Li Q. High throughput sequencing of small RNAs transcriptomes in two *Crassostrea* oysters identifies microRNAs involved in osmotic stress

response. *Sci Rep.* 2016;6 December 2015:22687. doi:10.1038/srep22687.

56. Huang J, Luo X, Huang M, Liu G, You W, Ke C. Identification and characteristics of muscle growth-related microRNA in the Pacific abalone, *Haliotis discus hannai*. *BMC Genomics.* 2018;19:1–11.

57. Picone B, Rhode C, Roodt-Wilding R. Identification and characterization of miRNAs transcriptome in the South African abalone, *Haliotis midae*. *Mar Genomics.* 2017;31:9–12. doi:10.1016/j.margen.2016.10.005.

58. Foster JS, McFall-Ngai MJ. Induction of apoptosis by cooperative bacteria in the morphogenesis of host epithelial tissues. *Dev Genes Evol.* 1998;208:295–303.

59. Lamarq LH, Mcfall-ngai MJ. Induction of a gradual, reversible morphogenesis of its host's epithelial brush border by *Vibrio fischeri* induction of a gradual, reversible morphogenesis of its host's epithelial brush border by *Vibrio fischeri*. 1998;66:777–85.

60. Troll J V. Taming the symbiont for coexistence: A host PGRP neutralizes a bacterial symbiont toxin. *Environ Microbiol.* 2011;12:2190–203.

61. Rader BA, Kremer N, Apicella MA, Goldman WE, McFall-Ngai MJ. Modulation of symbiont lipid signaling by host alkaline phosphatases in the squid-*Vibrio* symbiosis. *MBio.* 2012;3:e00093-12.

62. Nyholm S V., Deplancke B, Gaskins HR, Apicella MA, McFall-Ngai MJ. Roles of *Vibrio fischeri* and nonsymbiotic bacteria in the dynamics of mucus secretion during symbiont colonization of the *Euprymna scolopes* light organ. *Appl Environ Microbiol.* 2002;68:5113–22.

63. Jin P, Li S, Sun L, Lv C, Ma F. Transcriptome-wide analysis of microRNAs in *Branchiostoma belcheri* upon *Vibrio parahemolyticus* infection. *Dev Comp Immunol.* 2017;74:243–52. doi:10.1016/j.dci.2017.05.002.

64. Skalsky RL, Vanlandingham DL, Scholle F, Higgs S, Cullen BR. Identification of microRNAs expressed in two mosquito vectors, *Aedes albopictus* and *Culex quinquefasciatus*. *BMC Genomics.* 2010;11.

65. Li S, Mead EA, Liang S, Tu Z. Direct sequencing and expression analysis of a large number of miRNAs in *Aedes aegypti* and a multi-species survey of novel mosquito miRNAs. *BMC*

Genomics. 2009;10:1–17.

66. Qiang J, Tao F, He J, Sun L, Xu P, Bao W. Effects of exposure to *Streptococcus iniae* on microRNA expression in the head kidney of genetically improved farmed tilapia (*Oreochromis niloticus*). BMC Genomics. 2017;18:1–11.

67. Hu S, Liu L, Chang EB, Wang JY, Raufman JP. Butyrate inhibits pro-proliferative miR-92a by diminishing c-Myc-induced miR-17-92a cluster transcription in human colon cancer cells. Mol Cancer. 2015;14:1–15. doi:10.1186/s12943-015-0450-x.

68. Lai L, Song Y, Liu Y, Chen Q, Han Q, Chen W, et al. MicroRNA-92a negatively regulates toll-like receptor (TLR)-triggered inflammatory response in macrophages by targeting MKK4 kinase. J Biol Chem. 2013;288:7956–67.

69. Davidson SK, Koropatnick TA, Kossmehl R, Sycuro L, McFall-Ngai MJ. NO means “yes” in the squid-vibrio symbiosis: Nitric oxide (NO) during the initial stages of a beneficial association. Cell Microbiol. 2004;6:1139–51.

70. Small AL, McFall-Ngai MJ. Halide peroxidase in tissues that interact with bacteria in the host squid *Euprymna scolopes*. J Cell Biochem. 1999;72:445–57.

71. Vakulskas CA, Potts AH, Babitzke P, Ahmer BMM, Romeo T. Regulation of Bacterial Virulence by Csr (Rsm) Systems. Microbiol Mol Biol Rev. 2015;79:193–224.

72. Zuker M. Mfold web server for nucleic acid folding and hybridization prediction. Nucleic Acids Res. 2003;31:3406–15.

73. Wassarman KM, Storz G. 6S RNA regulates E. coli RNA polymerase activity. Cell. 2000;101:613–23.

Figures

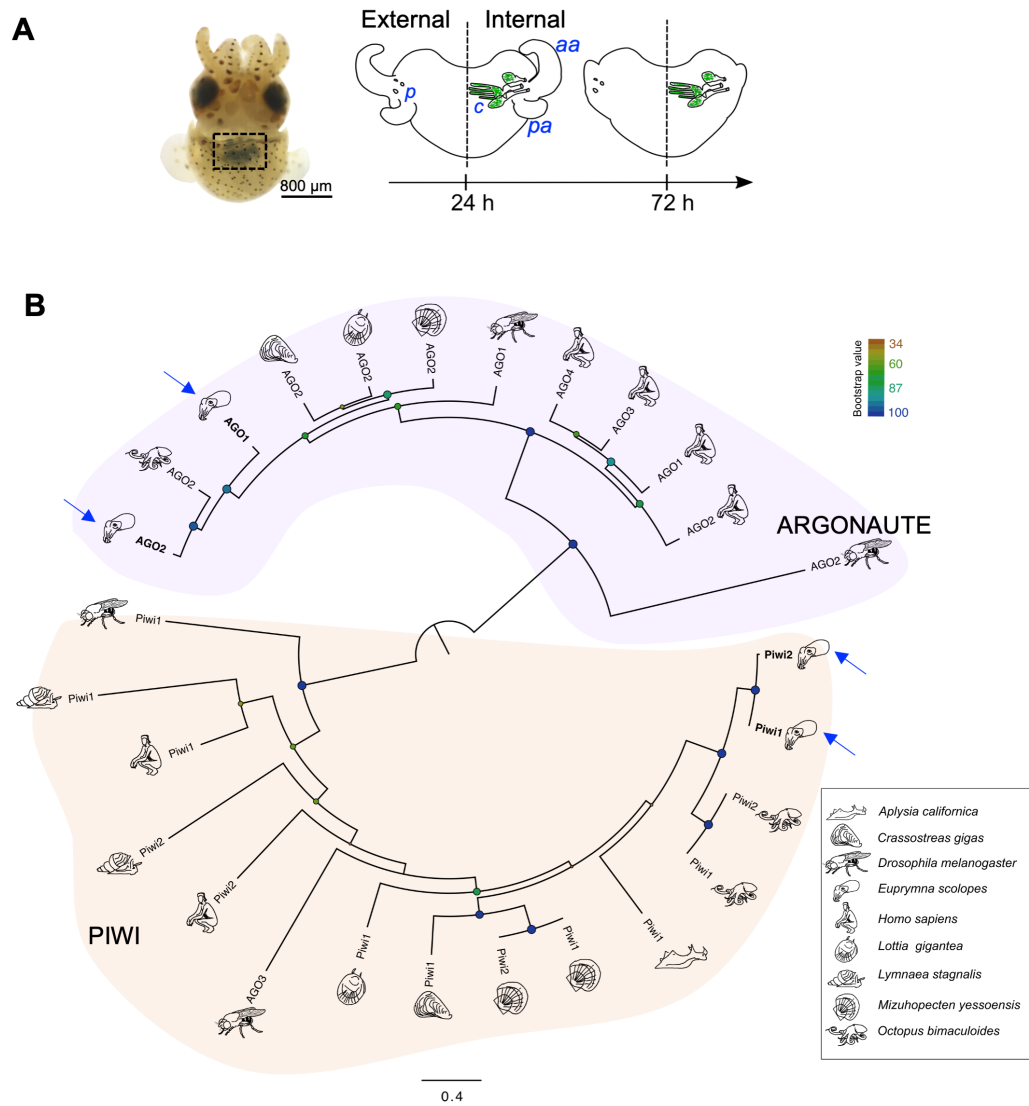


Fig. 1. The molluscan argonaute and PIWI gene repertoire. **A.** The juvenile *E. scolopes*. Light organ (dotted box), seen through ventral mantle tissue. Right panel: Early postembryonic development of the juvenile light organ. The light organ has 3 pores (*p*) that lead to the internal crypt spaces (*c*) where *V. fischeri* (green) is harbored. The surface tissues of the juvenile light organ including the anterior (*aa*) and posterior appendages (*pa*) regress during the first several days post-colonization. **B.** Phylogenetic analysis of PIWI-like and argonaute-like (AGO) proteins. Maximum likelihood analysis. Bootstrap values of particular nodes are represented as blue-to-orange circles. The scale bar represents amino acid substitution rate per site. Blue arrows indicate *E. scolopes*.

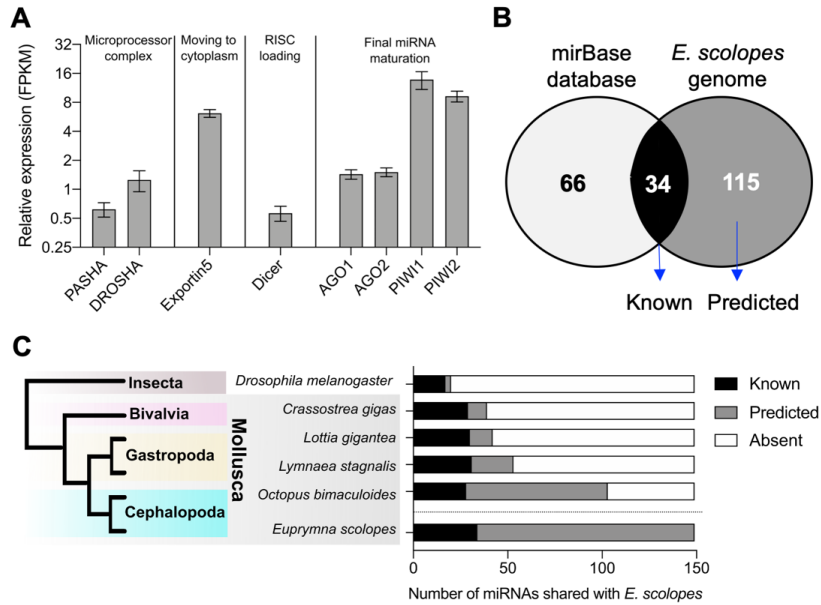


Fig. 2. Expression of miRNA-synthesis associated proteins and light-organ miRNA Database. A. Light-organ gene expression of miRNA machinery proteins 24 h post-hatching, expressed as Fragments Per Kilobase of transcript per Million mapped reads (FPKM). B. Venn diagram of miRNAs identified in the *E. scolopes* genome and mirBase database. C. Number of miRNAs found in the *E. scolopes* genome that are shared across organisms.

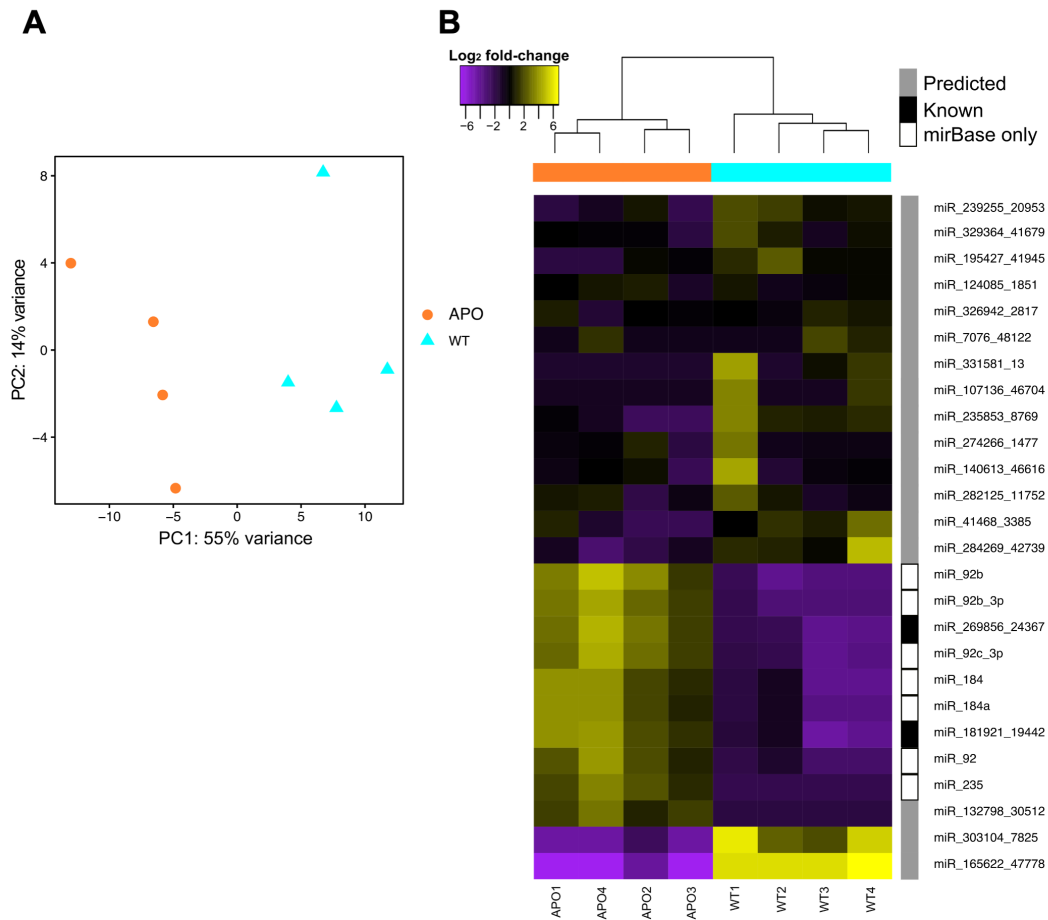


Fig. 3. The effect of symbiosis on the light-organ miRNA profile. A. Principal Components Analysis (PCA) of miRNA gene expression. PCA scatter plot shows the variance of the four biological replicates of colonized (WT) or uncolonized (APO) light organs. The percentages on each axis indicate the degree of variation explained by the principal components. B. Heatmap of expression values of the light-organ miRNAs that are differentially expressed (FDR<0.05, Fold-change>2) in responses to symbiosis. The bar to the left of the miRNA labels indicates the status of the miRNA as: Predicted in the genome (grey box), Known (black box), or only present in miRbase but not found within the genome (white box). See Fig. 2B.

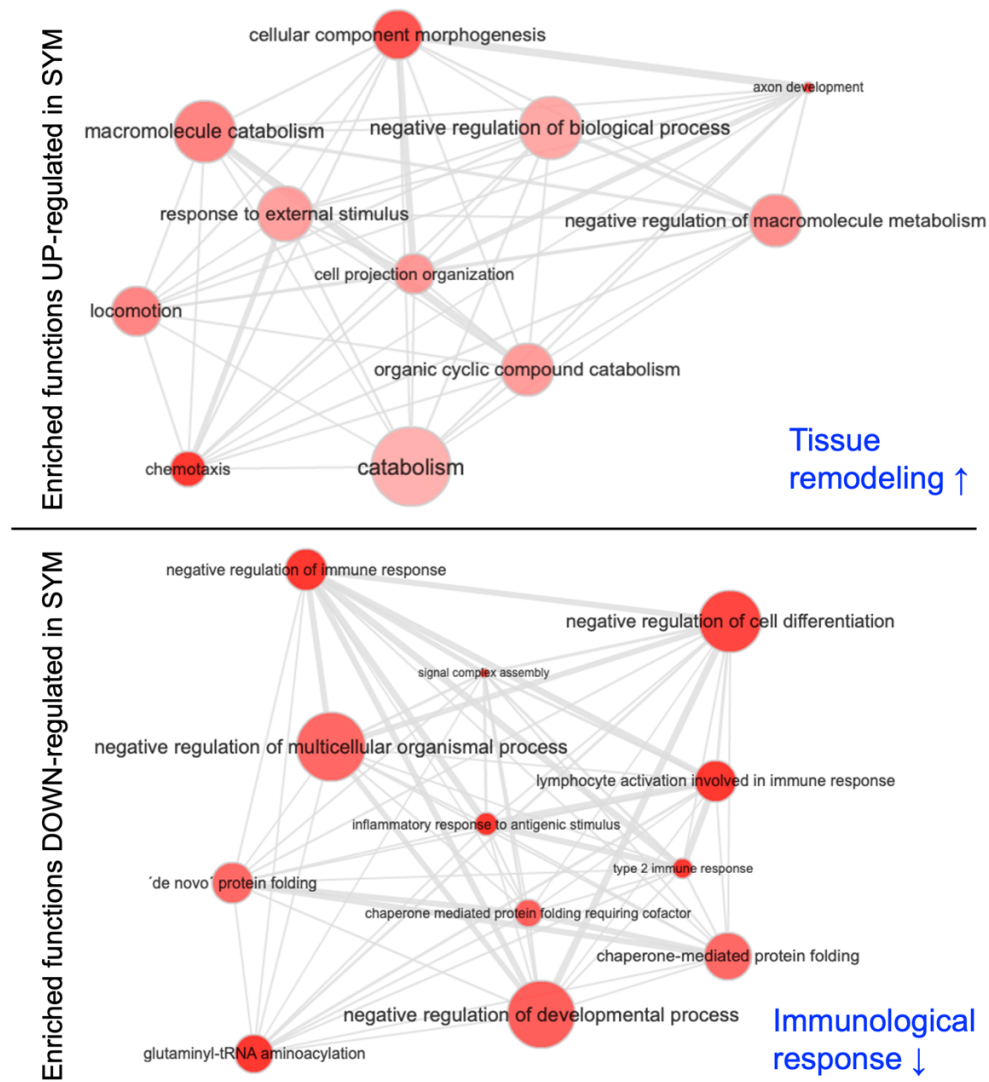


Fig. 4. Functional enrichment analysis of predicted miRNA target genes. Gene Ontology (GO) enrichment of predicted mRNA targets of differentially expressed miRNAs present in the *E. scolopes* genome. Darker red color indicates a higher statistical significance of GO terms, while bubble size indicates the frequency of the specific term in the Gene Ontology Annotation (GOA) Database. Grey lines link highly similar GO terms, where the width of the line indicates the degree of similarity. The predicted outcomes are reported in blue.

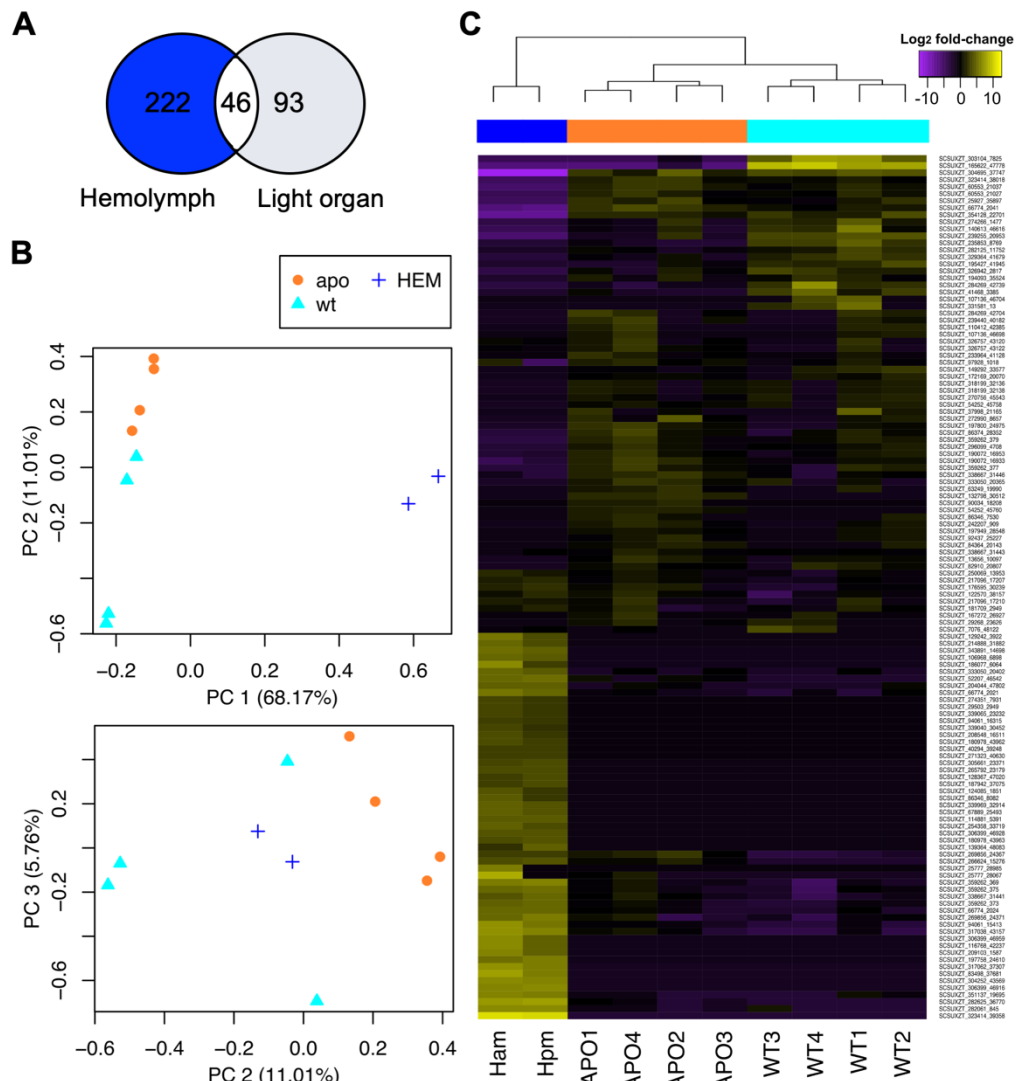


Fig. 5. Profiling of the circulating miRNAs. A. Comparison between predicted miRNAs identified in adult squid hemolymph and predicted miRNAs identified in juvenile light organ. B. Principal component (PC) analysis of expression profile from light organ miRNAs and hemolymph miRNAs (On top PC1 and PC2 on bottom PC2 and PC3). HEM: hemolymph; apo: light organ aposymbiotic; wt: light organ symbiotic. C. Heatmap of expression profile of miRNAs differentially expressed between light organ and hemolymph (FDR<0.05, Fold-change>2).

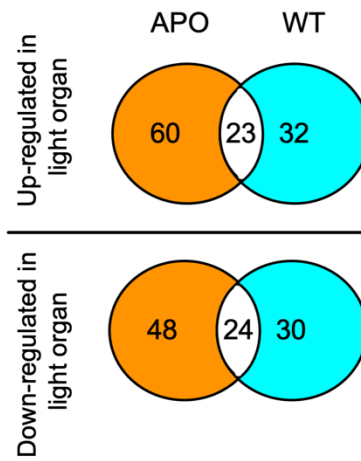


Fig. 6. The impact of symbiosis on miRNA expression. Venn diagram of differentially expressed miRNAs between hemolymph and aposymbiotic (APO) or symbiotic (WT) light organs.

Additional files

mRNA targets of miRNAs up-regulated in WT

provide t-lymphocyte towards residue ... catalyzed specialized **antigenic** neurocyte help mitogen aminoacylation 3'-5' ... amino inhibition ... linkage **number** ... lymphocyte adenosine **epitopes** down-regulation
expresses then **effector** antigen reaction cells can ... **alpha-beta** **immunological** ... coupling **stimulus** cytotoxicity acquires beta csi4-positive naive ... antigenically stops regulatory **receptor** alpha
activated 3'-hydroxy **immunogenic** downregulation ... reduces **chemokine** ... immune ... prevents differentiation memory exhibit t-cell **inflammatory** cytokine ... negative down group unspecialized first

mRNA targets of miRNAs up-regulated in APO

metabolites responds body regrowth **lower lipids** **higher** towards outgoing occurs pertaining action carries developing **along** remodeling
positive ... regeneration **cues** ... **agent** ... covers **repulsive** combination causes guidance **actin-binding**
through chemotaxis cone taxis while **sugars** de ... initially morphogenesis **guided** acquiring novo **attractive** directs chemotactic
activation cell-wall site trigger migration **concentration** fasciculation refers **receptors** efferent **pathfinding** signaling
axonogenesis defasciculation **cytoskeleton** directed **target** peptides potentials ... **bind** gradient growth

Fig. S1. Functional enrichment analysis of predicted miRNA target genes. Gene Ontology (GO) enrichment of predicted mRNA targets of differentially expressed miRNAs present in *E. scolopes* genome. Tag cloud displaying overrepresented words in the descriptions of the GO terms, with larger and darker letters signifying stronger overrepresentation.

Table S1: miRNAs identified by sequence similarity in mirBase database but not found within the *E. scolopes* genome

<u>miRNA iD</u>	<u>miRNA ID in miRBase</u>	<u>Total read count</u>
miR-92c-3p	ame-miR-92c-3p	9291
miR-1-3p	asu-miR-1-3p	4678
miR-981	lgi-miR-981	2214
miR-92b	bdo-miR-92b	1728
miR-184a	abu-miR-184a	1658
miR-184	aae-miR-184	1617
let-7a	abu-let-7a	1183
let-7-5p	ame-let-7-5p	1180
miR-750-3p	ame-miR-750-3p	1047
miR-133	bfl-miR-133	820
miR-375	abu-miR-375	729
miR-375-3p	bbe-miR-375-3p	725
miR-92b	cte-miR-92b	653
miR-31	abu-miR-31	640
miR-72-5p	asu-miR-72-5p	640
miR-1991	hru-miR-1991	633
miR-72	bma-miR-72	630
miR-2478	bta-miR-2478	626
miR-2c	aae-miR-2c	447
miR-2a-2	bdo-miR-2a-2	405
miR-2b	aae-miR-2b	402
miR-8-3p	dme-miR-8-3p	397
miR-2a	api-miR-2a	359
miR-92b-3p	aae-miR-92b-3p	348
miR-1	abu-miR-1	346
miR-96b	lgi-miR-96b	226
miR-31-5p	cli-miR-31-5p	219
miR-92	bma-miR-92	193
miR-981	aae-miR-981	159
miR-67-3p	mle-miR-67-3p	146
miR-7975	hsa-miR-7975	140
miR-133-3p	asu-miR-133-3p	127
miR-87-3p	ame-miR-87-3p	115
miR-92b-3p	bbe-miR-92b-3p	96
miR-235	cbn-miR-235	85
miR-184b	api-miR-184b	80

miR5658	ath-miR5658	73
miR8577	atr-miR8577	60
miR-92b	abu-miR-92b	43
miR-750	fhe-miR-750	37
bantam-3p	ame-bantam-3p	34
miR-12-5p	aae-miR-12-5p	33
let-7c	abu-let-7c	32
miR-79-3p	asu-miR-79-3p	30
miR-9-3p	bma-miR-9-3p	30
miR-29b-3p	chi-miR-29b-3p	28
miR-278	api-miR-278	25
miR-81	bma-miR-81	25
miR-2a-3p	asu-miR-2a-3p	20
miR5284b	mtr-miR5284b	20
miR-184-3p	asu-miR-184-3p	18
let-7g	abu-let-7g	17
miR-71-5p	ame-miR-71-5p	17
miR-1260	cfa-miR-92a	16
miR-317	aae-miR-317	16
miR-317-3p	cqu-miR-317-3p	16
miR-87	cbn-miR-87	16
miR-87a	api-miR-87a	16
miR-92a	abu-miR-92a	16
bantam	api-bantam	14
miR-92a-3p	ami-miR-92a-3p	14
miR-2g	cte-miR-2g	12
miR-745a-3p	mle-miR-745a-3p	12
miR-98-5p	ami-miR-98-5p	12
let-7	aga-let-7	11

Table S2. List of light-organ miRNAs found in the *E. scolopes* genome.

<u>miRNA ID</u>	<u>miRDeep 2 score</u>	<u>mature miRBase miRNA</u>	<u>consensus mature sequence</u>	<u>consensus precursor sequence</u>	<u>precursor coordinate</u>
miR_107136_46698	16.0	-	aagaucuuccuuggccaugga	aagaucuuccuuggccauggaagguccuuaauuuucc auggccuuaggaaaauuua	SCSUXZT_107136:543567..543625:+
miR_107136_46704	0.0	-	uguguguuuggguguguucu	uguauagcucuacguauguacgugcaguucacugu uauauguguguuuggguguguucu	SCSUXZT_107136:939336..939396:-
miR_110412_42385	1.3	-	uuccauaguuguuggagugccu	gugcuucauuacucuggggaugcugcuauuuua uaauccauaguuguuggagugccu	SCSUXZT_110412:1718584..1718644:+
miR_112063_2962	1.4	-	ucuaaccggccggcacaucagcu	ucuaaccggccggcacaucagcucauauaauc ggcagguaugcucggguguaag	SCSUXZT_112063:623179..623241:+
miR_116217_13558	1.7	-	uugcguaggugaauggcaua	uugcguaggugaauggcauaaaaggauauauaguuc uauagcacuugcuauagcaua	SCSUXZT_116217:3210391..3210450:+
miR_116768_40917	1.0	-	agggcccguaaguacuucaguc	cugaaguacuuaaggaccuuuagaaaguuucuauc agggcccguaaguacuucaguc	SCSUXZT_116768:4337060..4337119:+
miR_116768_40950	1.0	-	agggcccguaaguacuucaguc	cugaaguacuuaaggaccuuuagaaaguuucuauc agggcccguaaguacuucaguc	SCSUXZT_116768:4351651..4351710:-
miR_118262_28506	13.0	-	uuuuugacagaacggguucacu	uuuuugacagaacggguucacuaguauauuaaaaca aguguacaccuccgucaaaaug	SCSUXZT_118262:717912..717973:+
miR_118359_1348	5900.0	-	ugagaucauuguaaaacugguu	cugguuuacacaugauuuugcagauguaagacu ucugagaucauuguaaaacugguu	SCSUXZT_118359:3030277..3030339:-
miR_119465_47471	24.0	-	uagauucgaguccgggucgga	uagauucgaguccgggucggaauaaaaucagacuc ugaccggaauucgaaccuaca	SCSUXZT_119465:1909922..1909980:-
miR_122776_11889	2.6	-	uacccaugaucugccagauuag	agucuggcagauccagaaauuuuauugcuccuauua aaauacccaugaucugccagauuag	SCSUXZT_122776:7339125..7339186:+
miR_124085_1851	67.0	-	cuccuguuccugcgucagac	cuccuguuccugcgucagaccuagcuuuuuuuuu acagacucugcaguuuaaacaggaau	SCSUXZT_124085:8097318..8097381:-
miR_132798_30512	26.0	-	ugccuugccuucucuugccuugg	uagggcaauucggcugggucagcugauaaaauuac uauccuugccuucucuugccuugg	SCSUXZT_132798:6819629..6819691:-
miR_135923_216	6.9	-	uugucgagugcaaucaaga	uuuugauugcugcagcaagcuggguaaaagaaca gguuugcagugcaaucaaga	SCSUXZT_135923:895777..895837:-
miR_13656_10097	16.0	-	gcagaggauuaguuggccgaa	ucggccaacuauuccuugcccuuccuaagccgggc agaggauuaguuggccgaa	SCSUXZT_13656:2112642..2112698:+
miR_140613_46616	330.0	-	accgcgggugcagauuc	aucuguaccguggucgaaagccuagggcgagccc ggauaggagcaaacgggugcagauuc	SCSUXZT_140613:768295..768361:-
miR_144868_6090	1.2	-	uaaucucagcugguaaauaggag	uaaucucagcugguaaauaggagauaaacgucuc gaccuuaucagcugcgaauuga	SCSUXZT_144868:165712..165770:+
miR_144868_6094	6.5	-	uaaucucagcuaguauuuuagag	uaaucucagcuaguauuuuagaguuuucgauaguc ucaaguuaucagccagauuau	SCSUXZT_144868:177211..177270:+
miR_149292_33577	0.5	-	uagcagaguggcgaguggaa	ucacuguuuuuuuuuuuuuuuuuagcagagug gcgaguggaa	SCSUXZT_149292:3616896..3616943:+
miR_152170_10420	1.7	-	uaauagaaagucguuaguguca	uaauagaaagucguuagugucaaucauauugugac acuggcgaccuucaaaaacg	SCSUXZT_152170:15390..15447:+

miR_165622_47778	1.5	-	uauccuggaguguuugua	uauccuggaguguuugua gcuuugcaaaauaugucaggaugcu	SCSUXZT_165622:7339866..73 39926:+
miR_167272_26927	1.4	-	uggcuaccggauagggguc	ccguagauccugguuccauguuuaacauucauca uggcuaccggauagggguc	SCSUXZT_167272:2490..2547: +
miR_172169_20070	2.4	-	aacacccgagugagcggcugagg	aacacccgagugagcggcugaggauuacgaaauaugc cgagccuuacgaggguuucg	SCSUXZT_172169:268447..268 506:+
miR_175255_24920	0.2	-	aacuuuugaucgagaacag	guuccgcagcaaaaguuaacuccgcuacuucuuuug accucauuacucaaaugaaguagcagaguuacuuc uugaucgagaacag	SCSUXZT_175255:372573..372 661:-
miR_176595_30239	320.0	-	agcccuaugccuagucucuga	agcccuaugccuagucucugauguucuaaaauacu cagugacuugagcaaaaggacauc	SCSUXZT_176595:31171..3123 2:-
miR_177055_33310	1.3	-	uguacguucuguuuagggc	uguacguucuguuuagggcgaucgcccgcacuaaagu gacauc	SCSUXZT_177055:1660799..16 60842:+
miR_181709_2949	1.5	-	uggaagacuaaagaauuuuguuuuu	uggaagacuaaagaauuuuguuuuguuagucaga gaacaauagaucuuuauucucuga	SCSUXZT_181709:9938294..99 38355:-
miR_182134_27962	15.0	-	cccuagagacugggucuuaggcu	cccuagagacugggucuuaggcuaguugauaacaguu gccaagcaauagcuucuuaggcu	SCSUXZT_182134:493472..493 531:+
miR_186077_5448	27.0	-	uuuuuagcuguuuuucacgaga	ucgggaauagcggcauuagcuguaauuucgacugua uuuagcuguuuuucacgaga	SCSUXZT_186077:232838..232 895:-
miR_188031_36529	2.5	-	uacccaugaucugccagauuag	ugucuggcagaucaggaauuuuuuagcucccuuu aaauacccaugaucugccagauuag	SCSUXZT_188031:502..564:+
miR_190072_16933	1.2	-	uuaccuguugaaccgagcaagu	uuaccuguugaaccgagcaagugucaaaacac uguucucuucugaggguaau	SCSUXZT_190072:3158476..31 58534:-
miR_190072_16953	420.0	-	cuuaccuguaaaucggagaag	cuuaccuguaaaucggagaagugucaaaauagacaa gcuucucguuuacaggguaauuu	SCSUXZT_190072:8354902..83 54963:-
miR_191069_46057	4.9	-	ggaaccaacgcugacuuaaccu	ggaaccaacgcugacuuaaccugugacaugggaaagg uaagucagugcuaguuuucg	SCSUXZT_191069:47434..4749 0:-
miR_194093_35524	0.9	-	agauaugaugaucauuuauugcucc	agauaugaugaucauuuauugcucccuauaggagg uccagcacuaucugacuguccuuauuuu	SCSUXZT_194093:2456097..24 56163:+
miR_195427_41945	0.0	-	cuucacaagauuuucaau	ugaauucucuugauaggguuuucucucaagauuuag cucuugacaaaagucuaucacaagauuuucaau	SCSUXZT_195427:611111..611 183:+
miR_197800_24975	0.6	-	uuuucccgaaguugcgaauucg	uuuucccgaaguugcgaauucgcaaacuggaauca acgagauuuuccauuucgugaauuu	SCSUXZT_197800:3343131..33 43194:-
miR_197949_28548	9.0	-	ccugugcaaaaagucguuaagc	ccugugcaaaaagucguuaagccguugagccaagcga caagauuuugcguuaagcaacuucuuugcaugg	SCSUXZT_197949:9932462..99 32532:+
miR_198293_12597	440.0	-	ugcccuauaccucagucgaggug	ugcccuauaccucagucgagguguuuuuuuuuuuu cacagcugucagauaucgaggcacc	SCSUXZT_198293:88527..8859 0:-
miR_204044_47802	7.6	-	accacgcugguuugcugacagu	ugcuagcaaucaucguguuuauuuuuguccuccac cacgcugguuugcugacagu	SCSUXZT_204044:858239..858 296:-
miR_207646_13385	4.9	-	ugcgacuugaggauuuuuugac	ugcgacuugaggauuuuuugacuauuuugcaaaaa uccucaagucgca	SCSUXZT_207646:291174..291 224:+
miR_209041_5904	25.0	-	uggcgccguguaaacaucuaaccu	aggagguuuucaugggcgcuacacugcucagaaagug gcgccguguaaacaucuaaccu	SCSUXZT_209041:1321115..13 21173:-
miR_217630_29516	0.1	-	cggauauaggagacuucu	cggauauaggagacuucagauucuaucugcucu uauuuucggg	SCSUXZT_217630:1076646..10 76693:+

miR_224301_19577	0.2	-	ggaagacuuuaaagaauu	uucaaacuccuuacaucaacuuuuggguguggaa agacuuuaaagaauu	SCSUXZT_224301:170781..170 833:+
miR_233964_41128	9.9	-	uuuaagacugucccagggcu	cucguguaaacgauucgaagccuggaacauuugacga gguuuuaagacugucccagggcu	SCSUXZT_233964:2194721..21 94781:-
miR_235853_8769	1.9	-	cagaucuuuaaaacgca	cguuuuuuauaugauguaggaauauauauauauau auauacaaucccagaucauauaaauaacgca	SCSUXZT_235853:3052823..30 52891:+
miR_239255_20953	0.2	-	ucuuucgagaccgaacaa	ucuuucgagaccgaacaaagcaucgagccgagaga aca	SCSUXZT_239255:322455..322 495:-
miR_239440_40182	1.8	-	uuuagugcacauaacuggcuga	cugguuuugugaacuaagaucauuuuuuuaucaau auuuagugcacauaacuggcuga	SCSUXZT_239440:4983916..49 83976:-
miR_242207_909	1.7	-	accaggugugaauucaggua	ccugaguuuucacuggugucagagaguuuuuagauu uauagaccagcugugaauucaggua	SCSUXZT_242207:1778299..17 78362:+
miR_25713_23315	2.3	-	ucggguagucguuuaug	uuuuaggaccucuggcugaugacauagucggugu acguuuguaaug	SCSUXZT_25713:43001..43048 :+
miR_25777_28067	2.3	-	aaaaugcgucaaguuugcugc	agcggauucuggcgcguuuuuuauuuuuuucgaaa gugaaaaugcgucaaguuugcugc	SCSUXZT_25777:677394..6774 56:+
miR_25927_35897	0.7	-	uguacguacugucuguuc	uguacguacugucuguucguuuuugccccacauagua guagguggcggggcugcgggcucugcaagggcg gcggcugg	SCSUXZT_25927:655..736:-
miR_266624_15276	2.3	-	cggaacauaaggggccccuggga	ccggggccccuuagcuccguguuuugucgaucgugc ggaaacauaaggggccccuggga	SCSUXZT_266624:11446624..1 1446682:-
miR_269856_24371	72.0	-	agauauguuugauuuuuuggug	agauauguuugauuuuuuuggugugauuuuuu aauccaccaagaucauauaguccgcg	SCSUXZT_269856:3137316..31 37380:-
miR_270756_45543	0.5	-	uuuguacagagcucugcgug	ccagaagcuuuaucccggagacguguuuuguacaga gcucugcgug	SCSUXZT_270756:3081090..30 81137:+
miR_272990_8657	1.2	-	aacacuggaagggggauca	aaacaccuuucagcauuuuuagguccgaccguuu ggucugccuuucgucggacuuuugucgcaacacugg aagggggauc	SCSUXZT_272990:10382332..1 0382417:+
miR_274266_1477	1.4	-	eggcccgagagguuggg	caaccuuccgugcugugccaccguuccagggcccg agagguuggg	SCSUXZT_274266:1018442..10 18490:+
miR_282125_11752	18.0	-	gugcaucuuaguagaccuag	gugcaucuuaguagaccuagauugguuuuuuacau uuuuagggggacaaaagaucua	SCSUXZT_282125:759843..759 904:+
miR_282625_36770	2.0	-	auugcuaucggaugacuguuuau	auugcuaucggaugacuguuuauagagauaaacaug acauuuuucgaauguaauag	SCSUXZT_282625:1003776..10 03835:+
miR_284269_42704	0.5	-	uacuuuugcuguuuuagcu	uacuuuugcuguuuuagcuuuuucgauucuaauag ccaaccuccgacaagguugu	SCSUXZT_284269:4232639..42 32696:+
miR_284269_42739	1.0	-	cugaaggcaguuugaaga	cugaaggcaguuugaagaccugggugcaacaauugc aacuuuuuuuuuaccacauuuuuuugcuucggcua uagcauuagga	SCSUXZT_284269:689335..689 420:-
miR_286181_26697	19.0	-	ugcccuauaccugguccuggcc	ugcccuauaccugguccugccuuuuuugucugauu ggcugggauccaguguaugcggcgag	SCSUXZT_286181:1390241..13 90304:-
miR_286181_26706	1.6	-	uggcuaccggauuaggguc	ugcccuagauccugguuccauguuaacauuucau cauggcuaccggauuaggguc	SCSUXZT_286181:1458968..14 59027:-
miR_286189_11435	0.9	-	uuaguauagccaccgaug	uuaguauagccaccgaugagcagacuaacgcucau cuuuccgauacuagcu	SCSUXZT_286189:2656413..26 56466:-

miR_29268_23626	2.0	-	ugcuggaaacuuagaauauccc	ugcuggaaaccuuagaauauccc	SCSUXZT_29268:1395519..1395587:+
miR_296099_4708	57.0	-	aaaggguuucuguguuguucuca	uacauacuggauguugaagguuuccagaaaau agcaagacagacuuuuuugugacuuuuagcacc	SCSUXZT_296099:1594982..1595040:-
miR_303104_7825	2.4	-	gccggucggucggucgguc	aggguuucuguguuguucuca gccggucggucggucggucggucggccggucg	SCSUXZT_303104:1698462..1698516:+
miR_304252_42327	2.0	-	uuucaucauucacaaggcugca	cagccuugcagggugucaaaucgugugaaagacg uuucaucauucacaaggcugca	SCSUXZT_304252:5122639..5122698:+
miR_304695_37747	2400.0	-	gagacuaagcccucgacc	cuuggggugacguacuuaagagagacacaccacacu gcgaucuaaagagacuaagcccucgacc	SCSUXZT_304695:5379940..5380005:+
miR_306399_45260	1.3	-	uaaaaaucaagucugaggguuu	uaaaaucaagucugaggguuuuuaacuaaagaa cuuucugacuugaaaauuag	SCSUXZT_306399:4998975..4999033:+
miR_311210_531	0.1	-	aaccugaugucuacuguaug	ugcaucaagaagcagggaacuuuaauguaaaccug augucuacuguaug	SCSUXZT_311210:561276..561327:+
miR_317062_36051	2.3	-	ucgcgcgccaacuuccgucggu	cggcgucggugacgacgccagaugggccuccuucuc gcgcgccaacuuccgucggu	SCSUXZT_317062:1898976..1899033:+
miR_318199_32136	11.0	-	uguuaguugcacucaaaugac	uagugaccuguagcuaaagcguuugcauuccgaucuc uuguacgguguuuuuguuaguugcacucaaaugac	SCSUXZT_318199:29464..29536:-
miR_318199_32138	11.0	-	uguuaguugcacucaaaugac	uagugaccuguagcuaaagcguuugcauuccgaucuc uuguacgguguuuuuguuaguugcacucaaaugac	SCSUXZT_318199:115252..115324:-
miR_319888_22860	2.7	-	accggacguaucucagcguu	accggacguaucucagcguu uuuuguuaaauguuagugaacgcugaguucgucc gguaa	SCSUXZT_319888:1086326..1086404:+
miR_323414_38018	290.0	-	cucgggagacaagugagauguc	caucugacuuuccuccgagcauuaagcgaucuc ucgggagacaagugagauguc	SCSUXZT_323414:680137..680195:-
miR_326942_2817	0.4	-	guggaaggguuuuauag	gcuaaacuucuccacugcaguuagauagcagauac acucuggggaaggguuuuauag	SCSUXZT_326942:1243244..1243305:+
miR_329364_41679	0.6	-	gccccaaaucuagugacia	cagacugggaauggaaaagaguguaucgccccaaau ucuagugacia	SCSUXZT_329364:70482..70530:+
miR_331581_13	0.5	-	cggauaugagagacuucuu	cggauaugagagacuucuuauacuguccuacagcgc ucuuauauccggu	SCSUXZT_331581:1181445..1181495:-
miR_333050_20365	1.2	-	uccgcgaucacuuguuguauug	uguacgaacaagggcugcguugaauuuuuuagac auccgcgaucacuuguuguauug	SCSUXZT_333050:1043389..1043448:+
miR_333050_20402	0.7	-	acgcgaaccgcugcuaaccuugu	acgcgaaccgcugcuaaccuugucuaauucuaaguc caaggcaagcugcuuuaguggaa	SCSUXZT_333050:6556483..6556544:+
miR_338667_31441	0.8	-	ugacuagaucuaaccuacc	ugguuugaauugcuucuguccaaguagacaccgc ucaugacuagaucuaaccuacc	SCSUXZT_338667:207239..207301:+
miR_338667_31443	34.0	-	ucaccggguaaacaucauucgc	gggugguguucacccgguuugguuuuuuuuuagu ucaucaccggguaaacaucauucgc	SCSUXZT_338667:240282..240344:+
miR_338667_31446	93.0	-	gaugaauuuaaccggcacaug	gaugaauuuaaccggcacaugggucgauugcau caccggguaaacaucauucgc	SCSUXZT_338667:241089..241146:+
miR_342812_40253	570.0	-	ugacauaacuuggaacucuaaa	ugacauaacuuggaacucuaaaguuuuuuuuuga acuuagaauuccagguuacgcagc	SCSUXZT_342812:912229..912291:-
miR_351137_19695	7.7	-	accugccuuacucuauguuacau	accugccuuacucuauguuacauuucuuuuuu guagcugacugagacaaggacc	SCSUXZT_351137:448350..448410:-

miR_354128_22701	2300.0	-	uaguuuuccggauuaaaa	uaaaaugaugacuauacacuuuccggguauaaagacaa auaucgcauuuaaaauuuuccgcauuuaaguauuuuc cggauuuaaaa	SCSUXZT_354128:797319..797 403:-
miR_358499_269	1.7	-	ucucaauccucuucgcgcacaca	ugugcgggagagggaucgggugauuuuugauaacg ucucaauccucuucgcgcacaca	SCSUXZT_358499:134933..134 992:+
miR_359262_373	97.0	-	uaucaacagcuagcuuugaugagcu	cucaucaaaaugccgugauaugcugacaauagacuuau cacagcuagcuuugaugagcu	SCSUXZT_359262:382693..382 751:+
miR_359262_375	87.0	-	uaucaacagcuagcuuugaugagcu	cucaucaaaaugcugggauaugcugacaauaugacgu aucacagcuagcuuugaugagcu	SCSUXZT_359262:383019..383 079:+
miR_359262_377	100.0	-	uaucaacagcuagcuuugaugagcu	cuccucaaaaggcgugauacgugccaauaugacau aucacagcuagcuuugaugagcu	SCSUXZT_359262:383488..383 548:+
miR_359262_379	110.0	-	uaucaacagcuagcuuugaugagcu	cucaucaacugguugaugugcuaucuuugacauau cacagcuagcuuugaugagcu	SCSUXZT_359262:383687..383 745:+
miR_359262_384	440.0	-	ucaucaaaugggcugucauacg	ucaucaaaugggcugucauacccuuaaaucauca uucguauacacagccugcuuugaugag	SCSUXZT_359262:384732..384 795:+
miR_37998_21165	1.7	-	ccaggugcuguauugugcuc	ccaggugcuguauugugcucugcauuguuaccagu uguccggac	SCSUXZT_37998:4110304..411 0350:-
miR_43656_27391	4.2	-	cuaaguacaggugccgcaggag	cuaaguacaggugccgcaggaggucauugcgcaua cucaagcgacuccaguacuucua	SCSUXZT_43656:661672..6617 32:-
miR_52207_46542	2.2	-	caaacaccccgccgugcaaaa	caaacaccccgccgugcaaaagggaauucucucaccu ugucggcugaccgguuguuug	SCSUXZT_52207:1523707..152 3766:+
miR_54252_45758	20.0	-	acaagaggauagauuggucga	cggccaacucauccucuaaaccugaaaaagacaaggag augaguuggucga	SCSUXZT_54252:2465590..246 5641:-
miR_54252_45760	2.0	-	ucggugggacuuucguucguu	cgagggaaggcucgucaugacuugcaaacugaug aucggugggacuuucguucguu	SCSUXZT_54252:3419999..342 0058:-
miR_60553_21027	1.6	-	aguaagucaacguuguuucga	ggagccaacguaggcuaacuuuuuuccacauucaca gaaaguaagucaacguuguuucga	SCSUXZT_60553:547458..5475 20:+
miR_60553_21037	500.0	-	cugaagucuucgugggaccuc	agguccaggaaagucuuucaugagacugaaacgucug aagucuuucgugggaccuc	SCSUXZT_60553:582651..5827 07:+
miR_63249_19990	2.1	-	uuuccuaauggccuucccgugu	uuuccuaauggccuucccgugacuuuaccucacc acacgagaaucccguaaggguaac	SCSUXZT_63249:8134152..813 4213:+
miR_66549_43466	17.0	-	uuagcugucucaugaucuua	acggugaugagaucauuugucuuuaaaaucgauu agcugucucaugaucuua	SCSUXZT_66549:631055..6311 11:-
miR_66774_2024	0.5	-	uaaaugcauuacugguauug	cguacaaaagugcauucuaacagugucgauuaaaa acuguaaaugcauuacugguauug	SCSUXZT_66774:8392930..839 2993:-
miR_66774_2041	1.2	-	accugagaccguuaacuugu	accugagaccguuaacuuguaaccacauugaagac agguuacgcucuuaggcaca	SCSUXZT_66774:9411362..941 1419:-
miR_7076_48122	1.6	-	acauccacauguugacuu	acauccacauguugacuuugcuauaggccccucuc cgacgccgagucaacaauugggauugug	SCSUXZT_7076:7301670..7301 737:+
miR_81188_15097	6.1	-	cuggacacacaaugaacgguu	ccguucauacugaguccauuggaacacagggucuga agaacuggacacacaaugaacgguu	SCSUXZT_81188:6662075..666 2138:+
miR_82910_20807	18.0	-	uacuggccuacaacaucacaaa	ugggggagcuguuugcuuugauugcguuuaagau cauacuggccuacaacaucacaaa	SCSUXZT_82910:44660..44720 :+
miR_84364_20143	2.3	-	caggaucuuuagucacuagcugc	aguuauggguaaagcccuugcauucgaccagucuauc uaugcaggaucuuuagucacuagcugc	SCSUXZT_84364:46298..46362 :+

miR_84364_20234	2.3	-	caggauuuuagucacuagcugc	aguuaggguaaaagccuuugcauucgaccagucuauc	SCSUXZT_84364:260484..260548:-
miR_86346_7530	2.3	-	uggggagucugugaugguuuuu	uaugcaggauuuuagucacuagcugc	SCSUXZT_86346:1274523..1274584:-
miR_86374_28352	120.0	-	uuuuuggcacuugugaaauaac	ugcccuucacagguaucuccgguuuuuauaugucc	SCSUXZT_86374:14863..14924
miR_90034_18208	7.6	-	uuguugacguaacaccuugccc	cuggggagucugugaugguuuu	:+
miR_92437_25227	10.0	-	uuucuguccgagcacgggacu	uauuuggcacuuugugaauaacuucacuucuuuu	SCSUXZT_90034:4934733..4934795:-
miR_94061_15413	18.0	-	cuugugcgugugacagugacu	agauuauacaccggugccaaguuuaa	SCSUXZT_92437:5206835..5206893:+
miR_97712_33989	2.0	-	uaacugcguguggaagga	cgauggauuuguuacgucacugaugguauuuugcg	SCSUXZT_94061:77453..77509
miR_122570_38157	200.0	ssa-miR-9b-5p	auaaagcuagguuaccaaaggc	acauuguugacguaacaccuugccc	:+
miR_144868_6092	1.8	mle-miR-216b-3p	uaauaucagcugguauuccuga	ucucgucgucacgugggaaaguucgagccugaauuc	SCSUXZT_97712:24992415..24992475:+
miR_144868_6096	0.9	tur-miR-12a-5p	ugaguauuacauagguacuga	uucucguccgagcacgggacu	SCSUXZT_122570:2251394..2251455:+
miR_170183_47434	220.0	cqu-miR-8-3p	uaauacugucagguaaaguguc	gucgugucgacgcuuacuggaaacucauggauuc	SCSUXZT_144868:172659..172717:+
miR_181921_19442	860.0	bmo-miR-184-3p	uggacggagaacugauaagggc	ugugcgugugacagugacu	SCSUXZT_144868:178868..178928:+
miR_217096_17207	1100.0	sha-miR-133a	agcugguuugaaaucgggcaaaa	uuuaccuaccacgcugacgaagcucuucaaaaug	SCSUXZT_170183:672272..672333:-
miR_217096_17210	2700.0	crm-miR-1-3p	uggaauguaaagaaguauuguc	uuuaccugcguguaagga	SCSUXZT_181921:2110642..2110701:+
miR_219542_39997	22.0	ppa-miR-29b	uagcaccuuugaaaucaguac	ucuuugguuauucugcugaauugauugauauac	SCSUXZT_217096:610319..610383:-
miR_219542_39999	-0.1	ssa-miR-29a-3p	ccuggucucuucggcgcuuaga	uucuuuuguuuacucuaaguuuacucgaagu	SCSUXZT_217096:633920..633980:-
miR_247296_47945	300.0	mle-miR-281-5p	aaggagcauccgucgacagu	auggaauguaaagaaguauuguc	SCSUXZT_219542:682806..682868:+
miR_250069_13953	360.0	ame-miR-87-3p	cggccugaaaauuugucgcaaccu	ccuggucucuucggcgcuuaga	SCSUXZT_219542:898349..898406:+
miR_251866_44338	530.0	ame-miR-750-3p	ccagaucaaacuuccagcuc	aaggagcauccgucgacagcaaaaauagguacug	SCSUXZT_247296:2862608..2862666:-
miR_269856_24367	4900.0	dpu-miR-92	aaugcacucguccggccugc	ucauggaguugcucuuuac	SCSUXZT_250069:1126198..1126259:-
miR_282061_845	7.3	mle-miR-1992-3p	cgucaguggaugauugcuggua	cggccugaaaauuugucgcaaccucuccaguccaga	SCSUXZT_251866:48174..48255:-
miR_287196_34996	1098.6	ggo-miR-153	uugcauagucacaaaagugauc	aggugagcaaauguuucagguguag	SCSUXZT_269856:2926672..2926731:-
				aguuggaagguuuuugcauuuacauacauacaua	SCSUXZT_282061:3222379..3222442:-
				uauauauaucucugaacaaugccagaucaaacuu	SCSUXZT_287196:74..132:-
				ccagcuc	
				aggucgugauguuugcauuuugguuuuuugggc	
				aaauugcacucguccggccugc	
				cgucaguggaugauugcugguagucugauac	
				uuuauacagcaguuguaaccacugauuug	
				aagcuuuugauuuagcgauguagacuuacuaau	
				ugcauagucacaaaagugauc	

miR_287196_34998	-1.4	mml-miR-153-3p	uugcauagucacaaaagugauc	aagcuuuugugauuuagcgauuguagacuuacuaau	SCSUXZT_287196:16250..1630
miR_317038_43155	1.9	lgi-miR-745a	agcugccugaugaaagagcugucc	ugcauagucacaaaagugauc	8:-
miR_317038_43157	2.1	mle-miR-745b-3p	gagcugccaaaugaagggcugu	ccgguuuccuucagcugcuccuugcuacuagaucaa	SCSUXZT_317038:86317..8637
miR_326757_43120	1.2	lgi-miR-1994b	ugagacaguguguccuccu	gcugccugaugaaagagcugucc	6:+
miR_326757_43122	1.7	mle-miR-1994a-3p	ugagacaguguguccuccu	agucuuuccuuugugcaguuucucuaauucacgagag	SCSUXZT_317038:87163..8721
miR_334713_17593	1100.0	pca-miR-981-5p	uucguugucgacgaaaccugccu	cugccaaaugaagggcugu	9:+
miR_353736_30011	3.9	cqu-miR-124	uaaggcacgcggugaauugcgu	agguaguacaacugucgacgacgcuuugcauucgacg	SCSUXZT_326757:946439..946
miR_359262_367	70.0	sme-miR-71a-5p	ucuuacuaccugucuuucgag	ugagacaguguguccuccu	496:-
miR_359262_369	2.0	pte-miR-2g-3p	ucacagccagcuuugaugagc	agggcgguuacucugucguuugcuuugaacuuuac	SCSUXZT_326757:952594..952
miR_359262_371	1.8	lgi-miR-2d	uaucaacagccugcuuggaucag	ccucaugagacaguguguccuccu	655:-
miR_39696_45765	330.0	lva-miR-31-5p	aggcaagauuggcgauagcuga	acggguuucgugacagggcgagcauaaaucuaaaau	SCSUXZT_334713:3438841..34
miR_66774_2021	12.0	aga-miR-34	uggcagugugguuagcugguuuu	guucguugucgacgaaaccugccu	38902:+
miR_66774_2026	25.0	sfr-miR-317-3p	ugaacacagcugguguaucuggu	cguguucacuguguuggcuuuagugaaaagcuuacaa	SCSUXZT_353736:3449361..34
miR_66774_2043	610.0	mse-let-7a	ugagguaguagguuguauagu	uuaggcacgcggugaauugcgu	49420:+
miR_97928_1018	430.0	ipu-miR-375	uuuguucguucggcucgcguua	ugaaagacacggguagugagauugcuguaacugagacu	SCSUXZT_359262:381625..381
				ucuuacuaccugucuuucgag	684:+
				gcaucaaugcuggaugucauaguaauucuccuuggccu	SCSUXZT_359262:381897..381
				aucacagccagcuuugaugagc	956:+
				cugaccaaguggcugcgacauguaaacaucucucuc	SCSUXZT_359262:382087..382
				auaucacagccugcuuggaucag	147:+
				aggcaagauuggcgauagcugaauuaaauagacguca	SCSUXZT_39696:577808..5778
				gcugugcugcauguugccauc	66:-
				uggcagugugguuagcugguuuguaagccacacauac	SCSUXZT_66774:8384747..838
				aaccacuucugcacuuccaug	4806:-
				cggguaccauguuguguuugcagucuuuuuucuuug	SCSUXZT_66774:8487844..848
				ugaacacagcugguguaucuggu	7904:-
				ugagguaguagguuguauaguuaagaaauacaccuu	SCSUXZT_66774:9487744..948
				ucaaggagaacuguaacaaccuucuaucguuucc	7813:-
				acccgagccguuugugacaaggcgcugauuuuucug	SCSUXZT_97928:789208..7892
				cuuuguucguucggcucgcguua	68:-

Table S3. Differentially expressed miRNAs in response to symbiosis.

<u>miRNA ID</u>	<u>Up-regulated in</u>	<u>logFC</u>	<u>logCPM</u>	<u>PValue</u>	<u>FDR</u>
miR.235	APO	-7.0193716	7.26015181	0.00074023	0.00630806
miR_132798_30512	APO	-6.2465259	6.69669252	0.00248376	0.01872372
miR.92b.3p	APO	-5.680694	8.91319986	4.81E-08	2.35E-06
miR.92b	APO	-4.5972495	11.0951376	6.89E-08	2.60E-06
miR_269856_24367	APO	-3.4308763	13.5683884	1.32E-07	3.71E-06
miR.92c.3p	APO	-3.3359691	13.5387361	2.67E-07	6.54E-06
miR.92	APO	-3.0576654	8.09886346	0.0006611	0.00617031
miR_181921_19442	APO	-2.5332239	11.072212	0.00045161	0.00491755
miR.184	APO	-2.4389344	11.0524473	0.00058138	0.00569751
miR.184a	APO	-2.3430371	11.1015178	0.00080084	0.00654017
miR_124085_1851	WT	2.4901879	10.139029	0.00161612	0.01267041
miR_274266_1477	WT	3.04478211	9.71553029	0.00069497	0.00619153
miR_326942_2817	WT	3.17883746	9.71917972	0.00054497	0.00562182
miR_282125_11752	WT	3.60815532	7.40214698	6.48E-05	0.00079435
miR_239255_20953	WT	3.97625579	12.5593508	1.12E-05	0.00018316
miR_329364_41679	WT	4.00366645	8.46841894	4.37E-07	9.51E-06
miR_140613_46616	WT	4.34180676	11.0107201	3.17E-05	0.00041474
miR_195427_41945	WT	4.77003562	7.89866746	1.30E-05	0.00019644
miR_7076_48122	WT	5.45123711	6.10344738	0.00341299	0.02477579
miR_41468_3385	WT	6.0633243	9.38943905	5.15E-07	1.01E-05
miR_235853_8769	WT	6.41451478	9.05771551	3.61E-13	2.36E-11
miR_107136_46704	WT	7.40747589	6.95270443	0.00043344	0.00491755
miR_284269_42739	WT	8.09542697	11.8684665	7.97E-08	2.60E-06
miR_331581_13	WT	8.40204555	7.93408351	4.15E-06	7.40E-05
miR_303104_7825	WT	11.7237658	14.2725488	1.17E-16	1.15E-14
miR_165622_47778	WT	15.2455138	18.2303139	8.45E-27	1.66E-24

Table S4. Predicted mRNA targets of miRNAs differentially up-regulated in aposymbiosis (APO) or symbiosis (WT).

Target ID	Target description	miRNA Up-regulated in	GO IDs
TR192171 c0_g1_i1 m.11722	uncharacterized protein LOC111107827 isoform X7	APO	
TR192819 c3_g1_i1 m.7533	protein SDE2 homolog	APO	
TR20914 c11_g4_i1 m.10674	probable syndecan	APO	P:GO:0007411; C:GO:0016021
TR20914 c11_g4_i2 m.10677	probable syndecan	APO	P:GO:0007411; C:GO:0016021
TR20914 c11_g4_i4 m.10681	probable syndecan	APO	P:GO:0007411; C:GO:0016021
TR210868 c1_g2_i1 m.3915	dedicator of cytokinesis protein 9-like	APO	F:GO:0005085; P:GO:0007264
TR214861 c4_g3_i1 m.18200	monocarboxylate transporter 6	APO	C:GO:0016020
TR249086 c4_g1_i1 m.45434	SEC14-like protein 5 isoform X1	APO	
TR323284 c1_g1_i7 m.3002	sorbin and SH3 domain-containing protein 1-like isoform X12	APO	P:GO:0007015
TR323817 c12_g1_i2 m.37639	zinc finger E-box-binding homeobox 2-like isoform X1	APO	F:GO:0003676
TR340854 c0_g1_i1 m.41277	protein PAT1 homolog 1-like isoform X2	APO	P:GO:0000290; C:GO:0016021
TR351429 c0_g1_i1 m.41732	pancreatic triacylglycerol lipase-like	APO	F:GO:0052689
TR355393 c0_g2_i1 m.18539	regulator of nonsense transcripts 3A	APO	P:GO:0000184; F:GO:0003676
TR355393 c0_g2_i4 m.18541	regulator of nonsense transcripts 3A	APO	P:GO:0000184; F:GO:0003676
TR364483 c1_g1_i1 m.27282	brefeldin A-inhibited guanine nucleotide-exchange protein 3-like	APO	F:GO:0005086; P:GO:0032012
TR374418 c0_g5_i2 m.5933	titin homolog	APO	
TR431227 c1_g3_i1 m.30586	MAX gene-associated protein	APO	F:GO:0046983
TR434563 c1_g2_i8 m.23405	microtubule-associated serine/threonine-protein kinase 3-like isoform X4	APO	F:GO:0000287; F:GO:0004674; F:GO:0005524; P:GO:0006468
TR440297 c2_g1_i3 m.41261	Aminopeptidase N	APO	F:GO:0004177; P:GO:0006508; F:GO:0008237; F:GO:0008270; C:GO:0016020; C:GO:0016021
TR472968 c0_g2_i1 m.39995	transcription factor HES-1-like isoform X2	APO	F:GO:0003677; C:GO:0005634; P:GO:0006355; F:GO:0046983
TR475451 c2_g12_i1 m.874	carbonic anhydrase 2	APO	F:GO:0016829; C:GO:0044464; F:GO:0046872
TR484494 c0_g2_i1 m.46739	---NA---	APO	
TR544754 c5_g1_i1 m.45564	---NA---	APO	

TR554366 c1_g1_i1 m.29973	Na/Ca exchanger	APO	F:GO:0005432; P:GO:0006816; P:GO:0007154; C:GO:0016021; P:GO:0035725
TR561918 c3_g2_i1 m.7063	zinc finger BED domain-containing protein 4-like	APO	
TR578211 c4_g1_i1 m.6875	ubiquitin carboxyl-terminal hydrolase 15-like	APO	F:GO:0004843; P:GO:0006511; P:GO:0016579
TR578211 c4_g1_i2 m.6876	ubiquitin carboxyl-terminal hydrolase 15-like	APO	F:GO:0004843; P:GO:0006511; P:GO:0016579
TR593181 c4_g1_i1 m.32221	protein Fe65 homolog isoform X4	APO	F:GO:0001540
TR603747 c5_g2_i1 m.23391	pleckstrin homology domain-containing family A member 8-like	APO	C:GO:0005737; P:GO:0120009; F:GO:0120013
TR620168 c8_g2_i3 m.30621	myosin VIIa	APO	F:GO:0003774; F:GO:0005524; C:GO:0016459; F:GO:0051015
TR662291 c1_g1_i1 m.40860	ATP-dependent RNA helicase HAS1-like isoform X2	APO	F:GO:0003723; F:GO:0004386; F:GO:0005524
TR691595 c0_g2_i1 m.37830	hypothetical protein OCBIM_22038603mg	APO	
TR704792 c4_g1_i1 m.17929	transmembrane protein 131-like	APO	C:GO:0016021
TR83271 c3_g2_i1 m.29598	---NA---	APO	
isotig06990 m.5479	collagen alpha-1(XI) chain-like	APO	F:GO:0005201
isotig08334 m.10070	dystrophin-like isoform X2	APO	
c8040_f3p12_2996	Kielin/chordin-like protein	APO	P:GO:0010466; C:GO:0016020; C:GO:0016021; F:GO:0030414
c11581_f1p0_3510	---NA---	APO	
c13044_f1p20_2061	UNKNOWN	APO	
c18734_f2p3_2465	kielin/chordin-like protein	APO	P:GO:0010466; F:GO:0030414
c20937_f4p4_2955	synaptobrevin-like isoform X7	APO	C:GO:0016021; P:GO:0016192; C:GO:0030054; C:GO:0030672; C:GO:0043005
c26718_f1p5_2766	acid phosphatase type 7	APO	C:GO:0016020; F:GO:0016787
c27289_f1p4_2242	kielin/chordin-like protein	APO	P:GO:0010466; F:GO:0030414
c30352_f1p3_2764	eukaryotic translation initiation factor 3 subunit A-like	APO	P:GO:0001732; F:GO:0003743; C:GO:0005852; C:GO:0016282; C:GO:0033290
c34101_f1p0_3437	inner nuclear membrane protein Man1-like	APO	C:GO:0016020
c43035_f1p1_1991	CWF19-like protein 2	APO	
c44237_f1p1_1848	synaptobrevin-like isoform X7	APO	C:GO:0016021; P:GO:0016192; C:GO:0030054;

			C:GO:0030672; C:GO:0043005
c46298_f1p4_3292	---NA---	APO	
c59220_f1p1_1923	Regulator of nonsense transcripts 3A	APO	P:GO:0000184; F:GO:0003676
c69472_f1p2_3359	protein Fe65 homolog isoform X4	APO	F:GO:0001540
c70307_f1p5_1993	KH domain-containing, RNA-binding, signal transduction-associated protein 2-like isoform X2	APO	F:GO:0003723; C:GO:0005654; F:GO:0042802; P:GO:0051259
c77414_f2p2_1977	SWI/SNF-related matrix-associated actin-dependent regulator of chromatin subfamily E member 1-like	APO	F:GO:0003677; C:GO:0016514; P:GO:0043044
c80199_f1p3_3312	mediator of RNA polymerase II transcription subunit 24-like isoform X2	APO	C:GO:0016592
c81768_f1p0_2846	autophagy-related protein 9A	APO	C:GO:0016020; C:GO:0031410
c82647_f1p1_1948	myotubularin-related protein 2-like	APO	F:GO:0004725; P:GO:0035335
c85139_f1p3_1995	PREDICTED: uncharacterized protein LOC106874353 isoform X5	APO	
c91345_f1p2_2469	regulator of nonsense transcripts 3A	APO	P:GO:0000184; F:GO:0003676
c92635_f1p2_2401	PREDICTED: uncharacterized protein LOC106127467	APO	
c93450_f1p0_3465	ecdysone-induced protein 75B, isoforms C/D-like isoform X1	APO	F:GO:0005488; P:GO:0050794
c97609_f1p1_1986	probable syndecan	APO	P:GO:0007411; C:GO:0016021
c106436_f1p0_1000	---NA---	APO	
c119358_f5p2_1296	synaptobrevin isoform X2	APO	
c128331_f1p1_1318	synaptobrevin-like isoform X7	APO	C:GO:0016021; P:GO:0016192; C:GO:0030054; C:GO:0030672; C:GO:0043005
g74873.t1	hypothetical protein OCBIM_22037054mg, partial	APO	C:GO:0016020
g30101.t1	golgin subfamily A member 2-like	APO	C:GO:0005794
g68212.t1	PREDICTED: LOW QUALITY PROTEIN: uncharacterized protein LOC101856069	APO	
g15949.t1	hypothetical protein OCBIM_22018288mg	APO	
g51771.t1	PREDICTED: uncharacterized protein LOC105334976	APO	
g37298.t1	cilia- and flagella-associated protein 61	APO	
g36605.t1	uncharacterized protein LOC110459911 isoform X3	APO	
g27282.t1	histone-lysine N-methyltransferase SETMAR-like	APO	
g103017.t1	nipped-B-like protein	APO	F:GO:0003682; C:GO:0005634; P:GO:0007049; P:GO:0010468
g99392.t1	46 kDa FK506-binding nuclear protein-like isoform X1	APO	F:GO:0016853

g14889.t1	RNA-directed DNA polymerase from mobile element jockey-like	APO	F:GO:0003676; F:GO:0003964; P:GO:0006278; F:GO:0008270
g32522.t1	Retrovirus-related Pol polyprotein from transposon 17.6	APO	
g92470.t1	hypothetical protein OCBIM_22029953mg	APO	F:GO:0003676; F:GO:0003677
g28146.t1	protein HID1-like	APO	
g55747.t1	hemocyte protein-glutamine gamma-glutamyltransferase-like isoform X1	APO	F:GO:0016740
g13562.t1	potassium voltage-gated channel subfamily H member 8-like	APO	F:GO:0005249; C:GO:0005887; P:GO:0034765; P:GO:0042391; P:GO:0071805
g59859.t1	Serine/threonine-protein kinase haspin	APO	F:GO:0004672; F:GO:0005524; P:GO:0006468; F:GO:0016301; P:GO:0016310
g10287.t1	selenocysteine lyase-like	APO	F:GO:0003824; F:GO:0005488
g64402.t1	piggyBac transposable element-derived protein 3-like	APO	
g68180.t1	PREDICTED: uncharacterized protein LOC106633231	APO	
g3221.t1	eukaryotic translation initiation factor 4B-like	APO	F:GO:0003676
g31995.t1	CUGBP Elav-like family member 3-B isoform X6	APO	
g99799.t1	LOW QUALITY PROTEIN: uncharacterized protein LOC112561606	APO	P:GO:0007154; C:GO:0016020; C:GO:0016021
g82943.t1	E3 ubiquitin-protein ligase HECW2 isoform X1	APO	P:GO:0006511; P:GO:0016567; F:GO:0061630
g25333.t1	MAX gene-associated protein	APO	F:GO:0046983
g56987.t1	protein OS-9-like	APO	C:GO:0016020
g81269.t1	golgin subfamily A member 3-like	APO	P:GO:0007283; C:GO:0090498
g47883.t1	histone-lysine N-methyltransferase SETMAR-like	APO	F:GO:0000014; P:GO:0000729; P:GO:0000737; C:GO:0000793; F:GO:0003690; F:GO:0003697; C:GO:0005730; P:GO:0008283; P:GO:0015074; P:GO:0031297; C:GO:0035861; F:GO:0042800; F:GO:0042803; F:GO:0044547; P:GO:0044774; F:GO:0046975; P:GO:0051568; P:GO:0071157;

			P:GO:0097676; P:GO:2000373; P:GO:2001034; P:GO:2001251
g7460.t1	ATP-dependent RNA helicase cgh-1-like	APO	F:GO:0003676; F:GO:0004386; F:GO:0005524
g85481.t1	neurofibromin-like isoform X4	APO	
g29852.t1	Niemann-Pick C1 protein-like	APO	P:GO:0001666; C:GO:0016020; P:GO:0030301; P:GO:0035855; P:GO:0043009; P:GO:0055113
g95115.t1	tyrosine-protein kinase SRK2-like	APO	F:GO:0004672; P:GO:0016310
g48925.t1	small RNA 2'-O-methyltransferase-like	APO	P:GO:0001510; F:GO:0008171; F:GO:0008173
g34370.t1	ATPase family AAA domain-containing protein 5-like	APO	F:GO:0005524; P:GO:0032006
g30991.t1	WD repeat-containing protein 47-like isoform X1	APO	
g70207.t1	myosin VIIa	APO	F:GO:0003774; F:GO:0005524; C:GO:0016021; C:GO:0016459; F:GO:0051015
g13736.t1	PREDICTED: uncharacterized protein LOC106511844, partial	APO	
g1576.t1	chitin synthase	APO	F:GO:0000166; F:GO:0003824; C:GO:0016020
g44067.t1	neurogenic locus notch homolog protein 1	APO	F:GO:0005509; C:GO:0016020; C:GO:0016021
TR236563 c4_g1_i1 m.41411	electroneutral sodium bicarbonate exchanger 1-like	APO	P:GO:0006820; F:GO:0008509; C:GO:0016020
c37954_flp14_2283	Regulator of rDNA transcription protein 15	APO	
TRINITY_DN35533_c118_g1_i1	basic proline-rich protein-like	APO	
c54254_flp0_2262	hypothetical protein OCBIM_22030393mg	APO	
c40779_flp5_2361	probable syndecan	APO	P:GO:0007411; C:GO:0016021
TR445695 c0_g2_i1 m.32544	PREDICTED: uncharacterized protein LOC105342567	APO	P:GO:0007154; C:GO:0016020
TR101467 c8_g2_i2 m.24075	tissue factor pathway inhibitor-like	WT	F:GO:0004867; P:GO:0010951
TR109121 c2_g1_i1 m.29138	zinc finger protein 271-like	WT	F:GO:0003676
TR116179 c0_g2_i1 m.17608	sialin-like isoform X3	WT	C:GO:0016020
TR117107 c0_g2_i1 m.20986	collagen alpha-1(XII) chain-like	WT	F:GO:0005201; F:GO:0005509; F:GO:0030246; C:GO:0062023
TR14558 c0_g2_i1 m.2425	PREDICTED: uncharacterized protein C6orf62 homolog	WT	

TR14761 c0_g1_i2 m.7675	Mediator of RNA polymerase II transcription subunit 1	WT	C:GO:0005634
TR171269 c3_g1_i1 m.21784	E3 ubiquitin-protein ligase TRIM71	WT	F:GO:0008270; F:GO:0046872
TR172288 c0_g1_i2 m.44289	---NA---	WT	
TR223006 c4_g3_i1 m.30712	heparan sulfate glucosamine 3-O-sulfotransferase 5	WT	C:GO:0016020; F:GO:0016740
TR261284 c7_g2_i1 m.18380	protocadherin beta-15-like	WT	P:GO:0007155; C:GO:0016020
TR281882 c1_g1_i2 m.23160	E3 ubiquitin-protein ligase ubr3-like isoform X2	WT	F:GO:0008270; P:GO:0016567; F:GO:0061630; P:GO:0071596
TR282736 c0_g1_i1 m.15860	formin-like protein 2	WT	F:GO:0003779; P:GO:0008360; F:GO:0017048; P:GO:0030036
TR286202 c8_g4_i1 m.26924	zinc finger protein 436	WT	F:GO:0003676; F:GO:0003677
TR290108 c1_g1_i1 m.40462	transcription factor Sox-2-like	WT	F:GO:0003677; C:GO:0005634; P:GO:0006355
TR304300 c0_g2_i1 m.30104	protein SMG8-like	WT	P:GO:0000184
TR308402 c10_g1_i1 m.36935	succinate dehydrogenase assembly factor 3, mitochondrial-like	WT	C:GO:0005739; P:GO:0034553
TR313389 c7_g1_i4 m.29889	protein piccolo-like isoform X1	WT	C:GO:0005623; P:GO:0006886; C:GO:0016020; F:GO:0017137
TR313753 c0_g1_i1 m.27452	gastrula zinc finger protein XICGF26.1-like isoform X1	WT	F:GO:0003676
TR322436 c0_g1_i1 m.30873	N6-adenosine-methyltransferase 70 kDa subunit-like	WT	C:GO:0005634; F:GO:0016422; P:GO:0080009
TR335143 c7_g1_i1 m.14210	glutamine--tRNA ligase-like	WT	F:GO:0004819; F:GO:0005524; C:GO:0005737; P:GO:0006425
TR339557 c0_g1_i2 m.43989	heparan-alpha-glucosaminide N-acetyltransferase-like	WT	C:GO:0016020
TR342930 c3_g2_i1 m.19272	proline synthase co-transcribed bacterial homolog protein	WT	F:GO:0030170
TR342930 c3_g2_i2 m.19273	pyridoxal phosphate homeostasis protein	WT	F:GO:0030170
TR343054 c9_g1_i4 m.16560	protein phosphatase 1 regulatory subunit 27	WT	
TR344793 c1_g3_i1 m.38503	cytochrome P450 3A8-like isoform X2	WT	F:GO:0005488; F:GO:0016491
TR355088 c5_g1_i1 m.14995	Multiple epidermal growth factor-like domains protein 6	WT	F:GO:0004222; P:GO:0006508; F:GO:0008270; C:GO:0016020; C:GO:0016021
TR357153 c5_g1_i1 m.11687	Multiple epidermal growth factor-like domains protein 8	WT	F:GO:0005509; C:GO:0016021
TR358694 c1_g5_i1 m.2883	oocyte zinc finger protein XICOF6-like	WT	F:GO:0003676
TR362695 c8_g2_i2 m.36235	hypothetical protein BOW45_13000, partial	WT	

TR368322 c1_g1_i1 m.36677	gastrula zinc finger protein XICGF26.1-like isoform X1	WT	F:GO:0003676; F:GO:0003677
TR4245 c1_g1_i2 m.1776	ankyrin repeat domain-containing protein 17-like isoform X2	WT	F:GO:0003723
TR470762 c1_g1_i1 m.28218	BUD13 homolog	WT	P:GO:0000398; C:GO:0005684; C:GO:0070274
TR472128 c4_g1_i1 m.2427	PREDICTED: uncharacterized protein C6orf62 homolog	WT	
TR479119 c8_g3_i1 m.6205	serine-rich adhesin for platelets-like isoform X1	WT	
TR479119 c8_g3_i2 m.23309	mucin-5AC-like isoform X2	WT	
TR483191 c6_g1_i1 m.32303	early endosome antigen 1-like isoform X1	WT	F:GO:0003676; F:GO:0046872
TR484336 c3_g1_i1 m.33469	AT-rich interactive domain-containing protein 4B	WT	F:GO:0003677; C:GO:0005634
TR488186 c0_g1_i1 m.46367	calcium-independent protein kinase C isoform X1	WT	F:GO:0004697; F:GO:0005524; P:GO:0006468; C:GO:0016020; P:GO:0035556; F:GO:0046872
TR496671 c3_g1_i1 m.24165	RNA-binding protein MEX3B-like	WT	F:GO:0003723
TR499896 c1_g1_i1 m.29221	PREDICTED: uncharacterized protein LOC106870495	WT	C:GO:0016020
TR510446 c0_g1_i1 m.40153	beta-1,3-galactosyltransferase 1-like	WT	C:GO:0000139; P:GO:0006486; F:GO:0008378; C:GO:0016021
TR519265 c0_g1_i1 m.30336	disintegrin and metalloproteinase domain-containing protein 12-like	WT	F:GO:0004222; P:GO:0006508; P:GO:0007229; F:GO:0008237; C:GO:0016020; C:GO:0016021
TR531433 c2_g1_i1 m.32639	hypothetical protein EGW08_001840	WT	
TR53960 c0_g2_i1 m.3413	phosphatidylinositol phosphatase SAC2-like	WT	F:GO:0042578
TR549623 c3_g1_i1 m.27000	gastrula zinc finger protein XICGF8.2DB-like	WT	F:GO:0003676
TR561909 c7_g1_i1 m.34333	protein Wnt-5b-like	WT	F:GO:0005102; C:GO:0005576; P:GO:0007275; C:GO:0016021; P:GO:0016055
TR570240 c13_g1_i1 m.10190	PRDM9	WT	F:GO:0003676; P:GO:1900111
TR584256 c1_g1_i1 m.34944	zinc finger protein 420-like	WT	F:GO:0000976; P:GO:0002437; P:GO:0002829; F:GO:0003676; P:GO:0045629
TR593181 c4_g1_i1 m.32221	protein Fe65 homolog isoform X4	WT	F:GO:0001540
TR609903 c4_g2_i1 m.39009	spermatogenesis-associated protein 5-like	WT	F:GO:0005524
TR610792 c7_g1_i1 m.29257	PREDICTED: uncharacterized protein LOC106870380	WT	P:GO:0035556
TR61759 c10_g2_i1 m.31672	coatamer subunit delta-like	WT	C:GO:0000139; C:GO:0005829;

			P:GO:0006888; P:GO:0006890; P:GO:0015031; C:GO:0030126; P:GO:0051645
TR635015 c3_g1_i4 m.21682	protocadherin beta-15-like isoform X1	WT	F:GO:0005509; C:GO:0005886; P:GO:0007156; C:GO:0016021
TR640699 c0_g1_i1 m.45844	gastrula zinc finger protein XICGF57.1-like	WT	F:GO:0003676
TR642860 c3_g5_i1 m.7989	protocadherin beta-15-like isoform X1	WT	C:GO:0016020
TR64301 c1_g2_i2 m.22860	hsc70-interacting protein	WT	F:GO:0046983; P:GO:0051085
TR643063 c5_g2_i2 m.33313	rho GTPase-activating protein 17-like	WT	C:GO:0016021
TR667759 c6_g3_i5 m.41397	cysteine sulfinic acid decarboxylase-like	WT	C:GO:0016021; F:GO:0016831; P:GO:0019752; F:GO:0030170
TR705428 c1_g3_i1 m.5989	focal adhesion kinase 1-like isoform X2	WT	F:GO:0004713; F:GO:0005524; C:GO:0005856; C:GO:0005925; P:GO:0007172; P:GO:0018108
TR705650 c0_g1_i1 m.38827	sushi, von Willebrand factor type A, EGF and pentraxin domain-containing protein 1 isoform X2	WT	F:GO:0005509; C:GO:0016020; C:GO:0016021
TR706296 c0_g1_i1 m.26932	fatty acyl-CoA reductase 1-like	WT	P:GO:0006629; C:GO:0016021; P:GO:0055114; F:GO:0080019; F:GO:0102965
TR712224 c0_g1_i1 m.40960	radial spoke head protein 3 homolog B-like	WT	
TR716581 c0_g1_i1 m.24514	gastrula zinc finger protein XICGF26.1-like isoform X1	WT	F:GO:0003700; C:GO:0005654; F:GO:0043565; P:GO:0045892; P:GO:0045944
TR721009 c3_g6_i1 m.23890	PREDICTED: uncharacterized protein LOC105850876	WT	
TR73903 c8_g16_i1 m.43557	hypothetical protein OCBIM_22022350mg	WT	
TR81786 c6_g1_i2 m.15132	protein FAM184A-like	WT	
TR8884 c7_g2_i1 m.36124	zinc finger protein 271-like	WT	F:GO:0005488
TR93795 c7_g1_i1 m.28363	Protein SMG5	WT	
isotig01321 m.13435	enolase-phosphatase E1-like isoform X1	WT	F:GO:0046872
isotig07931 m.5857	phenylalanine-4-hydroxylase-like isoform X1	WT	F:GO:0004505; F:GO:0005506; P:GO:0006559; P:GO:0055114
c5078_f3p4_1453	COP9 signalosome complex subunit 6	WT	P:GO:0000338; C:GO:0008180
c8594_f2p4_2263	nuclear receptor-binding protein-like isoform X10	WT	
c9350_f1p0_2775	zinc finger protein 79 isoform X1	WT	

c10526_f1p1_2251	PREDICTED: uncharacterized protein LOC106878068	WT	C:GO:0016021
c11509_f4p14_3058	PREDICTED: uncharacterized protein LOC106874007 isoform X2	WT	
c11968_f2p0_2151	splicing factor, arginine/serine-rich 15-like	WT	F:GO:0003676; F:GO:0003723
c13349_f1p0_1391	---NA---	WT	
c13636_f3p2_2017	nuclear receptor-binding protein-like isoform X9	WT	
c14610_f1p0_2537	gastrula zinc finger protein XICGF26.1-like isoform X1	WT	F:GO:0003676
c18827_f1p1_3014	neuroglian-like	WT	C:GO:0016020; C:GO:0016021
c19483_f3p1_2267	hypothetical protein OCBIM_22035547mg, partial	WT	F:GO:0003676; F:GO:0008270
c21209_f1p0_1812	kelch domain-containing protein 4-like	WT	
c21684_f1p0_2447	---NA---	WT	
c27146_f1p11_2012	Rho GTPase	WT	F:GO:0003924; F:GO:0005525; P:GO:0007264
c27203_f1p4_2088	---NA---	WT	
c33160_f3p7_3236	probable serine/threonine-protein kinase DDB_G0267686 isoform X3	WT	
c33722_f1p0_1869	enolase-phosphatase E1 isoform X4	WT	F:GO:0046872
c35093_f1p0_1232	---NA---	WT	
c38166_f2p7_2627	PREDICTED: uncharacterized protein LOC106874007 isoform X2	WT	
c38932_f1p1_2599	caprin-1-like isoform X1	WT	
c41394_f1p0_2372	gastrula zinc finger protein XICGF8.2DB-like	WT	
c42943_f1p0_2736	---NA---	WT	
c42964_f1p16_3645	reticulon-1-A-like isoform X3	WT	C:GO:0005789; C:GO:0016021
c44521_f1p1_3419	exocyst complex component 6B-like isoform X2	WT	C:GO:0000145; P:GO:0006904
c45530_f1p0_2141	uncharacterized transporter slc-17.2-like	WT	C:GO:0016020; C:GO:0016021; P:GO:0055085
c47995_f1p1_2544	neuroglian-like	WT	C:GO:0016020; C:GO:0016021
c48993_f1p2_2347	dnaJ homolog subfamily B member 11	WT	F:GO:0005102; C:GO:0005615; C:GO:0005634; C:GO:0005788; P:GO:0006457; P:GO:0016556; P:GO:0032781; P:GO:0036498; P:GO:0050768; F:GO:0051082; P:GO:0051604
c52660_f2p1_1870	transcriptional coactivator YAP1-like isoform X3	WT	
c53150_f1p6_2368	hsc70-interacting protein	WT	F:GO:0046983; P:GO:0051085

c53390_flp0_2349	CDGSH iron-sulfur domain-containing protein 2 homolog A-like	WT	C:GO:0016021; C:GO:0043231; F:GO:0051537
c57662_flp6_3389	focal adhesion kinase 1-like isoform X14	WT	F:GO:0004713; F:GO:0005524; C:GO:0005856; C:GO:0005925; P:GO:0007172; P:GO:0018108
c58041_flp2_2832	transforming growth factor-beta-induced protein ig-h3-like	WT	C:GO:0005615; P:GO:0007155; P:GO:0030198; C:GO:0031012; F:GO:0050839
c59824_flp5_3436	synapse-associated protein 1-like isoform X2	WT	
c62347_flp1_3083	gastrula zinc finger protein XICGF26.1-like	WT	F:GO:0003676
c65710_flp0_2935	segment polarity protein dishevelled homolog DVL-3-like isoform X4	WT	P:GO:0016055; P:GO:0035556
c65863_flp0_2782	nef-associated protein 1-like	WT	F:GO:0016301; P:GO:0016310
c66015_flp0_2879	zinc finger protein 665-like	WT	F:GO:0005488
c66874_flp1_2903	splicing factor, arginine/serine-rich 15-like	WT	F:GO:0003723
c67807_flp1_2530	tyrosine-protein kinase Abl-like isoform X1	WT	F:GO:0004715; F:GO:0005524; P:GO:0018108
c68790_f2p4_2174	hypothetical protein OCBIM_22035547mg, partial	WT	F:GO:0003676; F:GO:0008270
c69350_flp1_1902	tyrosine-protein kinase Abl-like isoform X1	WT	F:GO:0000166; F:GO:0004713; P:GO:0006468
c69472_flp2_3359	protein Fe65 homolog isoform X4	WT	F:GO:0001540
c70107_f2p2_3685	innexin unc-9-like isoform X2	WT	C:GO:0016020
c71712_flp2_3149	autism susceptibility gene 2 protein homolog isoform X6	WT	
c74578_flp1_2249	collagen alpha-1(XXIII) chain-like	WT	
c77807_flp1_3491	ankyrin repeat and BTB/POZ domain-containing protein 1-like	WT	
c78075_flp0_2351	zinc finger protein 91-like	WT	F:GO:0003676; F:GO:0003677
c81108_flp0_3257	probable cation-transporting ATPase 13A3 isoform X2	WT	F:GO:0000166; C:GO:0016020; F:GO:0016787; F:GO:0043167
c81152_flp2_2996	potassium channel subfamily T member 1-like isoform X1	WT	P:GO:0006813; C:GO:0016021
c82503_flp4_2275	nuclear receptor-binding protein-like isoform X12	WT	F:GO:0004672; F:GO:0005524; P:GO:0006468
c91290_flp0_1831	---NA---	WT	
c93853_flp1_2481	gastrula zinc finger protein XICGF26.1-like isoform X1	WT	
c95696_flp0_2156	kin of IRRE-like protein 1	WT	F:GO:0005509; C:GO:0016020; C:GO:0016021

c96150_flp2_2547	transcription factor Sox-2-like	WT	F:GO:0003677; C:GO:0005634; P:GO:0006355
c97319_flp1_3750	ankyrin repeat domain-containing protein 17-like isoform X2	WT	F:GO:0003723
c98873_flp1_2009	ubiquitin-conjugating enzyme E2 variant 2	WT	C:GO:0005634; P:GO:0006281; P:GO:0016567
c122871_flp0_1230	hypothetical protein	WT	
c123028_flp1_1199	enolase-phosphatase E1-like isoform X1	WT	
c150843_flp0_1218	---NA---	WT	
c165949_flp0_1352	N-acetylserotonin O-methyltransferase-like protein	WT	F:GO:0008171; P:GO:0032259
c202608_f4p1_2709	glutamine--tRNA ligase-like	WT	F:GO:0004819; F:GO:0005524; C:GO:0005737; P:GO:0006425
g3220.t1	probable E3 ubiquitin-protein ligase MID2 isoform X3	WT	F:GO:0046872
g39704.t1	Gag-Pol polyprotein	WT	F:GO:0003676; F:GO:0004190; P:GO:0006508; P:GO:0015074; F:GO:0016787
g104855.t1	baculoviral IAP repeat-containing protein 7-like isoform X3	WT	
g10923.t1	transcription factor Sox-2-like	WT	F:GO:0003677; C:GO:0005634; P:GO:0006355
g87678.t1	---NA---	WT	
g5606.t1	cilia- and flagella-associated protein 70-like	WT	
g48769.t1	disintegrin and metalloproteinase domain-containing protein 12-like	WT	F:GO:0008237; C:GO:0016020
g104555.t1	1-phosphatidylinositol 4,5-bisphosphate phosphodiesterase epsilon-1-like	WT	P:GO:0006629; F:GO:0008081; P:GO:0035556
g38346.t1	Transposon Ty3-I Gag-Pol polyprotein	WT	F:GO:0003676; P:GO:0015074
g93262.t1	gastrula zinc finger protein XICGF26.1-like	WT	F:GO:0003676
g59987.t1	zinc finger protein 271-like	WT	F:GO:0005488
g68051.t1	predicted protein	WT	
g88658.t1	zinc finger protein OZF-like	WT	F:GO:0003676
g27374.t1	multidrug resistance-associated protein 1 isoform X1	WT	F:GO:0000166; P:GO:0006810; C:GO:0016021; F:GO:0016887; F:GO:0022857
g87195.t1	eukaryotic translation initiation factor 3 subunit A-like	WT	P:GO:0001732; F:GO:0003743; C:GO:0005852; C:GO:0016282; C:GO:0033290
g96398.t1	E3 ubiquitin-protein ligase UHRF1-like	WT	C:GO:0005634; F:GO:0046872

g82155.t1	serine/threonine-protein kinase LATS1-like	WT	P:GO:0000278; F:GO:0004674; F:GO:0005524; P:GO:0006468; P:GO:0035329
g75187.t1	Transposon TX1 uncharacterized 149 kDa protein	WT	F:GO:0097159; F:GO:1901363
g90737.t1	centrosomal protein of 295 kDa-like isoform X1	WT	C:GO:0005813
g85182.t1	protein dopey-1-like isoform X3	WT	C:GO:0005829; P:GO:0006895
g44266.t1	Transcriptional repressor CTCF	WT	F:GO:0003676
g61908.t1	bromodomain-containing protein 3 isoform X1	WT	
g55811.t1	protein SMG8-like	WT	P:GO:0000184
g686.t1	Collagen alpha-4(VI) chain	WT	C:GO:0005581
g73017.t1	zinc finger protein 420-like	WT	F:GO:0000976; P:GO:0002437; P:GO:0002829; F:GO:0003676; P:GO:0045629
g77954.t1	multiple epidermal growth factor-like domains protein 8	WT	F:GO:0005509; C:GO:0016020; C:GO:0016021
g44323.t1	small conductance calcium-activated potassium channel protein-like	WT	F:GO:0005249; F:GO:0005516; C:GO:0008076; F:GO:0016286; P:GO:0071805
g77971.t1	endoribonuclease Dicer-like	WT	F:GO:0003723; F:GO:0004525; P:GO:0006396; P:GO:0031047; P:GO:0090502
g17489.t1	ubiquitin carboxyl-terminal hydrolase 1-like	WT	P:GO:0006511; P:GO:0016579; F:GO:0036459
g70782.t1	GLTSCR1-like protein	WT	
g46283.t1	Multiple epidermal growth factor-like domains protein 6	WT	F:GO:0004222; P:GO:0006508; F:GO:0008270; C:GO:0016020; C:GO:0016021
g99507.t1	chromodomain-helicase-DNA-binding protein 4-like isoform X9	WT	F:GO:0005524; P:GO:0006325; P:GO:0007051; P:GO:0007098; C:GO:0016581; F:GO:0046872
g36174.t1	A disintegrin and metalloproteinase with thrombospondin motifs 7-like	WT	F:GO:0008237
g10987.t1	cysteine/serine-rich nuclear protein 3-like	WT	
g84152.t1	splicing factor, arginine/serine-rich 15-like	WT	F:GO:0003723
g1267.t1	Atrial natriuretic peptide receptor 1	WT	F:GO:0003824; P:GO:0009987
TR372995 c2_g1_i4 m.10263	retrovirus-related Pol polyprotein from transposon 17.6 isoform X1	WT	F:GO:0003676; P:GO:0015074

c71443_f2p0_2070	RUN and FYVE domain-containing protein 2-like isoform X3	WT	
TR348346 c2_g8_i2 m.9450	probable cation-transporting ATPase 13A3 isoform X2	WT	F:GO:0005488
c8981_f3p1_1992	lysosomal acid phosphatase	WT	C:GO:0016020; C:GO:0016021
TR286203 c3_g1_i8 m.12722	RUN and FYVE domain-containing protein 2-like isoform X1	WT	
TRINITY_DN35533_c116_g3_i1	predicted protein	WT	
c46614_f1p5_2694	chorion peroxidase-like	WT	F:GO:0004601; P:GO:0006979; F:GO:0020037; P:GO:0055114; P:GO:0098869
c70064_f1p0_2038	hemocyanin subunit 1	WT	F:GO:0016491; F:GO:0046872; P:GO:0055114
c86393_f1p26_4023	Transketolase-like protein 2	WT	F:GO:0003824
TR348346 c2_g8_i1 m.9448	probable cation-transporting ATPase 13A3 isoform X2	WT	F:GO:0000166; C:GO:0016020; F:GO:0016787; F:GO:0043167
TRINITY_DN35533_c117_g2_i1	hypothetical protein C9926_02940, partial	WT	C:GO:0016020; C:GO:0016021
c169023_f1p0_1028	---NA---	WT	
c19597_f1p3_2087	RUN and FYVE domain-containing protein 2-like isoform X4	WT	
c83101_f1p0_2632	Transposable element Tcb2 transposase	WT	F:GO:0003676; F:GO:0003677; P:GO:0006313; F:GO:0008270; P:GO:0015074; C:GO:0016020; C:GO:0016021; F:GO:0022857; P:GO:0055085
c48313_f1p3_2464	RUN and FYVE domain-containing protein 2-like isoform X2	WT	F:GO:0046872
TR286203 c3_g1_i7 m.12720	RUN and FYVE domain-containing protein 2-like isoform X2	WT	F:GO:0046872
TR274590 c1_g3_i1 m.42738	peptidyl-prolyl cis-trans isomerase-like 2	WT	P:GO:0006464; F:GO:0016853; F:GO:0140096
c77419_f3p3_2231	N-acetylserotonin O-methyltransferase-like protein	WT	F:GO:0008171; P:GO:0032259
c20372_f4p19_1536	APGWamide precursor	WT	F:GO:0005179; C:GO:0005576; P:GO:0010469
TR584256 c1_g1_i1 m.34944	zinc finger protein 420-like	WT	F:GO:0000976; P:GO:0002437; P:GO:0002829; F:GO:0003676; P:GO:0045629
TR705428 c1_g3_i1 m.5989	focal adhesion kinase 1-like isoform X2	WT	F:GO:0004713; F:GO:0005524; C:GO:0005856; C:GO:0005925;

			P:GO:0007172; P:GO:0018108
--	--	--	-------------------------------

miR_117701_37111	30.0	-	aucuagaaacacuugguccuga	aucuagaaacacuugguccugauggcaagacaaggucaagacaa gugugauacuagaugc	SCSUXZT_117701:776425.. 776485:-
miR_117884_25329	2.4	-	ggggaggauaaaaagaaaagc	uuuuuuuuuauccuccuuucggcauagaaaaggaggau gaaaaaagaaaagc	SCSUXZT_117884:3633114 ..3633170:+
miR_118262_28506	220.0	-	uuuuugacagaacggguucacu	uuuuugacagaacggguucacuaguauauuaaaacaagugua caccuccgucaaaaaug	SCSUXZT_118262:717912.. 717973:+
miR_118359_1348	95000.0	-	ugagaucauuguaaaacuggu	cugguuuucacaauuguuugcagaauuguaagacuucugag aucuuuguaaaacuggu	SCSUXZT_118359:3030278 ..3030339:-
miR_118467_35793	1800.0	-	guugugugauuuugucauggugu	cgugacuacucauuguuuugcuuacuuuugcguuguguga uuugucauggugu	SCSUXZT_118467:4688687 ..4688742:+
miR_118668_15085	3.1	-	cauagagcauuucuuacacug	guguaagaaaugcucuauguaugcaccagcacauagagcau uucuuacacug	SCSUXZT_118668:572639.. 572693:+
miR_119465_47471	2400.0	-	uagauucgaguccgggucgga	uagauucgaguccgggucggagauaaaauagacucugaccg gaaucgaaaccuaca	SCSUXZT_119465:1909922 ..1909980:-
miR_122776_11889	2.6	-	uaccaugaucugccagauuag	agucuggcagaucaaggaaauuuuauugcuccuauuuuuacc caugaucugccagauuag	SCSUXZT_122776:7339125 ..7339186:+
miR_122776_12619	18.0	-	gcagugguuccgguguggacuc	gcagugguuccgguguggacucuguuuccauugucgagucu uguuggggcuauugcauc	SCSUXZT_122776:1189382 1..11893881:+
miR_123089_5989	22.0	-	uaauggccauagaauagacaguuu	acucuuauucgagucguuuuaaagaaguauacuaauggcca uagaauagacaguuu	SCSUXZT_123089:2656544 ..2656601:+
miR_12408_38081	0.2	-	caaaaaauuugcguuguuu	caaaaaauuugcguuguuuauuagaugaaagucuaaaaa cgacauuuuuuugc	SCSUXZT_12408:277491..2 77549:-
miR_124085_1851	250.0	-	ugaaccaugguuaaagaacauu	ugaaccaugguuaaagaacauugguccgucaaaagugcaaugg ucuugaccaugauuuacc	SCSUXZT_124085:532728.. 532789:-
miR_124085_1893	2.7	-	ugaccaacaacuccucagaga	ugaccaacaacuccucagacucauuaaaauacuaagagaa gggucucugaugaguuuuuggucuc	SCSUXZT_124085:7444353 ..7444422:-
miR_125663_44640	1.9	-	aaccgaaucguucauuuaagag	aaccgaaucguucauuuaagaguaguuuaauucucuuaaaug aacgauuugguuuaa	SCSUXZT_125663:2098797 ..2098854:+
miR_128367_47020	2.3	-	uuuuguuucggauuuuguaauc	uuuuguaaaccgaaaauaggagaaaaauccaauuuuuuuuc uuuuguuucggauuuuguaauc	SCSUXZT_128367:3262125 ..3262190:-
miR_128838_39202	0.9	-	uuggaauaagauuagacaucu	uuggaauaagauuagacaucuacaguguaugucauaaaucu uauuccaaau	SCSUXZT_128838:418289.. 418342:+
miR_128838_39221	0.7	-	uuggaauaagauuagacaucu	uuggaauaagauuagacaucuacacuguaugucauaaaucu uauuccaaau	SCSUXZT_128838:418287.. 418340:-
miR_129194_17411	2.6	-	guggugguuucgucggcg	guggugguuucgucggcgucuuugagccgucgucgggucgc uaucaucguugc	SCSUXZT_129194:1225334 ..1225388:-
miR_129242_3922	2.8	-	uguguguguuugggucgcu	gcacgcgugugcagcgcgugugugucaguguguaugc gugugcuguguguuuugggucgcu	SCSUXZT_129242:1469452 ..1469520:-
miR_130181_6713	63.0	-	uccuacuuguaagacaucggcu	cagaugucucacaaguagaaauaagacuuaaaaauuccuacu guuagacaucggcu	SCSUXZT_130181:2681789 ..2681847:+
miR_132798_30512	1600.0	-	ugccuugccuucucuugccuugg	agggcaauucggcugguacuguguaaaaauacuugccu ugccuucucuugccuugg	SCSUXZT_132798:6819629 ..6819690:-
miR_133820_12508	57.0	-	cguguuguuuacacugggcgc	cguguuguuuacacugggcgcgaugugcgcacgcaaaaaa acacauggcaccagugaaaacaacacgca	SCSUXZT_133820:3762..38 35:+

miR_216861_40826	72.0	-	uugcauuguuaguugcauugc	uugcauuguuaguugcauugc gcauacgcaguguaau	SCSUXZT_216861:4372153 ..4372211:+
miR_217289_25747	2.1	-	cauuuauuuugccgguauaaaa	guauaccggcaaaaaauugcauugc uuuugccgguauaaaa	SCSUXZT_217289:144225.. 144284:+
miR_217630_30519	9.2	-	cgucacgcuagcguucauaggc	cugugaauuuagacugaggaguuaaa uagcguucauaggc	SCSUXZT_217630:3131331 ..3131388:+
miR_217941_42570	1.5	-	uaccugauuuauaccgacugaau	ucaguuagucuaaaacgaguagaagu ugauuuauaccgacugaau	SCSUXZT_217941:6759747 ..6759810:-
miR_218719_1338	1.5	-	ccaggugagaguggauggcuc	ccaggugagaguggauggcuc acuaaccucugc	SCSUXZT_218719:1825251 ..1825307:+
miR_218719_1360	0.3	-	uuugcuaagaauuuaggcc	uuugcuaagaauuuaggcc agcaaaau	SCSUXZT_218719:7551305 ..7551356:+
miR_219508_33160	7.2	-	aggcgugcugcuucgacaauu	aggcgugcugcuucgacaauu caaugcagccaauuga	SCSUXZT_219508:3744254 ..3744315:+
miR_220386_3844	0.0	-	aguggaggaccuagggaau	uccgguccucuccccgggggaaaagg agucguuccuagaggaggagaccuag ggaau	SCSUXZT_220386:124815.. 124897:-
miR_22265_7059	0.0	-	uuuuggaucuaauauaua	uuuuggaucuauauaua uauuuuggaucuaauaua	SCSUXZT_22265:6423846.. 6423911:+
miR_223353_2318	170.0	-	gcgauagcugcugacuccg	cgacgagcagcagcauagcuguguu auagcugcugacuccg	SCSUXZT_223353:2166121 ..2166182:+
miR_223353_2327	0.7	-	uccaggaccuagcguaaugg	acugcggcggucuuuggagguuuc ccauggcguaaugg	SCSUXZT_223353:5380617 ..5380675:+
miR_224453_34509	0.0	-	ucggcaucuuauagggacaa	guccauucagacgccaguuuuagag cagcacucuaaaaaucggcaucuuau agggacaa	SCSUXZT_224453:1969092 ..1969169:+
miR_225333_19326	12.0	-	uuccauauagaauguuugaug	uuccauauagaauguuugaug caacguucuaauaggcac	SCSUXZT_225333:558439.. 558501:+
miR_226854_46162	1.5	-	aagcacaagaauaaauggcugu	aagcacaagaauaaauggcugu uuuuuccuugucacugc	SCSUXZT_226854:1007578 ..1007639:+
miR_226854_46175	14.0	-	aggagccuuuguuggaugggc	aggagccuuuguuggaugggc uaauguugccuucuga	SCSUXZT_226854:1849609 ..1849668:-
miR_229437_15851	2.4	-	uguauuucguuucucug	uguauuucguuucucug uuuuucagcauauaggcagccacag gagaaggaguc	SCSUXZT_229437:913109.. 913190:-
miR_231264_6046	0.0	-	aaaccaugcagucugcugcu	aaaccaugcagucugcugcu ggaaggc	SCSUXZT_231264:627709.. 627759:+
miR_231759_34897	12.0	-	cgcaggacuuuuugauuguuu	cgcaggacuuuuugauuguuu cauuuagucggcgaa	SCSUXZT_231759:807820.. 807880:-
miR_233964_41128	3700.0	-	uuuaagacuguccacgggcu	cucguguacagucuaagccuggaac agacuguccacgggcu	SCSUXZT_233964:2194721 ..2194781:-
miR_234791_29767	0.0	-	uuuacacuggggcacgucgua	cgccuuucagaauuacacuccucc gcuuucagguuggagguuuacacug ggggcacgucgua	SCSUXZT_234791:1235652 ..1235737:+
miR_235771_36630	0.1	-	agggaacuucucugggcug	agggaacuucucugggcug cuggaagacagcucua	SCSUXZT_235771:1149422 ..1149482:+
miR_2363_8507	1.6	-	ccaggaaaccggagagacucaac	ccaggaaaccggagagacucaac ucucagguucuaug	SCSUXZT_2363:2167346..2 167406:-

miR_264863_15020	1.3	-	uaaaauaacuuucgacuaga	uaguuuaaguaauuuugcauuuuauuuuuguuuuuguaauu uaacuuucgacuaga	SCSUXZT_264863:3954898 ..3954955:-
miR_264863_15023	880.0	-	ucuccaaccaauuuucgguacc	ucuccaaccaauuuucgguaccuuauauaucaagugugguac caaagaugauuggagagau	SCSUXZT_264863:4821237 ..4821299:-
miR_265363_24307	19.0	-	uuuuugaaccuggaauucuuugu	uuuuugaaccuggaucuuuguugaccuuugaaauuaaaaau ccaaaguucaaaaagau	SCSUXZT_265363:44455..4 4515:-
miR_265780_2983	0.4	-	aaaacaaaaggacuuaucuu	guacaaguccuuuuugcggaugauaaaauucuaucaguuuc aaaacaaaaggacuuaucuu	SCSUXZT_265780:883958.. 884022:+
miR_265792_23167	0.4	-	aaucuaugacguucuga	aaucuaugacguucugauauauauauauauaccagaacg ucauauugaucgu	SCSUXZT_265792:2585941 ..2585997:-
miR_265792_23179	230.0	-	uagucugcaaucgacuuuaggu	uagucugcaaucgacuuuagguauucuuuuaccgaucugaag acggaaagcagacu	SCSUXZT_265792:5349617 ..5349673:-
miR_266624_16093	1.5	-	uccuugaugcgacacaugccg	guuugugacacauccaaguuuaguuggacuugaaccuaucuu gaugcgacacaugccg	SCSUXZT_266624:1531983 8..15319897:+
miR_266624_15276	2.2	-	cggaacauaaggcccccuggga	cgggggcccccuaagcuccguguuuugucgaucgugcggaaca uaaggggcccccuggga	SCSUXZT_266624:1144662 4..11446682:-
miR_267075_39675	1.4	-	ugucucauguauuuggaugu	ugucucauguauuuggauguugccucaguuuaccacaauuc aguccugagucuaa	SCSUXZT_267075:1408864 ..1408922:-
miR_269856_24371	6200.0	-	agauauguuugauuuuuuuggu	agauauguuugauuuuuuugguugauuuuuucuaucua ccaaguaucaaucauguccgc	SCSUXZT_269856:3137317 ..3137380:-
miR_26996_14255	2.5	-	gcaguuuuucugugguagccccc	gcaguuuuucugugguagcccccugcggggguuauucgua uugguggucccccggguuggggguguccauguuugaaaacagc uc	SCSUXZT_26996:7469..755 5:-
miR_270183_16742	1.0	-	uuagcguucggaacaaaugga	uuagcguucggaacaaauggaaguuguaacaacaauucuaau cauucgaacgguuauuc	SCSUXZT_270183:6147196 ..6147256:+
miR_270183_16765	1.0	-	uuagcguucggaacaaaugga	uuagcguucggaacaaauggaaguuguaacaacaauucuaau cauucgaacgguuauuc	SCSUXZT_270183:6075680 ..6075740:-
miR_271323_40630	0.0	-	uagacaucgaaauuuuac	guaaaauuuucacugucuguuuguaaaggugauugaauagaca ucgaaauuuuac	SCSUXZT_271323:1015867 ..1015923:-
miR_272983_200	2.3	-	aaaagaaaguugcucugcccca	gggcagagcaaguugcuuuuuggaauucauuuuuuuuuuuuuu gaaaguugcucugcccca	SCSUXZT_272983:478671.. 478732:-
miR_272990_9196	0.3	-	aguucaaucguucugaugcca	aguucaaucguucugaugcccaagauuuguuuuuuuuuuuuuu ucaagucaaauguuuga	SCSUXZT_272990:1162937 3..11629435:+
miR_274351_7931	1.5	-	auaaaacaaaacuguggac	auaaaacaaaacuguggacauuacugacugaaauuuuguccaa caauuuuuuuuuuauca	SCSUXZT_274351:46492..4 6553:-
miR_274597_17236	12.0	-	uaaaaaucaacaagaucug	uaaaaaucaacaagaucuggaauuuuuuuuuuuuuuuuuuuuu ugaauuuuuacuc	SCSUXZT_274597:4029159 ..4029216:+
miR_275003_28520	0.3	-	cgauauaacggcugucuc	aacagccguuuaucauuuagucuuucgagauaacggcugucuc aagaauaccaugagccgggucguuuuuuuuuuuuuuuuuuuuu	SCSUXZT_275003:1284411 ..1284454:-
miR_275274_1443	37.0	-	aucggcugagcgagucuuuc	aucggcugagcgagucuuucgaguuuuuuuuuuuuuuuuuuuu ucggcugagcgagucuuuc	SCSUXZT_275274:548888.. 548951:+
miR_276322_21037	2.9	-	auugucgauucggugcuuguac	acaagcaccgaucgacauuuuuuuuuuuuuuuuuuuuuuuuu uguac	SCSUXZT_276322:933642.. 933691:+
miR_279349_12395	6.1	-	cguaucagaacucugaccagcg	cguaucagaacucugaccagcguuuugaagacugcugucua aaauucugauaaga	SCSUXZT_279349:132830.. 132889:-

miR_292562_22283	2.7	-	ucugucuuagcaagaacgaaa	ucguucuuugcuaagacagaggcguaacgccucugucuuagca aagaacgaaa	SCSUXZT_292562:1822558 ..1822611:+
miR_292562_22294	2.7	-	ucugucuuagcaagaacgaaa	ucguucuuugcuaagacagaggcguaacgccucugucuuagca aagaacgaaa	SCSUXZT_292562:1822556 ..1822609:-
miR_29268_23626	2.0	-	ugcuggaaaccuuagaauaucc	ugcuggaaaccuuagaauauccugaagaguacaaaauacauac uggauguugaagguuuccagaaaau	SCSUXZT_29268:1395519.. 1395587:+
miR_294499_8437	2.8	-	agugacacuuuuguuuaaagcug	agugacacuuuuguuuaaagcuguuucacaaaauuugucuuagg cuuacacaaaauaggugcuc	SCSUXZT_294499:507031.. 507094:-
miR_294659_284	2.1	-	acggacacucauuuuuauagcuc	acggacacucauuuuuauagcucauccaaaaccgugcaauugaa ugaguguuuucuc	SCSUXZT_294659:324597.. 324654:+
miR_29503_2949	130.0	-	uuagaaccgugcugaauauau	uuagaaccgugcugaauauauuacguuauuuuuuacag uacgguucuuuaaac	SCSUXZT_29503:1408446.. 1408503:-
miR_295214_11412	0.4	-	aauuguagaauuccagaauGCCA	aauuguagaauuccagaauGCCAGAUGCCAGAUGCCAUUCUG UAUACUACAUAUUUC	SCSUXZT_295214:1326..13 85:+
miR_296099_5200	1600.0	-	aaagguuucuguguuuucua	agcaagacagacuuuuuugacuuuuagcacaaaggguu ucuguguuuucua	SCSUXZT_296099:1594982 ..1595040:-
miR_297276_139	2.3	-	caaaaauaacgucgguuuuga	caaaaauaacgucgguuuugacgauguuagaugcaaaaacgac auuuuuuugca	SCSUXZT_297276:118870.. 118926:-
miR_298677_16705	1.2	-	ucaucgucguaguaguagg	acuacgccacgacaggugauguuucuaaugcuaucaucaucgu cguaguaguagg	SCSUXZT_298677:114062.. 114119:+
miR_298677_16710	1.2	-	ucaucgucguaguaguagg	acuacgccacgacaggugauguuucuaaugcuaucaucaucgu cguaguaguagg	SCSUXZT_298677:162422.. 162479:-
miR_298706_6182	2.3	-	aacacggacagaagauuuu	aacacggacagaagauuuuucgucuaauagaagaaagcaug uucuguccauguugu	SCSUXZT_298706:30062..3 0121:+
miR_300214_49294	1.7	-	aaccuacacugagcaauagaagca	guucuaucgcucgucaguguaccuugacuauuuuaggauuuu gagauucaaaucuaagaacagucacacucagagcaauagaa gca	SCSUXZT_300214:1260889 ..1260979:-
miR_300567_26259	2.5	-	gaggauucggcaggguacu	guagccgguuugaauccucaggguuuuacacacgucaggauu cggcaggguacu	SCSUXZT_300567:1072022 ..1072079:+
miR_301846_3780	0.4	-	uuugaagcauuuugcgcgca	uuugaagcauuuugcgcgcaaaaauuuccgagaugcuuuuaa aa	SCSUXZT_301846:1054194 ..1054239:+
miR_301846_3802	0.1	-	ugguguuuuuucguacgcg	ugguguuuuuucguacgcgcauuuuuuuacgcauauagca uaaaaaaaauagcacaugcguauuuuuuuacgucaccacu	SCSUXZT_301846:4048464 ..4048545:+
miR_302001_41161	0.2	-	cagaaaggacauuuauac	cagaaaggacauuuaucaacuagacagaggacagucuuacucg gacacgagugaccgccgaugaugaugauguuguuaguauuu agaauagcuguggaaucuggauggaauagaauaacuuuuuagau agugaaaacaauuuuacguuuuuuccggucaugugcc	SCSUXZT_302001:911422.. 911508:-
miR_303915_24905	0.0	-	cguuuuuccggucagugcc	agugaaaacaauuuuacguuuuuuccggucaugugcc ucagguauuuugcgcacuuuuuccuucccaaguggcgac caacaugccugacg	SCSUXZT_303915:3387798 ..3387881:+
miR_304131_24295	11.0	-	ucagguauuuugcgcacau	ucagguauuuugcgcacuuuuuccuucccaaguggcgac caacaugccugacg	SCSUXZT_304131:2734696 ..2734753:-
miR_304252_43569	1.9	-	uuucauauucacaaggcugca	cagccuugcagguggucauuuacguguguaagacguuucau cauucacaaggcugca	SCSUXZT_304252:5122639 ..5122698:+
miR_304276_23400	2.6	-	ugacgaggaauucuguuuuua	aaaaccagaagucuccguaagguuuuuuuuuuuuacgccugac gaggaauucugguuuuaa	SCSUXZT_304276:3278772 ..3278834:-
miR_305052_40689	1.0	-	uuuuuugaacuacaggga	ccugaaguucaaaauuuuuuuuuuuuuuuuuuuuuuuuu uuuugaacuacaggga	SCSUXZT_305052:6049716 ..6049775:+

miR_305052_40718	1.7	-	cgggugcaucuuucagaaacu	cgggugcaucuuucagaaacugguucgacauagaagauuuccaa guuuuggaaagacgcgcaugga	SCSUXZT_305052:1096263 0..10962695:+
miR_305661_23371	0.9	-	ugagucuccugucgaacaa	uuauucgacgacgauuacuaaauaagauuuggaaauuuccau aaugugugauuugagucuccugucgaacaa	SCSUXZT_305661:1114290 ..1114365:+
miR_306399_46889	1.2	-	gagagacauugcugacugau	cagaaaaguggucuuccccauaagcacagccgauggagagac auugcugacugau	SCSUXZT_306399:3428788 ..3428845:+
miR_306399_45260	830.0	-	uaaaaucaagucugagggauuc	uaaaaucaagucugagggauucuuuuuacuaaagaacuucuu gacuugaaauuga	SCSUXZT_306399:4998975 ..4999032:+
miR_306399_46916	2000.0	-	ugucugugggaaagguuaguc	ugucugugggaaagguuagucuuuuuagaaacuaaacac uaaaccaaugacauu	SCSUXZT_306399:9845278 ..9845337:+
miR_306399_46928	330.0	-	uuccggaguuucacaccauc	uuccggaguuucacaccaucagaucaacuuauggaugu gaaccuccaga	SCSUXZT_306399:1262626 0..12626314:+
miR_306399_46959	1.1	-	gaaguuagcaacguagagccu	gaaguuagcaacguagagccuaccagucuaacauggguga ucauuuagaaauucaggugcuaucgugcuuuuaguuua	SCSUXZT_306399:4760125 ..4760208:-
miR_306649_35395	2.7	-	auucguauacaaucugaugcu	caucagauuuguaucgaaauuuuuuuuuuuuucguauacaauc ugaugcu	SCSUXZT_306649:2229157 ..2229207:+
miR_306649_35474	2.7	-	auucguauacaaucugaugcu	caucagauuuguaucgaaauuuuuuuuuuuuuuucguauacaauc gaugcu	SCSUXZT_306649:2229155 ..2229205:-
miR_307083_41719	1.9	-	uaauuucugaacuuugagau	cuuaacuucagaaaauacuauacauaguuuuuuuaguuuu ucugaacuuugagau	SCSUXZT_307083:6791756 ..6791815:+
miR_308370_14511	1.0	-	uguuucuggauggauuugcucacuc	uguuucuggauggauuugcucacucuggauucugggucuuug uagagccagcagucuuaccagggaacucugua	SCSUXZT_308370:6799274 ..6799349:-
miR_311210_726	0.5	-	ucucgauuuuguuuccguuuucc	ucucgauuuuguuuccguuuuccuggacuucuuuuuguuuacu ggaguccaggaauugcugauucaggaaggggcg	SCSUXZT_311210:8322267 ..8322342:+
miR_312102_19730	0.1	-	cauguggugcuguaagcaacuc	acagccuuucacagcaccacagcaacucaguuugcugugugc ugugaaagcaacuc	SCSUXZT_312102:95406..9 5464:-
miR_31387_9580	2.8	-	uaucgcguuucguuugugc	cgacguacgaaagcgcgaaauaagacguauacuuuuuuuuuau cgcgcuuucguuugugc	SCSUXZT_31387:474013..4 74076:-
miR_314363_15281	400.0	-	ugaagagaccgucaggucuguc	ugaagagaccgucaggucugugcuaagaauuuuacaacaa cacucacagacacgcgucugucacucacu	SCSUXZT_314363:291317.. 291389:-
miR_316645_5618	2.3	-	aaacgucgagacaauaaca	uuuuugcaucuccaguuuuuuugagauuuggucaaaacgug cugagacaauaaca	SCSUXZT_316645:1600529 ..1600586:-
miR_316868_21452	92.0	-	caggucuuuacuguguuuuc	caggucuuuacuguguuuucuuuuugcagaaaccaagcag uguuugaccagu	SCSUXZT_316868:1710729 ..1710784:+
miR_316868_21458	0.7	-	uaccuuguaugcuuugguaag	uaccuuguaugcuuugguaagacuguaaaacuguuuuccaacc auacacacaaggugg	SCSUXZT_316868:4504944 ..4505002:+
miR_316868_21460	0.7	-	uaccuuguaugcuuugguaag	uaccuuguaugcuuugguaagacuguaaaacuguuuuccaacc auacacacaaggugg	SCSUXZT_316868:4532282 ..4532340:+
miR_317062_37307	2.3	-	ucgcgcgcaacuuccgucggu	cggcgcgugggacgacgccagauugggccuucucgcgcg caacuuccgucggu	SCSUXZT_317062:1898976 ..1899033:+
miR_317151_3946	0.0	-	aagaaucuggacugaagca	aagaaucuggacugaagcaaaaaauugcuucaguccaggau uuuuuu	SCSUXZT_317151:2441261 ..2441312:+
miR_318199_33251	6.1	-	uaaagguuauuuuaguuugc	uaaagguuauuuuaguuugcaaaaguuuugcuaagagauugg cuuugccuagucugagauuaccuc	SCSUXZT_318199:2414393 ..2414464:-

miR_217096_17207	7100.0	sha-miR-133a	uugguccccuuaaccagcugu	agcugguugaaaucgggccaauuugacuaguccaaaggcauu uugguccccuuaaccagcugu	SCSUXZT_217096:610319.. 610383:-
miR_217096_17210	5600.0	crm-miR-1-3p	uggaauguaaagaaguauuguu	acaauucuuuuuacuaucucauagauuuacucgaaguuggaa uguaaagaaguauuguu	SCSUXZT_217096:633920.. 633980:-
miR_219542_39999	230.0	sla-miR-29b	uagcaccuuugaaaucaguuu	ccuggucucuucuggcgcuuagauauucuuucucuagcacca uuugaaaucaguuu	SCSUXZT_219542:898349.. 898406:+
miR_247296_47945	3400.0	mle-miR-281-5p	aaggagcauccgucgacagu	aaggagcauccgucgacagucagaaaauagguacugucaugg aguugcucuc	SCSUXZT_247296:2862613 ..2862666:-
miR_250069_13953	3100.0	egr-miR-87-3p	gugagcaaaguucagguguag	cggccugaaaauuugucucgaaccucuccaguccagaagguga gcaaaguucagguguag	SCSUXZT_250069:1126198 ..1126259:-
miR_251866_44338	3300.0	ame-miR-750-3p	ccagaucuaacucuccagcuca	aguuggaagguuagguuuuugcauauauacauauauauaua uauucucugaacaaugccagaucauacucuccagcuca	SCSUXZT_251866:48173..4 8255:-
miR_269856_24367	39000.0	dqu-miR-92c-3p	aaugcacucgucggccugc	aggucgugauguuugcauuuuuggguuuuuuugggcauuug cacucgucggccugc	SCSUXZT_269856:2926672 ..2926731:-
miR_282061_845	5600.0	lgi-miR-1992	ucagcaguuguccagauuug	cgucaguggauguugcugguagucugucugauuuuauca gcaguuguccagauuug	SCSUXZT_282061:3222379 ..3222442:-
miR_287196_34996	1200.0	ggo-miR-153	uugcauagucacaaaagugauc	uuuugugauuuagcgauuugagacuuacuaauuugcauaguc caaaagugauc	SCSUXZT_287196:74..128:-
miR_287196_34998	1200.0	gga-miR-153-3p	uugcauagucacaaaagugauc	uuuugugauuuagcgauuugagacuuacuaauuugcauaguc caaaagugauc	SCSUXZT_287196:16250..1 6304:-
miR_317038_43155	1000.0	lgi-miR-745a	agcugccugaugaagcugucc	cgguuccucucaggcugccuugcuacuuaugaucaagcugccu gauaagcugucc	SCSUXZT_317038:86318..8 6376:+
miR_317038_43157	2.1	mle-miR-745b-3p	gagcugccaaaugaaggcgugu	agucuuuccuuuggucagcuuucucuaauucacgagcugcca aauaaggcgugu	SCSUXZT_317038:87163..8 7219:+
miR_326757_43120	1.2	lgi-miR-1994b	ugagacaguguguccuccuc	gguaagacaaacugucgacgcuuugcauucgacugugagaca guguguccuccuc	SCSUXZT_326757:946438.. 946495:-
miR_326757_43122	1.7	mle-miR-1994a-3p	ugagacaguguguccuccu	ggcgguuacucugucguuuuugaacuuuaccucaugag acaguguguccuccu	SCSUXZT_326757:952594.. 952653:-
miR_334713_17593	20000.0	pca-miR-981-5p	uucguugucgacgaaaccugccu	acggguuucgucagcgagcauaaaauccauuuuugucgu ugucgacgaaaccugccu	SCSUXZT_334713:3438841 ..3438902:+
miR_353736_30011	800.0	cja-miR-124	uaaggcacgcgugaugcggu	guguucacugugugcuuuagugaaaagcuuacaauuagggc acgcgugaugcggu	SCSUXZT_353736:3449362 ..3449420:+
miR_353736_30011	1600.0	sme-miR-71a-5p	ugaaagacacggguagugagaug	ugaaagacacggguagugagcugcugacuugacuucuuac uaccugucuuucgag	SCSUXZT_359262:381625.. 381684:+
miR_359262_367	2.0	tcf-miR-2a-3p	ucacagccagcuuugaugagcc	caucaaugcuggaugucauaguaauucuuuggccuauacacag ccagcuuugaugagcc	SCSUXZT_359262:381898.. 381957:+
miR_359262_369	1.9	lgi-miR-2d	uauacagccugcuuggaucag	cugaccaaguggcugcagacuguuuaacuuucuucauauac agccugcuuggaucag	SCSUXZT_359262:382087.. 382147:+
miR_359262_371	-1.8	lgi-miR-2d	uauacagccugcuuggaucag	uauacagccugcuuggaucaguagaggcuuucugguauac auccugagccuuuaagaaaucugcagcguuugaaaaa	SCSUXZT_359262:382125.. 382207:+
miR_359262_372	1300.0	lva-miR-31-5p	aggcaagauuuggcauagcuga	aggcaagauuuggcauagcugaauuaauagcugcugcug cugcauugcgauc	SCSUXZT_39696:577808..5 77866:-
miR_66774_2021	2700.0	aga-miR-34	uggcagugugguagcugguuugu	uggcagugugguagcugguuuguaagccacacauacaaccac uauucgacacuccaug	SCSUXZT_66774:8384747.. 8384806:-

miR_66774_2026	2.1	cqu-miR-317-3p	ugaacacagcugggguaucug	gguaccauguuguguuugcagucuuuauucuuugugaacacag cugggguaucug	SCSUXZT_66774:8487846.. 8487902:-
miR_66774_2043	37000.0	tca-let-7-5p	ugagguaguagguuguauaguu	ugagguaguagguuguauaguuagaaaacaccauuucaagg agaacuguacaaccuucuaagcuuucc	SCSUXZT_66774:9487744.. 9487813:-
miR_97928_1018	1300.0	ami-miR-375-3p	uuuguucguucggcucgcguu	acccgagccguuugacaaggcgcugauuuuucugcuuugu ucguucggcucgcguu	SCSUXZT_97928:789209..7 89268:-

Table S6. Differentially expressed miRNAs between hemolymph and light organ from colonized (WT) or uncolonized squid.

miRNA ID	Up-regulated in	Contrast	logFC	logCPM	PValue	FDR
miR_323414_39358	HEM	HEM vs WT	17.19	16.07	1.10E-15	2.27E-13
miR_282625_36770	HEM	HEM vs WT	14.39	13.46	1.02E-08	7.02E-07
miR_317038_43157	HEM	HEM vs WT	5.30	13.65	1.10E-06	4.51E-05
miR_94061_15413	HEM	HEM vs WT	5.20	13.10	3.57E-06	0.0001225
miR_359262_369	HEM	HEM vs WT	4.48	14.62	5.45E-06	0.00014065
miR_83498_37681	HEM	HEM vs WT	13.01	12.28	5.46E-06	0.00014065
miR_317062_37307	HEM	HEM vs WT	12.56	11.91	1.94E-05	0.00040027
miR_306399_46916	HEM	HEM vs WT	12.44	11.81	3.08E-05	0.00057692
miR_304252_43569	HEM	HEM vs WT	12.35	11.74	3.89E-05	0.00066854
miR_52207_46542	HEM	HEM vs WT	11.98	11.44	0.00014235	0.00225574
miR_116768_42237	HEM	HEM vs WT	11.72	11.23	0.00046261	0.00680698
miR_25777_28067	HEM	HEM vs WT	13.05	12.32	0.00052513	0.00721176
miR_197758_24610	HEM	HEM vs WT	11.46	11.02	0.00066473	0.00855843
miR_306399_46959	HEM	HEM vs WT	11.52	11.07	0.00077027	0.00933391
miR_351137_19695	HEM	HEM vs WT	3.31	12.67	0.00092458	0.01014699
miR_209103_1587	HEM	HEM vs WT	11.37	10.95	0.00093589	0.01014699
miR_186077_6064	HEM	HEM vs WT	11.18	10.80	0.00269222	0.02772983
miR_269856_24371	HEM	HEM vs WT	3.04	13.27	0.0032712	0.03149211
miR_338667_31441	HEM	HEM vs WT	2.70	15.63	0.00336324	0.03149211
miR_359262_373	HEM	HEM vs WT	2.44	13.71	0.0041628	0.03728419
miR_266624_15276	HEM	HEM vs WT	10.67	10.39	0.00443005	0.03802458
miR_66774_2024	HEM	HEM vs WT	3.03	11.36	0.00558386	0.04448055
miR_106968_6898	HEM	HEM vs WT	10.39	10.17	0.00561405	0.04448055
miR_66774_2021	HEM	HEM vs WT	3.17	12.23	0.00605243	0.04493942
miR_282061_845	HEM	HEM vs WT	4.30	12.95	0.00610827	0.04493942
miR_343891_14698	HEM	HEM vs WT	10.52	10.27	0.00651578	0.04628453
miR_66774_2041	WT	HEM vs WT	-11.89	16.31	1.33E-11	1.37E-09
miR_190072_16953	WT	HEM vs WT	-6.73	13.33	7.22E-07	3.72E-05
miR_190072_16933	WT	HEM vs WT	-7.42	12.04	9.57E-06	0.00021907
miR_323414_39358	HEM	HEM vs APO	17.18	14.81	3.59E-27	7.40E-25
miR_83498_37681	HEM	HEM vs APO	13.12	11.00	6.46E-10	2.22E-08
miR_282625_36770	HEM	HEM vs APO	5.00	12.14	2.78E-09	8.17E-08
miR_317062_37307	HEM	HEM vs APO	12.64	10.59	5.33E-09	1.37E-07
miR_306399_46916	HEM	HEM vs APO	12.39	10.38	6.80E-09	1.56E-07
miR_304252_43569	HEM	HEM vs APO	12.36	10.34	1.20E-08	2.48E-07

miR_282061_845	HEM	HEM vs APO	4.75	11.52	4.30E-08	8.05E-07
miR_351137_19695	HEM	HEM vs APO	4.66	11.25	6.59E-08	1.13E-06
miR_116768_42237	HEM	HEM vs APO	11.88	9.94	1.10E-06	1.74E-05
miR_197758_24610	HEM	HEM vs APO	11.37	9.51	1.50E-06	2.20E-05
miR_209103_1587	HEM	HEM vs APO	11.48	9.60	1.68E-06	2.30E-05
miR_306399_46959	HEM	HEM vs APO	11.66	9.75	2.45E-06	3.16E-05
miR_94061_15413	HEM	HEM vs APO	3.49	12.02	5.25E-06	6.36E-05
miR_317038_43157	HEM	HEM vs APO	2.96	12.58	1.93E-05	0.00021487
miR_186077_6064	HEM	HEM vs APO	11.41	9.55	3.32E-05	0.00032595
miR_343891_14698	HEM	HEM vs APO	10.55	8.83	4.44E-05	0.000416
miR_106968_6898	HEM	HEM vs APO	10.43	8.73	7.85E-05	0.00070345
miR_129242_3922	HEM	HEM vs APO	10.59	8.87	9.29E-05	0.00073613
miR_359262_369	HEM	HEM vs APO	2.34	13.61	0.0001783	0.00136037
miR_214888_31882	HEM	HEM vs APO	10.09	8.46	0.00027085	0.00199267
miR_339969_32914	HEM	HEM vs APO	9.71	8.14	0.00032128	0.00208424
miR_66774_2021	HEM	HEM vs APO	2.77	10.98	0.00046271	0.00287984
miR_114881_5391	HEM	HEM vs APO	9.76	8.19	0.00048641	0.00287984
miR_67889_25493	HEM	HEM vs APO	9.82	8.23	0.00049074	0.00287984
miR_25777_28067	HEM	HEM vs APO	4.28	11.27	0.00050327	0.00287984
miR_254358_33719	HEM	HEM vs APO	9.56	8.02	0.00081583	0.00430924
miR_306399_46928	HEM	HEM vs APO	9.45	7.94	0.00084656	0.00435979
miR_25777_28985	HEM	HEM vs APO	10.24	8.58	0.00169852	0.00833082
miR_180978_43963	HEM	HEM vs APO	9.12	7.67	0.00239189	0.01145883
miR_86346_8082	HEM	HEM vs APO	9.08	7.64	0.00305436	0.01429994
miR_265792_23179	HEM	HEM vs APO	8.75	7.37	0.00372889	0.01685542
miR_305661_23371	HEM	HEM vs APO	8.78	7.40	0.00376383	0.01685542
miR_139364_48083	HEM	HEM vs APO	8.98	7.56	0.00453288	0.0195409
miR_124085_1851	HEM	HEM vs APO	8.85	7.45	0.00741967	0.03056903
miR_187942_37075	HEM	HEM vs APO	8.60	7.25	0.00783706	0.03151769
miR_128367_47020	HEM	HEM vs APO	8.61	7.26	0.00795592	0.03151769
miR_40294_39248	HEM	HEM vs APO	8.13	6.88	0.00987023	0.03836354
miR_271323_40630	HEM	HEM vs APO	8.19	6.92	0.01012067	0.03860847
miR_339065_23232	HEM	HEM vs APO	8.14	6.88	0.01063974	0.03985066
miR_180978_43962	HEM	HEM vs APO	8.43	7.12	0.01279542	0.04706888
miR_66774_2041	APO	HEM vs APO	-13.87	17.13	5.93E-25	6.11E-23
miR_190072_16933	APO	HEM vs APO	-9.74	13.11	6.22E-15	4.23E-13
miR_190072_16953	APO	HEM vs APO	-7.94	13.34	8.22E-15	4.23E-13
miR_338667_31446	APO	HEM vs APO	-8.40	11.73	4.80E-10	1.98E-08
miR_326757_43122	APO	HEM vs APO	-5.97	8.98	1.98E-05	0.00021487
miR_338667_31443	APO	HEM vs APO	-4.89	9.49	2.36E-05	0.00024268

miR_217096_17210	APO	HEM vs APO	-3.22	15.72	8.73E-05	0.00073613
miR_122570_38157	APO	HEM vs APO	-3.13	12.40	8.98E-05	0.00073613
miR_97928_1018	APO	HEM vs APO	-4.50	13.83	0.00029208	0.0020408
miR_217096_17207	APO	HEM vs APO	-2.62	15.37	0.0002972	0.0020408
miR_326757_43120	APO	HEM vs APO	-4.99	8.84	0.00032376	0.00208424
miR_250069_13953	APO	HEM vs APO	-2.48	13.68	0.00076531	0.0042609
miR_269856_24367	APO	HEM vs APO	-2.75	18.13	0.00081334	0.00430924
miR_176595_30239	APO	HEM vs APO	-2.53	13.54	0.00099567	0.00500263
miR_181709_2949	APO	HEM vs APO	-2.73	12.27	0.00481693	0.02025079

References

1. Moya A, Peretó J, Gil R, Latorre A. Learning how to live together: genomic insights into prokaryote–animal symbioses. *Nat Rev Genet.* 2008;9:218–29. doi:10.1038/nrg2319.
2. McFall-Ngai M, Hadfield MG, Bosch TCG, Carey H V., Domazet-Lošo T, Douglas AE, et al. Animals in a bacterial world, a new imperative for the life sciences. *Proc Natl Acad Sci.* 2013;110:3229–36. doi:10.1073/pnas.1218525110.
3. Montgomery MK, McFall-Ngai M. Bacterial symbionts induce host organ morphogenesis during early postembryonic development of the squid *Euprymna scolopes*. *Development.* 1994;120:1719–29. papers3://publication/uuid/BF5BB089-FA96-4EF6-8ED3-CAB940D15B66.
4. Kremer N, Philipp EER, Carpentier MC, Brennan CA, Kraemer L, Altura MA, et al. Initial symbiont contact orchestrates host-organ-wide transcriptional changes that prime tissue colonization. *Cell Host Microbe.* 2013;14:183–94.
5. Moriano-Gutierrez S, Koch EJ, Bussan H, Romano K, Belcaid M, Rey FE. Critical symbiont signals drive both local and systemic changes in diel and developmental host gene expression. *Proc Natl Acad Sci.* 2019;116:7990–9.
6. El Aidy S, Van Baarlen P, Derrien M, Lindenbergh-Kortleve DJ, Hooiveld G, Levenez F, et al. Temporal and spatial interplay of microbiota and intestinal mucosa drive establishment of immune homeostasis in conventionalized mice. *Mucosal Immunol.* 2012;5:567–79.
7. Rawls JF, Samuel BS, Gordon JI. Gnotobiotic zebrafish reveal evolutionarily conserved responses to the gut microbiota. *Proc Natl Acad Sci U S A.* 2004;101:4596–601.

8. Bartel DP, Chen CZ. Micromanagers of gene expression: The potentially widespread influence of metazoan microRNAs. *Nat Rev Genet.* 2004;5:396–400.
9. Agarwal V, Bell GW, Nam JW, Bartel DP. Predicting effective microRNA target sites in mammalian mRNAs. *Elife.* 2015;4:1–38.
10. Orang AV, Safaralizadeh R, Kazemzadeh-Bavili M. Mechanisms of miRNA-mediated gene regulation from common downregulation to mRNA-specific upregulation. *Int J Genomics.* 2014;2014 June 2013.
11. Vasudevan S, Steitz JA. AU-Rich-Element-Mediated Upregulation of Translation by FXR1 and Argonaute 2. *Cell.* 2007;128:1105–18.
12. Berezikov E. Evolution of microRNA diversity and regulation in animals. *Nat Rev Genet.* 2011;12:846–60. doi:10.1038/nrg3079.
13. Wheeler BM, Heimberg AM, Moy VN, Sperling EA, Holstein TW, Heber S, et al. The deep evolution of metazoan microRNAs. *Evol Dev.* 2009;11:50–68.
14. Mehrabadi M, Hussain M, Asgari S. MicroRNAome of *Spodoptera frugiperda* cells (Sf9) and its alteration following baculovirus infection. *J Gen Virol.* 2013;94 Pt_6:1385–97. doi:10.1099/vir.0.051060-0.
15. Mayoral JG, Hussain M, Joubert DA, Iturbe-Ormaetxe I, O’Neill SL, Asgari S. Wolbachia small noncoding RNAs and their role in cross-kingdom communications. *P Natl Acad Sci USA.* 2014;111:18721–6. doi:10.1073/pnas.1420131112.
16. Bartel DP. Metazoan MicroRNAs. *Cell.* 2018;173:20–51. doi:10.1016/j.cell.2018.03.006.
17. Murphy D, Dancis B, Brown JR. The evolution of core proteins involved in microRNA biogenesis. *BMC Evol Biol.* 2008;8:1–18.
18. Kozomara A, Birgaoanu M, Griffiths-Jones S. MiRBase: From microRNA sequences to function. *Nucleic Acids Res.* 2019;47:D155–62.
19. Lee KH, Ruby EG. Effect of the squid host on the abundance and distribution of symbiotic *Vibrio fischeri* in nature. *Appl Environ Microbiol.* 1994;60:1565–71. <http://www.ncbi.nlm.nih.gov/pubmed/16349257>.
20. Nawroth JC, Guo H, Koch E, Heath-Heckman EAC, Hermanson JC, Ruby EG, et al. Motile

cilia create fluid-mechanical microhabitats for the active recruitment of the host microbiome. *Proc Natl Acad Sci U S A*. 2017;114:9510–6.

21. Nyholm S V., Stabb E V., Ruby EG, McFall-Ngai MJ. Establishment of an animal-bacterial association: Recruiting symbiotic vibrios from the environment. *Proc Natl Acad Sci U S A*. 2000;97:10231–5.

22. Montgomery MK, McFall-Ngai MJ. The inductive role of bacterial symbionts in the morphogenesis of a squid light organ. 1995;35:372–80.

23. Lamarq LH, Mcfall-Ngai MJ. Induction of a Gradual , Reversible Morphogenesis of Its Host ' s Epithelial Brush Border by *Vibrio fischeri*. *Infect Immun*. 1998;66:777–85.

24. Chun CK, Scheetz TE, Bonaldo M de F, Brown B, Clemens A, Crookes-Goodson WJ, et al. An annotated cDNA library of juvenile *Euprymna scolopes* with and without colonization by the symbiont *Vibrio fischeri*. *BMC Genomics*. 2006;7:154.

25. Chun CK, Troll J V., Koroleva I, Brown B, Manzella L, Snir E, et al. Effects of colonization, luminescence, and autoinducer on host transcription during development of the squid-vibrio association. *Proc Natl Acad Sci U S A*. 2008;105:11323–8.

26. Boettcher KJ, Ruby EG. Depressed light emission by symbiotic *Vibrio fischeri* of the sepiolid squid *Euprymna scolopes*. *J Bacteriol*. 1990;172:3701–6. doi:10.1128/JB.172.7.3701-3706.1990.

27. Graf J, Dunlap P V, Ruby EG. Effect of transposon-induced motility mutations on colonization of the host light organ by *Vibrio fischeri*. *J Bacteriol*. 1994;176:6986–91. doi:10.1128/jb.176.22.6986-6991.1994.

28. Belcaid M, Casaburi G, McAnulty SJ, Schmidbauer H, Suria AM, Moriano-Gutierrez S, et al. Symbiotic organs shaped by distinct modes of genome evolution in cephalopods. *Proc Natl Acad Sci U S A*. 2019;116:3030–5.

29. Camacho C, Coulouris G, Avagyan V, Ma N, Papadopoulos J, Bealer K, et al. BLAST+: Architecture and applications. *BMC Bioinformatics*. 2009;10:1–9.

30. Gasteiger E, Gattiker A, Hoogland C, Ivanyi I, Appel RD, Bairoch A. ExpASY: The proteomics server for in-depth protein knowledge and analysis. *Nucleic Acids Res*.

2003;31:3784–8.

31. Katoh K, Standley DM. MAFFT multiple sequence alignment software version 7: Improvements in performance and usability. *Mol Biol Evol.* 2013;30:772–780.
32. Capella-Gutiérrez S, Silla-Martínez JM, Gabaldón T. trimAl: A tool for automated alignment trimming in large-scale phylogenetic analyses. *Bioinformatics.* 2009;25:1972–3.
33. Stamatakis A. RAxML version 8: A tool for phylogenetic analysis and post-analysis of large phylogenies. *Bioinformatics.* 2014;30:1312–3.
34. Langmead B, Salzberg SL. Fast gapped-read alignment with Bowtie 2. *Nat Methods.* 2012;9:357–9. doi:10.1038/nmeth.1923.
35. Li B, Dewey C. RSEM: accurate transcript quantification from RNA-Seq data with or without a reference genome. *BMC Bioinformatics.* 2011;12:323.
36. Andrews S, Krueger F, Seaman P, Pichon A, Biggins F, Wingett S. FastQC. A quality control tool for high throughput sequence data. Babraham Bioinformatics. Babraham Institute. 2015; Available online at: <http://www.bioinformatics.bab>.
<http://www.bioinformatics.babraham.ac.uk/projects/fastqc/>.
37. Bolger AM, Lohse M, Usadel B. Trimmomatic: a flexible trimmer for Illumina sequence data. *Bioinformatics.* 2014;30:2114–20. doi:10.1093/bioinformatics/btu170.
38. Martin M. Cutadapt removes adapter sequences from high-throughput sequencing reads. *EMBnet J.* 2011;17:10–2.
39. Friedländer MR, MacKowiak SD, Li N, Chen W, Rajewsky N. MiRDeep2 accurately identifies known and hundreds of novel microRNA genes in seven animal clades. *Nucleic Acids Res.* 2012;40:37–52.
40. Robinson MD, McCarthy DJ, Smyth GK. edgeR: A Bioconductor package for differential expression analysis of digital gene expression data. *Bioinformatics.* 2009;26:139–40.
41. Zhao S, Guo Y, Sheng Q, Shyr Y. Advanced Heat Map and Clustering Analysis Using Heatmap3. *Biomed Res Int.* 2014;2014:986048.
42. Enright AJ, John B, Gaul U, Tuschl T, Sander C, Marks DS. MicroRNA targets in *Drosophila*. *Genome Biol.* 2003;5:R1.

43. Götz S, García-Gómez JM, Terol J, Williams TD, Nagaraj SH, Nueda MJ, et al. High-throughput functional annotation and data mining with the Blast2GO suite. *Nucleic Acids Res.* 2008;36:3420–35.
44. Supek F, Bošnjak M, Škunca N, Šmuc T. Revigo summarizes and visualizes long lists of gene ontology terms. *PLoS One.* 2011;6:e21800.
45. Jehn J, Gebert D, Pipilescu F, Stern S, Kiefer JST, Hewel C, et al. PIWI genes and piRNAs are ubiquitously expressed in mollusks and show patterns of lineage-specific adaptation. *Commun Biol.* 2018;1:137. doi:10.1038/s42003-018-0141-4.
46. Zhou X, Liao Z, Jia Q, Cheng L, Li F. Identification and characterization of Piwi subfamily in insects. *Biochem Biophys Res Commun.* 2007;362:126–31.
47. Sohel MH. Extracellular/Circulating MicroRNAs: Release Mechanisms, Functions and Challenges. *Achiev Life Sci.* 2016;10:175–86. doi:10.1016/J.ALS.2016.11.007.
48. Valadi H, Ekström K, Bossios A, Sjöstrand M, Lee JJ, Lötvall JO. Exosome-mediated transfer of mRNAs and microRNAs is a novel mechanism of genetic exchange between cells. *Nat Cell Biol.* 2007;9:654–9. doi:10.1038/ncb1596.
49. Cortez MA, Bueso-Ramos C, Ferdin J, Lopez-Berestein G, Sood AK, Calin GA. MicroRNAs in body fluids--the mix of hormones and biomarkers. *Nat Rev Clin Oncol.* 2011;8:467–77. doi:10.1038/nrclinonc.2011.76.
50. Kremer N, Koch EJ, Filali AE, Zhou L, Heath-Heckman EAC, Ruby EG, et al. Persistent interactions with bacterial symbionts direct mature-host cell morphology and gene expression in the squid. *MSystems.* 2018;3:1–17.
51. Alles J, Fehlmann T, Fischer U, Backes C, Galata V, Minet M, et al. An estimate of the total number of true human miRNAs. *Nucleic Acids Res.* 2019;47:3353–64.
52. Wei P, He P, Zhang X, Li W, Zhang L, Guan J, et al. Identification and characterization of microRNAs in the gonads of *Crassostrea hongkongensis* using high-throughput sequencing. *Comp Biochem Physiol - Part D Genomics Proteomics.* 2019;31:100606. doi:10.1016/j.cbd.2019.100606.
53. Jiao Y, Zheng Z, Du X, Wang Q, Huang R, Deng Y, et al. Identification and characterization

- of microRNAs in pearl oyster *Pinctada martensii* by solexa deep sequencing. *Mar Biotechnol.* 2014;16:54–62.
54. Zhou Z, Wang L, Song L, Liu R, Zhang H, Huang M, et al. The identification and characteristics of immune-related MicroRNAs in haemocytes of oyster *Crassostrea gigas*. *PLoS One.* 2014;9:1–9.
55. Zhao X, Yu H, Kong L, Liu S, Li Q. High throughput sequencing of small RNAs transcriptomes in two *Crassostrea* oysters identifies microRNAs involved in osmotic stress response. *Sci Rep.* 2016;6 December 2015:22687. doi:10.1038/srep22687.
56. Huang J, Luo X, Huang M, Liu G, You W, Ke C. Identification and characteristics of muscle growth-related microRNA in the Pacific abalone, *Haliotis discus hannai*. *BMC Genomics.* 2018;19:1–11.
57. Picone B, Rhode C, Roodt-Wilding R. Identification and characterization of miRNAs transcriptome in the South African abalone, *Haliotis midae*. *Mar Genomics.* 2017;31:9–12. doi:10.1016/j.margen.2016.10.005.
58. Foster JS, McFall-Ngai MJ. Induction of apoptosis by cooperative bacteria in the morphogenesis of host epithelial tissues. *Dev Genes Evol.* 1998;208:295–303.
59. Lamarcq LH, Mcfall-ngai MJ. Induction of a gradual, reversible morphogenesis of its host's epithelial brush border by *Vibrio fischeri* induction of a gradual, reversible morphogenesis of its host's epithelial brush border by *Vibrio fischeri*. 1998;66:777–85.
60. Troll J V. Taming the symbiont for coexistence: A host PGRP neutralizes a bacterial symbiont toxin. *Environ Microbiol.* 2011;12:2190–203.
61. Rader BA, Kremer N, Apicella MA, Goldman WE, McFall-Ngai MJ. Modulation of symbiont lipid signaling by host alkaline phosphatases in the squid-*Vibrio* symbiosis. *MBio.* 2012;3:e00093-12.
62. Nyholm S V., Deplancke B, Gaskins HR, Apicella MA, McFall-Ngai MJ. Roles of *Vibrio fischeri* and nonsymbiotic bacteria in the dynamics of mucus secretion during symbiont colonization of the *Euprymna scolopes* light organ. *Appl Environ Microbiol.* 2002;68:5113–22.
63. Jin P, Li S, Sun L, Lv C, Ma F. Transcriptome-wide analysis of microRNAs in

- Branchiostoma belcheri upon *Vibrio parahemolyticus* infection. *Dev Comp Immunol*. 2017;74:243–52. doi:10.1016/j.dci.2017.05.002.
64. Skalsky RL, Vanlandingham DL, Scholle F, Higgs S, Cullen BR. Identification of microRNAs expressed in two mosquito vectors, *Aedes albopictus* and *Culex quinquefasciatus*. *BMC Genomics*. 2010;11.
65. Li S, Mead EA, Liang S, Tu Z. Direct sequencing and expression analysis of a large number of miRNAs in *Aedes aegypti* and a multi-species survey of novel mosquito miRNAs. *BMC Genomics*. 2009;10:1–17.
66. Qiang J, Tao F, He J, Sun L, Xu P, Bao W. Effects of exposure to *Streptococcus iniae* on microRNA expression in the head kidney of genetically improved farmed tilapia (*Oreochromis niloticus*). *BMC Genomics*. 2017;18:1–11.
67. Hu S, Liu L, Chang EB, Wang JY, Raufman JP. Butyrate inhibits pro-proliferative miR-92a by diminishing c-Myc-induced miR-17-92a cluster transcription in human colon cancer cells. *Mol Cancer*. 2015;14:1–15. doi:10.1186/s12943-015-0450-x.
68. Davidson SK, Koropatnick TA, Kossmehl R, Sycuro L, McFall-Ngai MJ. NO means “yes” in the squid-vibrio symbiosis: Nitric oxide (NO) during the initial stages of a beneficial association. *Cell Microbiol*. 2004;6:1139–51.
69. Small AL, McFall-Ngai MJ. Halide peroxidase in tissues that interact with bacteria in the host squid *Euprymna scolopes*. *J Cell Biochem*. 1999;72:445–57.

Appendix A

Additional Scientific contributions

In addition to the work described within this thesis, I performed research that was incorporated into the following seven publications:

Nikolakakis, K., Monfils, K., **Moriano-Gutierrez, S.**, Brennan, C. A., & Ruby, E. G. (2015). Characterization of the fatty-acid chemoreceptors VfcB and VfcB2 from *Vibrio fischeri*. *Applied and Environmental Microbiology*, AEM-02856.

For this project, I conducted the bioinformatic analysis to compare *V. fischeri* chemoreceptors among Vibrios.

Bongrand, C., Koch, E. J., **Moriano-Gutierrez, S.**, Cordero, O. X., McFall-Ngai, M., Polz, M. F., & Ruby, E. G. (2016). A genomic comparison of 13 symbiotic *Vibrio fischeri* isolates from the perspective of their host source and colonization behavior. *The ISME journal*, 10(12), 2907.

For this project, I conducted the comparative genomic analysis to compare 13 symbiotic *V. fischeri* isolates to show genetic differences between two different symbiont colonization behaviors.

Belcaid M, Casaburi G, McAnulty SJ, Schmidbaur H, Suria AM, **Moriano-Gutierrez S**, Pankey MS, Oakley TH, Kremer N, Koch EJ, Collins AJ, Nguyen H, Lek S, Goncharenko-Foster I, Minx P, Sodergren E, Weinstock G, Rokhsar DS, McFall-Ngai M, Simakov O, Foster JS, Nyholm SV. (2019). Symbiotic organs shaped by distinct modes of genome evolution in cephalopods. *Proceedings of the National Academy of Sciences*, doi: 10.1073/pnas.1817322116.

For this project, I contributed expression values and transcriptomes from several *E. scolopes* tissues to build a reference transcriptome.

Bongrand, C., **Moriano-Gutierrez, S.**, Arevalo, P., McFall-Ngai, M., Visick, K., Poltz, M., Ruby, E. Using colonization assays and comparative genomics to discover symbiosis behaviors and factors in *Vibrio fischeri* (2020). *mBio*, 11(2).

For this project, I conducted the comparative genomic analysis to compare light organ symbiotic *V. fischeri* isolates to isolates from other species to show genetic differences characteristics of light organ *E. scolopes* symbionts. I also conducted competition experiments between two *V. fischeri* strains.

Koch, E., **Moriano-Gutierrez, S.**, Mcfall-Ngai, M., Ruby, E., Liebeke, M. The impact of persistent colonization by *Vibrio fischeri* on the metabolome of the host squid *Euprymna scolopes* (2020). *Journal of experimental Biology*. Under review.

For this project, I extracted hemolymph from adult squid over different times of the day to characterize the *E. scolopes* metabolome in response to symbiosis.

Essock-Burns, T., **Moriano-Gutierrez, S.**, Goldman, W., S., Ruby, E., and M. McFall-Ngai. Differential deployment of products of a gene family across a symbiotic tissue landscape in the *Euprymna scolopes* – *Vibrio fischeri* symbiosis. Intended journal: *mBio*.

For this project, I conducted the gene expression analysis to determine cadherin response to light organ colonization.

Appendix B

Delivery of symbiont CsrB2 into host epithelium

A remaining question from **Chapter 3** of this dissertation is: do other symbiont sRNAs get into the host epithelium?

From the analysis OMVs RNA in Chapter 3, we found other sRNAs apart from SsrA. In addition, CsrB2 was also found in the squid hemolymph. *Vibrio fischeri* has two CsrB genes encode in its genome and its mechanism of action is shown in **Figure B1**. The expression levels of CsrB, CsrA and CsrD, the negative regulator of CsrB was studied over the growth curve of *V. fischeri* in rich media. While the CsrA levels remain constant over time, the expression of the regulators CsrB2 and CsrD do vary among the growth curve (**Figure B2**).

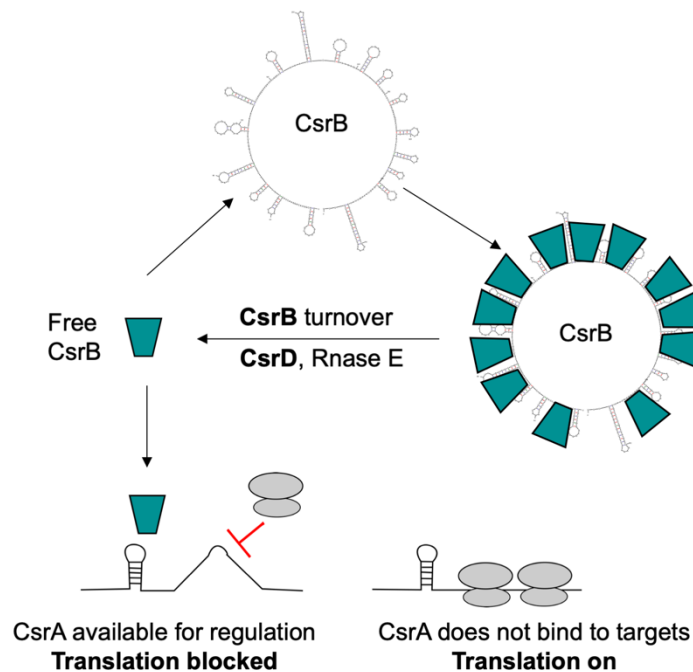


Figure B1. Outline of the Csr system. CsrA regulates mRNA targets by either blocking translation initiation, stabilizing or destabilizing mRNA, or resulting in premature transcriptional termination. The concentration of free CsrA depends on the levels of CsrB that bind to multiple CsrA and preventing them from binding their mRNA targets. Ribosomes are shown in grey. Adapted from (Vakulskas et al., 2015). The secondary structure prediction for *V. fischeri* CsrB2. was generated using with mFold (Zuker, 2003).

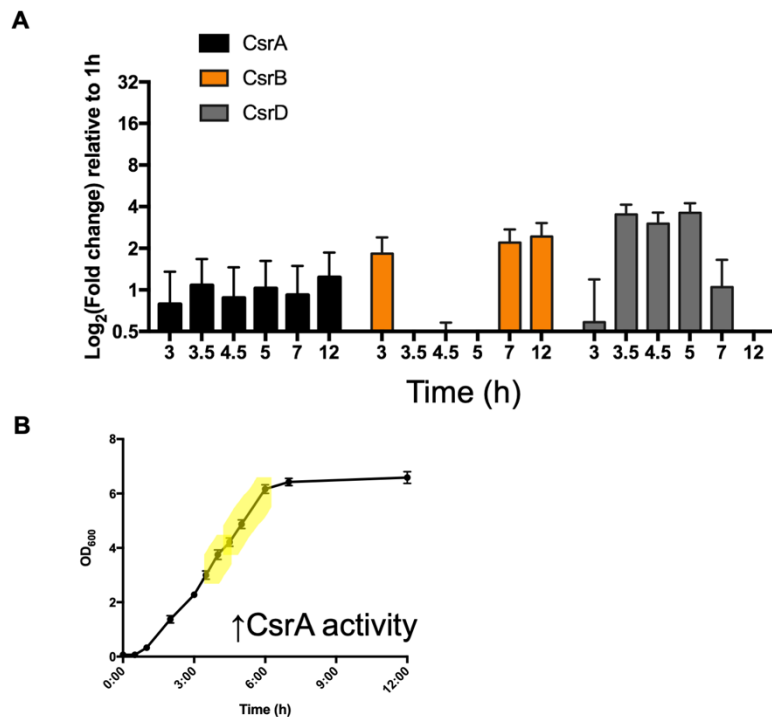


Figure B2. A. Expression levels of the Csr system over time of *V. fischeri* in rich media measured by qRT-PCR. **B.** Estimated bacterial density over time for the expression values obtained in Figure B2-A. Yellow shadow indicates growth curve period where the activity of CsrA is predicted high.

Two HCR probes for CsrB2 were design (**Table B1, Figure B3**), to localize the CsrB2 transcript within the light-organ crypts. CsrB2, as seen in chapter 3 with SsrA, also localizes within the host epithelium. SsrA localizes in abundance in the host cytoplasm, in constrast CsrB localizes mainly within the host nucleus (**Figure B4, Figure B5**). In less abundance, CsrB2, is also found within the cytoplasm of host epithelial cells (**Figure B6**).

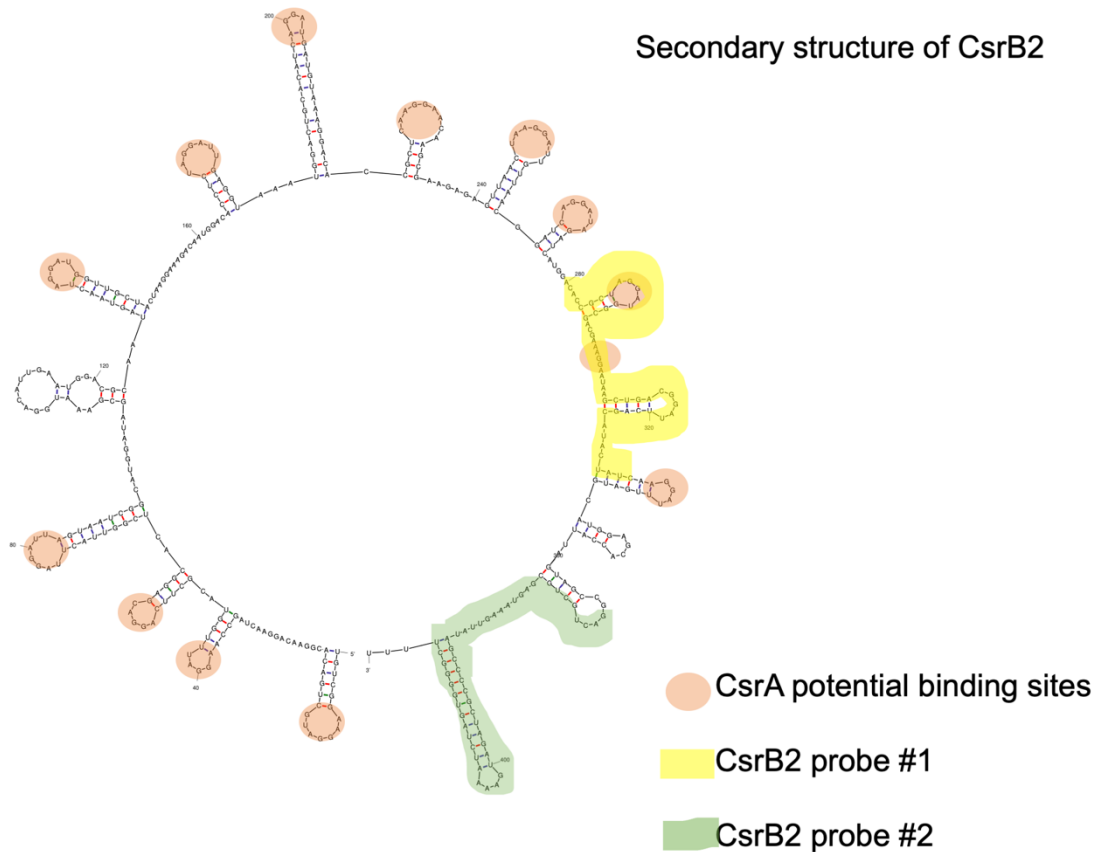


Figure B3. Secondary structure of *V. fischeri* CsrB2 determined by mFold (Zuker, 2003). Yellow and green indicate the binding target sequence of the HCR CsrB2 probes. Orange, indicate potential CsrA binding sites.

Table B1. Oligonucleotide sequences for localization of CsrB2 transcript.

Probe ID	Sequence
CsrB2-1-4	CCGCUAGGAUGGCGACGAAAGGAAUAAGCUGACGGAUUCAGCAUACUAUC
CsrB2-1-5	GACUGCUGCGAGUAAAGUUAUAGCCCCGCUAGAUGAAAAUCUAGUGGGGCU

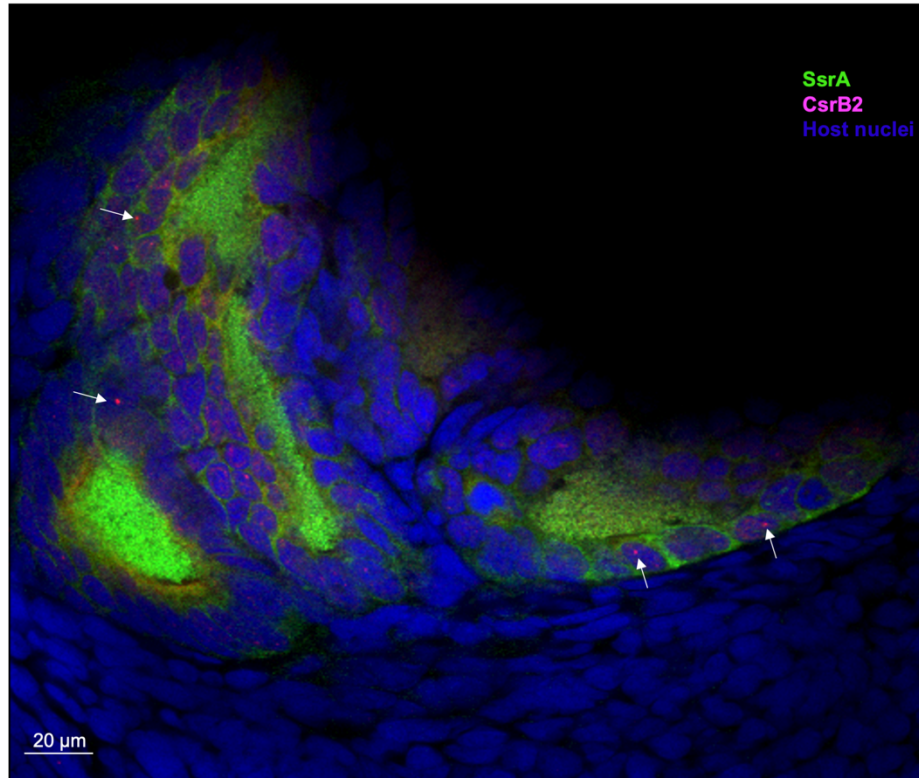


Figure B4. Localization of symbiont CsrB2 (red) transcript within the host epithelium. SsrA (green) is found in abundance within the cytoplasm. CsrB2 is found in the cytoplasm and within the host nucleus. White arrows point out high density areas of CsrB2 within the host nucleus.

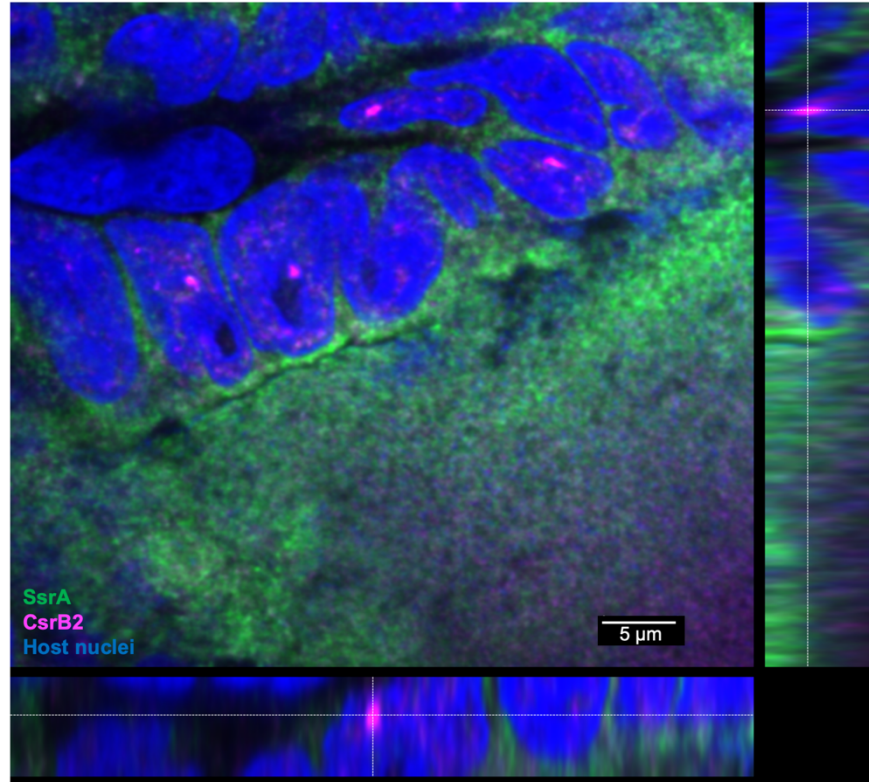


Figure B5. Localization of symbiont CsrB2 (pink) and SsrA (green) transcript by confocal microscopy. Orthogonal view showing CsrB2 transcript within the host nucleus.

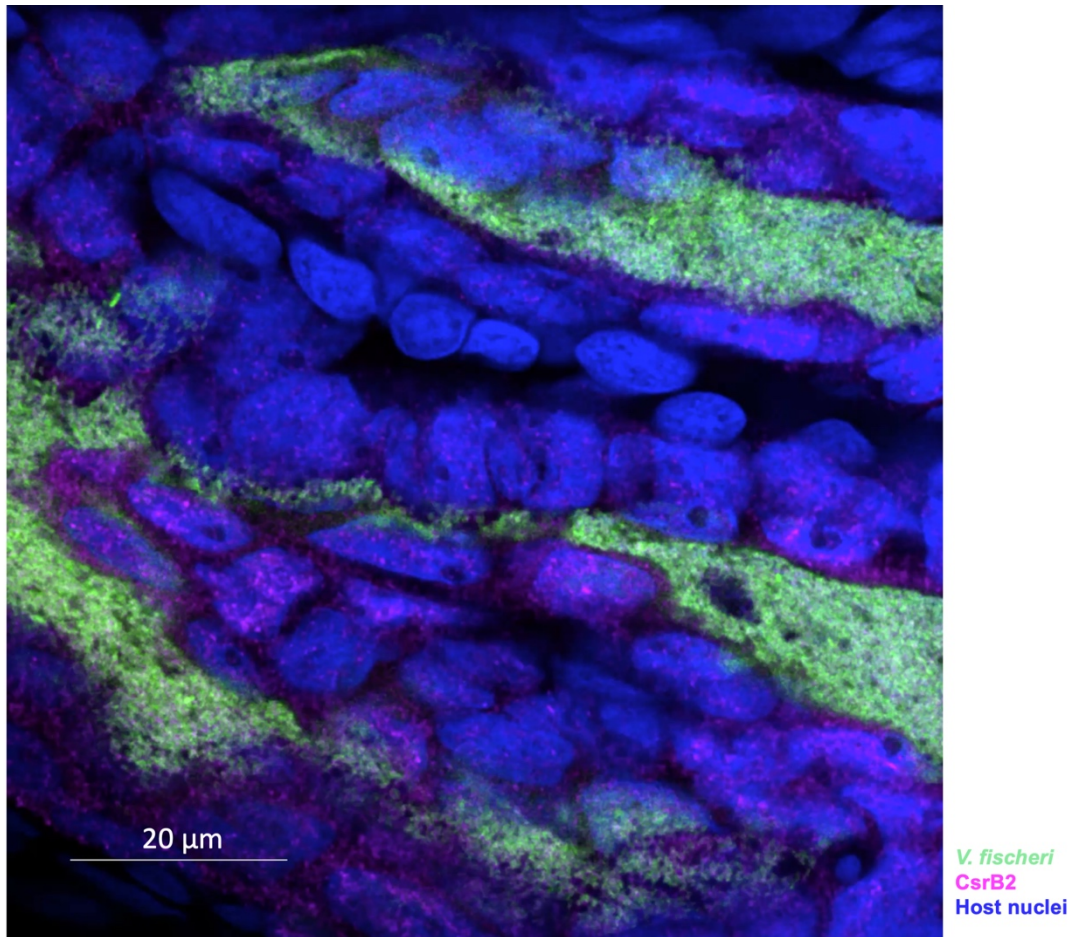


Figure B6. Localization of symbiont CsrB2 (pink) transcript by confocal microscopy. Light organ colonized for 24 h with labeled *V. fischeri* cells (green).

References

- Vakulskas, C.A., Potts, A.H., Babitzke, P., Ahmer, B.M.M., and Romeo, T. (2015). Regulation of Bacterial Virulence by Csr (Rsm) Systems. *Microbiol. Mol. Biol. Rev.* 79, 193–224.
- Zuker, M. (2003). Mfold web server for nucleic acid folding and hybridization prediction. *Nucleic Acids Res.* 31, 3406–3415.

Appendix C

Biogeography of symbiont gene expression in the light organ crypts

With HCR-FISH on juvenile light organs we have observed a characteristic pattern of symbiont gene expression within the host light-organ crypts for 16S, SsrA (seen in chapter 3) and SsrS bacterial non-coding RNAs after 24 h post-colonization (**Figure C1**). SsrS (6S RNA) is a transcription repressor during stationary phase by selectively binding to σ^{70} subunit of the RNA polymerase (Wassarman and Storz 2000). There is differential distribution for the expression of these ncRNAs within the colonized crypts, not only between crypts that are in different developmental stages (from the most mature crypt I to the least developmentally mature, crypt III) but also within a crypt. Questions

arise on how this heterogeneity between identical cells that reside in the same microenvironment and the possible functionality of this phenotypic subpopulations within the symbiont population when is host associated. How the phenotypic subpopulations in the light organ crypts (**Figure C1**) translate to beneficial functionality for the symbiont populations requires further investigation. That only the symbiont cells on the center of the light organ crypts show expression the global repressor of transcription SsrS, could be an indication that in the center of the crypts, cells are active

but not growing. We constructed a clean-deletion mutant of SsrS to study the dynamics of symbiont expression within the light organ. In competition with wild-type strain (WT), Δ *ssrS* is out-competed (**Figure C2**).

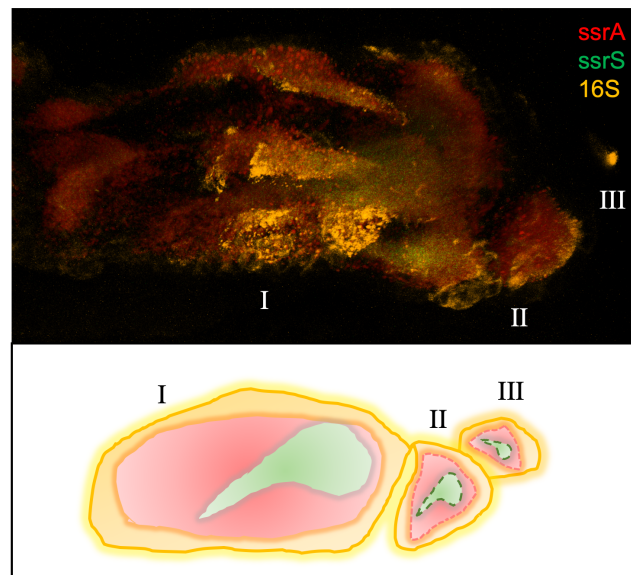


Figure C1. HCR-FISH of a juvenile light organ after 24 h post-colonization showing the different niches within the crypts with different bacterial expression profiles. SsrA (red) labeling strongest in the crypts lumen, 16S (yellow) along the edges. SsrS (green) is expressed only in the interior region of crypt I. Crypt II and III shows variable expression for SsrS and SsrA (dotted line).

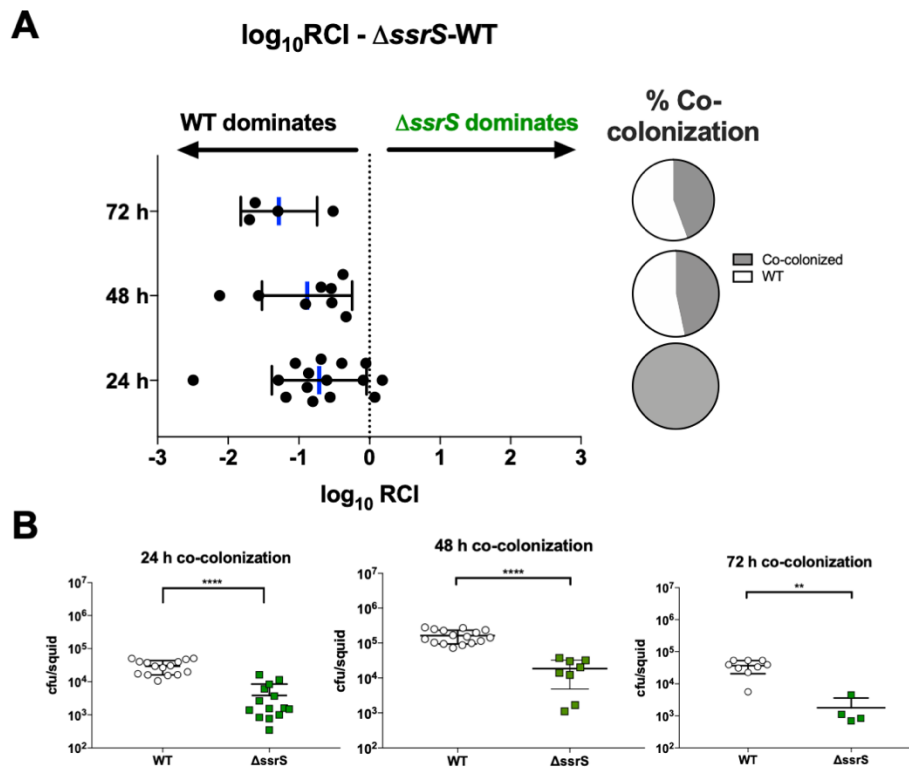


Figure C2. Competition of *ssrS* deletion mutant (ΔssrS) against wild-type strain (WT). **A.** Relative competitive index (RCI) over the first 3 days post-colonization. On the right panel percentage of co-colonization and single colonization overtime. **B.** Colony forming units (CFU) per squid after 24, 48 and 72 h post-colonization.

References

Wassarman, K.M., and Storz, G. (2000). 6S RNA regulates *E. coli* RNA polymerase activity. *Cell* 101, 613–623.